REPUBLIQUE ALGERIENNE DEMOCRATIQUE ET POPULAIRE MINISTERE DE L'ENSEIGNEMENT SUPERIEUR ET DE LA RECHERCHE SCIENTIFIQUE
UNIVERSITE ECHAHID HAMMA LAKHDAR EL-OUED
FACULTE DE THECHNOLOGIE
DEPARTEMENT DE GENIE DES PROCEDES ET PETROCHIMIE

THESE

Présenté en vue de l'obtention du diplôme de
Doctorat LMD
Filière : Génie Mécanique
Spécialité : Energétique

THEME DE LA THESE :

Élaboration et caractérisation d'un matériau composite renforcé par différents types de fibres

Présenté par :

RAHMANI Lalmi

Soutenu Le : 16/02/2026 devant le jury composé de :

Mr. BOUKHARI Ali	Professeur	Président	Université d'El-Oued
Mr. BEN HOUA Boubakeur	Professeur	Examinateur	Université d'El-Oued
Mr. BOULAHROUZ Salim	Professeur	Examinateur	Université de Khnchla
Mr. CHAHAOUI Oualid	Professeur	Examinateur	Université de Khnchla
Mr. DJOIDI Tarek	MCA	Examinateur	Université de Biskra
Mr. GHERBI Med Tahar	Professeur	Encadreur	Université d'El-Oued

Graduation year:2025-2026

ABSTRACT

This study aims to develop sustainable composite materials by reinforcing biodegradable matrices with treated natural fibers, with an emphasis on improving mechanical properties while reducing environmental impact. Techniques for surface modification, including alkali treatment and cold plasma, were employed to enhance the adhesion between fibers and the matrix, thereby increasing tensile, flexural, and compressive strength. Comprehensive characterization using FT-IR, SEM, and XRD confirmed changes in chemical composition and improved surface morphology after treatment. Mechanical assessments revealed that hybrids of plasma-processed wool and Periploca laevigata Aiton fiber (PLAF) achieved a tensile strength of 26.02 MPa and a Young's modulus of 2.35 GPa, exceeding the performance of the individual fiber composites. Flexural and compressive tests also showed improved load-bearing capacity, with the hybrid reaching 253.15 N and a compressive strength of 59.56 MPa. Cold plasma treatment was shown to be efficient in improving interfacial bonding by eliminating surface contaminants and altering fiber chemistry.

In addition to the above, we carry out an investigation into the low-velocity impact performance of four epoxy-based composite materials reinforced with natural fibers: Periploca laevigata Aiton fiber (PLAF), untreated wool fiber (WLF), NaOH-treated wool fiber (NWLF), and a hybrid composite (PLAWLF) that merges cold plasma-treated wool fiber with PLAF. The composites were created through vacuum infusion molding and evaluated at impact energy levels of 5 J, 10 J, 30 J, and 50 J to assess peak load, displacement at peak load, and energy absorption.

Research conducted on composites reinforced with treated horse tail hair fibers (THHF) demonstrated remarkable strength and rigidity. Alkaline-treated THHF showed an average single tensile strength of 129.34 MPa and a Young's modulus of 5.72 GPa. When incorporated into the matrix, the composite reached a tensile strength of 59.23 MPa and a flexural strength of 63.27 MPa, maintaining consistent compressive performance (66.14–78.82 MPa).

Keywords: Composites material, natural fiber, epoxy matrix, mechanical characteristic's, manufacturing process

Résumé

Cette étude vise à développer des matériaux composites durables en renforçant des matrices biodégradables avec des fibres naturelles traitées, en mettant l'accent sur l'amélioration des propriétés mécaniques tout en réduisant l'impact environnemental. Des techniques de modification de surface, telles que le traitement alcalin et le plasma froid, ont été employées pour améliorer l'adhésion entre les fibres et la matrice, augmentant ainsi la résistance à la traction, la flexion et la compression. La caractérisation approfondie utilisant FT-IR, MEB et DRX a confirmé les changements de composition chimique et l'amélioration de la morphologie de surface après traitement. Les essais mécaniques ont révélé que les hybrides de laine traitée au plasma et de fibres de Periploca laevigata Aiton (PLAF) ont atteint une résistance à la traction de 26,02 MPa et un module d'Young de 2,35 GPa, dépassant la performance des composites à fibres individuelles. Les tests de flexion et de compression ont également montré une capacité de charge accrue, l'hybride atteignant 253,15 N et une résistance à la compression de 59,56 MPa. Le traitement au plasma froid s'est révélé efficace pour améliorer l'adhésion interfaciale en éliminant les contaminants de surface et en modifiant la chimie des fibres.

En outre, nous avons réalisé une étude sur la performance aux chocs à faible vitesse de quatre matériaux composites à base d'époxy renforcés de fibres naturelles : la fibre de Periploca laevigata Aiton (PLAF), la fibre de laine non traitée (WLF), la fibre de laine traitée à la soude (NWLF), et un composite hybride (PLAWLF) combinant la laine traitée au plasma froid et la PLAF. Les composites ont été créés par moulage par infusion sous vide et évalués à des niveaux d'énergie d'impact de 5 J, 10 J, 30 J et 50 J afin d'analyser la charge maximale, le déplacement au pic de charge et l'absorption d'énergie.

Les recherches menées sur les composites renforcés par des fibres de crin de cheval traitées (THHF) ont démontré une résistance et une rigidité remarquables. Les fibres THHF traitées alcalinement ont présenté une résistance moyenne à la traction de 129,34 MPa et un module d'Young de 5,72 GPa. Lorsqu'elles sont intégrées à la matrice, le composite a atteint une résistance à la traction de 59,23 MPa et une résistance en flexion de 63,27 MPa, tout en maintenant des performances de compression constantes (66,14–78,82 MPa).

Mots-clés : Matériaux composites, fibres naturelles, matrice époxy, caractéristiques mécaniques, procédé de fabrication

الملخص

تهدف هذه الدراسة إلى تطوير مواد مركبة مستدامة من خلال تدعيم المصفوفات القابلة للتحلل الحيوي بألياف طبيعية معالجة، مع التركيز على تحسين الخصائص الميكانيكية وتقليل التأثير البيئي في الوقت نفسه .تم استخدام تقنيات لتعديل السطح، بما في ذلك المعالجة القلوية والمعالجة بالبلازما الباردة، لتعزيز الالتصاق بين الألياف والمصفوفة، مما أدى إلى زيادة مقاومة الشد والانحناء والضغط .أكدت التحليلات الشاملة باستخدام تقنيات FT-IR و SEM و XRDحدوث تغييرات في التركيب الكيميائي وتحسن في البنية السطحية بعد المعالجة .كشفت التقييمات الميكانيكية أن الهجائن المكوّنة من ألياف الصوف المعالجة بالبلازما وألياف نبات Periploca laevigata Aiton (PLAF) حقّقت مقاومة شد بلغت 26.02 ميغاباسكال ومعامل يونغ بلغ 2.35 غيغاباسكال، متجاوزة أداء المركبات أحادية الألياف .كما أظهرت اختبارات الانحناء والضغط تحسنًا في القدرة على تحمل الأحمال، حيث وصلت المقاومة إلى 253.15 نيوتن وقوة الضغط إلى 59.56 ميغاباسكال .وقد ثبت أن المعالجة بالبلازما الباردة فعالة في تحسين الترابط البيني من خلال إزالة الملوثات السطحية وتعديل التركيب الكيميائي للألياف.

بالإضافة إلى ما سبق، أجرينا تحقيقًا في أداء الصدمة منخفضة السرعة لأربعة مواد مركبة أساسها الإيبوكسي ومدعّمة بألياف طبيعية، وهي :ألياف Periploca laevigata Aiton (PLAF) ، ألياف الصوف غير المعالجة (WLF) ، ألياف الصوف المعالجة بهيدروكسيد الصوديوم (NWLF) ، والمركب الهجين (PLAWLF) الذي يجمع بين ألياف الصوف المعالجة بالبلازما الباردة وألياف PLAF. تم تصنيع هذه المركبات باستخدام تقنية القولبة بالحقن الفراغي، وتم تقييمها عند مستويات طاقة تصادم بلغت 5 جول، 10 جول، 30 جول، و 50جول لقياس الحمل الأقصى، والإزاحة عند الحمل الأقصى، وامتصاص الطاقة.

أظهرت الأبحاث التي أُجريت على المواد المركبة المدعّمة بألياف ذيل الحصان المعالجة (THHF) قوة وصلابة ملحوظتين .حيث سجلت الألياف المعالجة قلوياً متوسط مقاومة شد مفردة بلغ 129.34 ميغاباسكال ومعامل يونغ بلغ 5.72 غيغاباسكال .وعند دمجها في المصفوفة، وصلت مقاومة الشد في المركب إلى 59.23 ميغاباسكال، بينما بلغت مقاومة الانحناء 63.27 ميغاباسكال، مع الحفاظ على أداء ضغط مستقر يتراوح بين 66.14 و 78.82ميغاباسكال .

الكلمات المفتاحية: المواد المركبة, الالياف الطبيعية, الايبوكسي, مصفوفة البوليمر , الخصائص الميكانيكية, طرق التصنيع

ACKNOWLEDGEMENTS

It is with immense pride and gratitude that I present the culmination of several years of diligent research, conducted at the Department of Mechanical Engineering at the University of Chahid Hamma Lakhdar in El Oued.

First and foremost, I would like to express my deepest thanks to my thesis supervisor, **Pr. Mohammed Taher Gherbi**. His unwavering support, expert guidance, and insightful feedback have been absolutely invaluable throughout the entire research process. **Pr. Gherbi's** encouragement, dedication, and commitment to my academic and professional growth were fundamental in helping me navigate the challenges of this project and ultimately achieve the research goals. I am deeply honored to have had the opportunity to work under his supervision.

I am profoundly thankful to the esteemed professors who have contributed to the completion of this research, particularly **Pr. Oday Ibrahim Abdullah** from the University of Baghdad, Iraq, for his invaluable input and collaboration. Lastly, I wish to express my heartfelt appreciation to the members of the thesis committee for their keen interest in my research and for the honor of evaluating my work. Their thoughtful assessments and feedback have been instrumental in enhancing the quality of this thesis.

DEDICATION

First I would like to express my profound gratitude to my esteemed supervisor, **Pr. Mohammed Taher Gherbi**. His unwavering guidance, mentorship, and constant encouragement have been invaluable to me throughout this research. His dedication and expertise have not only shaped this work but have also inspired me to strive for excellence in everything I do.

To my dear mother and father, whose love and encouragement have been my foundation, guiding me through every step of this journey.

To my cherished family my wife, children, brothers and sister whose support and belief in me have been my greatest source of strength.

TABLE OF CONTENTS

Chapter II:

Mechanical Properties of Composites Material

Chapter III:

Test of Composites Material

Chapter IV:

Materials Employed, Methodologies Applied, and Characterization Approaches

Chapter V:

Results and discussions

LIST OF FIGURES

Figures of Chapter I

Figures of Chapter II

Figures of Chapter III

Figures of Chapter IV

Figures of Chapter V

LIST OF TABLES

Tables of Chapter I

Tables of Chapter II

Tables of Chapter III

Tables of Chapter IV

Tables of Chapter V

GLOSSARY

Axial stress difference (MPa) between two points on the curve,	$\Delta\sigma_a$
Applied force (N)	P
Bending stress on the outer surface (MPa).	σ^b
Change in length of the specimen, measured by the extensometer (mm).	ΔL
Compressive modulus (GPa),	E^C
Corresponding axial strain difference between the two points.	$\Delta\varepsilon_a$
Compressive Poisson's ratio,	v_c
Compressive strength (MPa or N/mm²)	C
Corresponding axial strain difference on the tangent.	$\Delta\varepsilon$
Dashpot viscosity (viscous component).	η
Density of test liquid (g/cm^3)	ρ_l
Density of fiber (g/cm^3)	ρ_f
Density of fiber (g/cm^3).	ρ_f
Density of cast resin (g/cm^3).	ρ_m
Density of fiber (g/cm³)	ρ_f
Density matrix (g/cm³)	ρ_m
Difference in midspan deflections at the corresponding points on the stress–Strain curves (mm).	$\Delta\delta$
Elastic Strain (instantaneous elastic deformation).	ε_2
Energy absorbed by the material.	E absorbed
Final gauge length (mm).	L_f
Final cross sectional area at the fracture.	A_f
Fiber weight in air (g)	W_1
Fiber weight in the test liquid (g)	W_2
Filament's average cross-sectional area (mm²).	A
Failure load (N).	F
Force as a function of displacement	F(δ)
Gauge length (mm).	L
Gauge length of the specimen (mm).	L
Glass Transition Temperature	Tg
Initial dry weight of the specimen (g)	W_0
Instantaneous cross sectional area (mm^2)	A_i
Initial gauge length (mm).	L_0
Kinetic energy of the impacting object (Joules)	E_k
Longitudinal tensile strength of fiber (MPa).	$\sigma^T{}_{1f}$
Longitudinal Young's modulus of fiber (GPa).	E_{Lf}

Linear density of fiber (g/m).	$\rho^{l}{}_{p}$
Lower strain limit	ε_{l}
Lateral compressive strains.	ε_{l2}
Lateral strain,	$\Delta\varepsilon_{l}$
Mass of the glass weighing bottle containing the sample after oven drying (g).	W_{3}
Maximum tensile load (N).	P
Measured (actual) density of the composite (g/cm³)	ρ_{c}
Mass of the fiber (g)	M_{f}:
Mass of the matrix (resin) (g)	M_{m}:
Maximum load the specimen can withstand before failure (N).	P_{ult}
Mass of the impacting object (kg)	m
Maximum displacement reached during the impact.	δmax
Normal vector to the surface.	n
Original cross-sectional area (mm^2).	A_0
Original cross sectional area.	A_{0}
Poisson's ratio in tension	v_{t}
Reduction in area.	R
Stress (MPa)	σ
Spring modulus (elastic component),	E:
Stress (MPa).	$\sigma(t)$
Strain.	$\varepsilon(t)$
Stress tensor.	σ_{ij}
Strain rate (rate of deformation).	$\frac{d\,\varepsilon\,(t)}{dt}$
Stress vector acting on the surface.	T
Stress difference on the tangent (MPa).	$\Delta\sigma$
Shear strength (MPa).	S
Specimen width (mm).	b
Specimen length (mm).	h
Span of the specimen (mm).	L
Tensile strength (N/mm^2)	T_{f}
Tensile modulus of fiber (N/mm^2).	E_{f}
True compliance (mm/N).	C
Tensile load at upper strain limit (N).	P_{u}
Tensile load at lower strain limit (N).	P_{l}
Theoretical density of the composite (g/cm³)	ρ_{t}
Tensile strength of composite (MPa).	T_{s}
Thickness of the specimen (mm).	h
Total initial energy of the impacting object.	E initial
Tensile modulus (GPa).	E^{T}

Upper strain limit	ε_u
Ultimate compressive force (N)	F_{ult}
Ultimate force at failure (N).	P_{ult}
Viscous Strain or viscous behavior (which accounts for the time-dependent Deformation of the material).	ε_1
Void content (%)	V_v
Velocity of the impacting object (m/s)	v
Weight fraction of fiber	W_f
Weight fraction of matrix	W_m
Weight of the specimen after immersion (g)	W_t
Initial dry weight of the specimen (g)	W_0
Width of the specimen (mm).	b

Abbreviations

CMCs : Ceramic matrix composites.

DMA: Dynamic Mechanical Analysis.

FTIR: Transform Infrared Spectroscopy.

FRP: Fiber-reinforced polymer.

LCM: Conventional liquid composite molding.

LFSM: Long Fiber Spray-up Molding.

MMCs: Metal matrix composites.

NWLF: NaOH-treated wool fiber.

PLAF : Periploca laevigata Aiton.

PMCs : Polymer matrix composites.

PVC: Polyvinyl chloride.

SEM: Scanning Electron Microscopy.

TMA: Thermomechanical Analysis.

Tg: Glass transition temperature.

THHF: Horse tail hair fibers.

WLF: Wool fibers.

XRD: X-ray diffraction.

LIST OF APPENDICES

GENERAL INTRODUCTION

I. General Introduction

The growing interest in sustainable and ecologically friendly materials has led to an increasing focus on natural fiber-reinforced polymer composites (NFRPCs). These composites are a desirable replacement for synthetic materials due to their biodegradability, renewability, affordability, and excellent mechanical characteristics[1, 2]. Natural fibers have been incorporated into composite materials for millennia, with initial uses traced back to approximately 7000 BC and more organized applications documented by 2800 BC [3]. Their attractiveness is attributed to characteristics including low density, high specific strength, resistance to corrosion, superior tensile performance, and compatibility with the environment [4, 5].

Industries including automotive, construction, aerospace, and packaging have progressively substituted synthetic reinforcements, such as glass fibers, with natural alternatives [6]. While glass fibers are known for their remarkable strength, their manufacturing process is energy-consuming, depends on finite resources, and lacks biodegradability. On the other hand, natural fibers offer numerous benefits, including affordability, abundant availability, better thermal insulation capabilities, opportunities for energy recovery, and improved safety for human health and the environment[7, 8].

The incorporation of natural fibers into polymer composites poses specific challenges. A significant issue is the hydrophilic nature of these fibers, primarily due to the presence of hydroxyl groups in cellulose, hemicellulose, and lignin. This property leads to insufficient interfacial bonding with hydrophobic polymer matrices, which ultimately results in reduced mechanical performance [9, 10].

Various surface modification techniques have been explored to enhance the adhesion between fibers and the matrix. Common chemical treatments, such as alkali (NaOH), silane, and acetylation, are often employed to clean the fiber surface and increase its roughness. In contrast, physical treatments like plasma or corona discharge are used to elevate surface energy [11, 12].

In this study, sheep wool was used as an animal fiber, and Periploca laevigata Aiton served as a plant fiber. Periploca laevigata Aiton is a heat-loving, perennial, deciduous shrub widely distributed across the Mediterranean region, including countries such as Spain, Algeria, Libya, Tunisia, Karpathos, Egypt, Crete, Malta, and Sicily. The plant is distinguished by drooping, arrow-shaped leaves and narrow, lanceolate branches. Its flowers are arranged in short axillary cymes, with reddish-brown lobes bordered in greenish-yellow and interspersed with incurved purplish filaments. The fruit is dry and consists of two smooth, fissured follicles containing anemocorous seeds.

In Algeria, Periploca laevigata Aiton is found in the GHARDAIA region, particularly in the arid valleys near METLILI, close to SIDI MEZGHISH (coordinates: 32°03'11" N, 3°34'36" E). The shrub typically grows to a height of 1–2 meters, with heavy branches and semi-lunar lobes. Each lobe encloses seeds covered with natural fiber that is short, lightweight, and disperses readily in the air once the lobes dry and split naturally.

Due to its delicate structure, the fibers were carefully extracted manually by opening the lobes and separating the seeds. The extracted fibers were then washed thoroughly with distilled water at 25°C, a temperature selected to preserve their structural integrity. After washing, the fibers were filtered and subjected to a 24-hour drying process at room temperature (25°C), ensuring that their natural properties were maintained for subsequent use.

NaOH treatment is distinguished by its high efficiency and cost-effectiveness. It effectively eliminates amorphous substances like hemicellulose, lignin, waxes, and pectin, thereby revealing cellulose fibrils and enhancing the mechanical interlocking with the surrounding matrix. [13, 14]. Additionally, cold plasma treatment has the capability to chemically modify the fiber surfaces without influencing their overall properties, resulting in improved wettability and adhesion. However, it is important to manage these treatments with precision, as excessive alterations may compromise fiber strength and jeopardize the composite's performance [15].Utilizing these fibers improves waste valorization and sustainability while also contributing to the development of cost-effective materials suitable for various structural and semi-structural applications[12]. However, studies on the mechanical characteristics and optimal treatment methods for these fibers obtained from arid regions remain limited.

This research intends to fill the current gap by examining both mono and hybrid composites that are strengthened with particular natural fibers obtained from the Algerian area. It highlights the creation and characterization of epoxy-based composite materials that integrate horse tail hair fibers (THHF) and wool fibers (WLF) in both their untreated and treated versions, as well as fibers from Periploca laevigata Aiton (PLAF). Additionally, the study investigates the collaboration of hybrid composites that combine plasma-treated wool with PLAF, referred to as PLAWLF. To remove surface impurities and enhance fiber texture, NaOH treatment was performed at concentrations ranging from 0.1% to 5% on WLF. Furthermore, cold plasma treatment was utilized to activate the fiber surface, thus improving its attachment to the epoxy matrix. Fourier Transform Infrared Spectroscopy (FTIR) was used to identify chemical alterations in both treated and untreated fibers, while Scanning Electron Microscopy (SEM) was applied to examine surface morphology and assess the interfacial bonding between the fibers and the matrix.

The findings indicated that hybrid composites, particularly PLAWLF, demonstrated the most superior overall performance. PLAWLF achieved an impressive tensile strength of 26.02 MPa, a Young’s modulus of 2.35 GPa, a flexural load capacity of 253.15 N, and a compressive strength of 59.56 MPa. The THHF-based composites performed well across all mechanical tests, achieving tensile strengths up to 59.23 MPa and flexural strengths over 63 MPa. Their compressive strength averaged 71.97 MPa, making them suitable candidates for applications requiring both strength and flexibility. These findings emphasize the efficacy of merging suitable surface treatments with hybridization methods to significantly enhance the characteristics of natural fiber-reinforced composites. Additionally, the effective use of underutilized desert-based fibers highlights their importance in promoting sustainable material alternatives. This study backs the creation of biodegradable, environmentally friendly composites with potential uses in numerous industries, such as automotive components, building panels, consumer products, and other engineering fields.

This study introduces a third investigation that builds upon two essential explorations into the mechanical characteristics of epoxy composites reinforced with untreated wool fiber (WLF), NaOH-treated wool fiber (NWLF), and Periploca laevigata Aiton fiber (PLAF). The emphasis of this new research is on a hybrid composite material (PLAWLF) that merges cold plasma-treated wool fiber with PLAF. All composites were fabricated using a uniform vacuum infusion molding technique to ensure consistency throughout the studies. The main objective of the third investigation is to evaluate the low-velocity impact performance at energy levels of 5 J, 10 J, 30 J, and 50 J. Critical performance metrics such as peak load, displacement at peak load, and absorbed energy were thoroughly analyzed. The PLAWLF composite displayed improved performance, achieving as much as 30% higher peak load and energy

absorption than NWLF, and a 24% enhancement over PLAF at an impact energy of 10 J. At 50 J, PLAWLF maintained its structural integrity and showed the highest load-bearing capability among all tested composites. These results highlight the substantial influence of hybridization and physical surface treatment (cold plasma) on enhancing fiber-matrix adhesion, crack resistance, and energy dissipation. Unlike the brittle failure seen in WLF and the restricted deformation of PLAF under high-impact conditions, PLAWLF showcased a balanced failure mode distinguished by both flexibility and toughness. This final phase of the research verifies that the combination of chemically and physically treated natural fibers within a hybrid design approach significantly boosts the impact resistance and mechanical endurance of bio-based composites. The findings provide insightful guidance for tailoring composite formulations for structural uses where strength and energy absorption are crucial, such as in automotive panels, protective enclosures, and aerospace interiors.

This thesis is organized into the following chapters:

Chapter I (Bibliographic Research and General Concepts)

This chapter provides a comprehensive review of the existing literature and the fundamental concepts relevant to this study.

Chapter II (Mechanical Properties of Composite Materials)

This chapter focuses on the mechanical behavior of composite materials reinforced with natural and/or animal fibers. It includes:

- Definition and significance of key mechanical properties such as tensile strength, compressive strength, shear strength, flexural strength, and impact resistance.
- Experimental techniques for evaluating mechanical properties (tensile, compressive, shear, and bending tests).
- Analysis of stress-strain behavior, modulus of elasticity, and failure mechanisms.
- Discussion on load transfer efficiency between matrix and fibers.
- Effect of fiber treatment, fiber length, and fiber dispersion on mechanical performance.
- Evaluation of performance differences between composites reinforced with Periploca laevigata Aiton, sheep wool.

Chapter III (Testing of Composite Materials)

This chapter presents the experimental evaluation of the composite materials developed in this study. It focuses on the methods and procedures used to characterize the mechanical, physical, and thermal behavior of the composites.

Chapter IV (Materials Employed, Methodologies Applied, and Characterization Approaches)

This chapter presents a detailed description of the materials used in this study, the experimental methodologies applied for composite preparation, and the characterization techniques employed to evaluate the physical, mechanical, and thermal properties of the composites.

Chapter V (Results and Discussions)

This chapter presents the experimental results obtained from the characterization of the developed composite materials and provides a detailed discussion of the findings. The analysis focuses on understanding the influence of fiber type, fiber content, and processing methods on the mechanical, thermal, and physical properties of the composites.

CHAPTER I

BIBLIOGRAPHIC RESEARCH AND GENERAL CONCEPTS

I. Introduction

A composite material is formed by merging two or more separate materials that have different properties to create a new material that displays improved characteristics. The elements maintain their unique properties and collaborate to boost the overall effectiveness of the composite[16].

Composites are extensively utilized in aerospace engineering because of their beneficial attributes, including low weight, high strength, and remarkable fatigue resistance. With the growing need for lighter and more efficient structures, composite materials now account for more than 50% of the overall weight in commercial aircraft[17].In addition to aerospace uses, green composites, which originate from renewable resources, have gained importance. These materials provide substantial advantages for both the industry and the environment, especially considering the decreasing availability of petroleum.

Natural fibers, especially, are acknowledged for their environmentally friendly characteristics, ability to be recycled, and beneficial traits in comparison to synthetic fibers[15].Green composites provide various benefits compared to traditional composites, such as reduced weight, enhanced flexibility, and sustainable manufacturing methods. Green composites are biodegradable, minimizing the potential for ecological damage [18]. The green composite lifecycle is represented in Figure **I.1**.

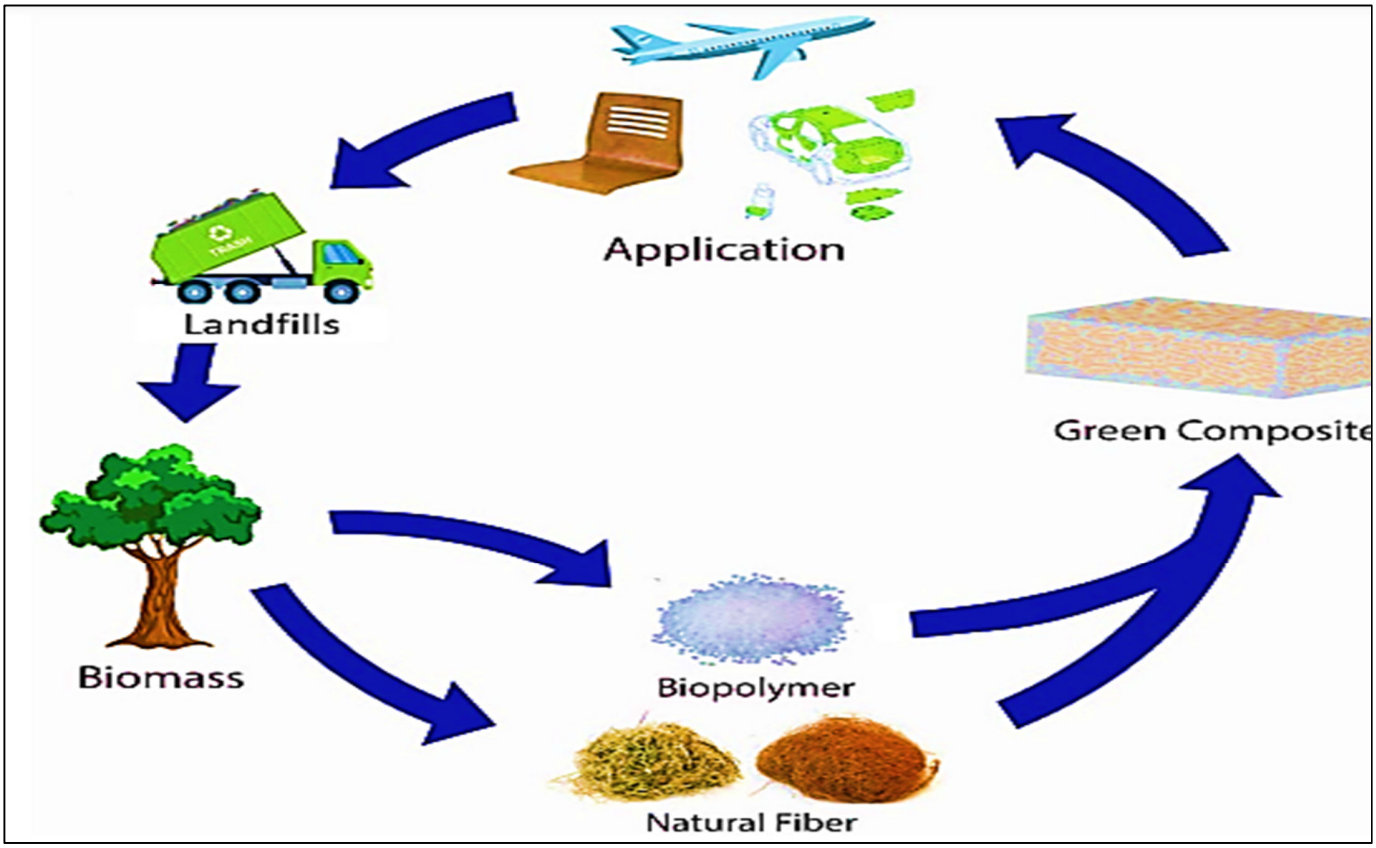

Figure 1.1: *Life cycle of green composites [18].*

Natural fiber composites are becoming increasingly significant because of their outstanding mechanical characteristics, ability to biodegrade, and broad accessibility, rendering them essential elements in sustainable manufacturing and environmentally friendly engineering solutions [19]. The utilization of non-biodegradable substances derived from non-renewable sources greatly adds to environmental contamination during the textile manufacturing process. In order to be eco-friendly, there is a growing interest in using biodegradable biopolymers obtained from leftover biomass, along with economical production methods, to replace or minimize the use of synthetic petrochemical-derived polymers [20].

Biopolymers, commonly referred to as bio-based polymers, are sustainable materials that can break down biologically. Derived from living entities, they break down quickly and provide several benefits, such as being lightweight, economical, plentiful, and renewable. They are divided into three primary categories according to their chemical makeup: (i) polysaccharides, (ii) proteins, and (iii) polyesters. Biopolymers may additionally be classified based on their origins, as shown in Figure **I. 2**[18].

Natural fiber composites provide a variety of benefits when compared to synthetic options, such as lighter weight, lower expenses, potential for recycling, and greater environmental sustainability. However, they also present significant challenges, including low impact resistance, restricted thermal stability, and high moisture uptake. These constraints can influence the long-term longevity and effectiveness of the composites, especially in severe environmental situations [21].One major problem with natural fiber composites is the lack of compatibility between hydrophilic fibers and the hydrophobic matrix. This incompatibility may lead to inadequate interfacial bonding, causing unfavorable characteristics in the composite. To address this issue, fiber surface treatments are commonly employed to improve their adhesion to the matrix and enhance the overall performance of the composite material [22].

Surface treatments are frequently used in the fabrication of natural fiber-reinforced composites to strengthen the interfacial bonding between the fiber and matrix. These treatments not only boost adhesion but also improve the mechanical characteristics of the fibers, including tensile strength, modulus, and elongation, thereby further enhancing the overall performance and longevity of the composite material [23]. Alkaline treatment is among the most frequently used methods for surface treatment. This approach works by breaking the hydrogen bonds in the fiber's network structure, resulting in a rise in surface roughness [24]. During the alteration process, alkaline treatment eliminates specific quantities of lignin, wax, and oils from the fiber's outer surface. It also breaks down cellulose into smaller units and reveals short-length crystallites, which boosts the fiber's engagement with the matrix and enhances the composite's overall effectiveness [25].

Some alteration techniques might be constrained by aspects such as inadequate mechanical performance, elevated equipment expenses, limited industrial scalability, and the requirement for specialized technology. Cold plasma treatment has garnered attention as a viable, durable, and environmentally friendly solution[26]. The engagement of cold plasma with the material surface can trigger surface etching and grafting, enhancing wettability, roughness, and adhesion. This improvement fortifies the fiber-matrix connection without adversely impacting the overall mechanical characteristics of the composite [27].

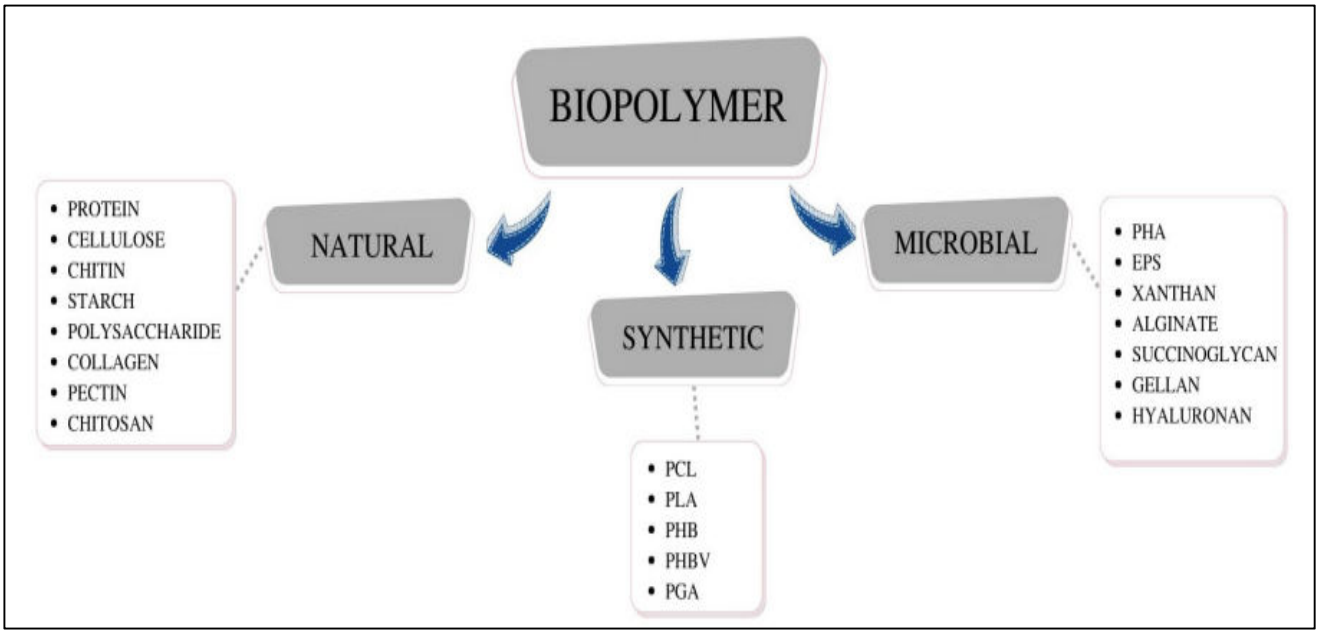

*Figure **I.2**:Classification of biopolymer [18].*

II. Composite material

Composites consist of materials that are formed from two or more phases that are chemically and physically distinct, which are separated by a clearly defined interface. These phases are intentionally combined to obtain enhanced structural or functional characteristics that the individual components alone cannot deliver [28]. Composites have emerged as an essential element in construction technology, providing notable benefits in strength, weight, and adaptability. By combining materials with unique physicochemical characteristics, they offer performance that exceeds that of conventional materials [29]. The matrix functions as the continuous phase that holds the reinforcement in a specific orientation, whereas the reinforcement provides strength to the matrix. The matrix and reinforcement are either chemically bonded or mechanically fastened together. The properties of a composite are determined by the combination of the matrix, reinforcement, and their interface [30].Composites are defined broadly to include contemporary synthetic composites like fiber- or particle-reinforced plastics, traditional materials like concrete, and natural materials like wood. These materials are now essential in engineering, particularly in areas where structural designs need to be both lightweight and extremely strong and stiff [31].

II.1. Classification of Composites

Composites are classified according to the kind of reinforcement and the matrix that is utilized. Types of reinforcement consist of fiber-reinforced, particle-reinforced, whisker-reinforced, and structural composites. The matrix phase divides composites into three primary categories: metal matrix composites (MMCs), polymer matrix composites (PMCs), and ceramic matrix composites (CMCs), as illustrated in Figure **I. 3**[18].

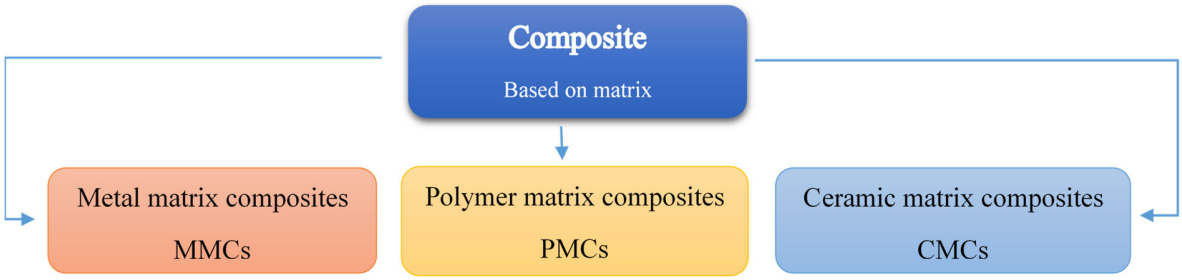

Figure I.3:*Classification of composites based on matrix[18] .*

II.1.1 Metal Matrix Composites (MMCs)

In metal matrix composites (MMCs), lightweight metals like aluminum, titanium, and magnesium, along with their alloys, are frequently employed as matrices. Of these, aluminum is the most commonly utilized because of its blend of outstanding strength, toughness, and resistance to corrosion and wear. These attributes render aluminum-based MMCs particularly useful in numerous engineering applications [30].

II.1.2 Ceramic Matrix Composites (CMCs)

For ceramic matrix composites (CMCs), silicon carbide (SiC) is commonly utilized as both the matrix and the reinforcement. Silicon carbide is preferred due to its remarkable thermal stability, strength, and wear resistance. In CMCs, silicon carbide reinforcements can exist in various forms to customize the composite's characteristics for particular applications, improving aspects such as toughness, thermal conductivity, and resistance to degradation at high temperatures [30].

II.1.3 Polymer Matrix Composites (PMCs)

The properties of Polymer Matrix Composites (PMCs) are affected by several elements, including the type of matrix, the reinforcement materials, the conditions under which they are processed, the microstructure, the composition, and the interfacial layer that exists between the matrix and the reinforcement. Typically, PMCs consist of thermoplastic or thermosetting plastics serving as the matrix, which is augmented with materials like carbon, glass, steel, or natural fibers. The advantages of polymers, such as ease of processing and low weight, render PMCs suitable for a wide range of applications with diverse characteristics [32].

a. Thermoplastic matrix

Thermoplastics consist of linear or branched chain molecules characterized by robust intramolecular bonds along with weaker intermolecular bonds. These substances can be reformed when subjected to heat and pressure, and they may be structured as either semi-crystalline or amorphous. Common instances of thermoplastics consist of polyethylene, polypropylene, polystyrene, nylons, polycarbonate, polyacetals, polyamide-imides, polyether ether ketone, poly-sulfone, polyphenylene sulfide, and polyether imide [33]. Thermoplastic resins, like polyethylene (PE), nylon, and polyvinyl chloride (PVC), are additionally utilized in PMCs for purposes that necessitate flexibility and simple processing [30].

*Table **I.1**: The general characteristics of thermoplastic polymers [34].*

Characteristics	PP	LDPE	PS	Nylon 6	Nylon 6,6
Density (g/cc)	0.899–0.92	0.910–0.925	1.04–1.06	1.12–1.14	1.13–1.15
Water abs (%)	0.01–0.02	< 0.015	0.03–0.10	1.3–1.8	1.0–1.6
Tg (°C)	–10 –23	–125	48	80	–
Tm (°C)	160–176	105–116	110–135	215	250–269
Heat deflection T (°C)	50–63	32–50	Max. 220	56–80	75–90
Tensile strength (MPa)	26–41.4	40–78	25–69	43–79	12.4–94
Elastic modulus (GPa)	0.95–1.77	0.055–0.38	4–5	2.9	2.5–3.9

b. Thermoset matrix

In polymer matrix composites (PMCs), the matrices are usually thermoset polymers that are cross-linked, like epoxy, polyester, and phenolic resins, which offer strength and durability. Glass fiber-reinforced thermoset polymers are especially appreciated for their superior strength-to-weight ratio and stiffness, rendering them perfect for application in automotive components [32].

Thermosets possess cross-linked or network structures in which covalent bonds link all molecules together. Unlike thermoplastics, they do not become soft when exposed to heat but rather break down. After they go through the cross-linking process and harden, they cannot be reformed. Typical examples of thermosets encompass epoxies, polyesters, phenolic, urea, melamine, silicone, and polyimides [33].

*Table **I.2**: Characteristics of thermoset polymers [34, 35].*

Characteristics	Polyester	Vinyl-Ester	Epoxy
Density (g/cc)	1.2–1.5	1.2–1.4	1.1–1.4
Elastic modulus (GPa)	2–4.5	3.1–3.8	3–6
Tensile strength (MPa)	40–90	69–83	35–100
Compressive strength (MPa)	90–250	100	100–200
Elongation (%)	2	4–7	1–6
Water absorption (24 h @ 20°C)	0.1–0.3	0.1	0.1–0.4

c. Elastomers

An elastomer is a type of polymer noted for its viscoelastic properties, usually displaying a low Young's modulus and a high yield strain in comparison to other substances. The word "elastomer," which comes from "elastic polymer," is frequently used synonymously with "rubber," although "rubber" is more frequently utilized when discussing vulcanized materials [33].

III. Natural fiber as reinforcement material

Natural fibers are classified into three primary groups: plant fibers, animal fibers, and mineral fibers (Figure **I. 4**). Plant fibers, a major category of natural fibers, mainly comprise cellulose, hemicellulose, lignin, and pectin. Famous plant fibers consist of cotton, jute, flax, ramie, sisal, and hemp. Cellulose fibers are mainly utilized in making paper and textiles. These fibers are additionally divided into seed fibers, leaf fibers, bast (stem) fibers, fruit fibers, and stalk fibers [36].

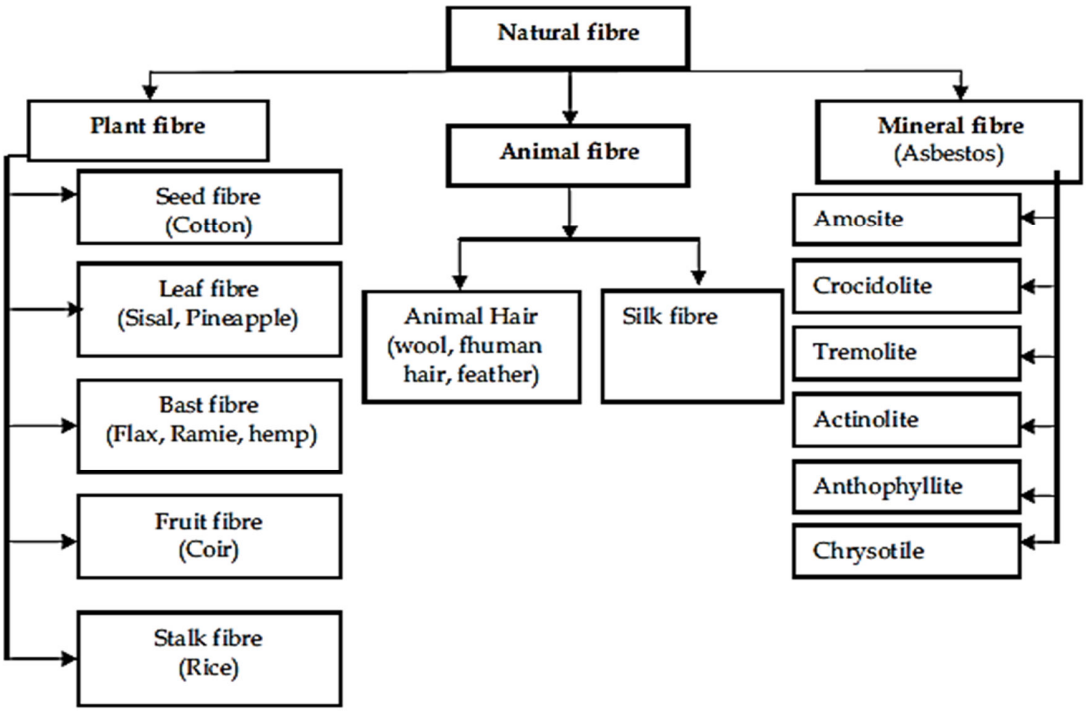

*Figure **I 4**: Classifications of natural fibers [36].*

Fiber-reinforced polymer (FRP) composites, identified as one of the most promising contemporary materials to substitute traditional metals and alloys in numerous structural applications, have garnered considerable interest in recent years [37]. Reinforced composites are currently the most frequently utilized form of polymer composite. These materials are made up of a polymer matrix that completely surrounds the reinforcing elements. In the absence of these reinforcements, the polymer would display considerably lower mechanical properties [38]. They provide advantages such as reduced tool wear, environmental sustainability, and easier disposal. However, they also have disadvantages, including insufficient thermal

and moisture resistance, lower durability, and weak adhesion to the matrix. Researchers are working to improve the adhesion between fibers and the matrix, as well as to enhance the mechanical properties of composites, by modifying the surfaces of natural fibers [36].

Figure **I.5** illustrates natural fibers sourced from their primary origins: bast, leaf, seed, wood, and grass. A wide variety of fibers can serve as reinforcements in structural applications, these fibers can be classified based on several criteria, including their length (short, long, or continuous), their strength and/or stiffness (low modulus, medium modulus, high modulus, or ultrahigh modulus), and their chemical composition (organic or inorganic) [39]. The inorganic fibers most commonly used in composites include glass, carbon, boron, ceramic, mineral, and metallic fibers. In contrast, the organic fibers typically utilized are primarily polymeric. When selecting a type of fiber, it is often necessary to balance mechanical properties, environmental durability, and cost considerations [40].

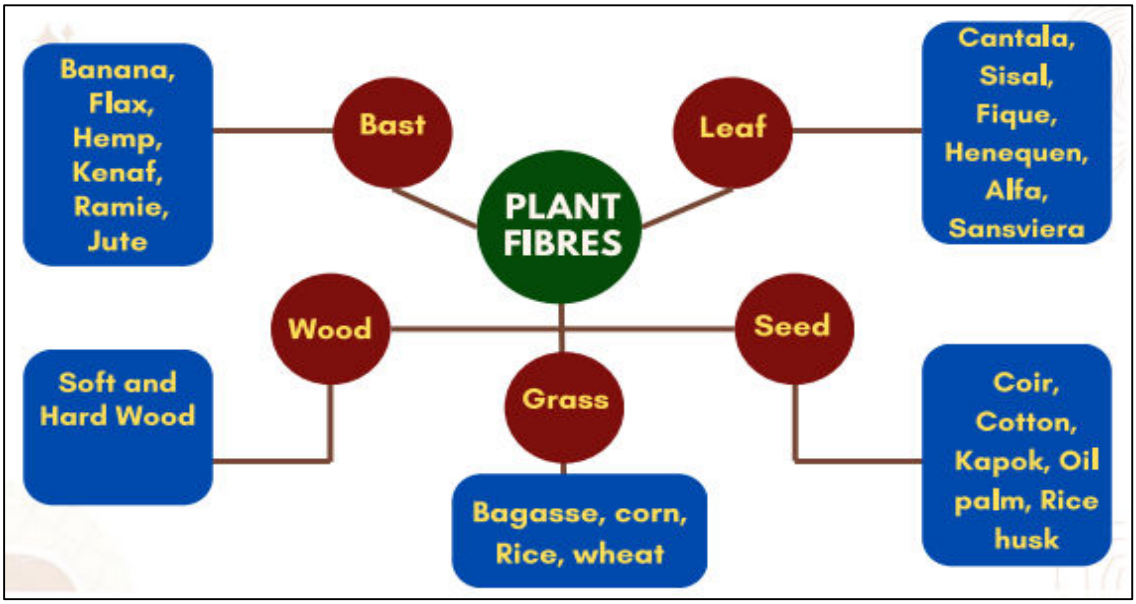

*Figure **I.5**:Types of plant fibers [39].*

III.1. Chemical Composition of Lignocellulosic Fibers

Lignocellulosic fibers consist of cellulose, hemicelluloses, lignin, ash, and various other components. The ratio of these constituents varies based on the fiber's source. Fibers that are rich in these components are known as lignocellulosic fibers [41]. Table**I.3** presents the composition of frequently used lignocellulosic fibers.

Plant biomass mainly consists of a lignocellulosic structure, which is characteristic of the majority of biomass materials. Within the cell walls of vascular tissues present in higher terrestrial plants, cellulose fibers are situated in an amorphous matrix made up of lignin and hemicellulose. These three polymers cellulose, hemicellulose, and lignin are linked together by both physical and covalent bonds, creating

lignocellulose, a composite substance that represents over 90% of the dry weight of plant cells, as illustrated in Figure **I. 6** [20].

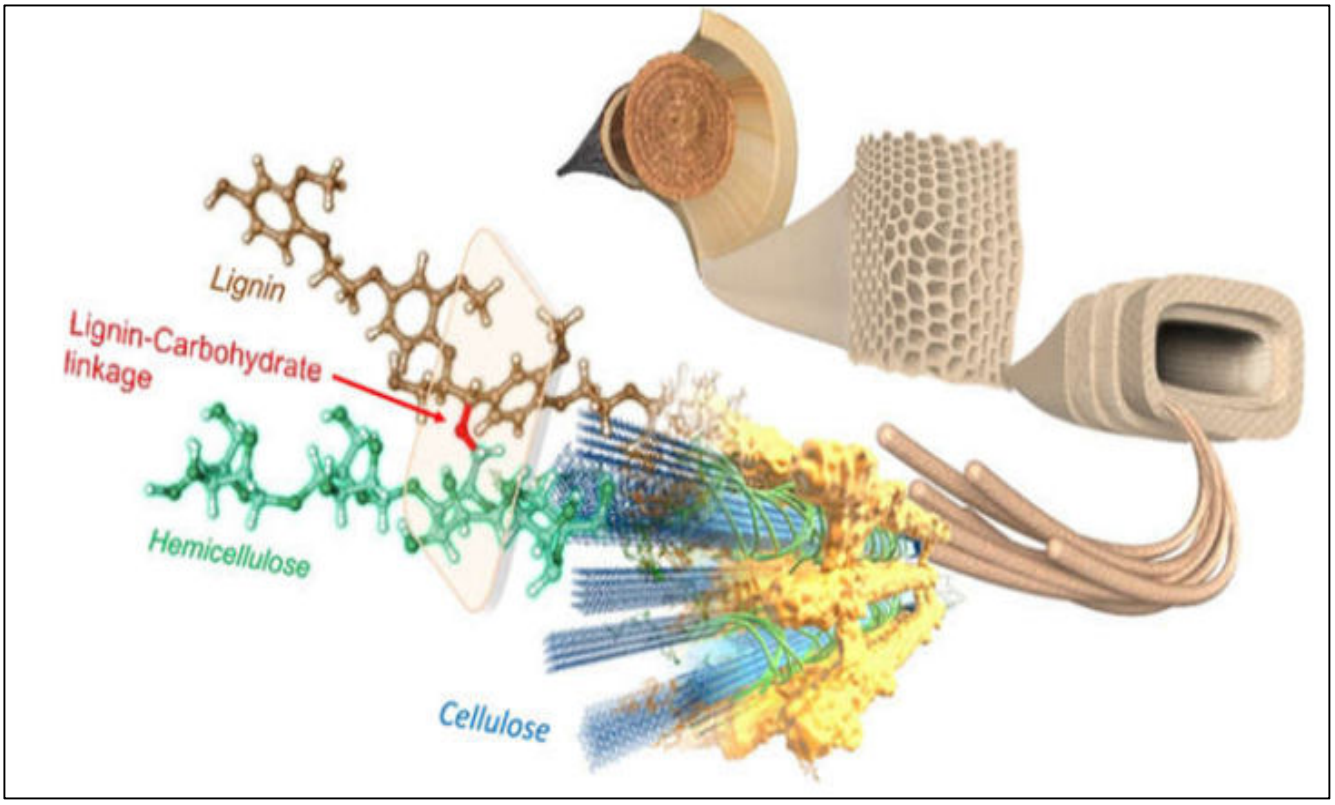

*Figure **I.6**:The Lignocellulose Matrix: Structure, Composition, and Function in Plant Cell Walls [20].*

III.1.1 Cellulose

The fiber is composed of multiple cell walls made up of aligned, reinforcing, semi-crystalline cellulose microfibrils embedded within a matrix of hemicellulose and lignin, exhibiting various compositions. Typically, these microfibrils have a diameter ranging from 10 to 30 nm and consist of 30 to 100 cellulose molecules arranged in an elongated chain configuration, which contributes to the mechanical strength of the fiber [42].Figure **I.7** illustrates the structure of fibrils, micro fibrils, and cellulose within the cell walls of a plant fiber.

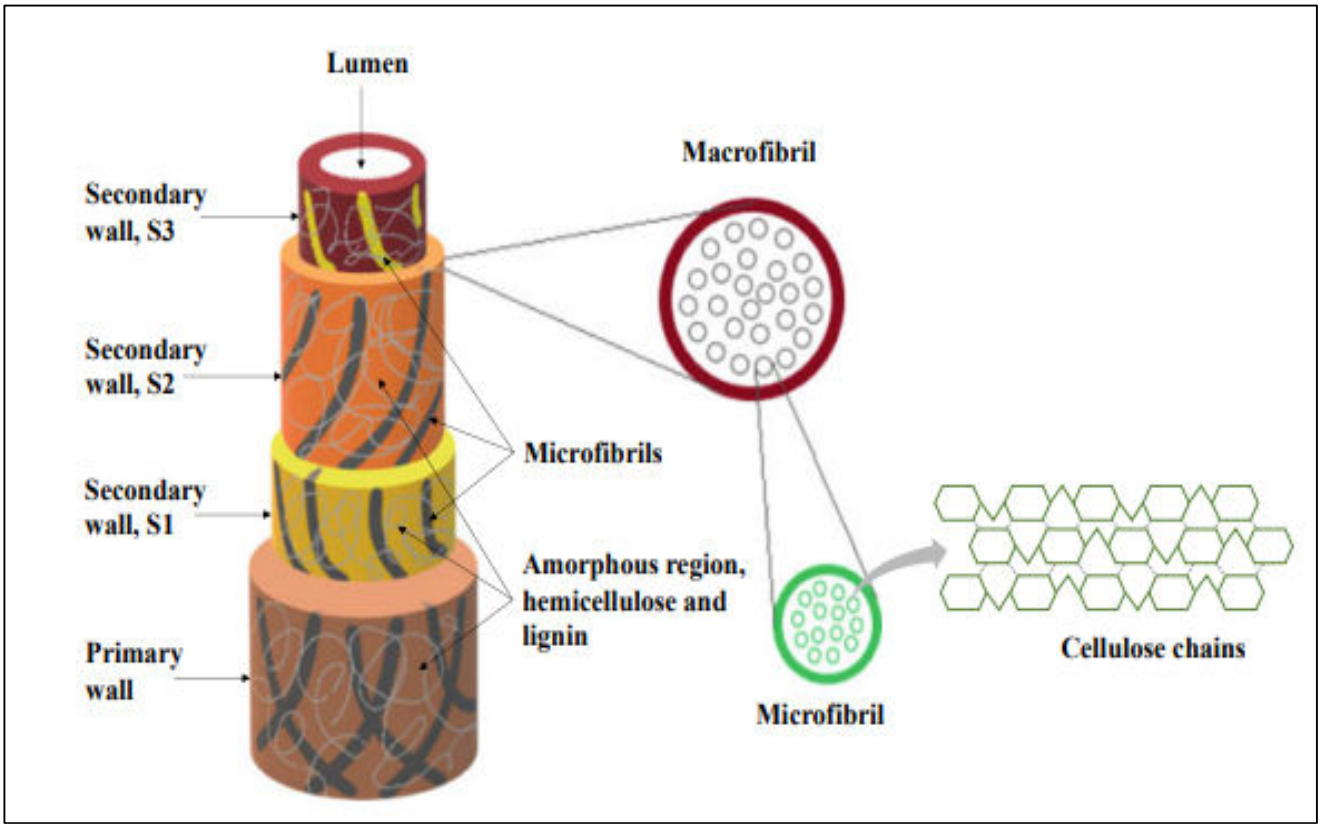

*Figure **I.7**: Schematic of plant fiber structure [43].*

As illustrated in Figure **I. 8,** cellulose (α-cellulose) serves as the main element of the majority of plant fibers. It is a linear macromolecule composed of consecutive D-anhydro-glucose ($C_6H_{11}O_5$) units, connected through β-1,4-glycosidic bonds, with a degree of polymerization approximately 10,000. Each repeating unit contains three hydroxyl groups, which play a vital role in establishing hydrogen bonds. These bonds assist in defining the crystalline structure and greatly affect the physical characteristics of cellulose-based materials [44].

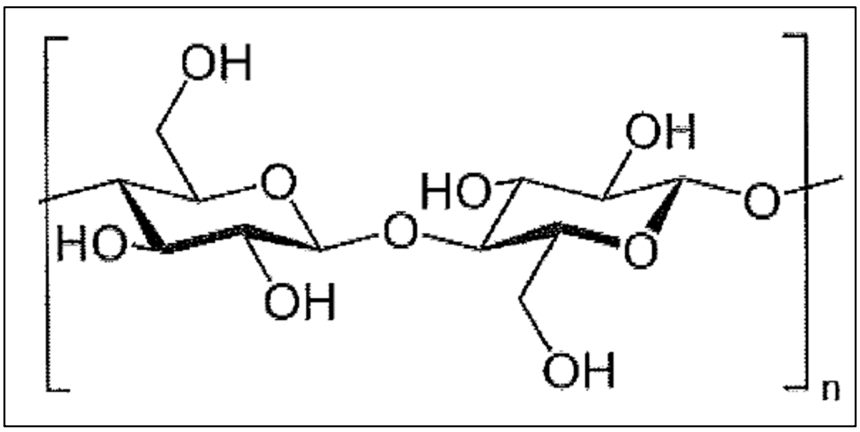

*Figure **I.8**: Molecule structure for cellulose [45].*

III.1.2. Hemicellulose

As illustrated in Figure **I. 9**, hemicelluloses consist of polysaccharides composed of a combination of sugars with 5- and 6-membered carbon rings. In contrast to cellulose, their polymer chains are shorter (having a degree of polymerization ranging from 50 to 300) and are branched, featuring side groups that enhance their non-crystalline nature. Hemicelluloses act as the supportive framework for cellulose microfibrils. They exhibit high hydrophilicity, dissolve in alkali, and are readily hydrolyzed under acidic conditions [44].

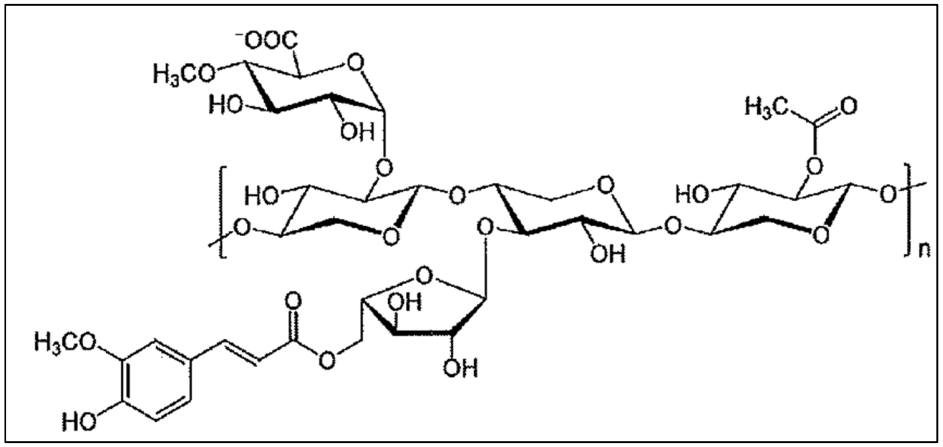

*Figure **I.9**: Molecule structure for Hemicelluloses [21].*

III.1.3. Lignin

As depicted in Figure **I.10**, lignin is an aromatic biopolymer that plays a crucial role in providing structural integrity to plant cell walls. However, its complex structure can impede microbial enzymatic processes, as it restricts the transport of sugars and ions across microbial cell membranes. Although the high concentration of aromatic compounds in lignin offers potential benefits for the bio-product industry, the challenge lies in identifying a suitable catalyst capable of effectively breaking the random chemical bonds in lignin without causing re-polymerization [46].

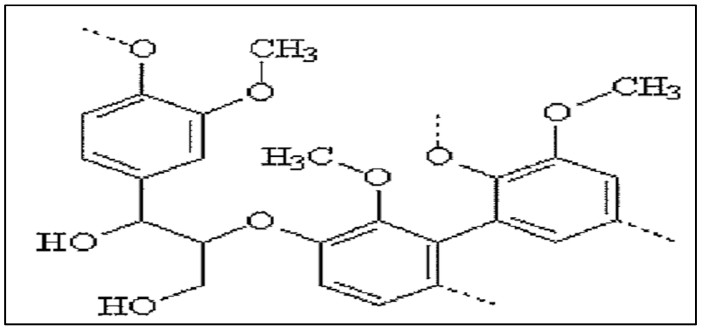

*Figure **I.10**: Molecule structure for Lignin[21].*

*Table **I.3**: The chemical constituent content in different natural fibers.*

Fiber Type	Cellulose (wt%)	Hemi-Celluloses (wt%)	Lignin (wt%)	Ref.
Flax	62-72	18.6–20.6	2–5	[41]
Hemp	55–90	12–22.4	2–10	[43]
Jute	45-72	13.6-24	9-26	[43]
Kenaf	31-72	8-21.5	8–21.5	[41]
Sisal	60–78	10–14.2	8-14	[47]
Abaca	53–68	17.5–25	5-15.1	[43]
Henequen	77.6	4–8	13.1	[34, 44]
Banana	63–64	10	5	[44]
Coir	26.2–43	17.2–37	22.2–45	[47]
Cotton	82.7–98	3-5.7	0.75	[43]
Bamboo	26	31	30	[47]

III.2. Mechanical properties of natural fibers

The mechanical properties of fibers are affected by factors including fiber quality, composition, and the age of the plant, which can lead to difficulties in achieving uniform results. While natural fibers may not attain the strength levels of graphite or aramid fibers, those derived from flax, jute, bamboo, and hemp demonstrate increased stiffness, with some also exhibiting comparable strength. The strength and stiffness of plant fibers are mainly influenced by the cellulose content and the spiral angle of the microfibrils found in the inner secondary cell wall of the fiber [37]. The mechanical properties of different natural fibers are provided in Table **I.4**.

*Table **I.4**: Properties of natural fibers derived from plant and animal [15, 18, 34, 37, 42].*

Fiber	Density (g/cm^3)	Diameter (µm)	TS (MPa)	Elongation at Break (%)	E (GPa)
Flax	1.5	17-20	300–1500	2.7-3.2	27.6
Jute	1.44-1.49	14–20	393–800	1.16–1.5	13-26.5
Sisal	1.45	200-400	400-938	3.7	9.4-22
Kenaf	1.2	13-33	930	1.6	53
Pineapple	0.8-1.6	20-80	413-1627	1.6	34.5-82.51

Banana	1.35	80-280	529–754	1-3.5	7.7-20.8
Coir	1.15-1.46	100–450	131–175	15–40	4–6
Ramie	1.51-1.55	40-60	400–938	1.2–3.8	61.4-128
Hemp	1.48-1.49	15-30	690	1.6	70
Wool	1.3	15-30	50-315	-	2.3-3.4
Cotton	1.5-1.6	11–22	287–800	3-8	2.3-5
Camel hair	-	20.04	212.15	-	5.79
Henequen	1.2	-	430-570	3.7-5.9	10.1-16.3
bamboo	0.6-1.1	-	140-230	2	11-17
Alfa	0.89	-	850	5.8	22
Abaca	1.5	-	400	3-10	12

III.3. Fiber extraction methods

Extraction denotes the process of moving a compound from its initial state, regardless of whether it is solid or liquid, into another phase. This process includes isolating the compound from a matrix for subsequent use or examination. Cellulosic fiber extraction can be accomplished in nano or micro forms through a range of chemical or mechanical methods. There are numerous techniques to extract cellulose from plant components that contain high cellulose content. The process generally consists of three primary steps: pre-hydrolysis, pulping, and bleaching. Pre-hydrolysis treatment employs either mineral acid or alkali to disrupt the matrix, aiding in the extraction of cellulose [48]. Extraction techniques are selected according to the particular plant sections from which the fiber is intended to be extracted. The choice of these techniques directly affects the features and qualities of the resulting composites made from the fibers [49].

III.3.1. Mechanical Decortication

As depicted in Figure **I. 11**, the extraction process starts by cutting the plant stalk with a slicer, which is then placed onto a transmission belt. The fibers move through an extrusion and feeding apparatus where the stalks slowly soften. These softened fibers are subsequently moved into a space between the scraper and the holding plate. A motor powers the scraper's rotating blades at high velocity, compressing and hitting the stalks to detach the fibers from the adjacent colloidal materials. The purified fibers are transported through the conveying device for additional processing [50].

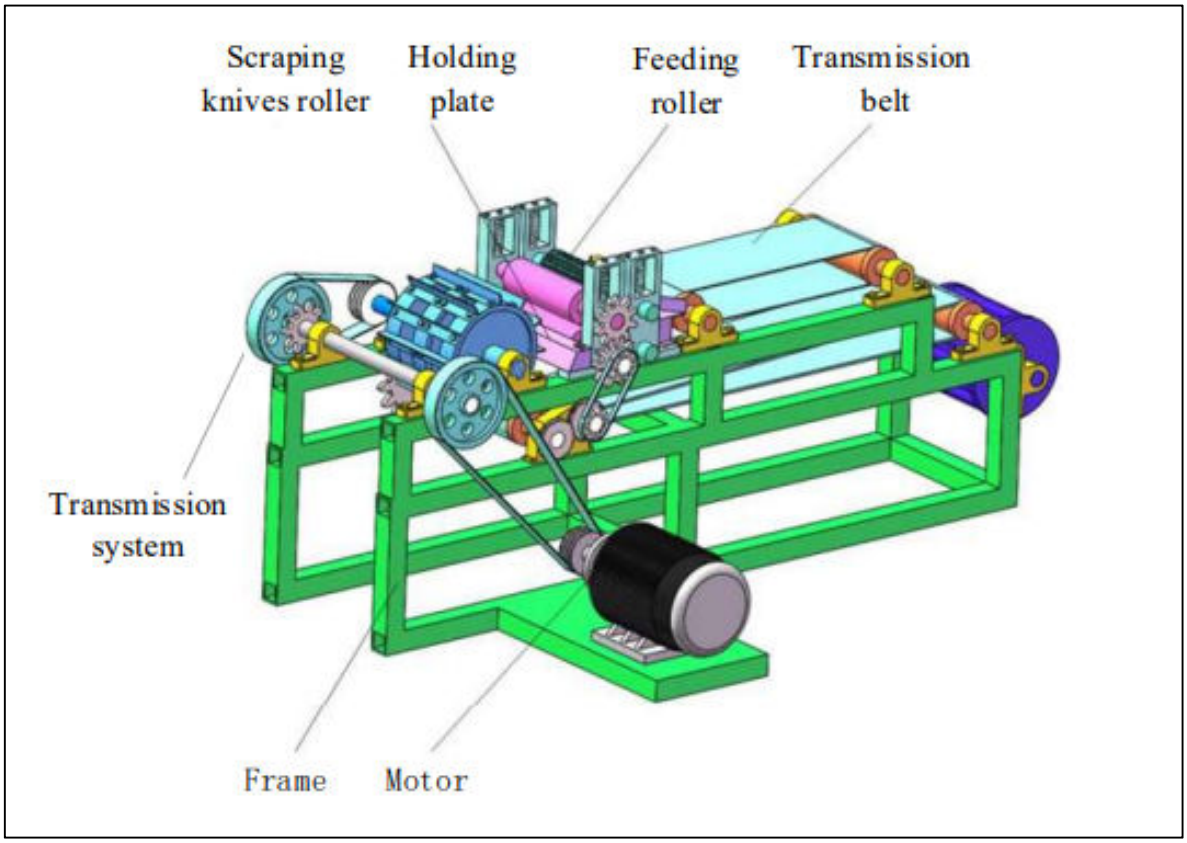

*Figure **I.11**: Structure of the Banana Stalk Fiber Extracting Machine with Scraping Type [50].*

III.3.2. Water Retting

Water retting is the predominant technique for generating natural fibers, where stalks are submerged in water to enable moisture to penetrate the roots and induce the outer layer to rupture. This procedure, which depends on damp air and decaying bacteria, generally spans several months in an oxygen-free setting. It is commonly performed in still or sluggish water bodies such as ponds, streams, and rivers. The timing of the harvest is vital for guaranteeing premium fibers for textile production [49]. Water retting is a widely employed method for extracting high-quality fibers. During this process, bacteria and moisture break down the cellular tissues and binding agents surrounding the fibers, which aids in the separation of individual fibers from the plant. Typically, this process lasts between 7 to 14 days, depending on the type of fiber being processed [51].

III.3.3. Degumming process

The industrialization of natural fibers involves eliminating non-cellulosic materials, a process referred to as degumming. Fibers obtained from plants like jute, ramie, kenaf, and hemp have been thoroughly researched and utilized for degumming and the creation of value-added products[52]. Degumming techniques for natural fibers encompass methods such as acid, alkali, steam explosion, ultrasonic,

microwave, bacteria, fungus, and enzyme treatments. Among these techniques, microbial degumming has proven effective in decreasing the chemical and energy use that is usually linked to conventional degumming approaches [53].

III.3.3.1. Chemical degumming

Chemical degumming is an intricate procedure that entails the elimination of contaminants such as pectin, hemicellulose, and lignin from fibers, usually employing alkali, inorganic acids, or oxidants. The process depends on the hydrolysis or oxidation of these contaminants, facilitating their removal while limiting harm to the cellulose. This procedure is intended to preserve the mechanical and physical attributes of the fiber to the greatest extent possible. Pectin and hemicellulose can be easily hydrolyzed in concentrated alkali solutions, whereas cellulose stays unaffected. Chemical degumming is classified into conventional and modern methods based on the reagents utilized [54].

III.3.3.2. Biological degumming

In the biological procedure of degumming, fiber gums are eliminated with the help of microorganisms that do not degrade cellulose or their extracellular enzymes. The two biological methods for degumming fundamentally adhere to the same degradation process, in which non-cellulose elements are decomposed by a sequence of polysaccharide-degrading enzymes. This method assists in eliminating impurities while preserving the integrity of the cellulose fibers [54].

a. Microbial degumming

Microbial degumming involves a process of microbial growth, metabolism, and enzymatic degradation[55]. Throughout this process, microbial strains use a portion of the gum hydrolysates as a carbon source for their metabolic functions [56]. This inhibits feedback inhibition of the degumming enzymes resulting from hydrolysis products like oligosaccharides or other low molecular weight sugars. Consequently, the gum is completely eliminated, improving the efficiency and effectiveness of the biological degumming process of ramie fibers [54].

b. Enzymatic degumming

Enzymatic degumming of ramie fibers requires the coordinated activity of multiple polysaccharide hydrolases, such as pectinase and hemicellulose-degrading enzymes like mannanase and xylanase [57]. Pectinase serves an essential function as a primase in this process. During the early phases of biological degumming, pectinase degrades the outer pectin materials, which loosens the cellular structure and facilitates improved access for hemicellulose and other degumming agents [53].

c. Biochemical degumming

A combination of biological and chemical processes has been suggested to reduce chemical and energy usage while maximizing the rate of gum removal from ramie fibers. This biochemical degumming method leverages the benefits of both biological and chemical techniques to achieve thorough gum removal[58]. However, it has significant disadvantages, including possible fiber damage and severe processing conditions. Furthermore, the technique entails intricate and time-consuming procedures associated with

chemical treatments and the cultivation of bacteria or enzymes, resulting in increased expenses and more complex operations [54].

IV. Surface modification of natural fibers

The main drawback of utilizing natural fibers as reinforcement in composites is the inadequate compatibility between the fiber and the matrix due to the hydrophilic nature of the fibers and the hydrophobic nature of polymer macromolecules [59]. To address this issue, methods for altering natural fibers are employed to improve their surface properties and strengthen their adhesion to various matrices [60]. The main techniques for modifying fiber surfaces are summarized as follows:

IV.1. Chemical treatments

IV.1.1. Alkaline treatment

Sodium hydroxide (NaOH) is the chemical most frequently utilized for bleaching and/or cleansing the surface of natural fibers. It leads to the creation and breaking down of short-length crystallites, altering the fine structure of native cellulose I into cellulose III [61]. The main goal of chemical treatment is to roughen the fiber surface, improving its adhesion to the binder matrix. This is achieved by ionizing the hydroxyl group and removing the hydrogen bonding from the fiber structure[62].

IV.1.2. Silane treatment

Chemical processing of natural fibers entails soaking them in a solution that contains silicon, referred to as silane treatment. This is accomplished by combining a silane agent with ethanol or distilled water. The silane coupling agent, possessing its hydroxyl groups, attaches to the hydroxyl groups on the fiber surface, enabling the silane to engage with the matrix resin and create robust bonds [63] As a bonding agent, silane aids in forming connections between inorganic and organic substances. This process enhances the bonding between the fiber and matrix, improving the mechanical characteristics by fortifying the interface bonds and offering reinforcement [64]. Silane treatment has emerged as an efficient supplementary approach to biological pre-treatment for surface alteration. While ruminant digestion eliminates non-cellulosic elements and generates active sites on fiber surfaces, silane coupling treatment further improves the interfacial adhesion between the fiber and matrix [65].

IV.1.3. Benzoylation treatment

Benzoylation is a method used to reduce the hydrophilic properties of fibers while improving the adhesion between the fibers and the matrix, thereby increasing the overall strength of the composites. In this process, the fibers are first subjected to treatment with sodium hydroxide (NaOH) and then exposed to benzoyl chloride (C_6H_5COCl) for a period of 15 minutes [66]. Subsequently, the fibers are separated, exposed to ethanol for 1 minute, and rinsed with distilled water. Ultimately, the fibers are dried in an oven at 80°C for 24 hours. This process yields fibers that exhibit greater thermal stability in comparison to untreated fibers[67].

IV.1.4. Acetylation Treatment

Acetylation is a process that involves the addition of an acetyl group to the surfaces of natural fibers, which reduces their affinity for water and enhances the stability of the resulting composites. This treatment strengthens the adhesion between the fibers and the matrix, resulting in more durable connections and improved characteristics for composites derived from natural fibers [68]. The hydroxyl (OH) groups found in the fibers interact with acetyl groups, causing the fibers to become more hydrophobic[69]. Generally, lignin and hemicellulose, which have hydroxyl groups, engage with acetyl groups during this process. Before the acetylation takes place, the fibers are typically treated with alkali. The alkali-treated fibers are subsequently immersed in glacial acetic acid for 1 hour and then soaked in acetic anhydride with two drops of concentrated sulfuric acid for 2-5 minutes [67].

IV.2. Physical treatment

IV.2.1. Cold plasma treatment

The term "plasma" was introduced by Irving Langmuir in 1928 to describe ionized gas characterized by an equal presence of ions and electrons. He noted that this gas resembled blood plasma due to its strong interactions and diverse constituents. While plasma in physics differs from blood plasma, a relationship exists between the two concepts in the context of plasma-assisted blood coagulation [70].Atmospheric-pressure plasma jets are gaining recognition for their ability to generate plasma in open environments, particularly in applications such as plasma medicine that require low gas temperatures. However, the high density of neutral atoms and molecules at atmospheric pressure leads to an increased frequency of collisions between electrons and atoms, which raises the gas temperature. To mitigate this issue, noble gases are often utilized. Recently, advancements have been made in the development of cold atmospheric-pressure air plasma jets, with some achieving gas temperatures that are nearly at room temperature[71].

Plasma treatment modifies the surface energy of polymers and natural fibers, resulting in crosslinking and the addition of reactive groups that can improve fiber strength. This process involves the bombardment of plasma, which causes chemical changes to the fiber surface, including surface erosion and an increase in functional groups like carboxyl and carbonyl. However, the effects of plasma treatment can vary across different types of fibers due to differences in their composition. Plasma reactions occur under non-equilibrium conditions, where various plasma species interact with the fiber surfaces, altering their structure [72].

The non-equilibrium atmospheric pressure, low temperature (cold) plasma jet, illustrated in Figure **I.12**.Cold plasma surface treatment modifies polymer surfaces by enhancing adhesion and wettability without damaging bulk properties. It improves mechanical strength by increasing the bonding potential between fibers and the matrix. The effects of plasma treatment depend on factors like gas composition, plasma conditions, and the presence of ions, electrons, radicals, and vacuum ultraviolet radiation, which contribute to etching, chemical activation, and cross-linking [73].

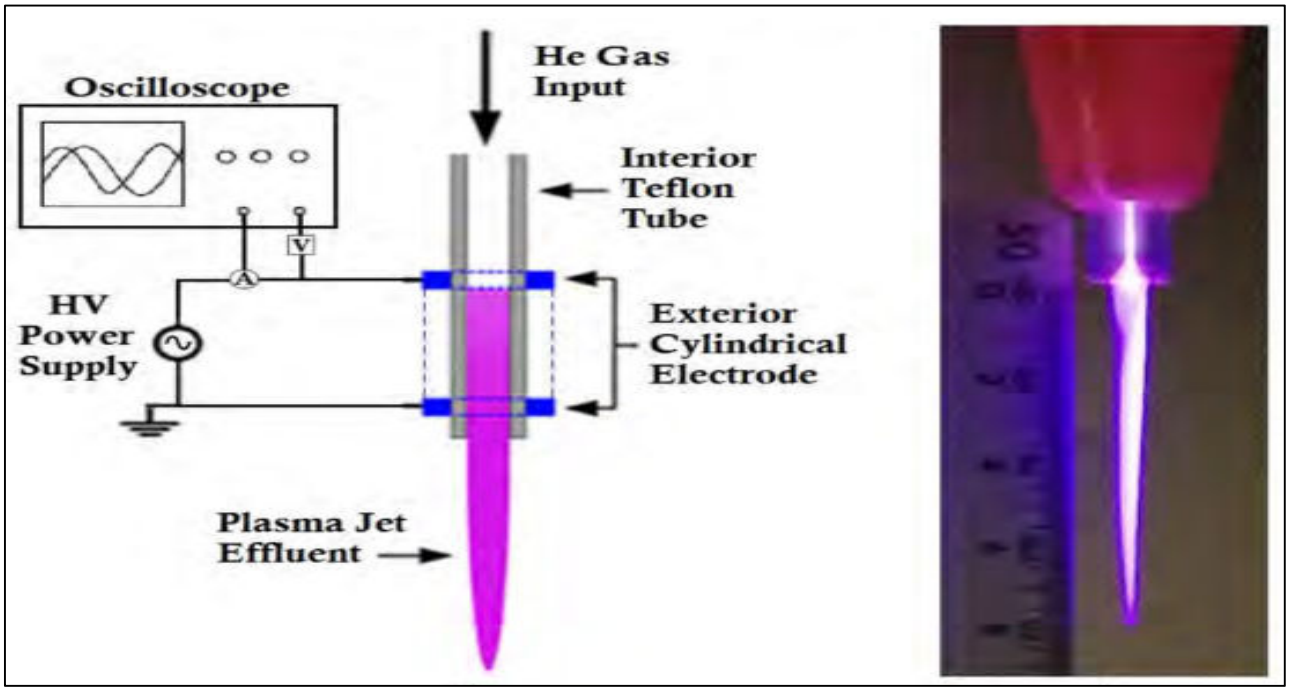

*Figure **I.12**: Cold Plasma illustrate process [73].*

V. Manufacture of Composite Materials

Selecting the appropriate manufacturing method is essential for converting raw materials into a superior final product. Key considerations when determining a composite manufacturing process encompass the dimensions and shape of the finished component, the required material characteristics, the manner in which raw materials are treated, the production rate, and the overall cost efficiency of the manufacturing method [74]. These techniques include a range of sophisticated methods like spray-up, resin transfer molding (RTM), vacuum infusion, vacuum-assisted RTM, compression molding, pultrusion, and filament winding, with each presenting distinct benefits for creating high-performance composite materials [75].

V.1. Vacuum-Assisted Resin Infusion (VARI)

One well-known technique for producing composites is the Vacuum Resin Infusion (VARI) method. In VARI, fibrous materials are set on a sturdy surface, encased with a net-shaped mold and bagging film. A vacuum pump extracts air from the space between the mold and bagging film, thereby compressing the fibers. This reduces air voids and results in composite components with enhanced mechanical properties [76]. VARI is a process that offers reduced costs for mass production, the ability to produce complex components in one step, and the potential for larger fiber volume fractions [77]. Nevertheless, there are certain limitations to consider: fluctuations in compaction pressure result in varying thicknesses, the surface finish is compromised due to creases in the vacuum bag, achieving high temperatures during the assembly process is challenging, and there is waste generated from non-reusable auxiliary materials [76].

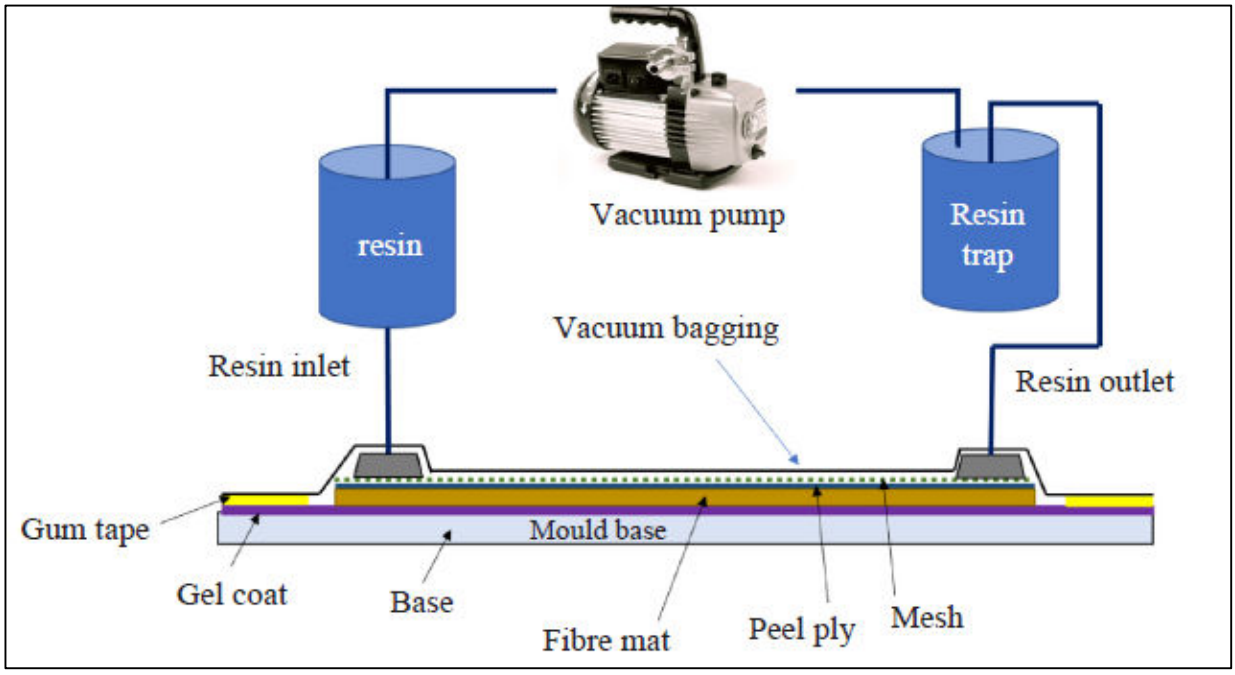

*Figure **I.13**: Vacuum infusion molding process [77].*

V.2. Compression molding

Compression molding is frequently utilized to produce structural components, where the mechanical characteristics are significantly affected by process variables like pressure, temperature, and compression speed. The movement of material during molding dictates the fiber orientation, which is crucial for maximizing the material's high stiffness and strength [78].Compression molding is acknowledged for its benefits, such as affordability, high efficiency, reduced internal stress, slight buckling deformation, strong mechanical stability, and outstanding repeatability in product production [79].Compression or hot-pressing methods require fewer tools compared to alternative techniques, offering both advantages and disadvantages. This approach allows for the production of complex shapes with outstanding dimensional precision, uniformity, mechanical strength, and spark resistance [75].The compression molding apparatus consists of the upper and lower heated platens, the upper mold section (core), the lower mold section (cavity), base plates, a moving plate, a hydraulic system, slide rods, and an ejector unit, as illustrated in Figure **I. 14**[80].

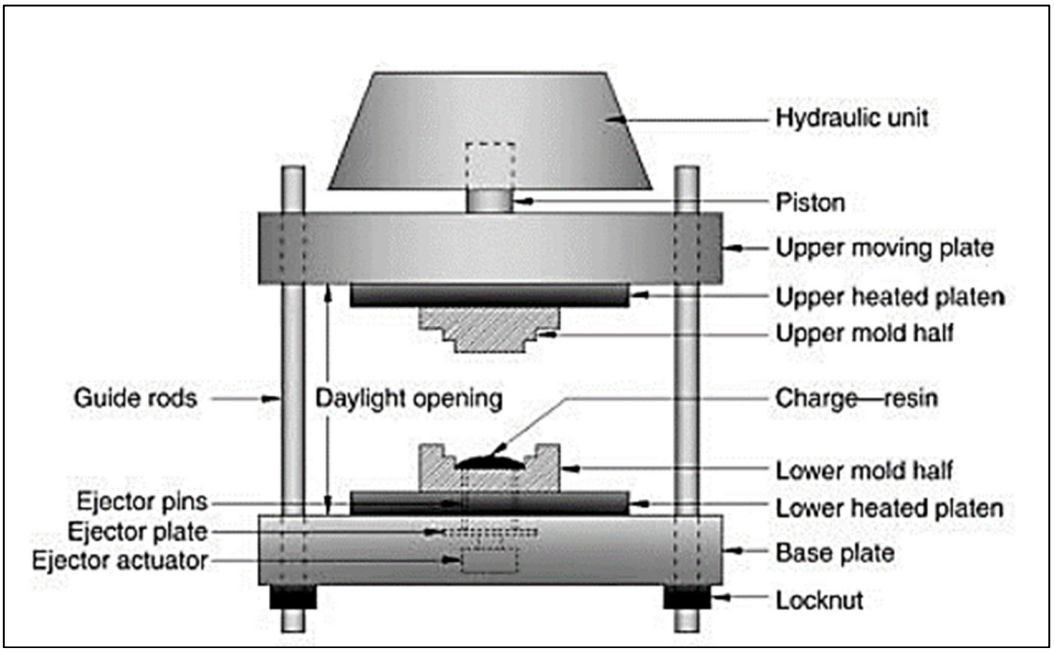

*Figure **I.14**: Schematic View of the Major Components of a Typical Compression Press [80].*

V.3. Hand lay-up

Hand layup is a widely used open molding method generally utilized for thermoset-based polymer matrix composites. It is preferred due to its straightforwardness, minimal tooling expenses, ease of manufacturing, and capacity to create a broad spectrum of part dimensions[81].However, this technique also has several disadvantages, including low production efficiency, extended cycle times, and possible fiber misalignment. In the hand layup procedure, fiber reinforcements are manually positioned into a mold, followed by the application of the polymer to the fibers using a brush or roller. The finished product is formed by stacking the materials in separate stages. At the beginning of the process, an anti-adhesive agent is applied to the mold surface to stop the polymer from adhering to it [82].Dry materials, including woven, knitted, stitched, or bonded textiles, are carefully positioned in the mold by hand. Next, a polymer matrix is applied to the reinforcing fibers with a brush or roller. Hand rollers are then utilized on the wet composite to improve the adhesion between the fibers and the matrix, ensuring uniform resin distribution. Ultimately, the composite goes through a curing phase, and when demolded, it is prepared [18].

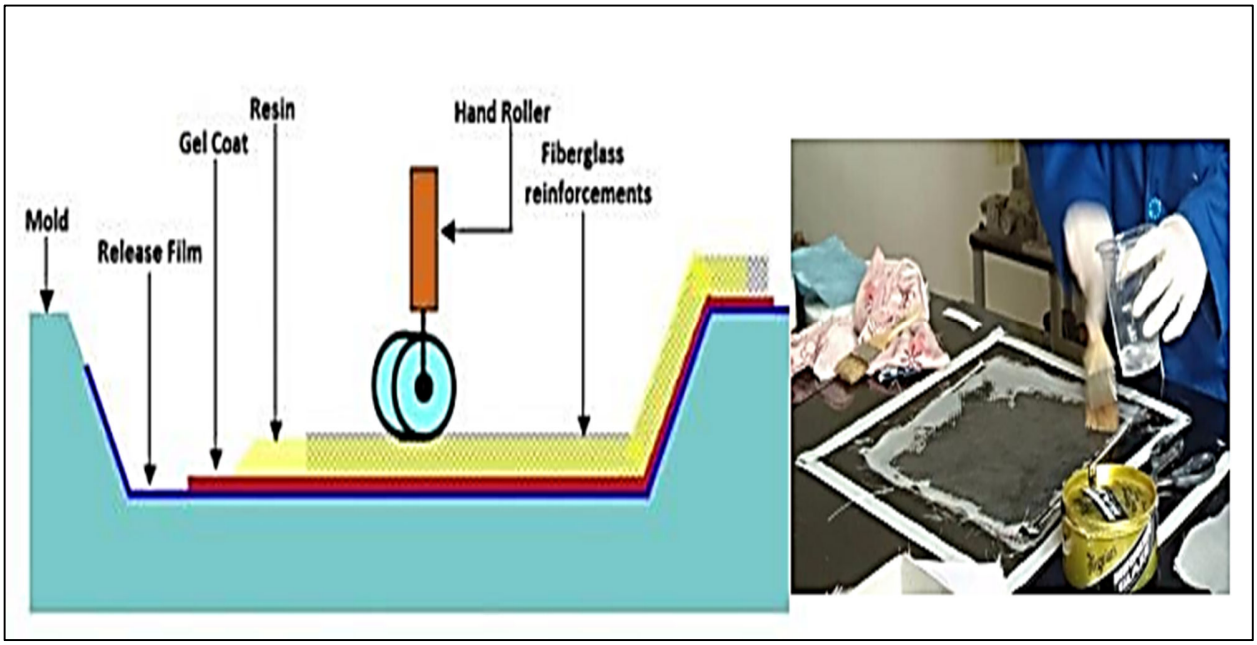

*Figure **I.15**: Hand lay-up technique [83].*

V.4. Filament Winding

Filament winding is a widely used out-of-autoclave manufacturing technique for producing continuous fiber-reinforced thermoplastic composites. Filament winding serves as an efficient, single-step production process for continuous fiber-reinforced polymer composites. It enables the rapid manufacturing of intricate shapes, including both axisymmetric and non-axisymmetric forms, along with closed-form structures. This method can be utilized for both thermoset and thermoplastic composites, although it is primarily used with thermosets [84]. The approach is largely automated, which serves as a significant benefit. While creating the product structure, it is essential to take into account the intricate impacts of the winding method's technological parameters, including helical winding on a sturdy mandrel or continuous winding on a supply mandrel. For example, to regulate the volumetric filling of the structure, it is vital to uphold the proper fiber tension by adding transverse layers. The tension present in both the external and internal layers may fluctuate considerably as a result of the helical winding process, causing variations in the stress-strain condition from the desired design values [85].Axisymmetric elements like pipes, tubes, drive shafts, and pressure vessels are frequently made using the filament winding technique. This approach is especially appropriate for axisymmetric components, providing numerous benefits compared to other production methods, such as the capacity to create parts with a high fiber volume fraction (60–80%) and exceptional specific strength. In filament winding, continuous fibers soaked in resin are wrapped around a spinning mandrel at a designated winding angle. Figure **I. 16** depicts the filament winding process [86].

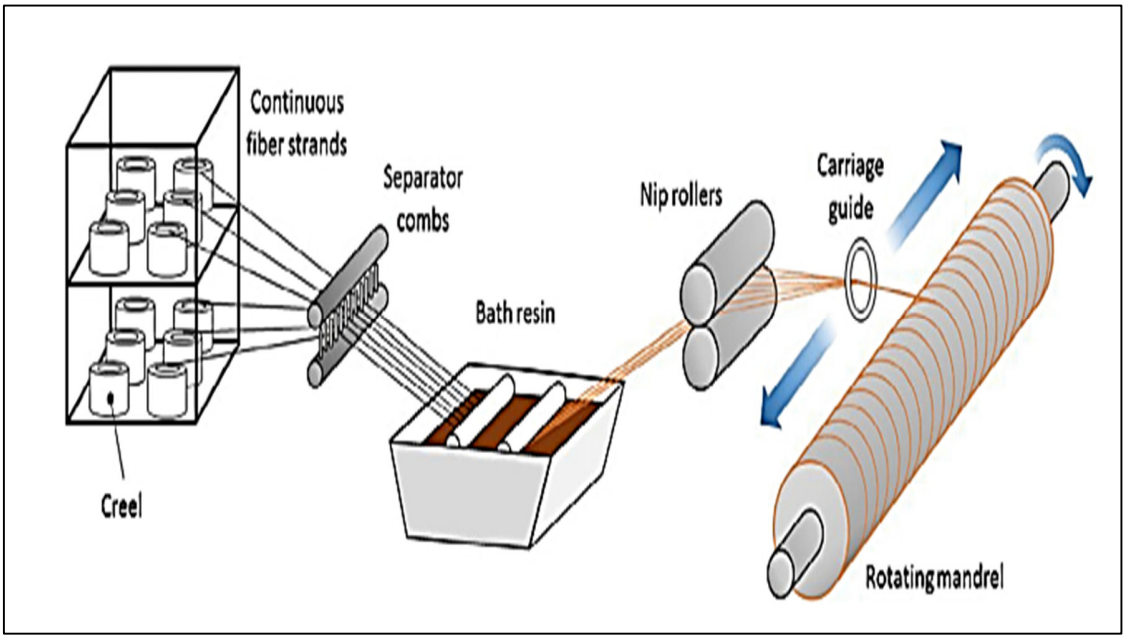

*Figure **I.16**: The filament winding process [86].*

V.5. Spray-Up

Spray-up is a composite molding technique where a resin matrix is applied through a spray gun utilizing compressed air. Concurrently, fiber or yarn reinforcement is trimmed, and the sprayed resin covers the trimmed fibers or yarn, which subsequently drop into the mold or board. This procedure can be repeated to reach the preferred thickness, enhancing its efficiency and flexibility for design modifications [87].

Long Fiber Spray-up Molding (LFSM) is distinct from conventional liquid composite molding (LCM) techniques as it utilizes exceptionally long chopped fiber strands as the primary reinforcement material. In LFSM, the chopped fibers are saturated with resin and sprayed vertically downward onto the surface of the mold. The spraying apparatus is attached to an actuator, enabling it to spray in any preferred pattern or direction. The experimental arrangement features a fiber chopper gun positioned at an angle, which sprays chopped glass fibers into a stream of resin. This stream of resin is propelled by a piston within a cylindrical tank, as illustrated in Figure **I. 17**[88].

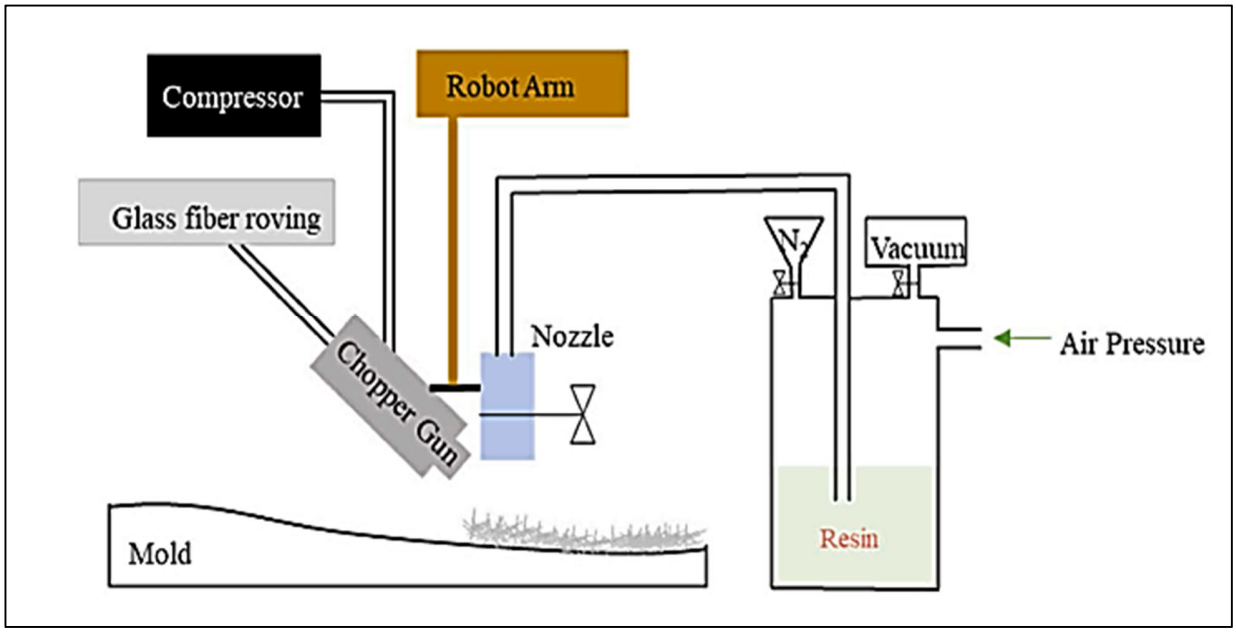

*Figure **I.17**: Spray-up Molding Schematic Diagram [88].*

V.6. Injection molding

Injection molding ranks as one of the most frequently used manufacturing methods for producing thermoplastic composite products, delivering high efficiency for industries such as transportation and energy [89]. Injection molding is characterized as a nonlinear, multivariable, and cyclical unsteady process, which makes it the most widely adopted molding method in plastics. It presents significant benefits regarding production efficiency and processing adaptability. The selection of process parameters for injection molding, generally determined through trial and error rooted in the expertise and practical experience of professionals, is an essential factor in ensuring the quality of the molded products [90]. The injection molding of thermoset composites is known as reactive injection molding; this method is quite intricate and is influenced by various factors, including material properties, mold design, and processing parameters. To predict the outcomes of the molding procedure and identify possible risks, simulation software is often utilized. Rheological modeling is particularly crucial in thermoset injection molding, as the material's flow properties significantly impact the entire molding operation [91]. Plastic injection molding serves as an excellent solution for lightweight automotive connector designs, proficient at managing complex geometries and structural features. This method provides advantages like cost-effectiveness and improved production efficiency, enabling the creation of complex structural components in a single step while ensuring high-quality finishes [92].

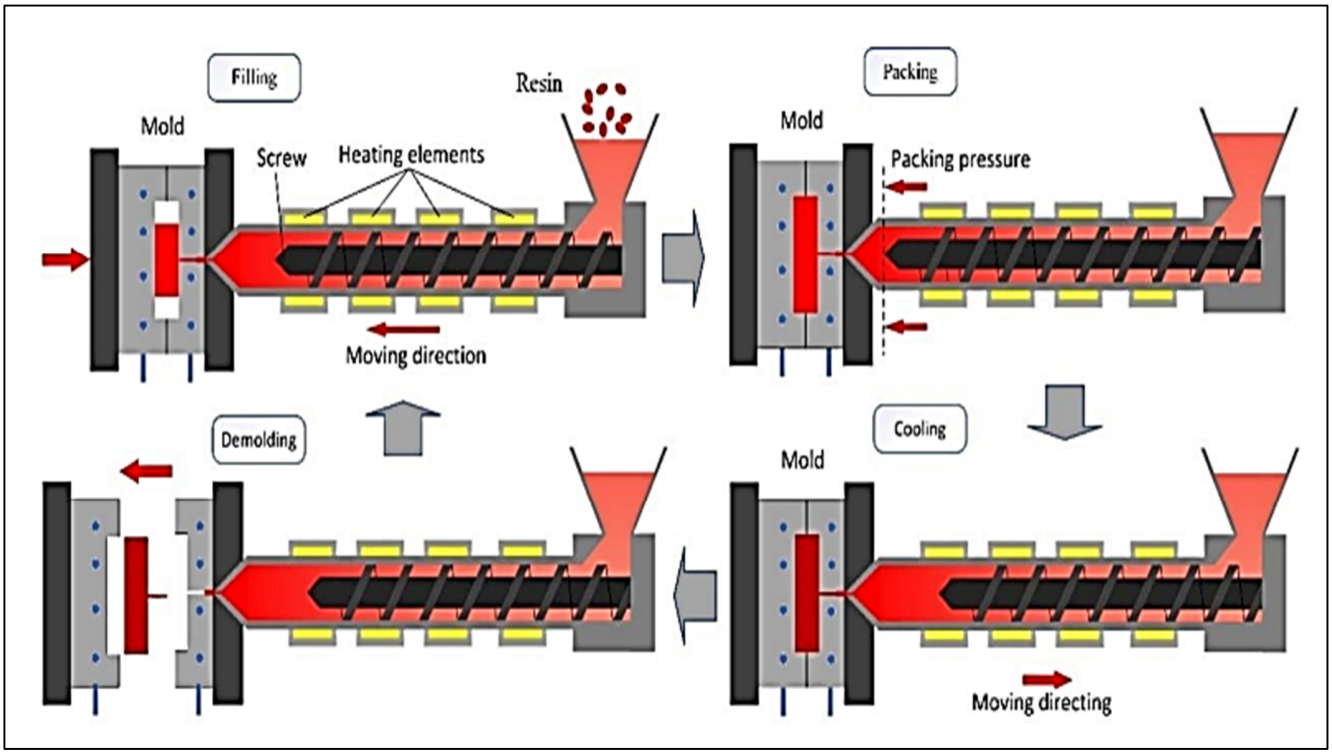

*Figure **I.18**: Injection molding techniques [92].*

CHAPTER II

Mechanical Properties of Composites Material

I. Introduction

The reinforcements establish a non-continuous phase within the material. Different shapes and sizes of reinforcements can be utilized, resulting in various structural forms for the resulting composite. Consequently, based on the geometry of the reinforcement, its shape, and the overall configuration of the composite, the following categories can be identified as illustrated in Figure **II.1**[93].

Phased composites are materials that combine multiple phases to enhance their performance. These composites include particulate, short fiber, flake, and unidirectional types, each offering unique benefits such as increased strength, stiffness, or barrier properties. Layered composites, such as laminated and sandwich composites, employ a layered structure to achieve superior strength, stiffness, and a reduction in weight.

In a composite material, the main structural components are the fiber reinforcements, which significantly increase the material's strength and stiffness. These reinforcements also enhance thermal stability and can either conduct or insulate heat and electricity, depending on the design specifications. On the other hand, the matrix binds the fibers together, giving the composite its shape and rigidity. It distributes loads among the fibers, protects them from damage, and influences the surface finish and transverse properties of the composite, making it essential to the overall performance of the material [93].

Composite materials have various mechanical behaviors that are distinct from those found in conventional engineering materials. Certain behaviors reflect merely adaptations of traditional characteristics, while others are entirely new and necessitate the creation of novel analytical and experimental methods. In contrast to the majority of typical engineering materials, which are homogeneous and isotropic, composite materials frequently display more intricate properties [94].

A homogeneous material has uniform properties throughout its entirety, although the properties may vary locally at different points within the material. For instance, a rubber or plastic containing a well-dispersed particulate filler may display uniform isotropic properties overall, but the individual properties of the polymer and the filler differ, which becomes apparent at a small scale [95].

An isotropic material exhibits the same characteristics in every direction from any point within the substance. A notable example of this is window glass, which demonstrates consistent behavior regardless of the direction in which its properties are assessed [95]. An isotropic body exhibits uniform material properties in all directions at any given point, demonstrating independence from orientation. Even when temperature affects these material properties, the body is still classified as isotropic if the characteristics remain consistent in every direction at each point. However, it is not considered homogeneous when subjected to a temperature gradient [96]. For isotropic materials, when a normal stress is applied, it results in extension along the direction of the stress and contraction in the perpendicular directions, without causing any shearing deformation. Similarly, when a shear stress is applied, it induces only shearing deformation, with no resulting extension or contraction in any direction [94].An orthotropic material, like a sheet, displays three mutually perpendicular planes of symmetry, with its characteristics varying in three orthogonal directions from any particular point [95].

An inhomogeneous object, conversely, does not possess uniform characteristics, with its properties differing based on location within the substance. Anisotropic substances refer to those whose characteristics change in various directions from any specific point, indicating they are not isotropic. A prime illustration of this is a woven or knitted fabric [95].

A ply or lamina refers to a flat sheet of material. Typically, a ply is characterized as a flat, unidirectional arrangement of fibers that are uniformly spaced and securely bonded to a matrix. Other variations of plies may include random fiber arrangements, such as chopped strand mat or foam sheets. Some plies may also display isotropic characteristics, as seen in foam-cored sandwich structures or packaging foils. A laminate consists of multiple plies or laminae that are adhered together [95].

A main classification of materials that can be described by fewer than 21 independent parameters includes monoclinic materials. These materials, characterized by 13 independent coefficients, demonstrate a solitary plane of elastic symmetry. This classification consists of three principal types of materials, categorized according to the arrangement of values within their compliance and stiffness matrices [97].

Composite material mechanics shares similarities with uniform materials like metals, particularly in equilibrium and compatibility, which remain unchanged regardless of material traits. However, the relationships that define material behavior differ; metals are usually isotropic, while composites with aligned fibers are often very anisotropic. The mechanical behavior of fiber-reinforced structures can be studied at two levels: micro mechanics focuses on the material properties from fibers, matrix, and their arrangement, while macro mechanics examines the overall stiffness and strength of the entire composite structure [98]. In micromechanical analysis, different parts of a composite material, like the matrix and fibers, are usually seen as uniform and the same in all directions. The composite is viewed as a mixed material with constant properties. Since fibers or particles are much smaller than the overall material volume, the whole composite can be treated as uniform at a larger scale. This simplification is important for studying the strength of components made from composite materials. Generally, composite materials face loads that cause linear elastic deformation, which can be explained using a modified version of Hooke's law[98].

The key distinction lies in the fact that isotropy remains unchanged by any dimensional scale, with the exception of atomic levels, which are not addressed in this chapter. In contrast, homogeneity is scale-dependent. Homogeneity refers to the uniformity of material properties across the entire volume of a material, which can vary depending on the size or scale of the analysis. On the other hand, isotropy ensures that material properties are consistent in all directions, regardless of the scale involved [95].

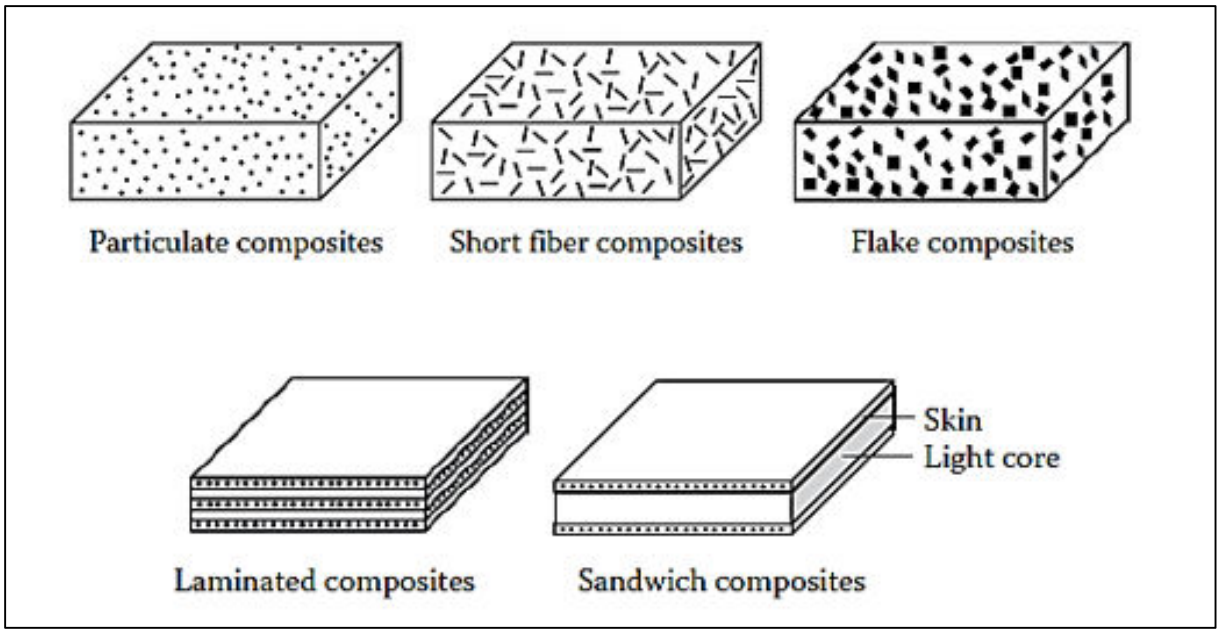

Figure II.1: Classification of Composites Based on Reinforcement Shape and Composite Form [93].

II. Viscoelasticity

The phrase "viscoelastic" has come into use to refer to materials that exhibit characteristics of both viscous fluids and elastic solids. Polymeric substances, recognized for their viscoelastic characteristics, can act as either fluids or solids based on the timescale or temperature [99]. Polycarbonate, a thermoplastic polymer, behaves like molten liquid at high processing temperatures but typically solidifies under normal conditions. Slightly above its glass transition temperature (Tg), it behaves like rubber, while below Tg, it can still show considerable deformation over a sufficiently extended testing duration. Ideal Hookean elastic solids accumulate energy when under load without losing it, whereas ideal Newtonian fluids release energy without retaining it under nonhydrostatic stress. In comparison, viscoelastic materials can both retain and release energy when under load [100].

II.1. Linear Viscoelasticity

A linear elastic solid exhibits a proportional connection between stress and strain that remains stable over time. Conversely, a linear viscoelastic solid also upholds a linear stress-strain relationship; however, this dependence fluctuates according to the load's time history. The mathematical conditions for linear viscoelasticity resemble those that dictate the linear behavior of different systems [100]. For a substance to display linear viscoelastic behavior, its reaction must meet two essential criteria. Firstly, proportionality has to be upheld, indicating that the connection between stress and strain is linear; if the applied stress is increased twofold, the resulting strain also increases twofold. Secondly, the substance must adhere to the principle of superposition, in which the overall response to various applied stresses or strains is equal to the total of the separate responses to each input[101, 102].

The tensile creep test, depicted in Figure **II. 2**, is the most frequently utilized technique for assessing viscoelastic properties. This testing process consists of applying a steady tensile stress to a sample and recording the resulting strain as a function of time [100, 103].

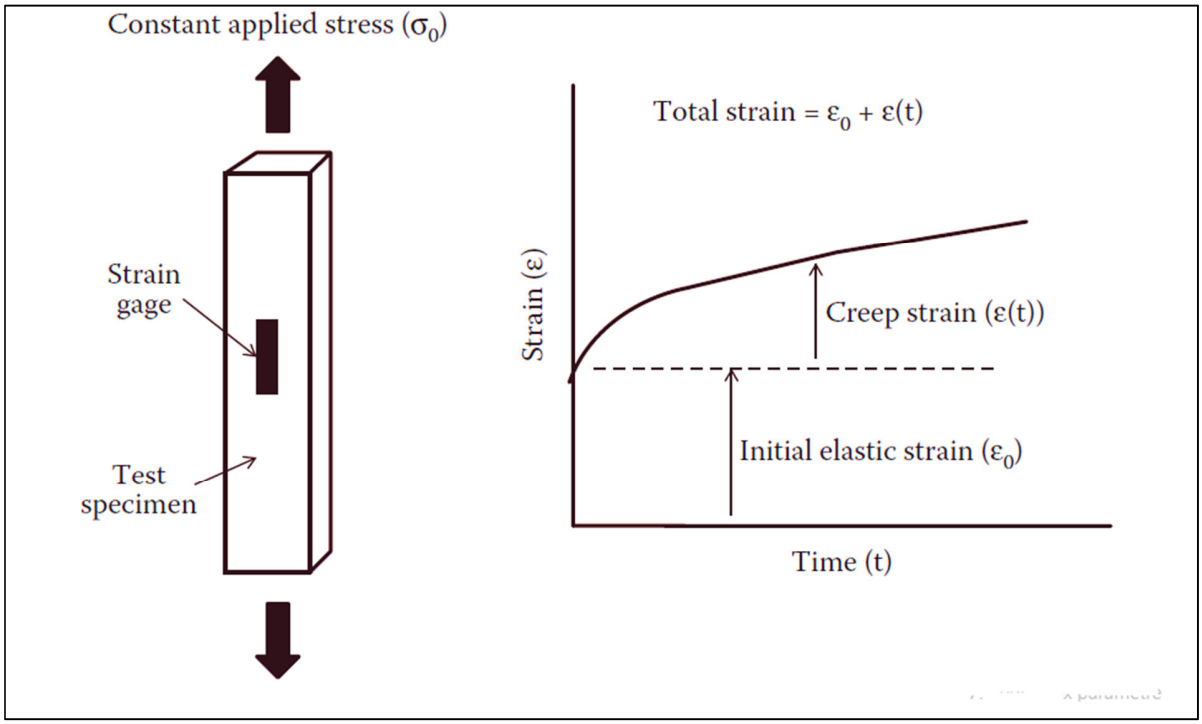

*Figure **II.2**: Tensile creep testing of a viscoelastic material involves applying a constant stress to the specimen and measuring the strain over time [100]*

Common models like the Maxwell and Kelvin-Voigt models merge these components to forecast material behavior. This method is effective for examining polymers, biological tissues, and foams, where both elastic and time-related responses hold significance [100].

II.1.1. Maxwell Model

The Maxwell model provides a simple depiction of linear viscoelasticity by combining an elastic spring and a viscous dashpot in a series configuration. The spring represents the material's elastic (immediate) response, while the dashpot illustrates the viscous (time-dependent) response. This model is employed to describe materials that exhibit both elastic and viscous characteristics, such as polymers [104, 105]. The Maxwell model of viscoelasticity is composed of two essential elements linked in series: a spring and a dashpot. The spring symbolizes the immediate elastic response of the material, adhering to Hooke's Law, which states that stress is directly proportional to strain. The dashpot symbolizes the viscous, time-dependent flow characteristics, dictated by Newton's law of viscosity, where stress is proportional to the rate of strain. This integration enables the Maxwell model to represent both instant elastic deformation and gradual viscous flow in response to applied loads[105, 106].

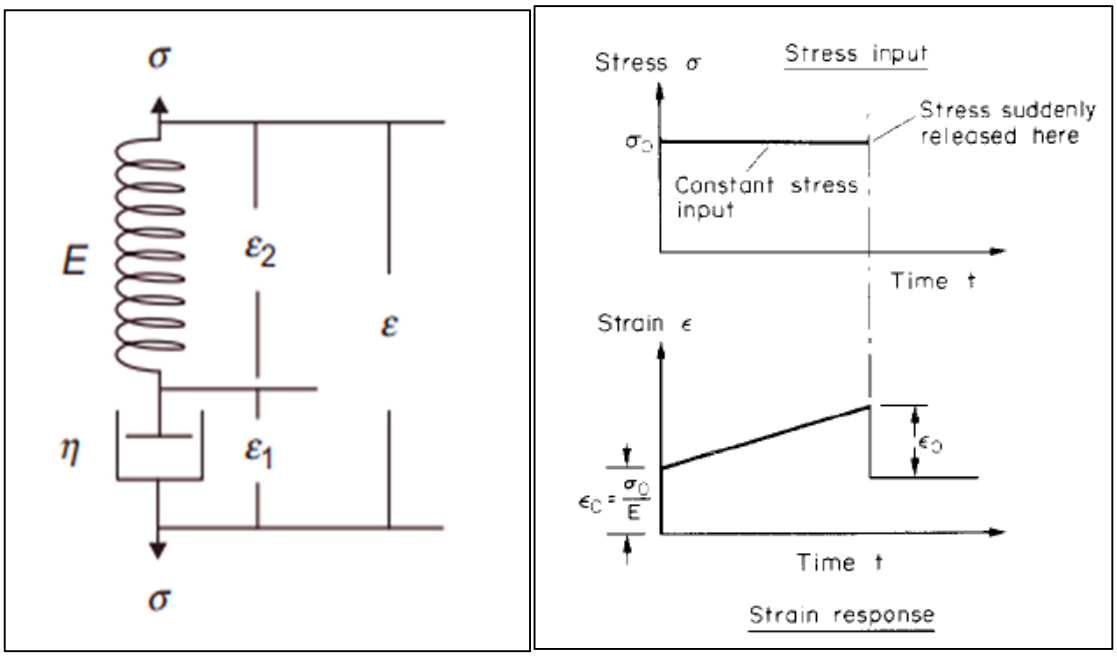

*Figure **II.3**: The Maxwell model [104, 105].*

As shown in Figure **II.3**, the Maxwell model has:

A spring (Hooke's Law):

$$\sigma = E\varepsilon_2 \Rightarrow \varepsilon_2 = \frac{\sigma}{\varepsilon} \tag{II.1}$$

$$\Rightarrow \frac{d\varepsilon_2}{dt} = \frac{1}{E}\frac{d\sigma}{dt} \tag{II.2}$$

A dashpot (Newton's Law of viscosity):

$$\sigma = \eta\frac{d\varepsilon_1}{dt} \Rightarrow \frac{d\varepsilon_1}{dt} = \frac{d\sigma}{\eta} \tag{II.3}$$

Since the spring and dashpot are in series:

The total strain is the sum of strains from both elements:

$$\varepsilon = \varepsilon_1 + \varepsilon_2 \tag{II.4}$$

The stress is the same in both elements:

$$\sigma = \sigma_1 = \sigma_2 \tag{II.5}$$

The final Governing Differential Equation of the Maxwell Model:

$$\frac{d\varepsilon}{dt} = \frac{1}{E}\frac{d\sigma}{dt} + \frac{\sigma}{\eta} \tag{II.6}$$

Where:

σ : Stress (MPa),

ε_2 : Elastic Strain (instantaneous elastic deformation).

ε_1 : Viscous Strain or viscous behavior (which accounts for the time-dependent deformation of the material).

E: Spring modulus (elastic component),

η : Dashpot viscosity (viscous component).

II.1.2. Kelvin-Voigt Model

The Kelvin-Voigt model is a fundamental representation of linear viscoelasticity, employed to describe materials that exhibit both elastic and viscous characteristics. Unlike the Maxwell model, which arranges the spring and dashpot in a series configuration, the Kelvin-Voigt model aligns them in parallel. This arrangement makes it suitable for materials that primarily exhibit recoverable deformation and immediate stress resistance. The model is represented by a spring-damper system, as shown in Figure **II.4**[107].

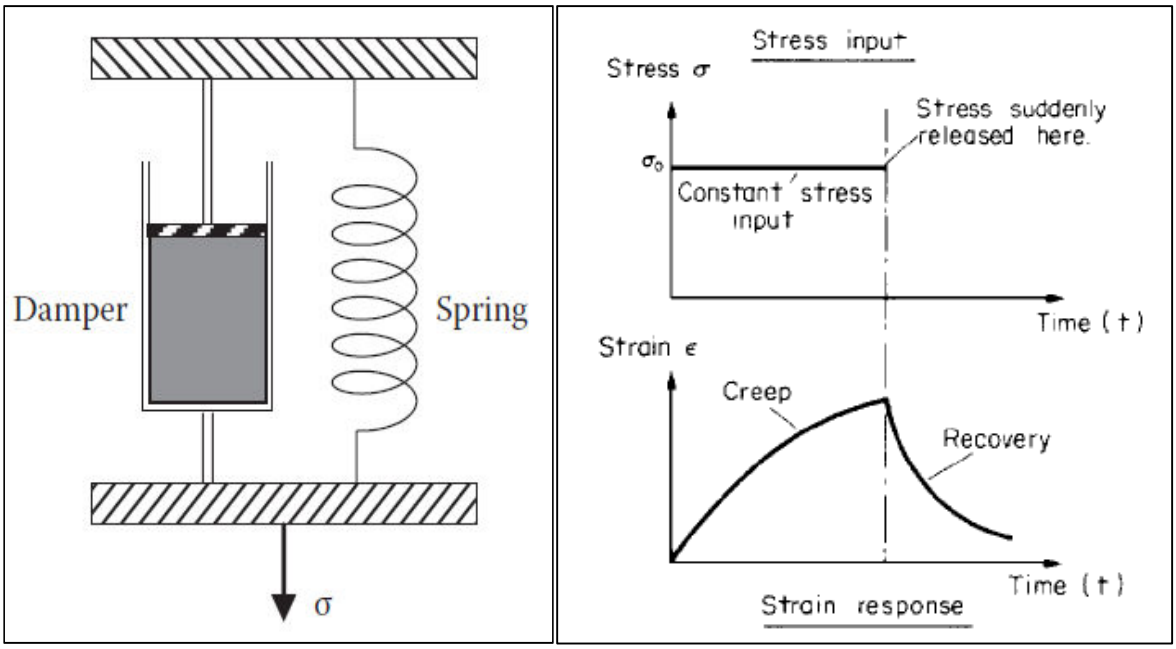

*Figure **II.4**: Kelvin–Voigt model element used for representing viscoelastic materials [105, 107].*

The spring represents the elastic component of the material, where stress is proportional to strain (Hooke's law). The dashpot represents the viscous component, where stress is proportional to the rate of strain (Newton's law of viscosity). In the Kelvin-Voigt model, both components work together, and the material resists deformation both instantly (elastic) and gradually (viscous)[104, 107].

In the Kelvin-Voigt model, the two components: a spring and a dashpot are connected in parallel.

Spring represent elastic element and follows Hooke's Law:

$$\sigma_e = E.\varepsilon \tag{II.7}$$

Dashpot represent viscous element and follows Newton's Law:

$$\sigma_v = \eta \frac{d\varepsilon}{dt} \tag{II.8}$$

Because they are in parallel, they share the same strain:

$$\varepsilon = \varepsilon_e = \varepsilon_v \tag{II.9}$$

But the total stress is the sum of stresses from both elements:

$$\sigma = \sigma_e + \sigma_v = E.\varepsilon + \eta \frac{d\varepsilon}{dt} \tag{II.10}$$

Governing Differential Equation of Kelvin-Voigt**:**

$$\sigma(t) = E.\varepsilon(t) + \eta \frac{d\varepsilon(t)}{dt} \tag{II.11}$$

Where:

$\sigma(t)$: Stress (MPa).

$\varepsilon(t)$: Strain.

E: Elastic modulus of the spring (elastic component).

η: Viscosity of the dashpot (viscous component).

$\frac{d\varepsilon(t)}{dt}$: The strain rate (rate of deformation).

*Table **II.1**: Comparison between Maxwell Model and Kelvin-Voigt Model.*

Aspect	**Maxwell Model**	**Kelvin-Voigt Model**
Configuration	Spring and dashpot in series	Spring and dashpot in parallel
Total Stress	Same in both elements: $\sigma = \sigma_1 = \sigma_2$	Sum of stresses: $\sigma = \sigma_e + \sigma_v$
Total Strain	Sum of strains: $\varepsilon = \varepsilon_1 + \varepsilon_2$	Same strain in both elements: $\varepsilon = \varepsilon_e = \varepsilon_v$
Governing Equation	$\frac{d\varepsilon}{dt} = \frac{1}{E}\frac{d\sigma}{dt} + \frac{\sigma}{\eta}$	$\sigma(t) = E.\varepsilon(t) + \eta \frac{d\varepsilon(t)}{dt}$
Behavior	Stress Relaxation constant strain leads to decreasing str**ess**	Creep Behavior constant stress leads to increasing strain
Recovery	No full recovery, may experience permanent deformation	Full recovery, no permanent deformation after stress removal
Applications	Materials that show viscous flow under stress (polymers)	Materials that show creep and recovery (rubbers)

II.2. Mechanical Behavior

The mechanical properties of a material outline how it deforms or reacts when subjected to an external load or force. Important mechanical characteristics consist of strength, hardness, stiffness, and ductility. Forces can be applied in three main types: tension, compression, and shear, illustrated in Figure **II. 5**. A variety of tests for mechanical properties have been created to assess how materials react to these loads. As these test outcomes are frequently relied upon by regulatory organizations, it is vital that the methodologies are uniform and standardized. In the U.S., ASTM International serves as the primary authority for standardized testing protocols [108].

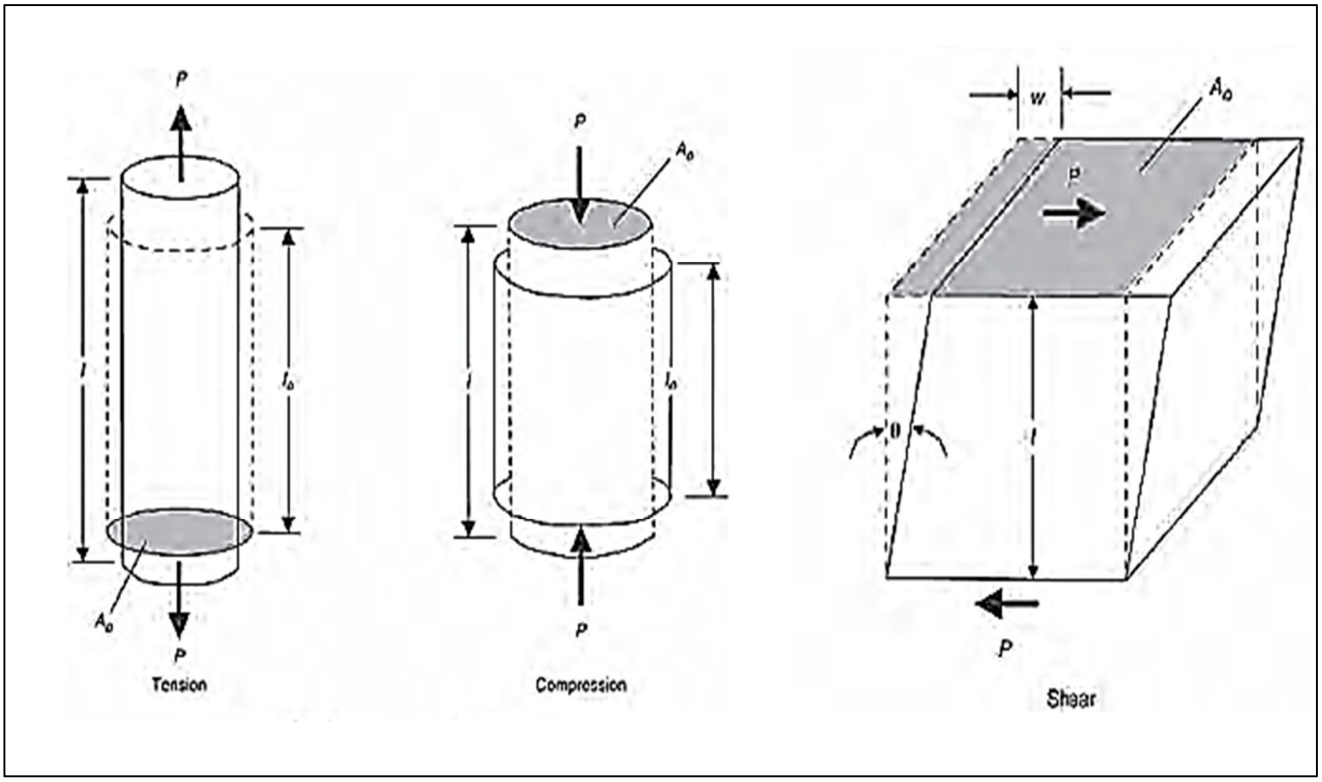

*Figure **II.5**: Stress source [108].*

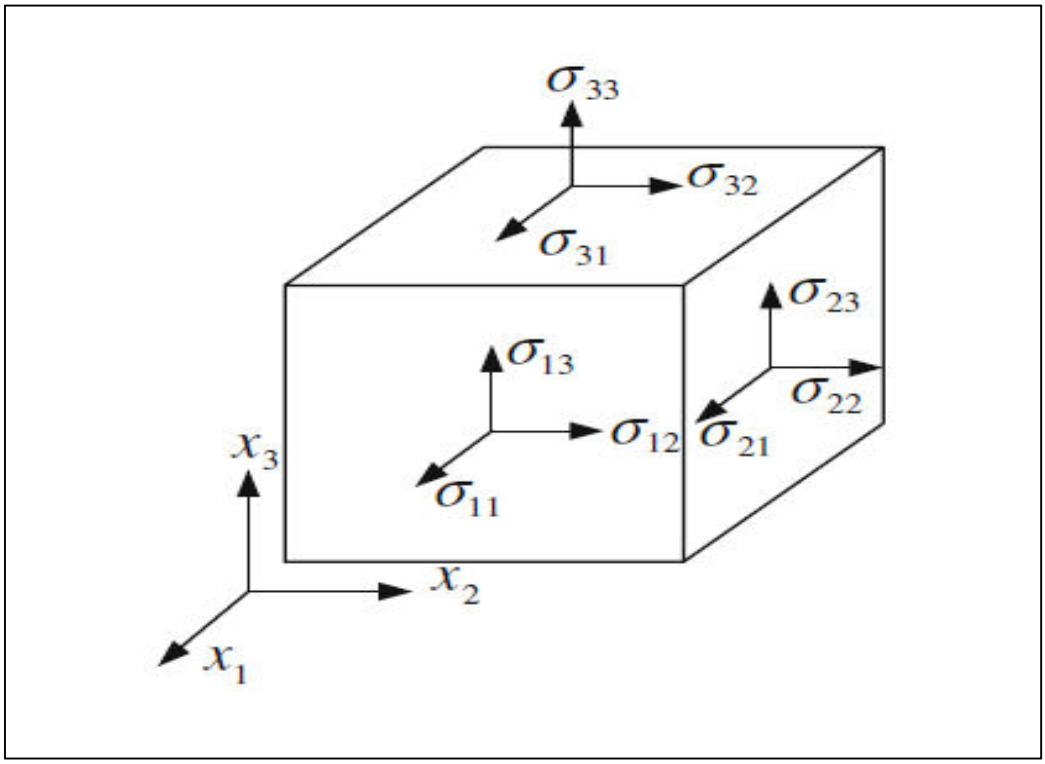

*Figure **II.6**: Stress components [109].*

A body is generally considered a deformable continuous medium. The main objective of the analysis is to identify the stresses and strains induced by external loads. At any location within a continuous body, regardless of being in equilibrium or in motion due to external forces, the stress state can be depicted by the stress components on three mutually perpendicular planes intersecting that point[110].If an infinitesimally small volume element surrounding the point is shaped like a rectangular parallelepiped with faces aligned to the coordinate planes, the stress components $\sigma_{ij}$are as illustrated in Figure **II.6**[109].

The initial subscript of σ signifies the direction perpendicular to the plane, whereas the following subscript represents the direction of the stress component. The components σ_{11}, σ_{22}, σ_{33}, which act perpendicular to the surfaces, are known as normal stresses, whereas the remaining components, which act parallel to the surfaces, are referred to as shear stresses. When the body's movements are overlooked, the stress components will display symmetry. By examining the stress components on planes that are orthogonal to the coordinate axes, it is possible to ascertain the stress vector t on any surface defined by a unit outward normal vector n that intersects the point, employing Cauchy's formula [109].

$$t_i = \sigma_i \cdot n_j \tag{II.12}$$

Or in vector notation:

$$t = \sigma \cdot n \tag{II.13}$$

Where:

T: The stress vector acting on the surface.

σ : The stress tensor.

n : The unit normal vector to the surface.

σ_{ij} : The components of the stress tensor.

And i indicates the direction of the stress vector and j corresponds to the direction of the surface's normal.

II.2.1. Hook's Law

The essential relationship between stress and strain was initially presented by Robert Hooke in 1678. Consequently, the basic relationship between stress and strain in the elastic region is often referred to as Hooke's law. This principle asserts that strain (ε) in an elastic substance is directly proportional to the applied stress (σ) [144].For axial loading, the proportionality constant is known as Young's modulus, E. In the case of shear loading, the proportionality constant is termed the shear modulus G. For triaxial or pressure loading, the constant is generally referred to as the bulk modulus K [111].

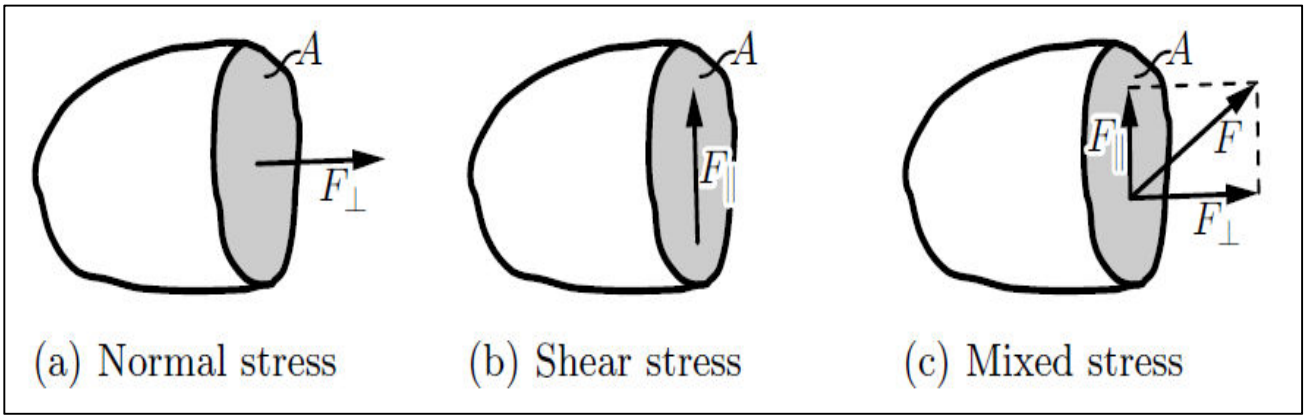

*Figure **II.7**: Stress types: (a) Normal stress, (b) Shear stress, and (d) Mixed stress [112].*

In continuous media, the stress tensor σ_{ij} fully defines the state of stress, while the strain tensor ε_{ij} describes the state of deformation. A substance is categorized as elastic if it changes shape when a load is applied but reverts to its initial dimensions once the load is removed. In other terms, elastic substances demonstrate a direct analytical correlation between stress and strain. When this correlation is linear, it is typically called the generalized Hooke's law, and these substances are known as linear elastic materials. If a linear elastic substance is maintained at a stable temperature and undergoes no stress in its unstrained condition, the generalized Hooke's law can be formulated as follows [109, 113]:

$$\sigma_{ij} = C_{ijkl}\varepsilon_{kl} \tag{II.14}$$

II.2.2. Definitions of stress and strain

Load and displacement information may suffice for certain product assessments; however, a thorough analysis of material properties requires size-independent factors like stress and strain. These fundamental concepts are typically defined in two widely accepted formats, the first of which is predominantly used in engineering applications [96]:

$$\sigma_{eng} = \frac{P}{A_0} \tag{II.15}$$

And

$$\varepsilon_{eng} = \frac{L_f - L_0}{L_0} \tag{II.16}$$

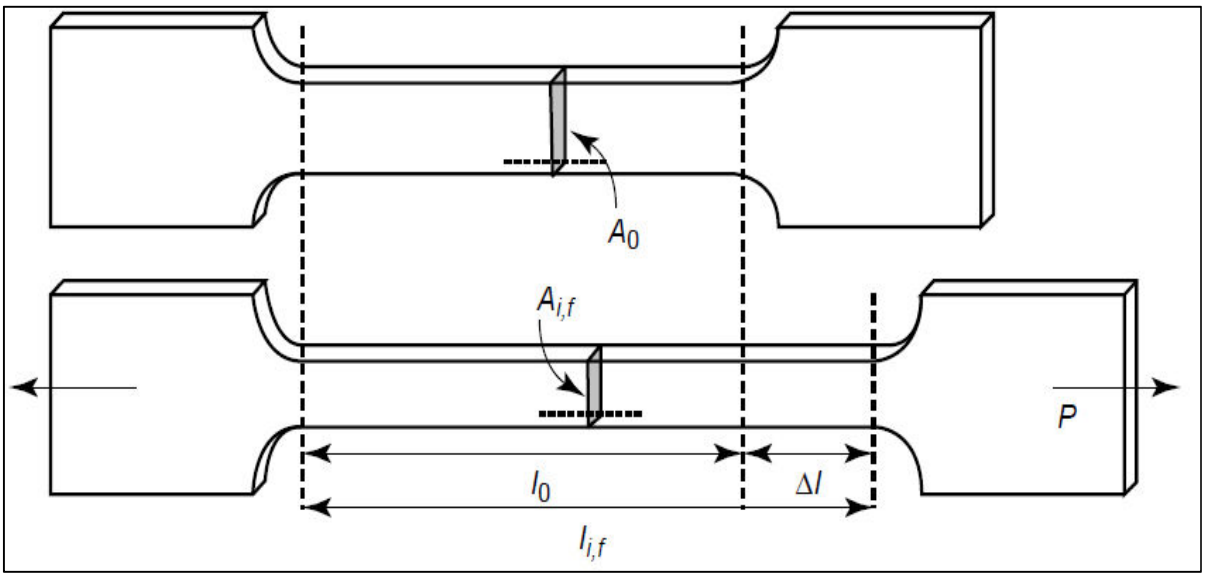

*Figure **II.8**: A schematic representation shows a rectangular tensile specimen before loading, during loading, after loading [96].*

Cylindrical specimens with circular cross-sections are also commonly used, and the same definitions apply to both shapes. As shown in Figure **II.8**, stress and strain can alternatively be defined as[96]:

$$\sigma_{true} = \frac{P}{A_i} \tag{II.17}$$

$$\varepsilon_{true} = \ln \frac{L_f}{L_0} \tag{II.18}$$

The formula for true strain is obtained by integrating the engineering strain expression over the length change from L_0 to L_f, ensuring that the accumulated strain is considered for each infinitesimal increment. The primary distinction between the definitions of true stress and true strain exists in recognizing the connection between gauge length (L) and the alterations in cross-sectional area (ΔA) throughout plastic deformation. When a specimen undergoes tensile deformation, its cross-sectional area generally reduces.

Where:

P : The load (N)

A_i : The instantaneous cross sectional area (mm^2)

L_f : The final gauge length (mm).

L_0 : The initial gauge length (mm).

II.2.3. Tensile Properties

The tensile test is the predominant method used to assess the mechanical properties of materials. This test provides crucial insights into a material's ductility and fracture behavior. By applying a tensile force to a specimen and measuring its deformation or elongation using a load frame, the tensile properties of the material can be determined. The load can be converted into engineering stress (σ) by dividing it by the specimen's original cross-sectional area (A_0)[108]:

$$S = \frac{P}{A_0} \tag{II.19}$$

Where:

P: The load (N).

A_0: The original cross-sectional area (mm^2).

The engineering strain ε is calculated by dividing the change in gauge length by the original gauge length:

$$\varepsilon = \frac{L - L_0}{L_0} \tag{II.20}$$

Where:

L : The gauge length (mm).

L_0 : The original gauge length (mm).

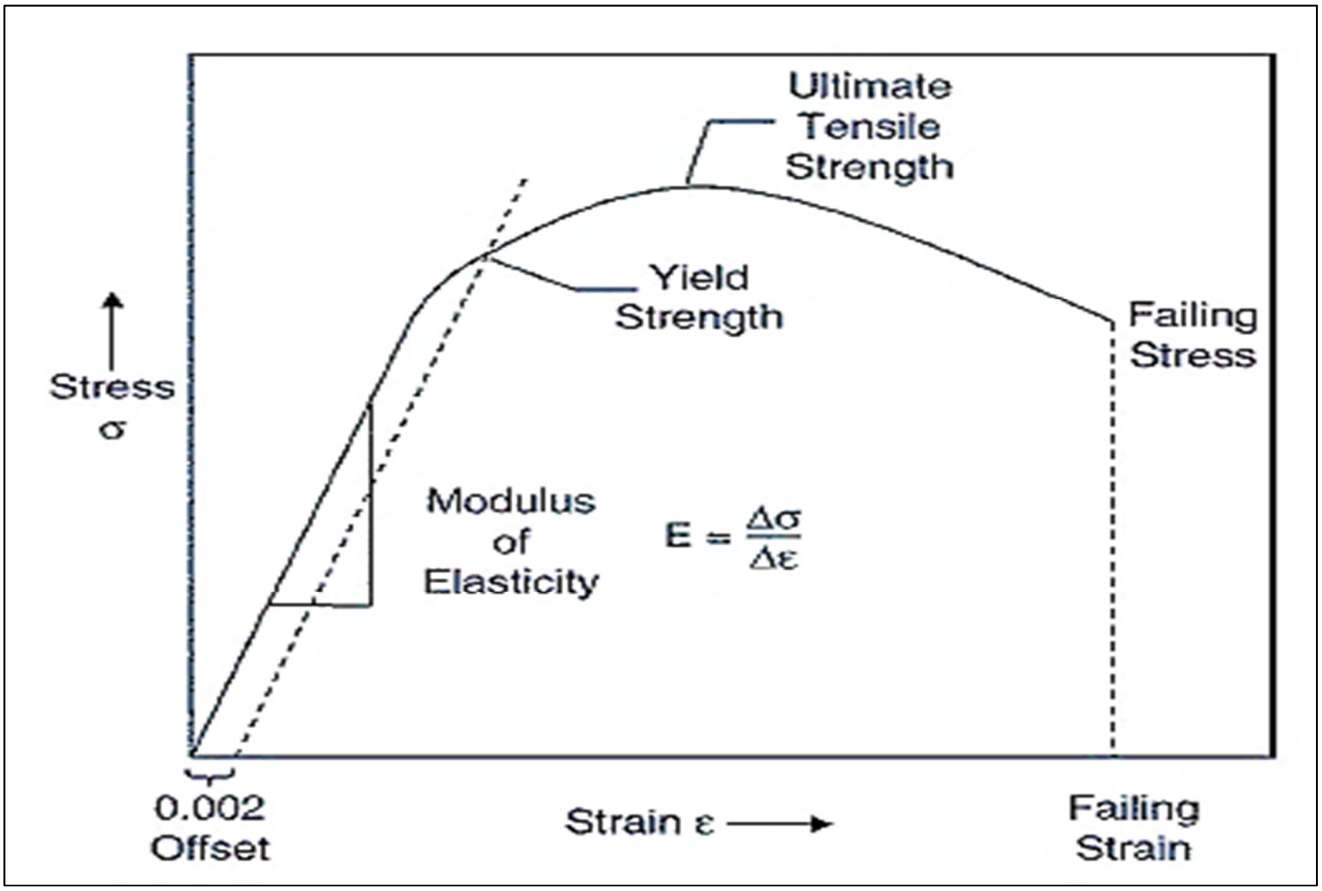

*Figure **II.9**: Stress-strain curve. Source [108].*

As illustrated in Figure **II.9**, the maximum tensile strength represents the highest stress attained during a tensile test. While this figure is commonly referenced, it is rarely utilized in design applications. In the case of ductile metals, static design is primarily based on yield strength, as the objective is to prevent any plastic deformation. In contrast, for brittle metals, which exhibit minimal plastic deformation, tensile strength can be used as a design reference, adjusted with a suitable safety factor [108].

II.2.4. Ductility

Ductility measures derived from the tension test include the engineering strain at fracture (ε_f) and the reduction of area at fracture (q), both typically expressed as percentages. The engineering strain at failure is often reported as percent elongation. These properties are determined after fracture by reassembling the specimen and measuring its final length (L_f) and the final cross-sectional area at the fracture (A_f). Percent elongation is calculated using:

$$\varepsilon_f = \frac{L_f - L_0}{L_0} x100\% \quad \text{(II.21)}$$

Where:

L_f : The final length after fracture (mm).

L_0 : The original gauge length (mm).

The reduction in area can be determined using the formula:

$$R = \frac{A_0 - A_f}{A_0} x100 \quad \text{(II.22)}$$

Where:

R: Reduction in area.

A_f : The final cross sectional area at the fracture.

A_0 : The original cross sectional area.

Poisson's ratio (v) is defined as the ratio of the lateral strain (ε_t) to the longitudinal strain (ε_l):

$$v = \frac{\varepsilon_t}{\varepsilon_l} \quad \text{(II.23)}$$

The slope of the initial linear portion of the stress-strain curve, as shown in Figure **II.9**, represents the modulus of elasticity, also known as Young's modulus:

$$E = \frac{\Delta\sigma}{\Delta\varepsilon} \quad \text{(II.24)}$$

The modulus of elasticity (E) quantifies the stiffness of a material. An elevated modulus signifies reduced elastic strain for a specific stress, indicating that materials with greater moduli are stiffer than those with lesser moduli. Since it is vital for determining deflections in beams and various structural components, the modulus of elasticity serves as an important design factor. It is derived from the atomic binding forces, which cannot be modified without altering the intrinsic characteristics of the material, rendering the modulus of elasticity one of the mechanical properties least influenced by microstructure [108].

II.2.5. Glass Transitions

The glass transition temperature (Tg) is a critical threshold at which polymers transition from a hard, brittle, and rigid glassy state to a more flexible and rubbery state. This phenomenon occurs because, at temperatures below Tg, the polymer chains are effectively "frozen," displaying limited mobility. In contrast, when the temperature exceeds Tg, molecular motion increases, allowing for greater flexibility [114].

Polymers may be categorized as amorphous or crystalline depending on their structure, which profoundly affects their mechanical, thermal, and optical characteristics. Amorphous polymers: These polymers do not possess a consistent, repeating molecular arrangement, indicating that their chains are organized in a random manner [115, 116]. Polymers in crystals exhibit a more uniform molecular structure, with their chains aligning in alternating patterns and forming areas of crystallization. Crystalline polymers also feature a melting point, beyond which the structured crystalline form transitions into a more amorphous state [117].Below the glass transition temperature (Tg), polymers behave as rigid glasses. In this state, the polymer chains have limited molecular motion, resulting in a solid and brittle material [118].

When the temperature surpasses Tg, the polymer chains acquire increased mobility, and the material shifts into a rubbery condition. In this condition, the polymer becomes pliable and soft. The material might display elastic properties, akin to rubber, allowing it to experience reversible deformation when subjected to stress. This indicates that the polymer can revert to its initial form once the deformation is alleviated, which is characteristic of elastomers [93].

II.3. Stress-Strain Properties of Fiber-Reinforced Materials

The assessment emphasizes the differences found within a small material element made up of many fibers arranged in a single layer. This method allows for a seamless transition into the study of composite materials, which consist of fiber-reinforced substances. It is unrealistic to evaluate the behavior of each single fiber during an extensive structural evaluation, given that existing computational resources are inadequate for such detailed analysis. However, composite materials often fail due to broken fibers, compromised connections between the fibers and the matrix, or the breakdown of the matrix itself [119].

II.3.1. Isotropic material

An isotropic material is a material that exhibits identical mechanical and physical properties in all directions. This means that its response to applied forces, such as stress and strain, remains the same

regardless of the direction of loading. In the context of elasticity, an isotropic material has uniform elastic properties, meaning its stiffness, strength, and deformation behavior are independent of orientation[114].

II.3.2. Anisotropic material

An anisotropic material is a material whose mechanical and physical properties vary depending on the direction of measurement. Unlike isotropic materials, anisotropic materials do not exhibit uniform behavior when subjected to stress or strain from different directions. This directional dependence is due to the material's internal structure, such as the arrangement of fibers, crystals, or layers [114].

II.3.3. Orthotropic material

An orthotropic material is a specific type of anisotropic material that has three mutually perpendicular planes of symmetry, meaning its mechanical properties vary along three distinct axes but remain constant within each plane. These materials have different stiffness, strength, and elasticity in each of the three principal directions [120].

II.3.4. Homogeneous material

A homogeneous material is one that has a uniform composition and consistent properties throughout its entire volume. This means that its mechanical and physical characteristics, such as strength, density, and elasticity, remain unchanged regardless of the location within the material. Homogeneous materials can be either isotropic, exhibiting the same properties in all directions, or anisotropic, where properties vary based on direction [120].

II.3.5. Monoclinic material

A monoclinic material is a type of anisotropic material that has a single plane of elastic symmetry, meaning its mechanical properties vary in different directions but remain consistent within that plane. It is characterized by 13independentelasticconstants, making it more complex than orthotropic or isotropic materials. Examples of monoclinic materials include certain crystals, minerals like gypsum, and some composite materials with layered structures [120].

II.4. Stress and Strain in Fiber-Reinforced Materials

In the evaluation of fiber-reinforced materials, an orthogonal coordinate framework referred to as 1-2-3 is utilized. In this framework, the 1-axis corresponds with the orientation of the fibers, the 2-axis is at a right angle to the fibers within the layer, and the 3-axis is at a right angle to the layer itself. The 1-axis indicates the fiber orientation, while the 2 and 3 axes are regarded as matrix directions. The phrase "transverse direction" denotes the orientation that is at right angles to the fibers. The specific matrix

direction, whether it is 2 or 3, will be specified in the appropriate context. Stresses, strains, and strengths are indicated within this main material coordinate system [119]. Figure **II.10**, illustrates an isolated layer and the orientation of the principal material coordinate system.:

- The 1-axis is aligned with the fiber direction (longitudinal direction).
- The 2-axis lies in the plane of the layer, perpendicular to the fibers (matrix direction).
- The 3-axis is perpendicular to the plane of the layer, also perpendicular to the fibers.

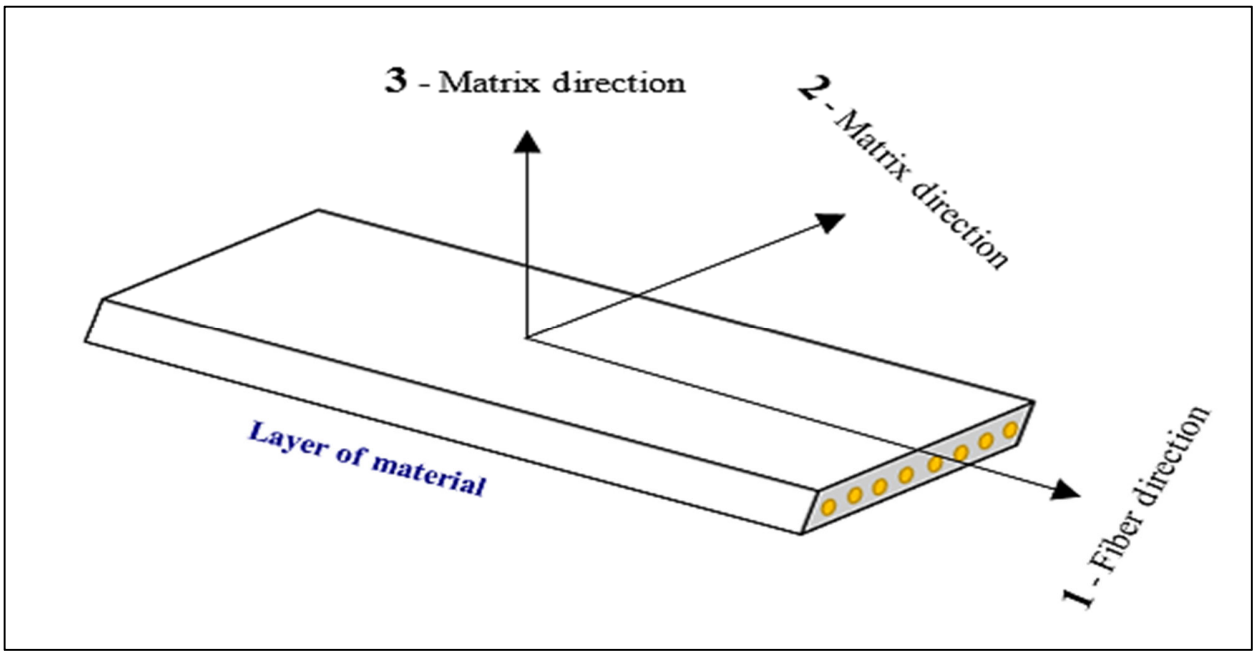

*Figure **II.10**: Material coordinate system [119].*

The effect of fiber reinforcement is uniformly distributed throughout the material, leading us to consider the fiber-matrix system as a single homogeneous entity. This assumption aids in the analysis of fiber-reinforced composites. However, it is crucial to note that this composite does not display consistent properties in all directions. Typically, it exhibits greater strength and stiffness along the 1 direction (parallel to the fibers) compared to the 2 and 3 directions (perpendicular to the fibers). A material that demonstrates varying properties in three mutually perpendicular directions is classified as orthotropic. Therefore, a layer made from such a material is considered orthotropic [119].

The 1-2, 1-3, and 2-3 planes are mutually perpendicular to one another, and the material's properties are symmetrical with respect to each of these planes. A material that demonstrates uniform properties in all directions, indicating that it behaves consistently regardless of orientation, is referred to as isotropic [119].

Figure **II.11** depicts a small element of smeared fiber-reinforced material subjected to stresses on its six bounding surfaces. The small volume is considered to be taken from a layer. The normal stress on the face of the element with its outward normal in the 1 direction is denoted as σ_1. The shear stress acting in the 2

direction on that face is labeled as τ_{12}, and the shear stress in the 3 direction on that face is labeled as τ_{13}. The normal and shear stresses on the other faces are similarly designated.

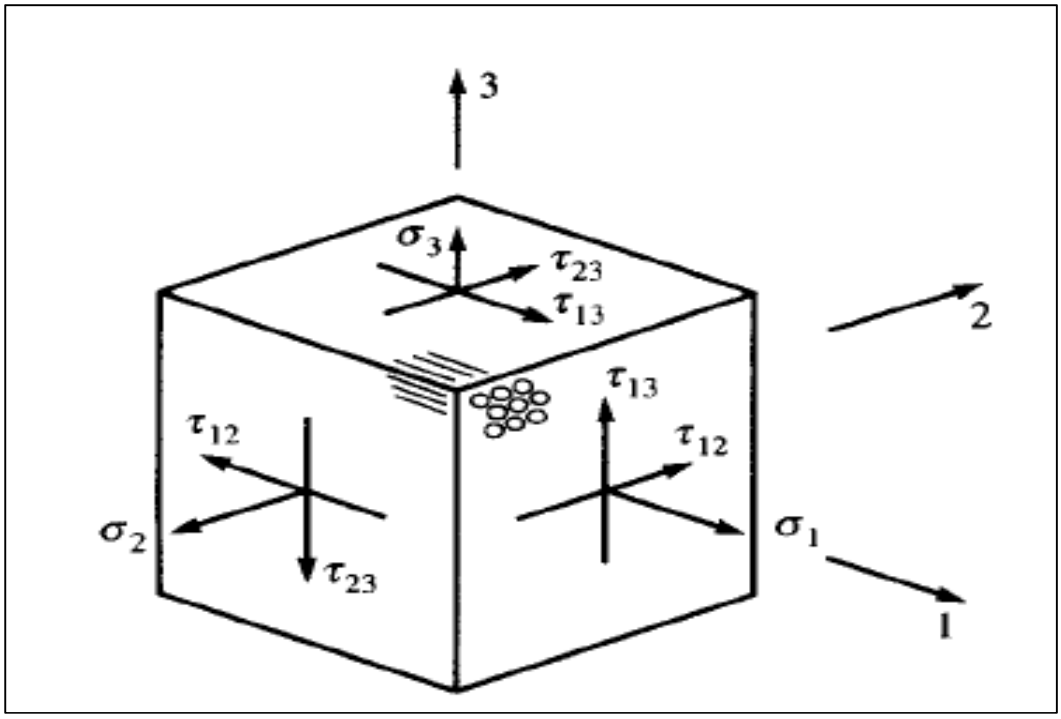

*Figure **II.11**: Stresses in element [119].*

The extensional strain responses of the element, as referenced in the 1-2-3 coordinate system, are represent as $\varepsilon_1, \varepsilon_2$ and ε_3, while the engineering shear strain responses are denoted as γ_{12}, γ_{23}, and γ_{13}. In this notation, ε_1 represents the stretching of the element in the fiber direction, γ_{12} refers to the change in angle in the 1-2 plane, and so on. The stress-strain relationship for the small element will be developed by analyzing the response of the element to each of the six stress components. Since only linear elastic behavior is considered, the superposition principle will be applied to determine the overall response of the element under a complex or combined stress state [119].

Figure **II.12.a** shows the element subjected to a tensile normal stress in the 1 direction, denoted as σ_1. Figure**II.12. b** and Figure **II.12.d** depict three different views of the element, illustrating how it deforms under this tensile stress.

The tensile normal stress σ_1 causes the element to elongate in the 1 direction. Due to Poisson's effect, there is also a contraction in the 2 and 3 directions. However, there is no inherent reason to assume that the contractions in the 2 and 3 directions are equal. Furthermore, nothing has been expressed to suggest that the element has to contract; it might actually expand. Although contraction is common for a single layer, laminates can be engineered to expand instead of contracting. Laminate Poisson's ratios, which dictate this behavior, will be examined later [93].The extensional strain in the 1 direction is related to the

tensile normal stress in the 1 direction by the tensile modulus of the equivalent smeared material in the fiber direction, ε_1. The relationship between these quantities is[119]:

$$\varepsilon_1 = \frac{\sigma_1}{E_1} \tag{II.25}$$

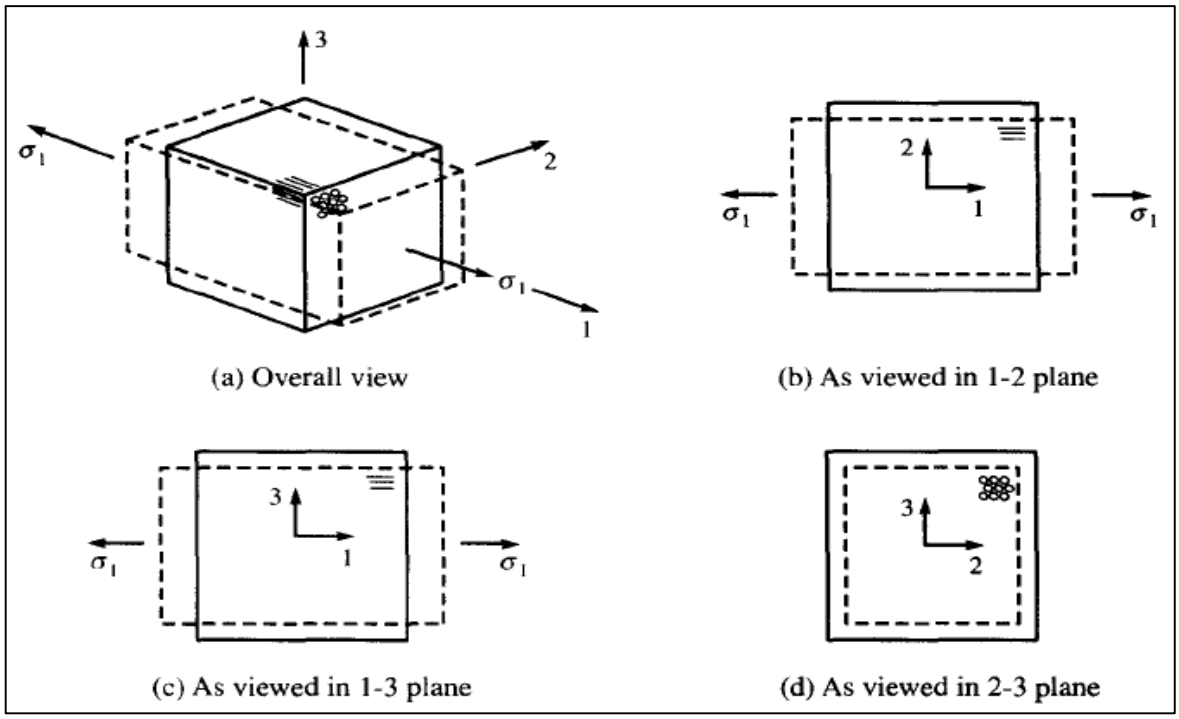

*Figure **II.12**: Deformation of an element [119].*

The Poisson's ratio, often denoted by v_{12}, is a material property that describes the relationship between the longitudinal strain (in the direction of the applied force) and the lateral strain (in the perpendicular direction to the applied force). When referring to the contraction in the 2-direction and extension in the 1-direction, the Poisson's ratio is defined mathematically as:

$$v_{12} = -\frac{\varepsilon_2}{\varepsilon_1} \tag{II.26}$$

The negative sign indicates that an extension in one direction (the 1-direction) typically causes a contraction in the perpendicular direction (the 2-direction). This relationship is essential in understanding material deformation under stress. The Poisson's ratio ν_{12} can indeed be related to Young's modulus E. The relationship between these quantities is fundamental in materials science and mechanical engineering. The general relationship is:

$$\varepsilon_2 = -v_{12} \cdot \varepsilon_1 = -v_{12} \cdot \frac{\sigma_1}{E_1} \tag{II.27}$$

Given that the second subscript in v_{13} refers to the direction of contraction (or lateral strain), the Poisson's ratio refers to the contraction in the 3-direction due to extension in the 1-direction. Specifically:

$$v_{13} = -\frac{\varepsilon_3}{\varepsilon_1} \tag{II.28}$$

$$\Rightarrow \varepsilon_3 = -v_{13} \cdot \varepsilon_1 = -v_{13} \cdot \frac{\sigma_1}{E_1} \tag{II.29}$$

If a tensile normal stress is applied in the 2-direction instead of the 1-direction, the element of smeared material will deform as shown in Figure II.13. Due to the material's softness in the direction perpendicular to the fibers, it will elongate more easily in the 2-direction than in the 1-direction. However, the rigid fibers resist lateral contraction, significantly minimizing the contraction in the 1-direction, counteracting the typical Poisson effect.

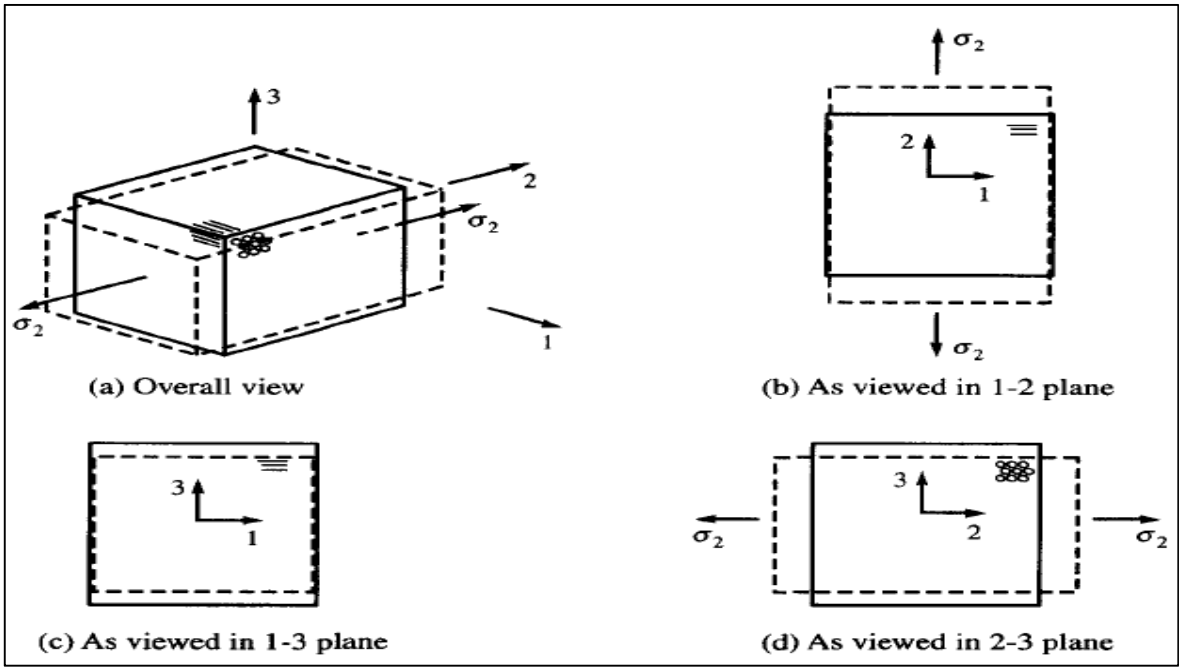

*Figure **II.13**: Deformation of an element [119].*

In contrast, the contraction in the 3-direction will be significant because only the matrix and the soft diametral direction of the fiber are resisting deformation. For the loading scenario shown in Figure **II.13**, the tensile normal stress in the 2-direction σ_2, and the extensional strain in the 2-direction are related by another extensional modulus through the following relationship:

$$\varepsilon_2 = \frac{\sigma_2}{E_2} \tag{II.30}$$

Using the subscript convention established for Poisson's ratios, the contraction in the 1-direction is related to the extension in the 2-direction by another Poisson's ratio, which is defined as:

$$v_{21} = -\frac{\varepsilon_1}{\varepsilon_2} \tag{II.31}$$

As a result, due to the tensile normal stress σ_2 applied in the 2-direction:

$$\varepsilon_1 = -v_{21} \cdot \varepsilon_2 = -v_{21} \cdot \frac{\sigma_2}{E_2} \tag{II.32}$$

This means that as the material extends in the 2-direction due to the applied stress, it will contract in the 3-direction by an amount determined by v_{23}.

$$v_{23} = -\frac{\varepsilon_3}{\varepsilon_2} \tag{II.33}$$

Rearranging the expression, we get:

$$\varepsilon_3 = -v_{23} \cdot \varepsilon_2 = -v_{23} \cdot \frac{\sigma_2}{E_2} \tag{II.34}$$

Finally, if only a tensile normal stress σ_3 is applied, the strains in the three directions can be determined using the general relationships for Poisson's ratios and the material's behavior in response to stress. The strain in each direction is related to the applied stress in a way that accounts for both the longitudinal strain in the direction of the applied stress and the lateral strains in the perpendicular directions. The strain in the 3-direction is the direct extension due to the applied stress σ_3, which can be written as:

$$\varepsilon_3 = \frac{\sigma_3}{E_3} \tag{II.35}$$

$$\varepsilon_1 = -v_{31} \cdot \varepsilon_3 = -v_{31} \cdot \frac{\sigma_3}{E_3} \tag{II.36}$$

$$\varepsilon_2 = -v_{32} \cdot \varepsilon_3 = -v_{32} \cdot \frac{\sigma_3}{E_3} \tag{II.37}$$

E_3 is the extensional modulus in the 3-direction, ν_{32} relates the contraction in the 2-direction to the extension in the 3-direction, and ν_{31} connects the contraction in the 1-direction to the extension in the 3-direction. This applies when only the stress σ_3 is applied. Due to the differing stiffness between the fibers and the matrix, the σ_3 stress causes minimal contraction in the 1-direction. However, as shown in Figure **II.14**, the contraction in the 2-direction will be much more significant.

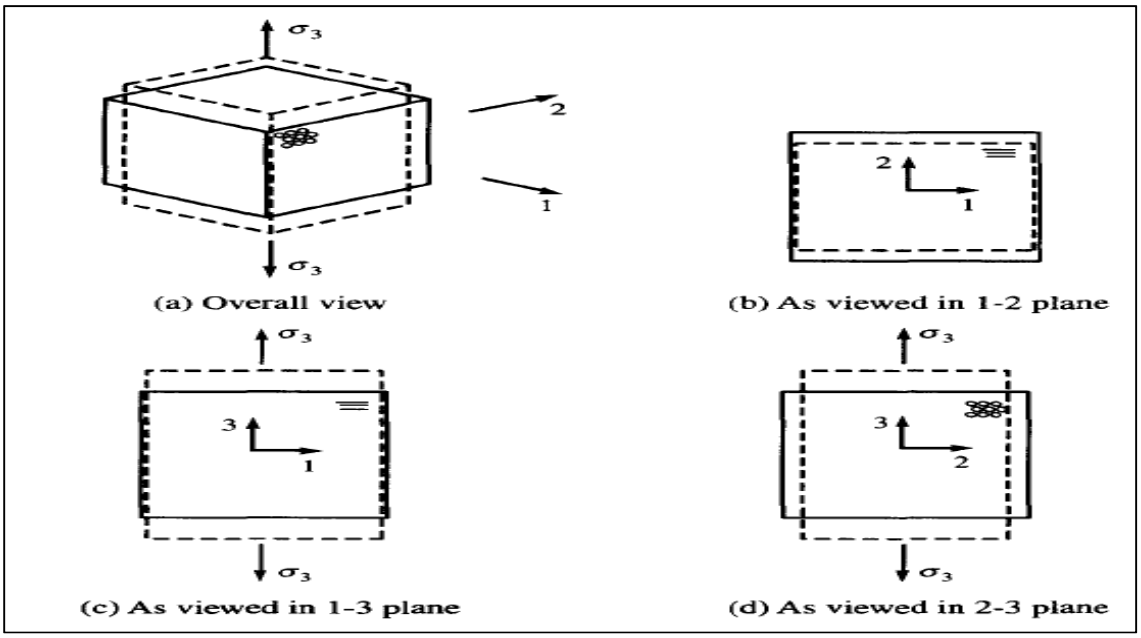

*Figure **II.14**: Deformation of an element [119].*

If all three tensile stresses are applied simultaneously, the strain in any one direction is the result of the combined effects of each applied stress. The total strain in any direction can be expressed as a sum of the individual strains caused by each of the applied stresses, taking into account the material's Poisson's ratios and moduli. Mathematically, this can be written as:

$$\varepsilon_1 = \frac{1}{E_1}\left(\sigma_1 - v_{12}\cdot\sigma_2 - v_{13}\cdot\sigma_3\right) \tag{II.38}$$

$$\varepsilon_2 = \frac{1}{E_2}\left(\sigma_2 - v_{21}\cdot\sigma_1 - v_{23}\cdot\sigma_3\right) \tag{II.39}$$

$$\varepsilon_3 = \frac{1}{E_3}\left(\sigma_3 - v_{31}\cdot\sigma_1 - v_{32}\cdot\sigma_2\right) \tag{II.40}$$

The strain in any direction due to the simultaneous application of tensile stresses in all three directions can be expressed in matrix form as:

$$\begin{pmatrix} \varepsilon_1 \\ \varepsilon_2 \\ \varepsilon_3 \end{pmatrix} = \begin{pmatrix} \frac{1}{E_1} & \frac{-v_{21}}{E_2} & \frac{-v_{31}}{E_3} \\ \frac{-v_{12}}{E_1} & \frac{1}{E_2} & \frac{-v_{32}}{E_3} \\ \frac{-v_{13}}{E_1} & \frac{-v_{23}}{E_2} & \frac{1}{E_3} \end{pmatrix} \cdot \begin{pmatrix} \sigma_1 \\ \sigma_2 \\ \sigma_3 \end{pmatrix} \quad \text{(II.41)}$$

The effects of shear stress in an orthotropic material are less complex compared to the normal stresses, as there is no coupling among the three shear deformations. This means that the shear strain in one direction is independent of the shear stresses applied in the other directions. In an orthotropic material, each shear stress only affects the corresponding shear strain in its own plane, without influencing the shear deformation in the other planes.

As illustrated in Figure **II.15**, when shear stresses are applied in one direction (τ_{12} , τ_{23}andτ_{31}), the correspond shear strain (γ_{12} , γ_{23}, and γ_{31}) is calculated independently, based on the material's shear moduli. The shear strain γ_{23} due to the shear stress τ_{23} is given by:

$$\gamma_{23} = \frac{\tau_{23}}{G_{23}} \quad \text{(II.42)}$$

Where G_{23} is the shear modulus in the 2-3 plane, and similarly for the other shear moduli in their respective planes. Thus, in an orthotropic material, each shear stress is only responsible for its corresponding shear strain, and there is no interdependence between the shear strains in different directions.

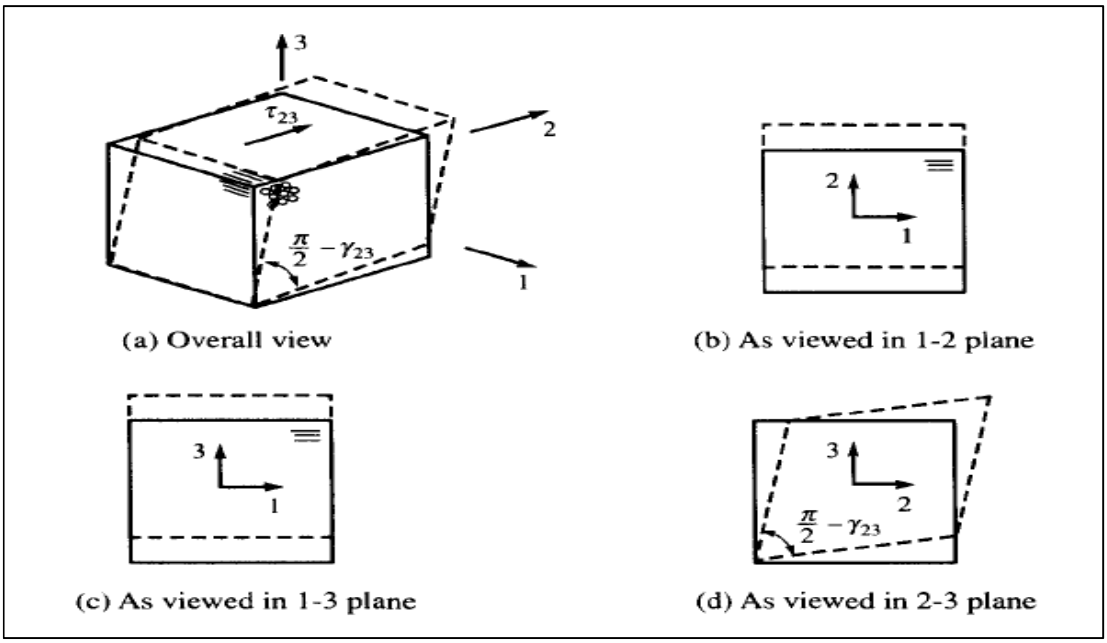

*Figure **II.15**: Deformation of an element [119].*

The convention for shear in the 2-3 plane can be straightforwardly applied to the 1-3 and 1-2 planes as well. As shown in Figure **II.16**, a shear stress τ_{13} alters the right angles in the 1-3 plane, while all other angles in the cube stay orthogonal.

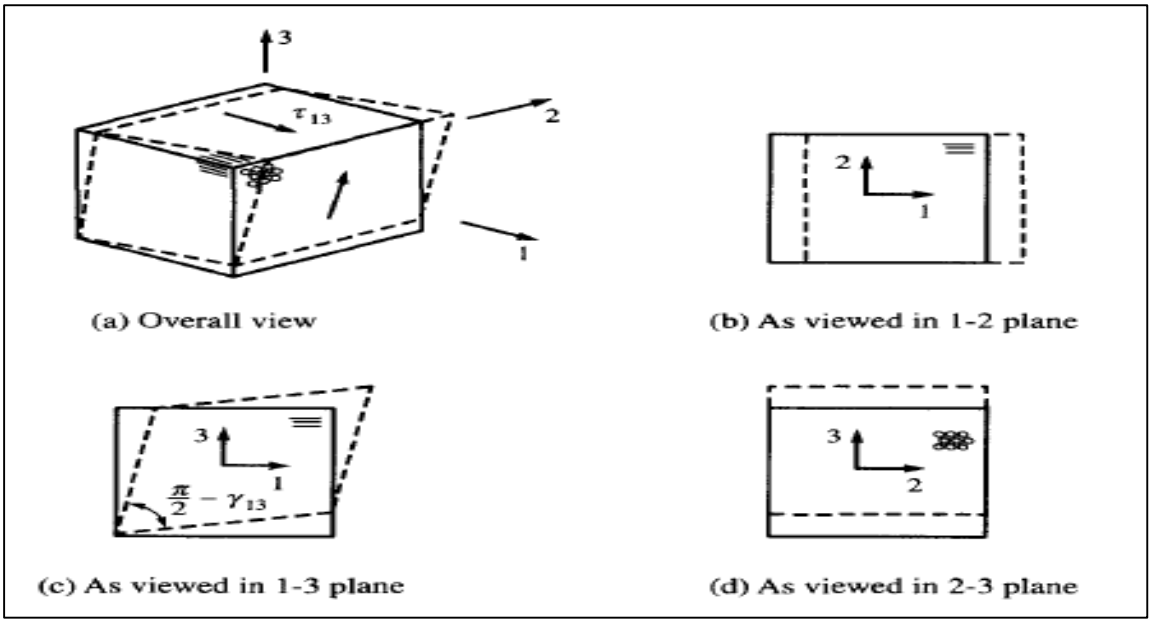

*Figure **II.16**: Deformation of an element [119].*

Similarly, as depicted in Figure **II.17**, a shear stress τ_{12} affects only the angles in the 1-2 plane, causing them to deform. As a result:

$$\gamma_{13} = \frac{\tau_{13}}{G_{13}} \tag{II.43}$$

And

$$\gamma_{12} = \frac{\tau_{12}}{G_{12}} \tag{II.44}$$

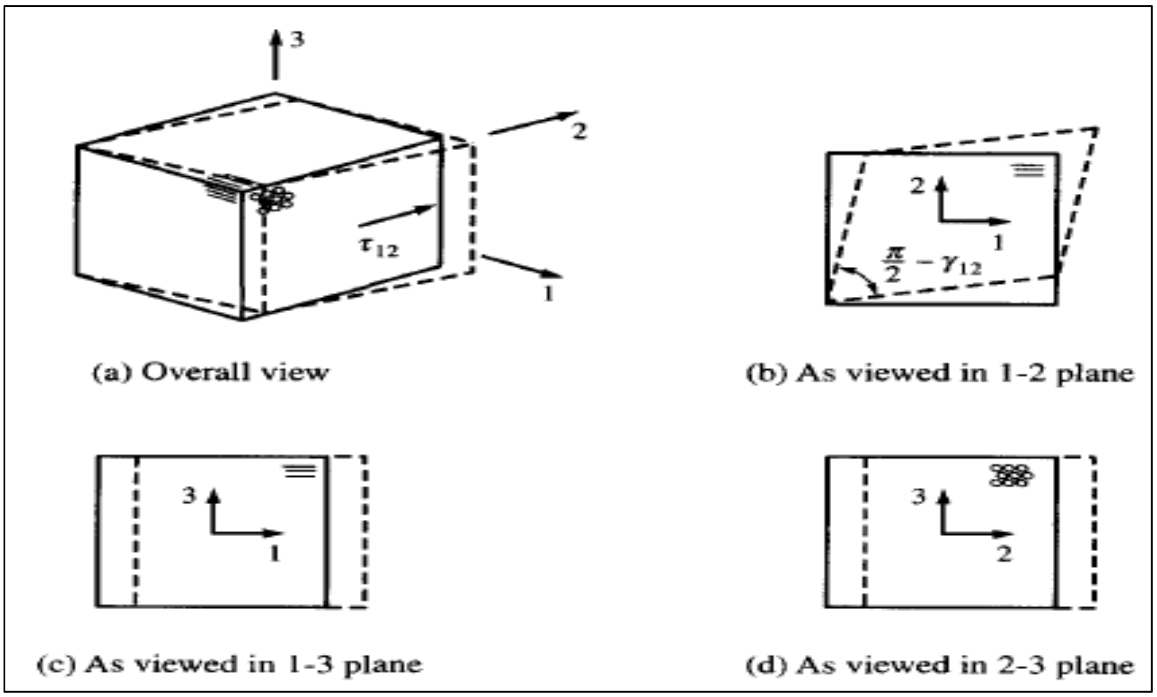

*Figure **II.17**: Deformation of an element [119].*

The quantities G_{13} and G_{12} represent the shear moduli in the 1-3 and 1-2 planes, respectively. The different extensional moduli, Poisson's ratios, and shear moduli are collectively known as engineering constants, or engineering properties. The analysis of fiber-reinforced composites relies on understanding the numerical values of these engineering constants, as they are crucial for predicting the material's behavior under various loading conditions. Before we proceed, it is important to note that implicit in the discussion so far is the assumption that:

$$\tau_{12} = \tau_{21}, \tau_{31} = \tau_{13}, \tau_{32} = \tau_{32} \tag{II.45}$$

This means that the shear stresses in the off-diagonal directions are symmetric, with the stress in one plane being equal to the stress in the corresponding plane, but with the indices swapped. This symmetry simplifies the analysis of shear stresses and their corresponding strains. Also, in the application of the theory of elasticity to the analysis of composite materials, the definitions of the tensor shear strains are given as:

$$\gamma_{ij} = \frac{\partial u_i}{\partial x_j} + \frac{\partial u_j}{\partial x_i} \tag{II.46}$$

Where γ_{ij} represents the shear strain tensor, u_i and u_j are the displacement components in the I and j directions, respectively. These definitions allow the shear strains to be expressed in terms of the changes in displacement in the directions normal and parallel to the plane of shear. The shear strain components describe the deformation of the material under shear stress, which is essential for understanding the behavior of composite materials. The shear strain components can be written as:

$$\gamma_{ij} = 2\varepsilon_{ij} \tag{II.47}$$

Where γ_{ij} is the shear strain and ε_{ij} is the engineering shear strain (also sometimes referred to as the strain in the material under shear stress). The factor of 2 comes from the definition of shear strain in the context of tensor analysis, where the total shear strain is twice the engineering shear strain. This relationship helps simplify the calculations in the analysis of composite materials, especially when considering the behavior of the material under shear stress.

$$\varepsilon_{12} = \frac{\gamma_{12}}{2}, \varepsilon_{13} = \frac{\gamma_{13}}{2}, \varepsilon_{23} = \frac{\gamma_{23}}{2} \tag{II.48}$$

Finally, it will be assumed that the elastic properties of the composite in compression in the 1, 2, and 3 directions are the same as those in tension. This assumption simplifies the analysis, as it means that the material behaves symmetrically under both tensile and compressive stresses. When considering the elastic properties of a composite material in both tension and compression, and assuming that the material behaves symmetrically under both tensile and compressive stresses, the relationships between the stresses and strains can be expressed in a matrix form that includes 9 components. This includes normal stresses, shear stresses, and their corresponding strains. The matrix form of the relationships between the 9 stress components σ_{ij} and the 9 strain components ε_{ij} is:

$$\begin{pmatrix}\sigma_1\\ \sigma_2\\ \sigma_3\\ \gamma_{23}\\ \gamma_{13}\\ \gamma_{12}\end{pmatrix}=\begin{pmatrix}\frac{1}{E_1} & -\frac{v_{21}}{E_2} & -\frac{v_{31}}{E_3} & 0 & 0 & 0\\ -\frac{v_{12}}{E_1} & \frac{1}{E_2} & -\frac{v_{23}}{E_3} & 0 & 0 & 0\\ -\frac{v_{13}}{E_1} & -\frac{v_{23}}{E_2} & \frac{1}{E_3} & 0 & 0 & 0\\ 0 & 0 & 0 & \frac{1}{G_{23}} & 0 & 0\\ 0 & 0 & 0 & 0 & \frac{1}{G_{13}} & 0\\ 0 & 0 & 0 & 0 & 0 & \frac{1}{G_{12}}\end{pmatrix}.\begin{pmatrix}\sigma_1\\ \sigma_2\\ \sigma_3\\ \tau_{23}\\ \tau_{13}\\ \tau_{12}\end{pmatrix} \quad \text{(II.49)}$$

The square 6x6 matrix of material properties that describes the relationship between the stresses and strains in a composite material is called the compliance matrix. This matrix relates the applied stresses to the resulting strains, and it incorporates the material's elastic properties, such as the Young's moduli, Poisson's ratios, and shear moduli. Typically represented by S, the stress-strain relationships are expressed in terms of S for an orthotropic material, the compliance matrix is represented as:

$$\begin{pmatrix}\sigma_1\\ \sigma_2\\ \sigma_3\\ \gamma_{23}\\ \gamma_{13}\\ \gamma_{12}\end{pmatrix}=\begin{pmatrix}S_{11} & S_{12} & S_{13} & 0 & 0 & 0\\ S_{21} & S_{22} & S_{23} & 0 & 0 & 0\\ S_{31} & S_{32} & S_{33} & 0 & 0 & 0\\ 0 & 0 & 0 & S_{44} & 0 & 0\\ 0 & 0 & 0 & 0 & S_{55} & 0\\ 0 & 0 & 0 & 0 & 0 & S_{66}\end{pmatrix}.\begin{pmatrix}\sigma_1\\ \sigma_2\\ \sigma_3\\ \tau_{23}\\ \tau_{13}\\ \tau_{12}\end{pmatrix} \quad \text{(II.50)}$$

The inverse of the compliance matrix is the stiffness matrix, also known as the modulus matrix or elasticity matrix, denoted as C. This matrix relates the stress components to the strain components and describes the material's response to applied forces. For an isotropic material, the stiffness matrix is the inverse of the compliance matrix. The stress-strain relationship, using the stiffness matrix, is given by:

$$\begin{pmatrix}\sigma_1\\ \sigma_2\\ \sigma_3\\ \tau_{23}\\ \tau_{13}\\ \tau_{12}\end{pmatrix}=\begin{pmatrix}C_{11} & C_{12} & C_{13} & 0 & 0 & 0\\ C_{21} & C_{22} & C_{23} & 0 & 0 & 0\\ C_{31} & C_{32} & C_{33} & 0 & 0 & 0\\ 0 & 0 & 0 & C_{44} & 0 & 0\\ 0 & 0 & 0 & 0 & C_{55} & 0\\ 0 & 0 & 0 & 0 & 0 & C_{66}\end{pmatrix}.\begin{pmatrix}\sigma_1\\ \sigma_2\\ \sigma_3\\ \gamma_{23}\\ \gamma_{13}\\ \gamma_{12}\end{pmatrix} \quad \text{(II.51)}$$

For an anisotropic material, the material properties vary in all directions, and there is no symmetry in the material's behavior. This type of material requires a full 6x6 compliance matrix to account for the varying properties in all directions, including the interactions between normal and shear stresses and strains. The compliance matrix for an anisotropic material relates the strains to the stresses in all directions. It is generally written in the following form:

$$\begin{pmatrix} \sigma_1 \\ \sigma_2 \\ \sigma_3 \\ \tau_{23} \\ \tau_{13} \\ \tau_{12} \end{pmatrix} = \begin{pmatrix} S_{11} & S_{12} & S_{13} & S_{14} & S_{15} & S_{16} \\ S_{21} & S_{22} & S_{23} & S_{24} & S_{25} & S_{26} \\ S_{31} & S_{32} & S_{33} & S_{34} & S_{35} & S_{36} \\ S_{41} & S_{42} & S_{43} & S_{44} & S_{45} & S_{46} \\ S_{51} & S_{52} & S_{53} & S_{54} & S_{55} & S_{56} \\ S_{61} & S_{63} & S_{63} & S_{64} & S_{65} & S_{66} \end{pmatrix} \cdot \begin{pmatrix} \sigma_1 \\ \sigma_2 \\ \sigma_3 \\ \gamma_{23} \\ \gamma_{13} \\ \gamma_{12} \end{pmatrix} \quad \text{(II.52)}$$

CHAPTER III

Mechanical Testing of Composite Materials

I. Introduction

Composite materials and products are developed from raw constituent materials, with testing conducted at various levels, as explored in this chapter. Unlike isotropic materials, composites are inherently anisotropic, requiring a broader set of material parameters for design, analysis, quality control, and quality assurance. Consequently, composite testing is more complex, and significant research has been conducted in this field. However, the test methods discussed here are not exhaustive. The primary goal of testing is to generate valuable data on the mechanical and non-mechanical properties of a material or structure.

The most common objective of testing is to generate data for product design and analysis. Material selection and preliminary design calculations are typically based on material properties available in the literature. Another key objective of testing is quality control and quality assurance, ensuring that materials and products meet specified standards and performance requirements. It is crucial to identify the materials actually used in product manufacturing, and some level of testing may still be necessary for quality control and quality assurance purposes.

The third key objective is materials research, aimed at enhancing existing materials and developing new, more efficient material systems. Tests can be broadly classified into different levels: coupon-level tests (including constituent-level tests on fibers and resin, lamina-level tests, and laminate-level tests), structural element-level tests, and component-level tests. Component-level tests are further divided into subscale and full-scale component-level tests.

Composite laminates may contain holes, cutouts, bonded interfaces, and other discontinuities. Tests for designing such structural elements or ensuring quality control fall under this level. While standard test coupons exist for certain cases, such as lamina or laminate tensile strength with a hole and interface adhesive strength, specially designed subscale test components are sometimes used for specific testing needs. Following these guidelines helps manufacturers and researchers develop and assess materials and products, ensuring results that are accurate and consistent with industry practices.

Standard test methods are essential for evaluating the mechanical and non-mechanical properties of materials such as fibers, resins, laminae, and laminates. These methods ensure consistency, accuracy, and reproducibility across tests, which is crucial for material performance evaluation and product development. A typical standard test method covers several key components to define the parameters and procedures for testing. These include the scope of the test, test specimen and sampling, apparatus, equipment, and machinery, physical principles, test procedure, and calculation and reporting of results.

The scope of the test defines the purpose and application, specifying the material or product being tested and the conditions under which the test is applicable. It clarifies the specific property being measured, whether mechanical, thermal, or another characteristic. The test specimen and sampling section specifies how the test specimens should be prepared and how they represent the material or product being

tested. It includes the dimensions, number of specimens, and how to sample the material to ensure uniformity and fairness in testing.

The apparatus, equipment, and machinery section outlines the specific equipment required, including machines, instruments, and other devices. It defines calibration, setup, and operation procedures to ensure accurate results, and may specify tolerances for equipment performance. The physical principle section explains the scientific or physical principles behind the test, describing how the material's behavior is measured and providing context for understanding the test results.

The test procedure section provides step-by-step instructions for conducting the test, including how to apply the load or stimulus, the environmental conditions to maintain (e.g., temperature, humidity), the duration of the test, and how to handle the specimens during and after the test. This ensures consistent testing, regardless of the tester. Finally, the calculation and reporting of results section outlines how to process raw data, including formulas for calculations and statistical methods. It also defines the format for reporting results, ensuring clarity and consistency, which is essential for comparing results across different tests or labs.

Various organizations, such as ASTM (American Society for Testing and Materials) and ISO (International Organization for Standardization), work to develop, revise, and promote these standards. They collaborate with industry experts, researchers, and manufacturers to ensure that standards remain up-to-date and reflect current technology. These organizations also provide certifications and guidelines to ensure that testing is conducted in accordance with established norms. Standards play a crucial role in ensuring the quality, consistency, and reliability of testing methods for composite materials [93].

II. Tests on Reinforcement

II.1. Non mechanical Tests on Reinforcement

Non-mechanical tests are used to evaluate properties like thermal stability, moisture absorption, chemical resistance, and other environmental factors that could impact the performance of reinforcement materials. Table **III.1**show the common test methods for these parameters[93].

*Table **III.1**. Standard Testing Procedures for Non-Mechanical Properties of Reinforcements [93].*

Parameter	Description	Principle of Testing	ASTM Standard
Density	Mass per unit volume	Method of displacement	ASTM D792
		Archimedes principle	ASTM D3800
		Density-gradient column	ASTM D1505
Moisture content	Mass of moisture per unit mass of reinforcement	Moisture removal by oven drying and weighing	ASTM D123

Filament diameter	Diameter of individual filament	Plan metering, indirect method based on density and linear density	ASTM D3379
Tex	Mass per unit length	Direct measurement and vibroscope procedure	ASTM D1577
Fabric construction	Filament count and weave	Direct counting	ASTM D3775
Fabric areal density	Mass per unit area	Direct measurement	ASTM D3776

II.1.1. Density

The density of both continuous and discontinuous high-modulus fibers can be measured according to ASTM D3800 using either the buoyancy method, based on Archimedes' principle, or the sink–float method [125]. The fiber density calculated by dividing its mass by this volume:

$$\rho_f = \frac{W_1}{\frac{W_2 - W_1}{\rho_l}} \tag{III.1}$$

Where:

W_1: Fiber weight in air (g)

W_2: Fiber weight in the test liquid (g)

ρ_f: Density of fiber (g/cm^3)

ρ_l: Density of test liquid (g/cm^3)

II.1.2. Moisture content

A standard test method for measuring the moisture content of roving, yarns, or fabrics typically involves using a small fabric piece or a roll of roving weighing around 2 g. The process starts by drying and weighing a glass weighing bottle. The sample is then placed in the bottle, weighed at room temperature, and heated at 105–110°C to remove moisture[93]. After heating, the sample and container are reweighed, and the moisture content is calculated based on the difference between the initial and final weights. The moisture content (M.C) of the sample is calculated using the following formula [8]:

$$M.C(\%) = \frac{W_2 - W_3}{W_3 - W_1} x100 \quad \text{(III.2)}$$

Where:

W_1: Mass of the empty glass weighing bottle (g).

W_2: Mass of the glass weighing bottle containing the sample before moisture removal (g).

W_3: Mass of the glass weighing bottle containing the sample after oven drying (g).

II.1.3. Filament diameter

The diameter of an individual filament can be determined using two methods: direct measurement through photomicrography and an indirect calculation based on linear density and material density.

a. **Direct Measurement (Planimeter Method)**

This method involves capturing a high-magnification photomicrograph of the filament cross-section at 2000–3000 times magnification**.** The cross-sectional area is then measured using a planimeter, a device designed to determine irregular areas. The filament diameter is then derived from the measured area, ensuring a precise and accurate determination of individual fiber dimensions.

b. **Indirect Calculation Method**

An alternative approach estimates the filament's cross-sectional area (F_{CSA}) using its tex value (weight in grams per kilometer) and density (g/mm²). The formula used is:

$$F_{CSA} = \frac{Tex}{Density} \quad \text{(III.3)}$$

Since this method relies on measuring a bundle of fibers, it provides only an average filament diameter rather than the exact measurement of a single filament. Proper unit conversion is crucial to ensure accuracy in this approach. While the direct method offers greater precision, the indirect method is useful for obtaining a quick estimate of filament dimensions, especially when handling large fiber bundles. Then, the average filament diameter is given by:

$$d_f = 2x\sqrt{\frac{A}{\pi}} \quad \text{(III.4)}$$

II.1.4 Tex

Tex is a commonly used unit for measuring the linear density of fibers, representing the mass per unit length of either an individual filament or a fiber bundle (such as strand or yarn). It is defined as the mass in grams per 1000 meters of fiber. ASTM D1577 prescribes two primary methods for determining the tex of fibers: the direct mass measurement method and the vibroscope procedure[121]. In the direct mass measurement method, a fiber of a known length, typically 1000 meters, is cut and weighed using a precision balance. The tex value is then calculated by dividing the mass of the fiber (in grams) by its length (in kilometers). This method is straightforward and commonly used for coarser fibers or fiber bundles. The vibroscope procedure is a non-destructive method that measures the natural frequency of vibration of the fiber to determine its mass per unit length. This method is especially useful for delicate or fine fibers, where direct weighing might not be feasible. Both methods provide accurate measurements, with the vibroscope being preferred for fine fibers and the direct method typically used for coarser fibers or fiber bundles.

In the direct method, tex is easily calculated by dividing the mass (in milligrams) by the length (in millimeters) of the fiber and multiplying the ratio by 1000. However, this method is not suitable for individual filaments shorter than 30 mm, as it may not provide accurate measurements for such small lengths. In the vibroscope method, the fundamental resonant frequency of an individual fiber is measured using a vibroscope. By applying known conditions, such as the length of the fiber and the tension applied, the linear density (tex) can be calculated from the fiber's fundamental resonant frequency of transverse vibration. This method is particularly useful for staple fibers with low linear density, as it allows for precise measurements without needing to directly weigh the fibers.

II.1.5. Fabric construction

Two key parameters that define fabric construction are filament counted weave. These factors are essential because they directly affect various fabric characteristics, such as handleability, drapeability, stability, fabric thickness, and how the fiber properties transition into fabric properties. ASTM D3775 outlines the standard procedure for measuring filament count in fabrics, which involves directly counting the filaments under suitable magnification. This measurement plays a significant role in determining the overall structure and behavior of the fabric.

II.1.6. Areal density of fabric

Fabric areal density, or mass per unit area, can be determined through the tests prescribed by ASTM D3776. The procedure involves directly measuring the mass of a fabric specimen with specified dimensions. To calculate the areal density, the net mass of the fabric is divided by the product of the

specimen's length and width. This method provides a straightforward way to determine the fabric's mass per unit area.

II.2. Mechanical Tests on Reinforcement

The test methods for the following mechanical properties of reinforcements are covered:

- Tensile strength and modulus of a single filament
- Tensile strength and modulus of a tow
- Breaking strength of fabric

Table **III.2** provides a summary of the test methods for these mechanical properties.

*Table **III.2**. Standard Test Methods for Mechanical Parameters of Reinforcements [93].*

Parameter	Principle of Testing	ASTM Standard
Tensile strength and modulus of a single filament	Loading till failure	ASTM D3379
Tensile strength and modulus of a bundle of filaments	Loading till failure	ASTM D4018
Breaking strength of a fabric	Loading till failure	ASTM D7018/D5034/D5035

II.2.1. Tensile Properties by Single-Filament Tensile Testing

Single-filament tensile testing is used to measure the tensile strength and modulus of individual fibers. This method involves applying a gradually increasing load to a single filament until it breaks, allowing for the measurement of the force required for failure as well as the deformation of the fiber under stress. The tensile strength and modulus of fibers can be determined using the single-filament tensile testing method in accordance with ASTM D3379.

In single-filament tensile testing, the test specimen consists of an individual fiber of adequate length, carefully separated from a dry strand to avoid damage or stress concentrations. To facilitate handling and ensure accurate alignment during testing, the filament is mounted on a slotted cardboard tab, as illustrated in Figure **III.1.**

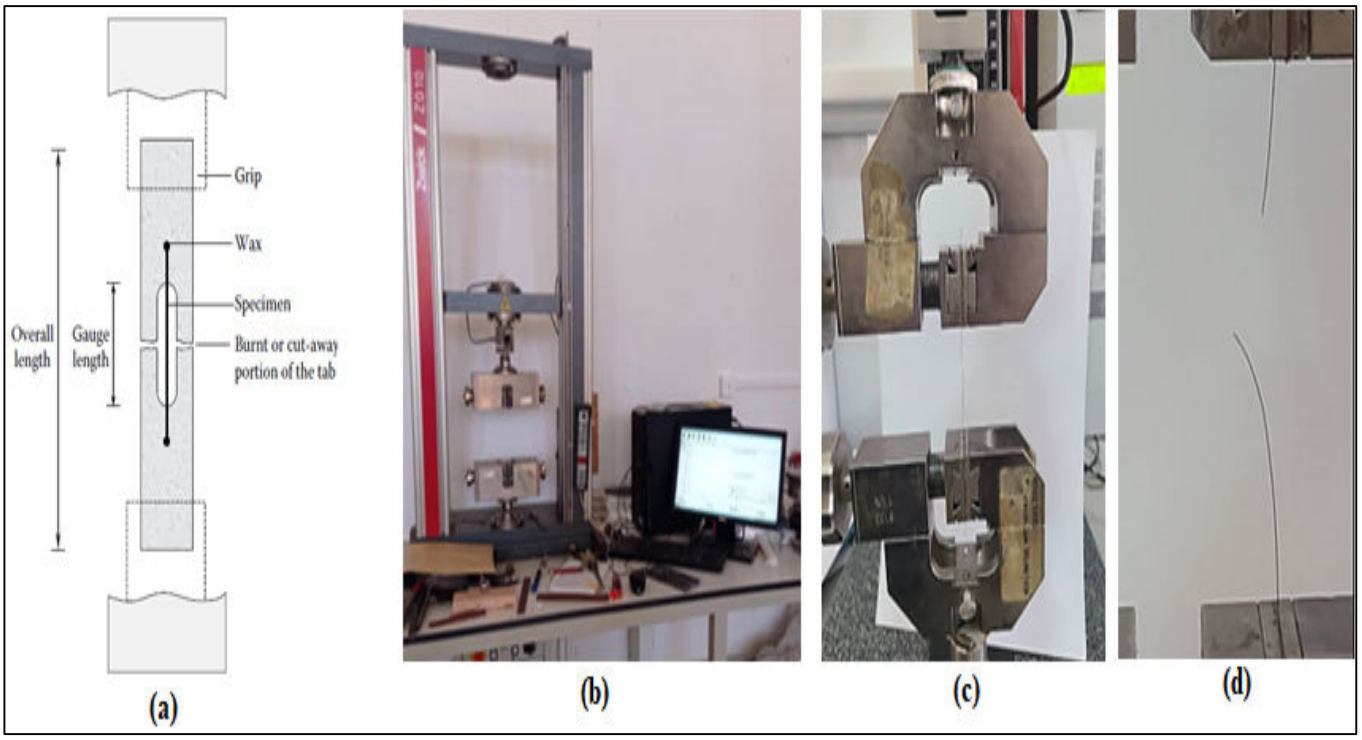

*Figure **III.1**: Single-Filament Tensile Testing Method (ASTM D3379-75): (a) Schema of tensile test equipment) [93], (b) Zwick/Roell Z10 machine, (c) sample under tensile force, (d) Specimen after failure.*

This mounting technique helps maintain the filament's straightness and prevents premature failure due to misalignment. The tabbed specimen is then clamped into a tensile testing machine, where the filament is subjected to a gradually increasing tensile load until failure. The applied load and the corresponding elongation are continuously recorded during the test. To ensure statistically meaningful results, a large number of specimens are tested. Tensile strength is calculated by dividing the failure load by the average cross-sectional area of the filament. This can be expressed as:

$$T_f = \frac{F}{A} \tag{III.5}$$

Where:

T_f: Tensile strength (N/mm^2)

F: The failure load (N).

A: The filament's average cross-sectional area (mm^2).

II.2.2. Determination of Filament Cross-Sectional Area and Tensile Modulus

a. Filament Cross-Sectional Area Measurement

The cross-sectional area of a filament is essential for accurate tensile property calculations. ASTM D3379 prescribes two methods for its determination:

The direct method for determining filament cross-sectional area involves capturing a photomicrograph of the filament at a magnification of 2000–3000×, followed by measuring the cross-sectional area using a planimeter to ensure precise assessment of the filament's actual shape.

The filament's linear density Ld (g/mm) is divided by its material density d (g/mm³) to estimate the cross-sectional area (mm²):

$$A = \frac{Ld}{d} \tag{III.6}$$

b. Tensile Modulus Determination

The tensile modulus of a filament is derived from load-elongation data through the following process: Multiple specimens with different gauge lengths are tested under controlled tension. The elongation per unit load (apparent compliance) is calculated for each specimen. A gauge length–compliance curve is plotted, typically showing a linear relationship. The intercept at zero-gauge length represents system compliance, which is subtracted from apparent compliance to determine true compliance. Finally, the modulus is obtained by dividing the specimen gauge length by the product of true compliance and filament cross-sectional area.

The tensile modulus of a filament is determined through compliance analysis by testing multiple specimens with varying gauge lengths under controlled tension. A gauge length vs. compliance curve is plotted, which generally shows a linear relationship. The intercept of this curve represents the system compliance, which accounts for the deformation of the testing apparatus. To obtain the true compliance, the system compliance is subtracted from the apparent compliance, which is the elongation per unit load. Finally, the tensile modulus is calculated by dividing the specimen gauge length by the product of the true compliance and the filament's cross-sectional area. The tensile modulus is calculated using the following relationship:

$$E_f = \frac{L}{CA} \tag{III.7}$$

Where:

E_f : Tensile modulus of fiber (N/mm²).

L: Gauge length of the specimen (mm).

C: True compliance (mm/N).

A: Average filament area of cross-section (mm^2).

II.2.3. Tensile Properties by Tow Tensile Testing

Selecting individual filaments and mounting them on tabs can be a challenging process, often leading to inaccuracies, particularly when determining modulus. As an alternative, the tensile strength and modulus of fibers can be determined using the tow tensile testing method prescribed by ASTM D4018. This method provides a more reliable and efficient way to obtain these properties, as it involves testing a bundle of fibers rather than individual filaments. In addition to tensile strength and modulus, this method also allows for the determination of other important parameters such as the fiber's density and linear density (mass per unit length). The specimen for this test is a bundle of fibers that are impregnated with a suitable resin and then consolidated. The resin must be compatible with the fiber and any applied sizing. The impregnation and consolidation processes ensure the specimen is easier to handle and allow for uniform loading of the individual filaments during the test. Depending on the specimen configuration, tabs may or may not be used. For tabbed specimens, the gauge length between tabs is set to 150 mm, while untabbed specimens are designed with sufficient length to achieve a 150 mm gauge length between grips. The tensile test involves pulling the resin-impregnated and consolidated fiber bundle in a calibrated tensile testing machine until failure occurs. To accurately determine the fiber modulus, an extensiometer is attached to the specimen during testing. This method not only provides accurate measurements of tensile strength and modulus but also gives important additional data such as density and linear density, which are critical for evaluating fiber performance in composite materials. The tensile strength and modulus of the fiber are calculated using the following formulas:

$$\sigma^{T}{}_{1f} = \left(\frac{\rho_f}{\rho^{l}{}_{p}}\right).P \tag{III.8}$$

$$E_{Lf} = \left(\frac{\rho_f}{\rho^{l}{}_{p}}\right).\left(\frac{P_u - p_l}{\varepsilon_u - \varepsilon_l}\right) \tag{III.9}$$

Where:

$\sigma^{T}{}_{1f}$: Longitudinal tensile strength of fiber (MPa).

ρ_f : Density of fiber (g/cm^3).

ρ^{l}_{p} : Linear density of fiber (g/m).

P: Maximum tensile load (N).

E_{Lf} : Longitudinal Young's modulus of fiber (GPa).

P_u : Tensile load at upper strain limit (N).

P_l : Tensile load at lower strain limit (N).

ε_u : Upper strain limit

ε_l : Lower strain limit

II.2.4. Breaking Strength of Fabric

The breaking strength of a fabric refers to the tensile failure load per unit width, typically expressed as N per 25 mm. ASTM D5035 provides a method for determining the breaking strength and elongation of fabrics using strip specimens of width 25 mm or 50 mm, with a minimum length of 150 mm. The specimens are often cut along the warp and fill directions, depending on the requirements. The breaking strength is calculated by recording the load at failure during the test [135].

Additionally, ASTM D5034 outlines an alternative method known as the grab test, which is commonly used to measure the breaking strength and elongation of fabrics. In this method, a specimen of fabric with a width of 100 mm and a length ranging from 200–250 mm is tested. Two slits are made in the fabric, located midway between the two ends, leaving a central 25 mm section uncut [136]. This approach is particularly useful for evaluating the strength of fabrics that are subjected to real-world conditions. The breaking strength is determined by the load at which the fabric fails during testing.

II.3. Tests on matrix

II.3.1. Non mechanical Tests on Matrix

The density of cast resin and the viscosity of liquid resin are two essential non mechanical parameters of matrix materials, providing crucial information for the design and processing of Polymer Matrix Composites (PMCs). Another significant parameter is the glass transition temperature (Tg), which plays a critical role in determining in-process thermal cycles and the service temperature range of the material. Beyond these, other factors such as volatile content also hold importance, especially in specific resin systems where they can affect the overall performance. In the upcoming sections, we will explore the standard test methods used for determining resin density, viscosity, and Tg.

II.3.1.1. Density

The liquid displacement method (ASTM D792) is used to determine the density of cast resin based on Archimedes' principle. The process involves weighing the resin specimen both in air and in water. The weight difference between the specimen in air and water gives the weight of the displaced water [137]. Knowing the density of water (approximately 1 g/cm³), the volume of the resin sample is calculated. Finally, the density of the resin is obtained by dividing the specimen's weight in air by its calculated volume. The formula for calculating the resin density is:

$$\rho_m = \frac{W_1}{W_1 - W_2} \tag{III.10}$$

Where:

ρ_m : Density of cast resin (g/cm^3).

W_1: Weight of the cast resin sample in air (g).

W_2: Weight of the cast resin sample fully immersed in water (g).

In the density-gradient method, a specimen is cut from the cast resin into a suitable shape and size, ensuring the center of volume is identifiable. The specimen is placed in a density-gradient column, which contains a solution of linearly varying density, created by mixing two suitable liquids and maintaining a precise temperature. A standard glass float of known density is first placed into the column to record its equilibrium position relative to a reference plane. The glass float is removed without disturbing the gradient, and then another glass float with a different known density is introduced, followed by the specimen. The equilibrium positions of each are recorded. The density of the specimen is determined by linear interpolation between the known densities of the floats, using the following formula:

$$\rho_m = (\rho_2 - \rho_1).\left|\frac{Z_m - Z_1}{Z_2 - Z_1}\right| + \rho_1 \tag{III.11}$$

Where:

ρ_m , ρ_1 and ρ_2 : densities of the cast resin sample and the two standard glass floats, respectively (g/cm^3)

$Z_m, Z_1,\ Z_2$ distances, w.r.t. an arbitrary datum, of the cast resin sample and the two standard glass floats, respectively (mm).

II.3.1.2. Viscosity

Viscosity is a crucial property of liquid resins, directly influencing the proper impregnation of reinforcement materials during manufacturing. It is a key parameter evaluated for quality control and acceptance processes in resin-based composite production. There are several methods for measuring viscosity, with three commonly used instruments being:

a. Rotational-Type Viscometers (Brookfield viscometers)

These are based on the principle that the torque required to turn a spindle in a viscous fluid is proportional to the fluid's viscosity. In these instruments, a spindle is immersed in the fluid, and a calibrated spring measures the torque, which is displayed as a viscosity reading. ASTM D2393 outlines the standard method for measuring resin viscosity using this type of instrument[93].

b. U-Tube Viscometer (Ostwald's)

This device works on the capillary principle. It consists of a U-shaped glass tube with precise dimensions. The fluid is drawn through one arm and allowed to flow through the other. The time it takes for the fluid to pass between two marked levels is used to determine the viscosity of the liquid.

c. Flow-Cup Viscometer

This instrument comprises a cup with an orifice through which the fluid is allowed to flow. The time taken for a known volume of the fluid to pass through the orifice is used to determine its kinematic viscosity.

II.3.1.3. Glass Transition Temperature (Tg)

Tg refers to the temperature at which a polymer matrix undergoes a transition from a glassy state to a rubbery state as it is heated. In the glassy state, the molecular segments of the material can only move vibrationally, with no relative movement between them. In contrast, in the rubbery state, the molecular segments can move relative to each other. This transition occurs at a specific temperature, known as Tg.

When the material is heated and reaches this temperature, its modulus (rigidity) decreases significantly, often by several orders of magnitude. This change is accompanied by a shift in heat capacity and coefficient of thermal expansion (CTE). Tg is crucial because it indicates the maximum service temperature for the resin matrix, beyond which the material may lose its structural integrity and performance.

Tg is influenced by the molecular structure of the resin and the curing conditions. Specifically, the Tg of a resin matrix cured at a higher temperature tends to be higher than that of the same material cured at a

lower temperature. This property is critical in determining the suitability of the resin for specific applications where temperature resistance is essential.

a. Differential Scanning Calorimetry (DSC)

DSC is the most widely used method to determine Tg. It measures the heat flow into or out of a sample as a function of temperature. When a polymer transitions from the glassy to the rubbery state, there is an endothermic heat absorption due to the molecular motion starting. This results in a change in the heat flow, which can be used to determine the Tg[93]

b. Dynamic Mechanical Analysis (DMA)

DMA measures the mechanical response of a polymer sample as it is subjected to oscillatory stress over a range of temperatures. The storage modulus (which reflects the material's elasticity) and loss modulus (which reflects the material's viscosity) are measured, and the Tg can be identified as the temperature where there is a significant drop in storage modulus.

Tg is identified in DMA as the temperature where the storage modulus drops significantly, and the loss modulus reaches its peak**.** This point marks the transition from a rigid (glassy) state to a more flexible (rubbery) state[93].

c. Thermomechanical Analysis (TMA)

Thermomechanical Analysis (TMA) is a technique used to measure the dimensional changes of a material as it is heated or cooled under a controlled force. This method is particularly useful for characterizing how materials expand or contract with temperature, which can be correlated with specific thermal transitions, such as the glass transition temperature (Tg)**.** TMA measures the dimensional changes of a material as it is heated or cooled under a controlled force. The glass transition temperature (Tg) can be identified as the temperature where there is a sharp increase in the dimensional change, marking the transition from a rigid (glassy) state to a more flexible (rubbery) state[93].

II.4. Mechanical Tests on Matrix

Mechanical testing of the matrix material in composites is crucial for evaluating its performance and suitability for various applications. These tests assess key properties such as strength, stiffness, and durability, which are essential for ensuring the matrix can effectively support and bond with reinforcing fibers. Common mechanical tests include tensile, compressive, flexural, and impact testing, each providing insights into how the matrix behaves under different loading conditions. These tests help in understanding the matrix's ability to withstand stresses, its deformation characteristics, and its overall structural integrity in composite materials[93]

II.4.1. Tensile Properties

The tensile properties of neat cast resin are commonly determined using a dog-bone-shaped specimen, as specified by ASTM D638. The most widely used specimen dimensions are 165 mm in overall length, 19 mm in overall width, and 3.2 mm in thickness, with a gauge section of 50 mm length and 13 mm width. During testing, the specimen is subjected to tension by gripping it in a testing machine, which moves at a constant cross-head speed[122]. The tensile strength is calculated by dividing the maximum force by the average original cross-sectional area in the gauge section. Extensometers are used to monitor elongation, and force-extension curves are continuously recorded. The modulus is calculated from the initial linear portion of the curve, where the difference in stresses between two points is divided by the difference in strains at those points. This method provides accurate measurements of both tensile strength and modulus.

II.4.2. Compressive Properties

The compressive properties of neat cast resin are evaluated using the standard method outlined in ASTM D695. The typical test specimen is either a short cylinder (12.7 mm diameter × 25 mm height) or a prism (12.7 mm × 12.7 mm × 25 mm). The specimen is placed between two hardened, flat plates of a compression tool, ensuring that the end faces are parallel and aligned with the plunger of the testing machine. During the test, compressive force is applied at a constant cross-head rate of 1.3 mm/min until the yield point is reached[123, 124].

After yielding, the cross-head speed is increased to 5–6 mm/min to continue loading until failure. The compressive strength is calculated by dividing the maximum compressive force by the original minimum cross-sectional area of the specimen. To determine stress–strain data, a compressometer is used to record the force–displacement curve, from which the modulus of elasticity is calculated by drawing a tangent to the initial linear portion of the curve.

II.4.3. Shear Properties of Cast Resins

The shear properties of cast resins can be evaluated using two primary methods.

II.4.3.1. V-notched Beam Method

The ASTM D5379 test method is commonly used to evaluate the shear properties of composite materials at the lamina or laminate level. This test involves a V-notched specimen, which is subjected to a shear force to assess its response to shear stress. The V-notched beam test provides critical data on the material's shear strength, stiffness**,** and toughness, making it particularly valuable for analyzing fiber-reinforced composites and other advanced materials. This method ensures accurate characterization of shear behavior, aiding in material selection, quality control, and structural design[125].

II.4.3.2. Torsion Cylinder Method

This method is employed to determine the shear modulus of structural materials, including cast resins**,** by evaluating their response to torsional forces. The test involves subjecting a solid cylinder or a hollow tube to an externally applied torque, which induces twisting deformation in the specimen. By precisely measuring the angle of twist under the applied load, the shear modulus (G) can be accurately calculated. This technique provides critical insights into a material's resistance to shear deformation**,** making it particularly valuable for applications requiring high torsional rigidity and strength. The procedure follows the standards outlined in ASTM E143, ensuring reliable and repeatable results.

III. Tests for Lamina/Laminate Properties

Lamina and laminate properties are crucial for understanding the mechanical performance of composite materials, especially fiber-reinforced composites. These tests evaluate how individual layers (lamina) and multiple layers (laminate) of composite materials behave under various loading conditions. Below are the key tests used to assess lamina/laminate properties:

III.1. Non-Mechanical Tests on Laminae

Non-mechanical tests are crucial for evaluating the physical, chemical, and thermal properties of composite materials, especially laminae (individual layers) within laminates. These tests help assess the quality, durability, and performance of composite materials under different environmental conditions. Below are the key non-mechanical tests commonly used for laminae in composite materials:

III.2. Density Measurement

The density of a cured composite material is an important property that influences its mechanical and thermal behavior. It plays a significant role in applications where weight reduction is crucial, such as in aerospace, automotive, and structural engineering. The principles and methodology for measuring the density of a cured composite material are similar to those used for cast resins. One of the most commonly used methods for this measurement is the liquid displacement method, as outlined in ASTM D792.

III.3. Void Content

Void content represents the percentage of air gaps or voids present in a composite material, which are formed due to incomplete resin infiltration, trapped air, or improper curing. It is calculated as the difference between the theoretical density and the measured density of the composite. ASTM D2734 is a standard test method used to determine the void content in reinforced polymer matrix composites. Void content is a crucial parameter in composite materials because excessive voids can significantly reduce mechanical properties such as strength, stiffness, and durability [126]**.**

$$V_v = \left(\frac{\rho_t - \rho_c}{\rho_t} \right) \quad \text{(III.12)}$$

Where:

V_v: Void content (%)

ρ_t: Theoretical density of the composite (g/cm³)

ρ_c: Measured (actual) density of the composite (g/cm³)

The theoretical density is based on the known densities of the fiber and resin:

$$\rho_t = \left(\frac{1}{\frac{W_f}{\rho_f} + \frac{W_m}{\rho_m}} \right) \quad \text{(III.13)}$$

Where:

W_f, W_m: Weight fractions of fiber and matrix

ρ_f, ρ_m: Densities of fiber and matrix (g/cm³)

The weight fractions are calculated using the following equations:

$$W_f = \frac{M_f}{M_f + M_m} \quad \text{(III.14)}$$

And

$$W_m = \frac{M_m}{M_f + M_m} \quad \text{(III.15)}$$

Where:

M_f: Mass of the fiber (g)

M_m: Mass of the matrix (resin) (g)

III.4. Water Absorption

Water in epoxy composites exists as condensed water in fractures and molecularly dispersed water in the matrix. Incorporating hydrophilic lignocellulosic fibers increases moisture absorption due to hydroxyl groups forming hydrogen bonds with water. This leads to poor fiber-matrix compatibility, reduced interfacial bonding, and dimensional instability, which can impact the composite's mechanical properties and durability[126]. Water absorption studies were conducted in accordance with ASTM D570, which specifies procedures for determining the water absorption characteristics of polymeric materials. The test involves immersing a composite specimen in water at a controlled temperature for a specified duration. After immersion, the specimen is removed, surface water is wiped off, and the specimen is immediately weighed. The percentage of water absorbed is calculated using the formula[127]:

$$W_{abs}(\%) = \frac{W_t - W_0}{W_0} x100 \qquad \text{(III.16)}$$

Where:

W_t: Weight of the specimen after immersion (g)

W_0: Initial dry weight of the specimen (g)

III.5. Mechanical Property Testing of a Lamina

The mechanical properties of a lamina play a crucial role in the design and analysis of composite materials. These properties can be categorized into the following groups:

III.5.1. Tension properties

Tension Testing is a crucial mechanical test used to assess a material's behavior under tensile forces. It provides essential data for understanding a material's strength, elasticity, and ductility, which are key for engineering design and material selection. During the test, a specimen is subjected to a gradually increasing tensile force until failure, and several important properties are measured:

a. Tensile Strength:

Tensile Strength is the maximum stress a material can withstand while being stretched. It represents the material's resistance to breaking under tension. Young's Modulus, measures the material's stiffness by defining the ratio of stress to strain in the elastic region of the material's stress-strain curve.

To ensure that the specimen fails in the gauge section under a uniaxial stress state, it is important to use standard specimen shapes that promote failure in the intended area. For isotropic materials and materials

with low orthotropic**,** dog-bone-shaped (Figure**III.2**) or dumb-bell-shaped specimens are typically used. These specimens have a tapered width in the central section, as specified by ASTM D 638. This shape helps concentrate the applied stress in the gauge section, ensuring that the material fails in a controlled and predictable manner during the tension test.

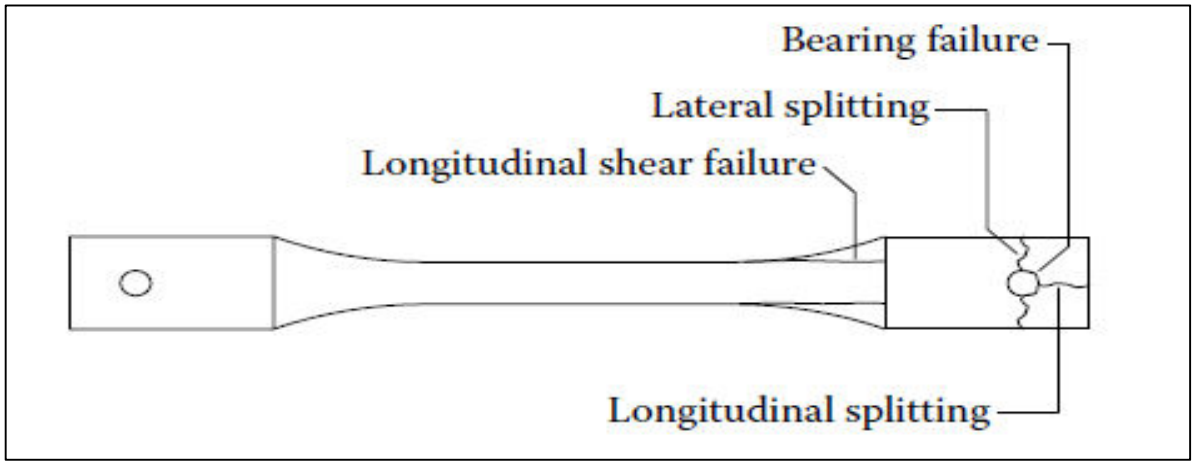

*Figure **III.2**: A dog-bone-shaped tensile test specimen with end holes is a variation of the standard dog-bone or dumb-bell-shaped specimen, commonly used in tensile testing [93].*

Several standard specimens and test procedures are commonly used for tensile testing, including ASTMD3039, BS 2782, and ISO 527. Among these, ASTM D3039 is perhaps the most widely recognized and accepted standard. The standard specimen as per ASTM D3039 (shown in Figure **III.3**) typically has a simple rectangular shape.

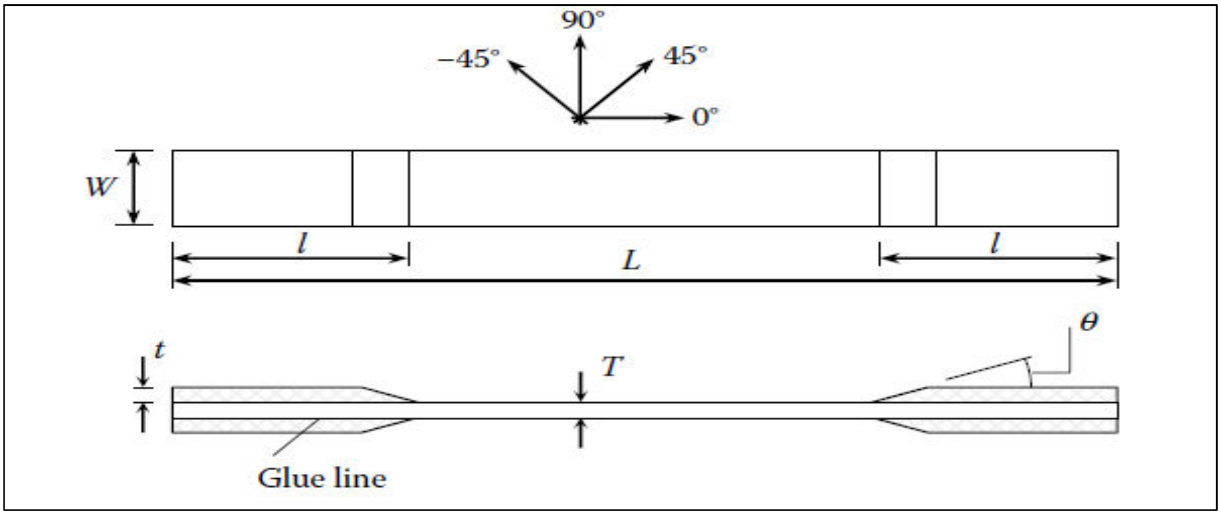

*Figure **III.3**: The tension test specimen as described in ASTM Standard D3039/D3039M-08, titled Standard Test Method for Tensile Properties of Polymer Matrix Composite Materials [93].*

The recommended dimensions for the tension test specimen are detailed in Table **III.3**. It's important to note that the specific dimensions of the specimen can vary based on factors such as the type of material, the laminate fabrication method, and other material-specific considerations. These variations ensure that the specimen is appropriately tailored to the particular characteristics of the material being tested, allowing for accurate and reliable measurement of its tensile properties**.**

*Table **III.3**: Standard Tensile Test Specimen as Recommended by ASTM D3039 [93].*

Type	**Unidirectional (0°)**	**Unidirectional (90°)**	**Balanced and Symmetric**	**Random and Discontinuous**
Overall Length, L (mm)	250	175	250	250
Width, W (mm)	15	25	25	25
Thickness, T (mm)	1.0	2.0	2.5	2.5
Tab Length, l (mm)	56	25	a	a
Tab Thickness, t (mm)	1.5	1.5	a	a
Tab Bevel Angle, θ (°)	7–90	90	a	a

Note:(a) indicates that the dimensions or specifications are not applicable or vary based on the specific material or test conditions[93].

Tensile strength can be calculated using the following formula:

$$T_s = \frac{P_{ult}}{A} \tag{III.17}$$

Where:

T_S: Tensile strength of composite (MPa).

P_{ult} : The maximum load the specimen can withstand before failure (N).This refers to the maximum load that the material can withstand before it fails or breaks. It is the peak value observed on the load **vs.** elongation (or strain) curve during the tensile test. The ultimate tensile load is often used to calculate the tensile strength of a material.

A: The average area of the specimen's gauge section (mm^2).

To calculate the modulus (Young's Modulus) from the stress-strain curve, stress is calculated from each data point by dividing the applied load (P) by the average cross-sectional area (A)**.** The formula for stress at any data point is:

$$\sigma = \frac{P}{A} \tag{III.18}$$

Where:

σ : Axial tensile stress at any data point (MPa)

P: Tensile load at any data point (N). This refers to the load value at any specific moment or data point during the tensile test. It can be measured at various stages of the test, such as at a certain elongation or strain value. The load may increase or decrease as the material undergoes elastic or plastic deformation.

$$\varepsilon = \frac{\Delta L}{L_0} \tag{III.19}$$

Where:

ΔL: The change in length of the specimen, measured by the extensometer (mm).

L_0: The original length of the specimen (mm).

b. Tensile modulus

The Tangent Modulus (also known as the elastic modulus in the linear portion of the stress-strain curve) is the slope of the tangent line to the stress-strain curve at any given point within the elastic region of a material. It represents the instantaneous stiffness of the material at that point, which means it tells you how much stress is required to produce a small change in strain at that specific point. The tangent modulus is primarily defined in the elastic region of the stress-strain curve, where the material behaves in a linear-elastic manner, and the stress is proportional to the strain. In this region, the material returns to its original shape once the stress is removed. For calculate Tangent Modulus (Figure **III.4**):

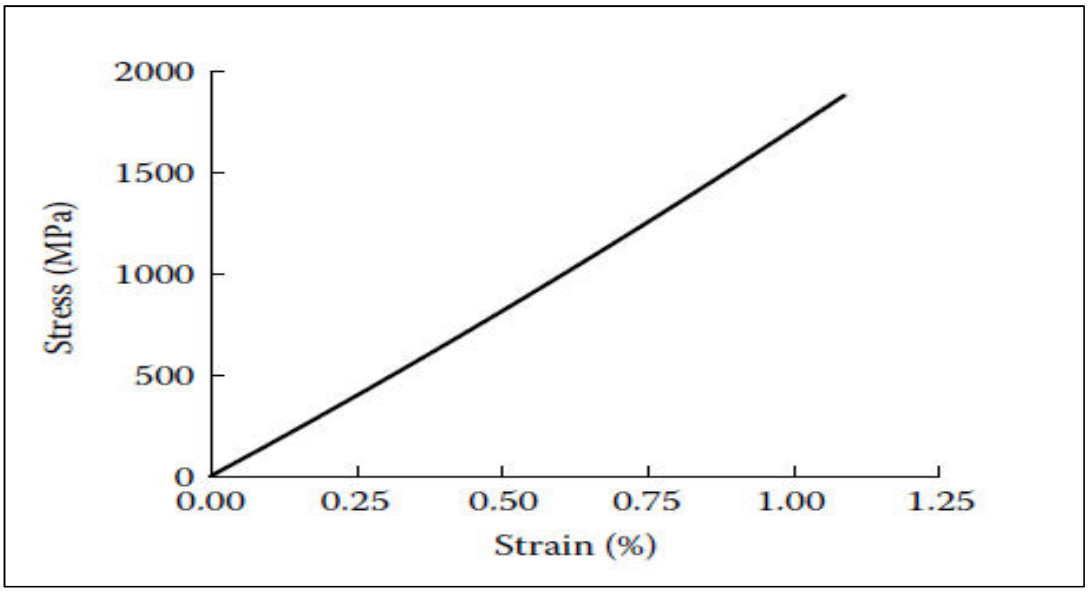

*Figure **III.4**: A schematic representation of a typical tensile stress-strain curve [93].*

a. Obtain the Stress-Strain Data**:** First, you need the stress-strain curve of the material. The curve is typically obtained from a tensile test, where stress is plotted against strain.
b. Select a Point**:** Choose a point on the curve where you want to determine the tangent modulus. This point should ideally lie within the elastic region (where the material behaves elastically).
c. Draw a Tangent Line: At the selected point, draw a tangent line to the curve. This tangent line represents the instantaneous stiffness of the material at that specific point.
d. Calculate the Slope**:** The slope of this tangent line is the tangent modulus. If you have the data points from the stress-strain curve, you can calculate the slope between two points near the selected point to approximate the tangent modulus.

For example, if the stress at point 1 is σ_1 and at point 2 is σ_2, and the strain at point 1 is ε_1 and at point 2 is ε_2, the tangent modulus can be approximated as:

$$E^T = \frac{\sigma_1 - \sigma_2}{\varepsilon_1 - \varepsilon_2} = \frac{\Delta\sigma}{\Delta\varepsilon} \qquad \text{(III.20)}$$

Where:

E^T : Tensile modulus (GPa).

$\Delta\sigma$: Stress difference on the tangent (MPa).

$\Delta\varepsilon$: Corresponding axial strain difference on the tangent.

Poisson's ratio ($\mathcal{V}_t$) is a fundamental mechanical property that defines the relationship between axial and lateral deformation in a material subjected to uniaxial stress. It is expressed as the ratio of lateral strain (perpendicular contraction or expansion) to axial strain (elongation or compression) when a material is subjected to a tensile or compressive load. When a tensile test is performed, the material elongates in the direction of the applied load (axial direction), while simultaneously contracting in the transverse (perpendicular) direction. Conversely, under compressive loading, the material shortens axially and expands laterally. Poisson's ratio quantifies this effect, providing insight into the material's deformation behavior and its tendency to maintain volume during mechanical loading.

$$v_t = -\frac{\Delta\varepsilon_l}{\Delta\varepsilon_a} \tag{III.21}$$

Where:

v_t: Poisson's ratio in tension.

$\Delta\varepsilon_l$: Lateral strain difference corresponding to the longitudinal strain difference.

$\Delta\varepsilon_a$: Axial strain difference.

c. Compressive properties

In a compression test, a gradually increasing compressive force is applied to a specimen until failure, while recording its response to the load. The force versus strain (or displacement) data, along with the specimen's geometry, are used to calculate key compressive properties such as compressive strength, modulus, and yield strength. The ultimate compressive force, which is the maximum force the material withstands before failure, is a critical parameter. This test helps evaluate a material's ability to resist deformation and failure under compressive loads, making it essential for structural and engineering applications.

Under compressive loads, materials typically exhibit two broad failure modes: material failure and global buckling. Material failure occurs when the internal structure of the material can no longer withstand the applied load, leading to fracture or plastic deformation Global buckling, on the other hand, is a structural instability that causes the specimen to bend or collapse due to excessive compressive forces. When a composite material is subjected to longitudinal compression (force applied parallel to the fiber direction), several failure modes can occur, including:

1- Fiber microbuckling in extension occurs when compressive stresses cause localized fiber instability, leading to slight out-of-plane bending of the fibers even in the direction of axial compression, resulting in structural weakening.

2- Fiber Microbuckling in Shear: A more common form, where fibers buckle due to instability under combined axial and shear stresses, often leading to a kink band formation and progressive collapse of fiber alignment.
3- Transverse Tensile Failure of the Matrix and Fiber/Matrix Interface: Under compressive loading, tensile stresses perpendicular to the loading direction can develop, causing cracks in the matrix or at the fiber-matrix interface due to weak adhesion or low transverse tensile strength.
4- Shear Failure by Fiber Kinking: This occurs when shear stresses exceed the critical limit, causing fibers to misalign in a kinked pattern, often leading to localized shear band formation and overall failure.

When a composite material is subjected to transverse compression meaning the compressive force is applied perpendicular to the fiber direction several failure modes can occur due to the anisotropic nature of the material and the relative weakness of the matrix in that direction. These include:

1- Compression Failure of the Matrix: The matrix, being less stiff and strong than the fibers, can collapse or yield under high compressive stress, leading to local crushing and material degradation.
2- Shear Failure of the Matrix: High shear stresses can cause the matrix to deform or crack along shear planes, especially in areas where stress concentration occurs.
3- Fiber Crushing: Although fibers are generally stronger in the axial direction, they may be crushed when compressed from the side, particularly in brittle fiber systems like carbon or glass.
4- Fiber-to-Matrix Interface Failure: Poor bonding or stress mismatch between fiber and matrix can lead to delamination or debonding at the interface, especially under transverse loading, where interfacial shear stresses are significant.

According to ASTM D3410, the standard compression test specimen is a simple flat strip with a constant rectangular cross-section, which may or may not include end tabs as shown in Figure **III.5**. The primary consideration in designing the specimen dimensions such as width, thickness, and gauge length is to prevent Euler buckling during testing. To achieve this, the specimen geometry must be tailored based on the material's anticipated compressive strength and modulus. In general, materials with lower compressive strength and modulus require thicker specimen**s** to maintain structural stability and ensure accurate measurement of compressive properties without premature buckling[128].

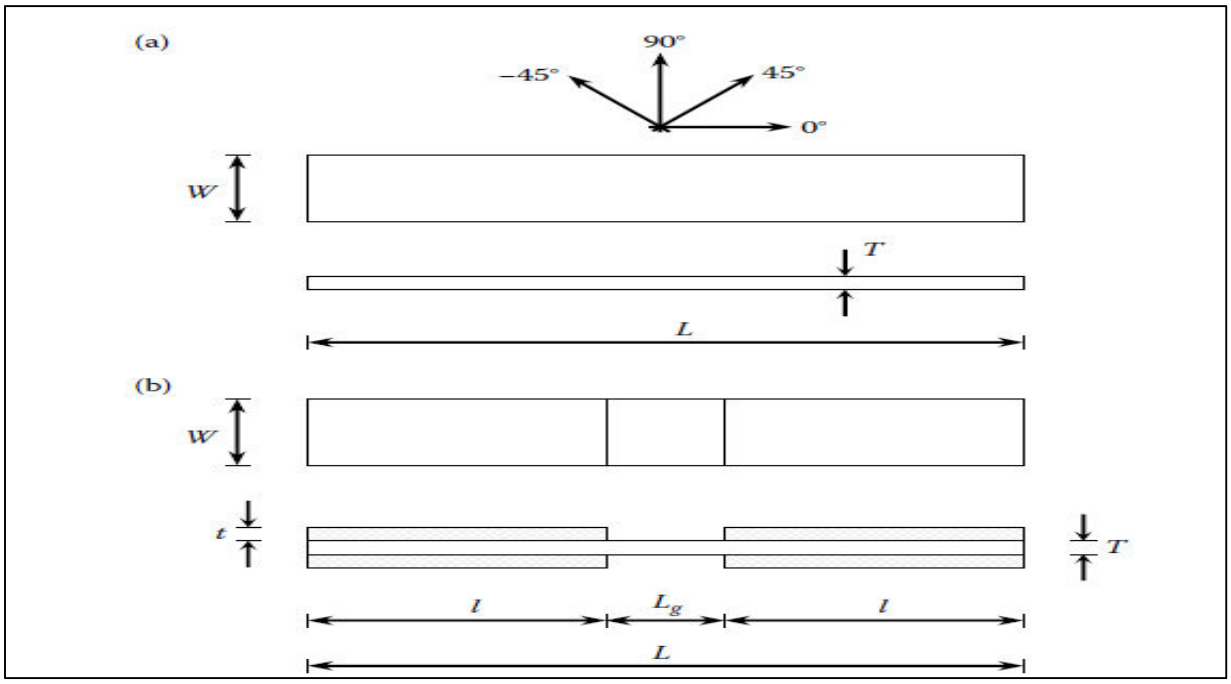

*Figure **III.5**: Compression Test Specimen: (a) Compression test specimen without end tabs, (b) Specimen with bonded tabs at both ends adapted from ASTM standard D3410/D3410M-03[93].*

The gauge length in compression testing must ensure a uniform uniaxial stress distribution while avoiding buckling. For shear-loaded specimens, a thicker specimen demands a longer gauge length to maintain stress uniformity. This length also depends on the ratio of longitudinal to shear modulus. Thus, selecting an appropriate gauge length is a trade-off between minimizing buckling and ensuring stress uniformity. ASTM D3410 provides recommended dimensions to balance these factors, assuming pinned-end column buckling conditions as given in Table **III.4.**

*Table **III.4**: Standard Compression Test Specimen Dimensions (ASTM D3410) [93].*

Type	Unidirectional (0°)	Unidirectional (90°)	Specially Orthotropic
Overall length, *L* (mm)	140–155	140–155	140-155
Gauge length, *Lg* (mm)	10–25	10-25	10-25
Width, *W* (mm)	10	25	25
Thickness, *T* (mm)	1.00–10.91	1.00–10.91	1.00–10.91
Tab length, *l* (mm)	65	65	65
Tab thickness, *t* (mm)	1.5	1.5	1.5

Compressive strength is determined by dividing the ultimate compressive force by the average cross-sectional area of the specimen:

$$C = \frac{F_{ult}}{A} \tag{III.22}$$

Where:

C: Compressive strength (MPa or N/mm²)

F_{ult} : Ultimate compressive force (N)

A: Average cross-sectional area (mm²)

Stress–strain curves are essential for calculating the modulus of elasticity (Young's modulus) of a material. At each data point during the test, **stress** is calculated by dividing the applied load by the average cross-sectional area of the specimen:

$$\sigma = \frac{F}{A} \tag{III.23}$$

Where:

σ : Axial compressive stress at any data point (MPa).

F: Applied compressive load at that data point (N).

A: Average cross-sectional area at the gauge section (mm^2)

The axial and lateral strains are calculated by averaging the readings from the two back-to-back strain gauges placed on the specimen. The axial and lateral strains at any given data point can be expressed as follows:

Axial strain:

$$\varepsilon_a = \frac{\varepsilon_{a1} + \varepsilon_{a2}}{2} \tag{III.24}$$

Where:

ε_{a1} and ε_{a2} are the axial compressive strains measured by Gauge 1 and Gauge 2, respectively, at the same data point.

Lateral stress:

$$\varepsilon_l = \frac{\varepsilon_{l1} + \varepsilon_{l2}}{2} \tag{III.25}$$

Where:

ε_{l1} and ε_{l2} are the lateral compressive strains measured by Gauge 1 and Gauge 2, respectively, at the same data point.

The secant modulus or chord modulus is a measure of the material's stiffness calculated as the slope of the line (secant or chord) connecting two points on the stress–strain curve. It is given by the following formula:

$$E^C = \frac{\Delta\sigma_a}{\Delta\varepsilon_a} \tag{III.26}$$

Where:

E^C : The compressive modulus (GPa),

$\Delta\sigma_a$: The axial stress difference (MPa) between two points on the curve,

$\Delta\varepsilon_a$: The corresponding axial strain difference between the two points.

Additionally, the compressive Poisson's ratio can be calculated from the axial and lateral strains using the following relationship:

$$v_c = -\frac{\Delta\varepsilon_l}{\Delta\varepsilon_a} \tag{III.27}$$

Where:

v_c : The compressive Poisson’s ratio,

$\Delta\varepsilon_l$: The lateral strain,

III.2.3. Shear properties

The primary goal of shear testing is to evaluate two key properties: (i) the shear modulus and (ii) the shear strength. Various testing techniques exist to assess the shear characteristics of composite materials, which are generally classified into two main types: in-plane shear tests and interlaminar shear tests.

III.2.3.1. The Short Beam Shear Test

Short beam shear test is based on the principles of three-point beam bending. In this test, a beam is supported at both ends and loaded in the center, generating both bending and shear stresses within the beam. The bending stresses are maximal at the top and bottom surfaces of the beam, being compressive at the top and tensile at the bottom beneath the loading point. For elastic materials, the bending stresses vary linearly across the thickness and change sign at the neutral plane, where the bending stresses become zero. In contrast, the interlaminar shear stresses follow a parabolic distribution, being zero at the top and bottom faces and peaking at the neutral plane, where the material is subjected to pure shear [93].

ASTM D2344 specifies two standard specimen types for the short beam shear test, the flat beam and the curved beam (Figure **III.6**). The span-to-thickness ratio should be limited to 4:1. Additional recommended dimensions are as follows: specimen thickness (minimum), h = 2 mm, specimen length, L = 6 h. and Specimen width, b = 2 h [105,133].

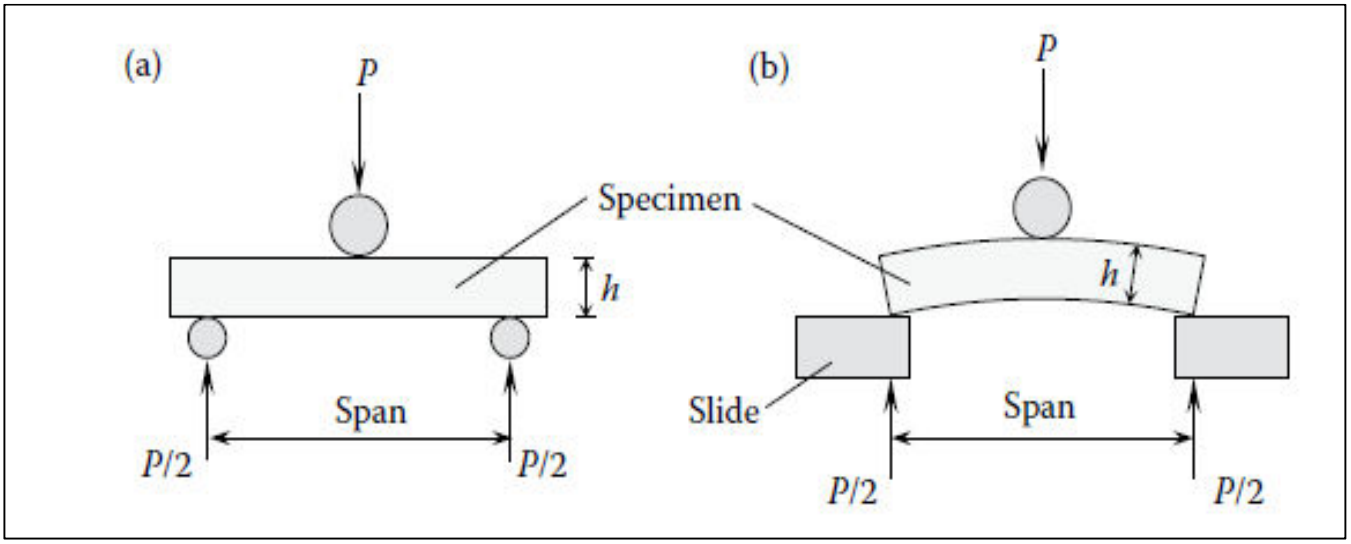

*Figure **III.6**: Short beam shear test: (a) Flat specimen, (b) Curved specimen. (Adapted from ASTM Standard D2344/D2344M-00, Standard Test Method for Short-Beam Strength of Polymer Matrix Composite Materials and Their Laminates, ASTM International, 2006.) [93].*

The specimen is supported on 3-mm-diameter rollers, with a central concentrated force applied using a 6-mm-diameter loading nose. Typically, load versus cross-head movement data is recorded, along with the final failure load. The interlaminar strength (also referred to as short beam strength) is calculated as follows:

$$S = \frac{3P_{ult}}{4bh} \tag{III.28}$$

Where:

S: Shear strength (MPa).

P_{ult} : Ultimate force at failure (N).

h : Specimen length (mm).

b : Specimen width (mm).

III.2.4. Flexural properties

The purpose of flexural testing is to measure both the flexural modulus and flexural strength of a material. Unlike tensile, compressive, or shear properties, however, flexural modulus and strength are not considered fundamental material properties. This is because bending induces a complex stress state that combines tensile, compressive, and shear stresses. Consequently, flexural values are not directly applicable for precise design calculations. Nevertheless, due to the straightforward nature of the test specimens and procedures, flexural tests are commonly employed particularly for material comparison and quality control purposes. The most commonly used method for flexural testing are the three-point bending test

III.2.4.1. Three-Point Flexure Test

The three-point flexural test, as specified by ASTM D790, serves as a standard technique for measuring the flexural strength and modulus of materials [134].

In a three-point flexure test, the specimen typically consists of a flat beam with a uniform rectangular cross-section [45]. While the precise dimensions of the specimen are not critical, it is essential to maintain an appropriate support span-to-thickness (L/h) ratio to ensure the specimen fails in bending rather than in shear. This ratio, which ranges from 16:1 to 60:1, depends on the material's tensile strength relative to its interlaminar shear strength [93].

The specimen is carefully placed on a properly aligned test fixture within the testing machine and loaded via a central loading nose by moving the cross-head at a constant speed. During the three-point bending process, the bending moment reaches its maximum at the midpoint of the span (as shown in Figure **III.7**). The highest bending stress develops at the outer surface of the specimen and is calculated accordingly[93]:

$$\sigma^{b} = \frac{3PL}{2bh^{2}} \tag{III.29}$$

Where:

σ^b : Bending stress on the outer surface (MPa).

P : Applied force (N).

L : Span of the specimen (mm).

b : Width of the specimen (mm).

h : Thickness of the specimen (mm).

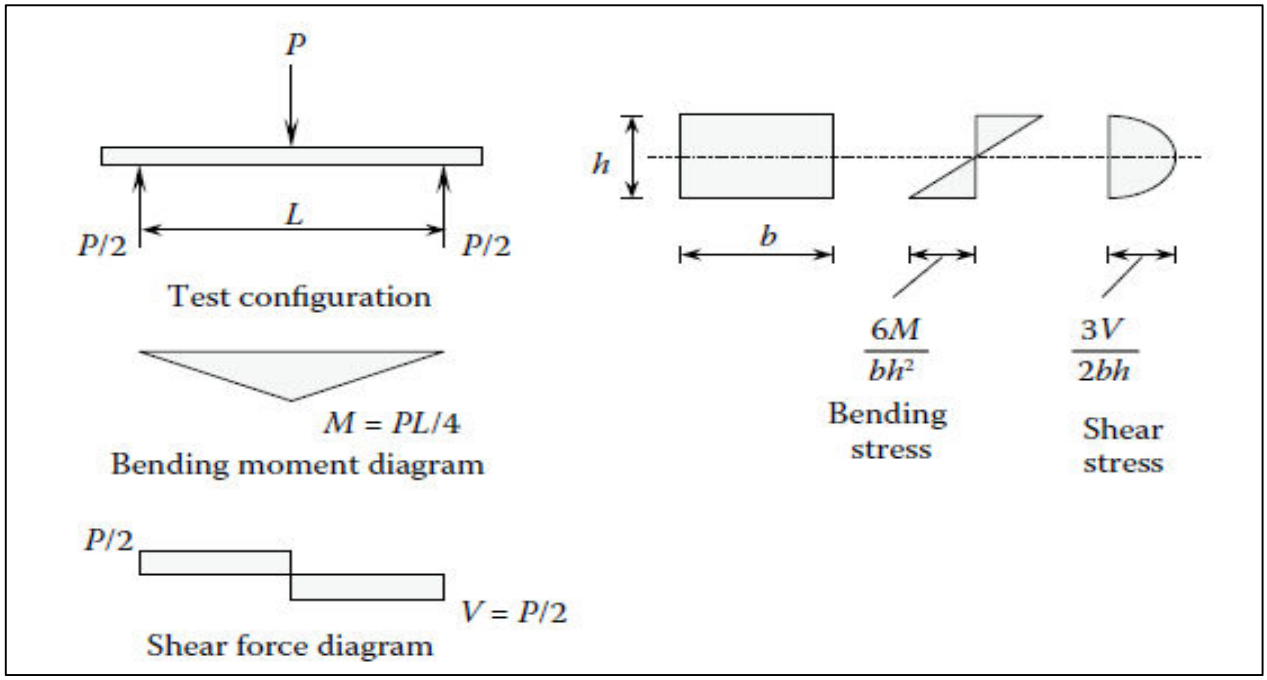

*Figure **III.7**: Configuration of the three-point flexure test and corresponding diagrams of bending stress and shear stress [93].*

The bending strain is calculated as:

$$\varepsilon^b = \frac{6\delta \cdot h}{L^2} \tag{III.30}$$

Where δ is the midspan deflection (deflection at the midpoint of the span).

The flexural modulus is determined from the initial linear region of the bending stress versus bending strain curve using the following equation:

$$E^b = \frac{L^3}{4bh^3}\left(\frac{\Delta P}{\Delta \delta}\right) \tag{III.31}$$

Where:

ΔP: Difference in applied forces at two points in the initial linear portion of the bending stress–bending strain plot (N).

$\Delta\delta$: Difference in midspan deflections at the corresponding points on the stress–strain curves (mm).

L: Span of the specimen (mm).

b : Width of the specimen (mm).

h : Thickness of the specimen (mm).

III.2.5. Low Velocity Impact Test

Low velocity impact (LVI) denotes an impact scenario in which the impacting object collides with the material at relatively low speeds, generally below 10 m/s. Although the velocity is low, such impacts can inflict considerable damage on composite materials due to their unique characteristics. Composites, including fiber-reinforced polymer (FRP) materials, are favored for their excellent strength-to-weight ratios and adaptability. Nevertheless, under low-velocity impacts, these materials may experience concealed or internal damage, such as matrix cracking, fiber breakage, and delamination, which can significantly compromise their structural integrity. When an object strikes a material, it imparts kinetic energy to that material. This energy can lead to deformation, cracking, or even penetration, contingent upon the energy level, the material type, and the impact geometry.

The impact test is intended to assess how a sample of a specific material, such as polymers, ceramics, or composites, reacts to a sudden application of force. This test serves to measure the toughness, brittleness, notch sensitivity, and impact strength of engineering materials under quick loading conditions. Being able to measure the impact characteristics is particularly beneficial for product safety and liability. Different types of impact test specimens include notches like V-notch, U-notch, and keyhole notch. Typically, impact testing uses Charpy and Izod specimen designs. The main difference between the Izod and Charpy tests lies in the notch's orientation facing the striker. In the Charpy test, the specimen is supported horizontally between two vertical beams, while in the Izod test, the sample is positioned vertically, similar to a fence post [129].

III.2.5.1. Charpy impact test

The Charpy impact test, established in 1900 by Georges Augustin Albert Charpy (1865-1945), is widely regarded as one of the most effective and economical methods for evaluating the toughness of materials. This test measures the energy absorbed by a standard notched specimen when it fails under an impact load. It serves as a valuable quality control technique for determining notch sensitivity and impact toughness in a variety of engineering materials, including metals, composites, ceramics, and plastics. A typical Charpy impact test specimen measures 55 mm x 10 mm x 10 mm and includes a notch on one of the larger sides, as illustrated in Figure e **III. 8**. The test quantifies the energy absorbed by the notched sample during fracture caused by an impact force. The procedure involves striking the specimen with a hammer connected to a pendulum arm, while the sample is securely clamped at both ends. The hammer strikes the side opposite the notch, and the energy absorbed is precisely measured by observing the decrease in the pendulum arm's motion[129]

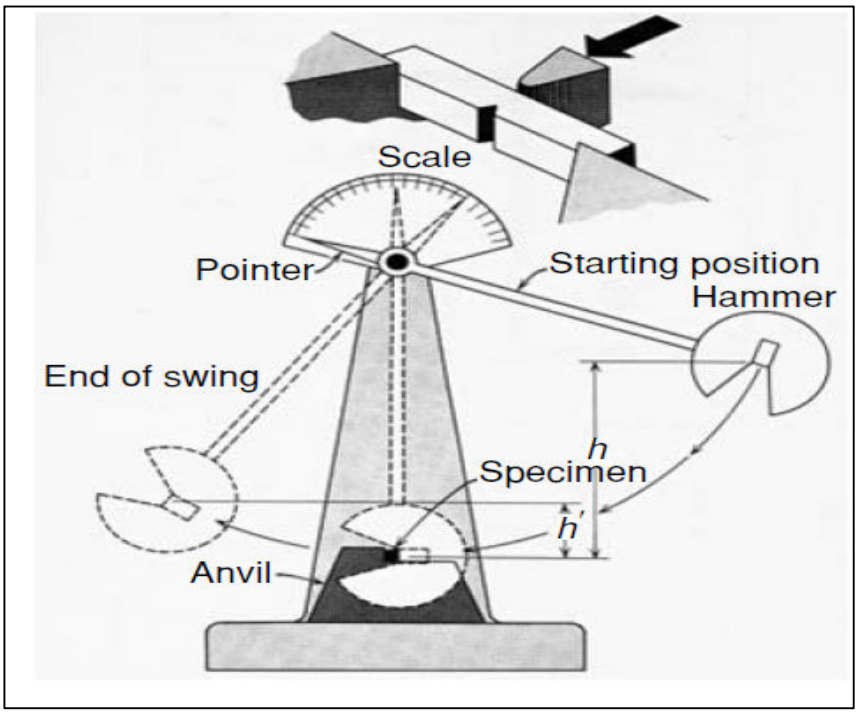

*Figure **III. 8**: Charpy test apparatus and specimen. A swinging hammer strikes the specimen. The elevation the pendulum reaches post-breakage reflects the energy taken in. From H. W. Hayden, W. G. Moffatt, and J. Wulff, Structure and Properties of Material[129].*

III.2.5.2. Izod impact test

The Izod impact test, named after the English engineer Edwin Gilbert Izod, is akin to the Charpy impact test and is employed to assess materials at low temperatures. In this method, a specimen is shaped into either a square or round form, featuring one, two, or three notches measuring 70 mm by 15 mm by 3 mm. The test utilizes a pendulum with a designated weight at the end of its arm, which swings downward to strike the specimen that is firmly held in a vertical position. The apparatus for creating the V-notch and performing the impact test is depicted in Fig. 1.4. The impact strength is evaluated by measuring the

energy loss of the pendulum, which is determined by precisely measuring the decrease in height of its swing. Furthermore, researchers have defined impact strength as the capacity of polymer composites to endure high-energy impacts without breaking. They have also observed that in fiber-reinforced and hybrid polymer composites, the impact properties are affected by the characteristics of the individual fibers used in hybridization, as well as the interlaminar and interfacial bonding between the fibers and the matrix[129].

III.2.5.3. Impact energy and transfer energy

The transfer of energy is a crucial principle in low-velocity impact (LVI) testing, wherein the kinetic energy from the impacting object is conveyed to the material under examination. This transfer may result in different types of deformation and failure in the material, influenced by its characteristics and the impact's energy level. When an object impacts a material, it has kinetic energy that is transferred to the material. The key energy equation for impact is:

$$E_k = \frac{1}{2} m v^2 \tag{III.32}$$

Where:

E_k: Kinetic energy of the impacting object (Joules)

m: Mass of the impacting object (kg)

v**:** Velocity of the impacting object (m/s)

III.2.5.4. Energy Absorption

The substance takes in a portion of the energy from the impact when it undergoes deformation. This energy absorption is generally represented as the space beneath the force-displacement graph throughout the experiment. The level of energy that gets absorbed serves as an indicator of the material's resilience. To determine the absorbed energy, the following equation can be used:

$$E_{absorpation} = \int_0^{\delta \max} F(\delta).d\delta \tag{III.33}$$

Where:

F(δ): Force as a function of displacement

δmax: Maximum displacement reached during the impact.

III.2.5.5. Rebound Energy

Rebound energy is the energy that is not absorbed by the material and is returned to the impacting object. The resilience of a material is influenced by its flexibility and rigidity. More flexible materials tend to rebound more efficiently, while those that are more brittle may absorb greater energy, resulting in a reduced rebound effect. It can be calculated as:

$$E_{rebound} = E_{initial} - E_{absorbed} \quad \text{(III.33)}$$

Where:

E initial: Total initial energy of the impacting object.

E absorbed: Energy absorbed by the material.

CHAPTER IV

Materials Employed, Methodologies Applied, and Characterization Approaches

I. Introduction

This chapter presents a comprehensive overview of the materials and procedures employed in this research. The methodologies and techniques implemented are thoroughly described herein. The study involved the execution of the following experimental activities:

Selection and Preparation of Natural Fiber and Resin: natural fibers and the epoxy resin matrix were meticulously selected based on their physical and mechanical properties to ensure compatibility. The fibers were then cleaned, treated, and dried as required, while the resin and hardener were prepared according to the manufacturer's specifications to achieve optimal performance during composite fabrication.

Composite Fabrication Techniques: suitable fabrication techniques were utilized to produce the composite specimens, adhering to standardized protocols to ensure uniformity and structural integrity. The process involved accurate weighing, proper mixing of the resin and hardener, and careful fiber placement within the mold. This was followed by curing under controlled conditions to achieve the desired composite structure.

Characterization and Analysis: the fabricated composite specimens were subjected to a range of characterization techniques to assess their physical, structural, and morphological properties. These analyses provided insights into fiber-matrix interaction, surface quality, and the overall integrity of the composites, serving as a foundation for evaluating their mechanical performance.

Mechanical Testing of Composites: a comprehensive set of mechanical tests was performed to evaluate the strength, stiffness, and durability of the composite materials under various loading conditions. These tests included tensile, flexural, and compressive strength assessments, providing critical data on the composites' ability to withstand mechanical stresses and validating their suitability for structural applications.

II. Experimental I: Fabrication of Single and Hybrid Composites Based on Wool Fiber and Periploca laevigata Aiton (PLA) Fibers

This experiment focused on the fabrication of both single-fiber and hybrid composite materials using untreated and treated wool fibers, as well as Periploca laevigata Aiton (PLA) fibers. The aim was to develop and compare the mechanical and structural performance of composites reinforced with individual fibers versus hybrid reinforcement.

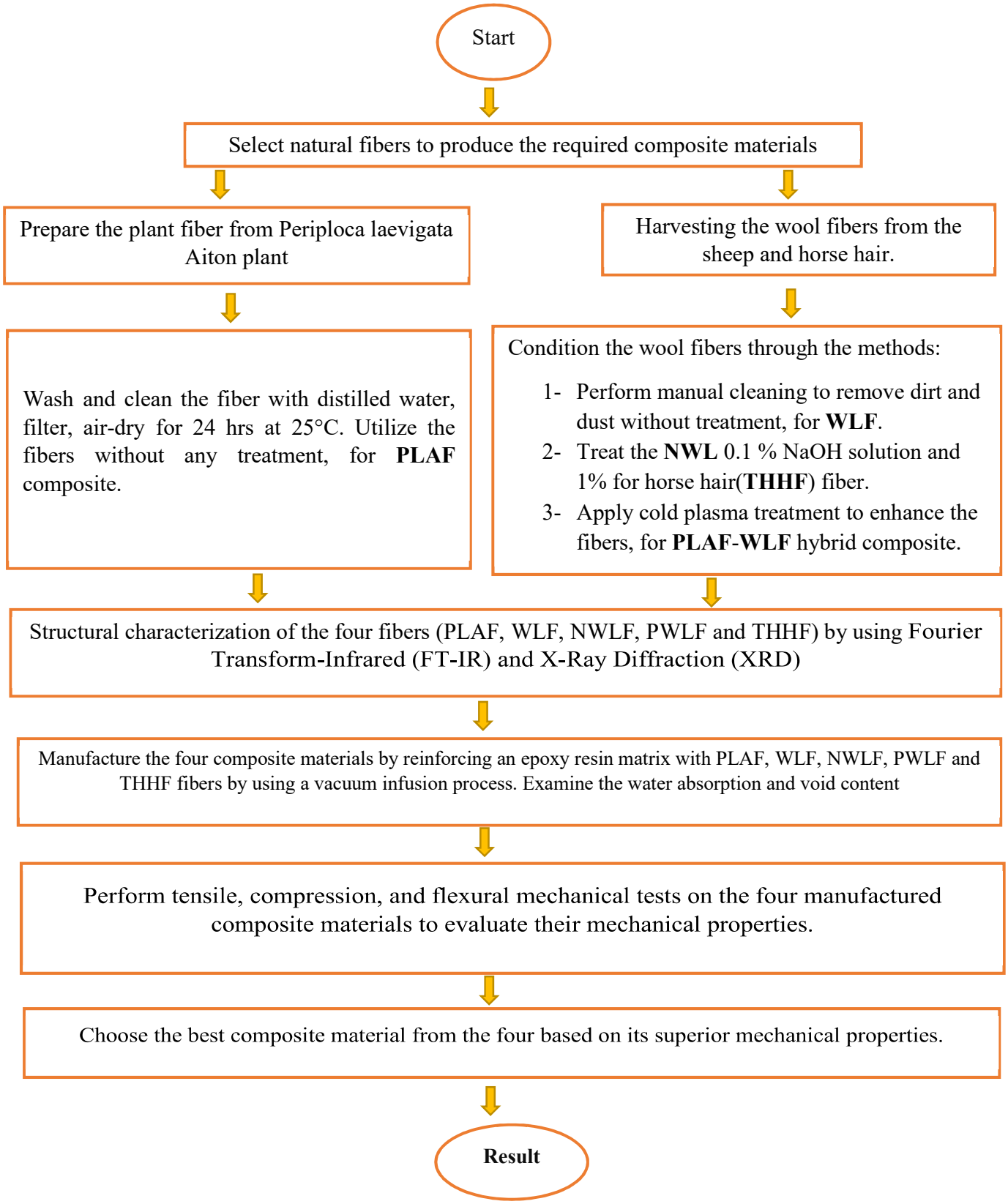

Figure **IV.1:** Applied Methodology [8].

II.1. Materials

II.1.1. Natural Fibers Selection

II.1.1.1. Wool fiber (WLF)

Animal fibers, such as sheep wool, alpaca hair, goat hair, horse hair, and fibers from other hairy mammals, are widely used in various industries. Wool, in particular, has been a staple in the clothing and textile sectors and will continue to play an important role in emerging applications. The process of transforming raw sheep wool into fabric involves several key steps: shearing, washing, drying, grading, sorting, carding, spinning, weaving, and finishing. Wool samples used in this study were sourced from sheep in the GHARDAÏA region of Algeria (Figure **IV.2**). The wool was sheared during the spring, resulting in greasy, raw wool that contained significant amounts of dirt, sand, oil, and dried sweat. One portion of this wool was manually cleaned to remove the dirt and dust, while another portion was treated with a 0.1% NaOH solution, and a third portion underwent treatment using cold plasma.

*Figure **IV.2**: Natural wool fiber sample.*

After cleaning, the wool fibers were combed through a series of thin metal teeth to untangle and smooth them. The fibers were then arranged into a flat strip, known as a weave, which was eventually spun into fine threads. After carding, the fibers were stretched and twisted to make them finer and ready for the spinning process. Figure **IV.3** illustrates the entire manufacturing process as depicted in this study.

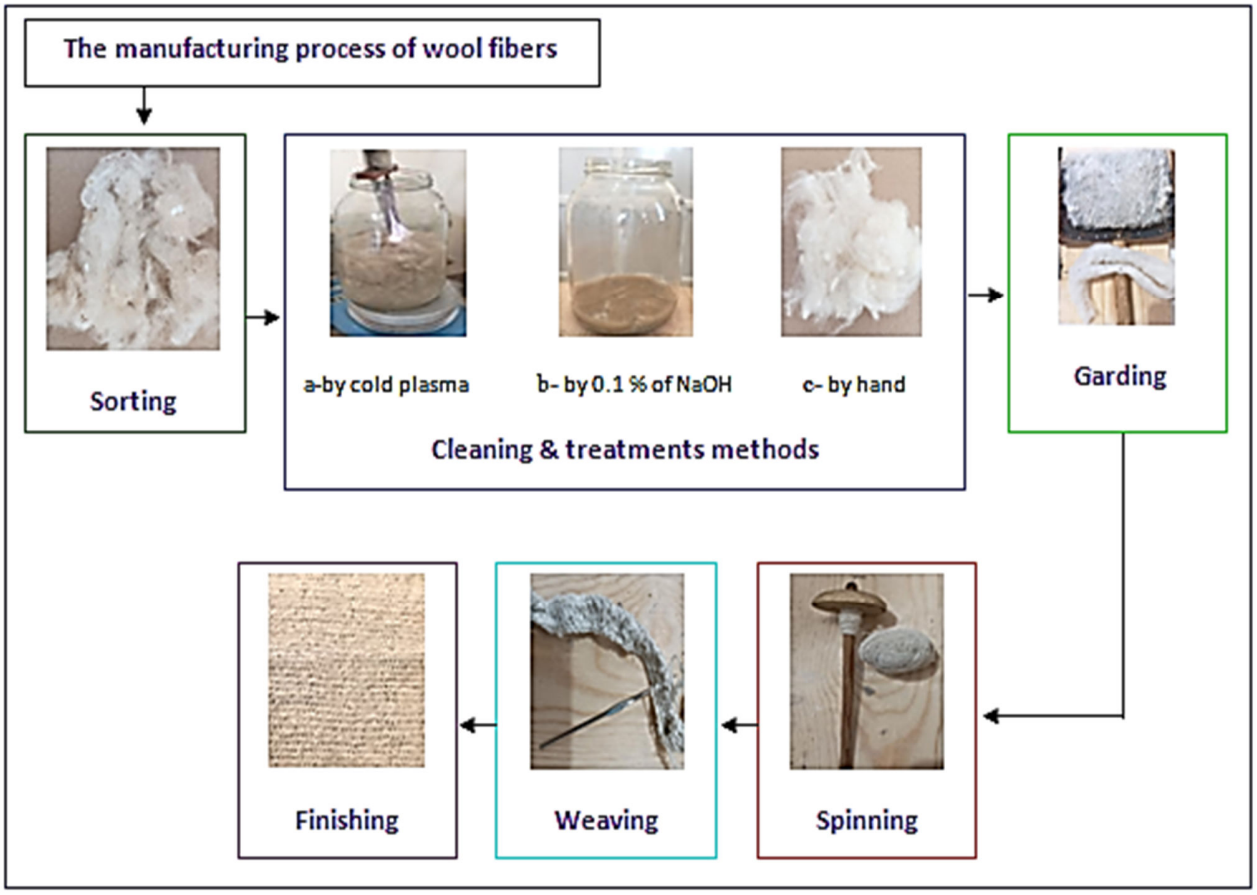

*Figure **IV.3**: Preparation of Wool Fiber, (a) Cold plasma treatment, (b) Treatment with 0.1% NaOH, and (c) Manual cleaning [8].*

II.1.1.2. Periploca laevigata Aiton (PLAF)

PLAF a perennial, heat-loving deciduous shrub, is commonly found across various regions of the Mediterranean, including Spain, Algeria, Libya, Tunisia, Karpathos, Egypt, Crete, Malta, and Sicily. This plant features drooping leaves and slender, lance-shaped branches. Its flowers are arranged in short, axillary cymes, with reddish-brown lobes bordered by a greenish-yellow hue, alternating with purplish, curved filaments. The fruit is dry and consists of two smooth, fissured follicles that contain anemocorous seeds[130, 131].

The fibers of Periploca laevigata Aiton are lightweight and short, easily carried by the wind once the lobes dry and crack naturally, as depicted in FigureIV.4a, Figure IV.4b, and Figure IV.4c. Given the delicate nature of the fibers and their natural characteristics, no extensive processing has been applied. The lobes were manually opened to extract the fibers, separating them from the seeds. The fibers were then thoroughly washed with distilled water at a temperature of 25°C, which helps to maintain their

structural integrity. After washing, the fibers were filtered and left to air dry at room temperature for 24 hours.

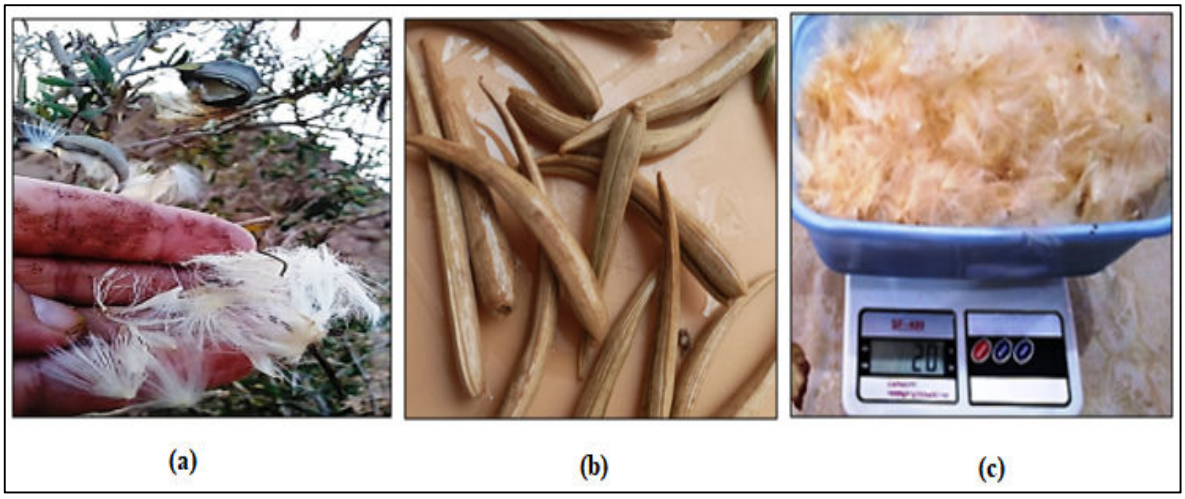

*Figure **IV.4**: The Periploca laevigata plant and its fibers. (a) Periploca laevigata Aiton plant, (b) Lobes containing fibers, and (c) Extracted fibers from the lobes.*

II.1.2. Fiber treatment

II.1.2.1. Chemical treatment method

Natural fibers are inherently hydrophilic, which presents significant challenges when incorporating them into polymeric composites due to the presence of hydroxyl groups in components such as lignin, cellulose, and waxes. The natural fibers' sensitivity to water complicates their integration with hydrophobic matrices. To address this issue, natural fibers must undergo treatment prior to the fabrication of green composite materials. Chemical treatments are commonly used to remove impurities and particles from the fiber surface, improving the bond between the fiber and the matrix and enhancing interfacial adhesion[81, 132].

Alkaline treatment, in particular, effectively disrupts the hydrogen bonds in the fiber's network structure, reducing moisture absorption, decreasing fiber diameter, and increasing the aspect ratio. This treatment also enhances surface roughness, promoting better mechanical cross-linking and exposing more cellulose on the fiber surface. Sodium hydroxide (NaOH) is one of the most widely used alkaline treatments for natural fibers[133, 134].

In this study, wool fibers were treated by immersion in a 5% NaOH solution for 30 minutes, which initiated fiber degradation. Further treatment with NaOH at varying concentrations (5%, 3%) led to different degrees of structural breakdown. The NaOH concentration was gradually reduced to a practical

0.1%, with each treatment lasting one hour. This concentration resulted in a uniformly rough fiber surface. After the treatment, the wool fibers were thoroughly washed with distilled water and dried at room temperature (25°C) for three days. Thus, 0.1% NaOH was selected as the optimal concentration for the chemical treatment in this experiment.

II.1.2.2. Cold plasma treatment method

Plasma surface treatment plays a crucial role in industrial applications due to its effectiveness and environmentally friendly nature. Cold plasma treatment is widely used to modify the surface properties of various fibers, including short glass, carbon, cellulose, polyimide, aramid, and others. Air plasma treatment has been employed to enhance the adhesion between cellulose fibers and thermoplastic starch matrices. Scanning electron microscopy (SEM) analysis of fractured surfaces reveals a significant improvement in the adhesion between treated cellulose fibers and the thermoplastic starch matrix[135, 136].

In this study, the applied electric field was generated using a gliding arc discharge powered by a 9 kV source operating at a frequency of 60 Hz. Atmospheric air was used as the gas, with a flow rate of 800 L/min. As shown in Figures **IV.5**, the plasma jet discharge extended about 5 cm, directly influencing the natural fiber's surface. The gliding arc discharge reactor was equipped with two diverging stainless steel electrodes, each 1 mm thick, positioned at the bottom of the feed gas nozzle. As shown in Figure IV.5 the wool fibers were placed in a container with a diameter of 10 cm and a thickness of 1 cm, filled with distilled water. The fibers were exposed to the cold plasma inside this container, randomly moved within the plasma jet for a set duration under ambient temperature. The fibers were kept 5 cm away from the plasma jet's flow during processing. The plasma treatment lasted for 60 minutes. Afterward, the treated wool fibers were immersed in ionized water for four hours, washed with distilled water, and left to dry at room temperature for three days. Prior to use, the fibers were dried in an oven at 60°C for 24 hours.

*Figure **IV.5**: Wool fiber under cold plasma jet.*

II.1.2. Epoxy and hardener

As shown in Figure **IV.6**, the resin matrix intended for reinforcement in this study with natural fibers is Duraclear Epoxy, supplied by AGEL Chemicals Company. Its properties and specifications are listed in Table **IV.1**.

*Table **IV.1**: Properties and Specifications of Duraclear Epoxy [8].*

Item	Specifications
Density (specific density at 25ºC)	1.12epoxy,0.97hardener
Mix Ratio (volume)	2:1
Mix Ratio (weight)	100:43
Viscosity (A/B/Mixed at 25 ºC)	1850/35/280
Mixed Density specific density at 25ºC	1.07
Pot Life at 25ºC	90 min
Tack Free Time at 35ºC	24 hrs
Color	White
PH	7 to 9
Recommended Full Cure	Seven days at 25°C
Gel time @ 22ºC in a 150-gram mass	5.5 hrs
Maximum casting depth	1.27-2.54 cm

*Figure **IV.6**: Duraclear epoxy and hardener.*

II.1.3. Structural Characterization of WF and PLA Natural Fibers

II.1.3.1. Fourier Transformation Infrared (FT-IR)

The samples were analyzed using FTIR Shimadzu, IR Affinity-1, Fourier Transform Infrared (Figure **IV.7a**) with a resolution of 8. To investigate changes in chemical composition, 0.02 g of each sample was ground and mixed with 0.198 g of KBr powder. The mixture was then ground on a KBr disc and compressed at 70 kN for 2 minutes. FTIR analysis was performed over a wavenumber range of 400–4000 cm^{-1}, with 20 scans conducted for each sample.

*Figure **IV.7**: Shimadzu, IR Affinity-1, Fourier Transform Infrared.*

II.1.3.2. X-ray diffraction (XRD)

The diffraction pattern was recorded by measuring the intensities of diffraction lines through steps taken by the source and detector. Using the X-ray diffraction instrument, we recorded the diffraction pattern of the investigated material. X-ray diffraction spectroscopy was performed with a wavelength of λCuK = 1.54 Å, over 2θ scan angles ranging from 10° to 90° (Figure **IV.8a**, and Figure **IV.8b**)

*Figure **IV.8**: X-ray diffraction instrument.*

II.1.3.3. Scanning electron microscopy (SEM)

The scanning electron microscope, SEM, Leo Supra 55, Zeiss Inc., Oberkochen, Germany (Figure **IV.9**) was configured with specific settings to ensure effective analysis. The voltage was set to 10 kV, the beam current to 5 µA, and the spot size to 10 nm. The acceleration angle was also adjusted to optimize the morphological examination of the four composites. These carefully selected parameters were intended to provide precise and detailed imaging during the SEM analysis.

*Figure **IV.9**: SEM, Leo Supra 55, Zeiss Inc., Oberkochen, Germany.*

II.2. Fabrication of Composite Materials

In this study, the vacuum infusion molding process was employed to manufacture the composite material, addressing challenges often encountered with manual lay-up and spray-up methods. This modern composite manufacturing technique holds potential to replace traditional methods. The principle of vacuum infusion involves creating a vacuum to draw air into the mold through negative pressure, simultaneously pulling resin into the mold and impregnating the reinforcement material. This process eliminates the risk of trapped air within the composite and ensures consistent purity across repetitions, as the process is governed by the equipment design rather than the operator's skill [25].

After forming the resin layer and matrix, excess resin is removed from the mold via suction, ensuring a uniform thickness distribution along the part. Materials produced using vacuum infusion have a higher fiber-to-resin ratio compared to those made by the hand lay-up method, resulting in stronger and lighter composites. As shown in Figure **IV.10**, the mold used in this study measures 300 mm x 250 mm x 4 mm. Fibers were weighed using a sensitive balance, and the required amounts of epoxy and hardener were calculated. Regardless of fiber type or treatment, all fibers were dried at 60°C to prevent voids, moisture, and ensure good fiber-matrix adhesion. The mold surface was meticulously cleaned and coated with a release agent for easy removal and optimal surface finish.

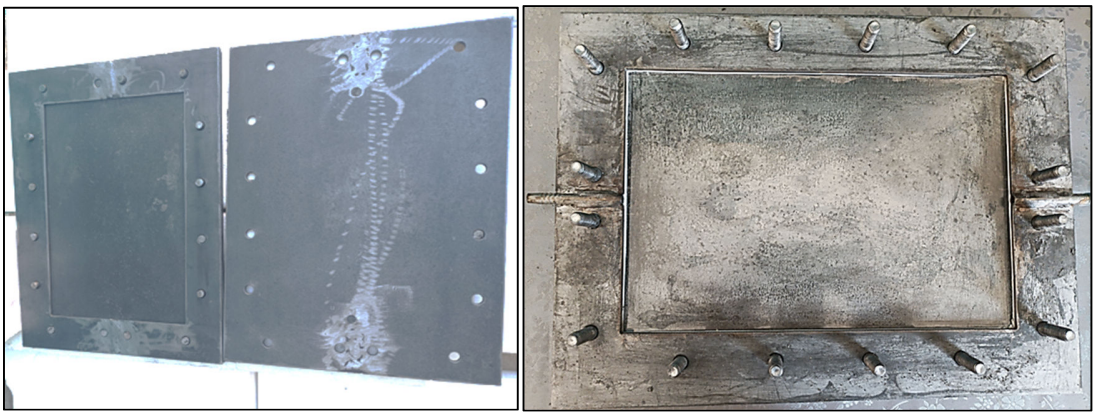

*Figure **IV.10** : Mold dimensions 300 mm x 250 mm x 4 mm.*

Once the fiber preparation was complete, it was placed in the mold, which was then covered with an additional layer. The experimental setup, shown in Figure **IV. 11**, clearly illustrates the apparatus used. The inlet hose is connected to the resin tank, while the outlet hose leads to the resin trap. After the vacuum pump was installed and the circuit completed, the pump began operating, causing the resin to flow into the mold due to pressure differences, until reaching the output section. The vacuum pressure used to suction the epoxy resin was 30 mHg. Figures **IV.12**to outline the sequential steps in the composite manufacturing process, and the final specimens, which were positioned in a controlled environment.

*Figure **IV.11**: Vacuum Infusion Molding Process for Composite Material Manufacturing.*

*Figures **IV.12**: Manufacturing process steps, and the final products.*

Previous studies suggest that increasing wool fiber content has minimal impact on tensile stress or elastic modulus. Various studies have used volume fractions of 30/70, 40/60, and 50/50, with 30/70 being the minimum ratio before mechanical properties begin to decline. A 50/50 ratio exhibits higher moisture absorption compared to a 60/40 ratio, which in turn demonstrates greater chemical absorption than the 50/50 ratio. When the fiber content exceeds 50%, mechanical properties deteriorate. To achieve a lightweight composite with favorable mechanical properties, this study emphasizes reducing the wool content and incorporating plant fibers. This approach improves properties such as low water absorption, low density, and lightweight characteristics. Therefore, we selected a fiber content of 30% wool, maintaining this proportion when adding plant fibers to reduce the wool percentage.

The selection of fiber types, treatments, and weight fractions is guided by the objective to explore the influence of natural and hybrid fibers on composite mechanical performance, while balancing density, processability, and fiber-matrix adhesion. The experimental design allows a comparative evaluation of untreated, chemically treated, and hybrid fiber-reinforced composites.

For the WLF and NWLF (30 wt.%) is a relatively high fiber content was chosen to maximize reinforcement while maintaining processability. For wool fibers, 30 wt.% provides sufficient mechanical reinforcement without compromising resin flow during molding. PLAF (15 wt.%) is lower fiber fraction for plant fiber was selected to reduce composite density and accommodate the relatively short fiber length,

preventing agglomeration and void formation. The hybrid PLAF-WLF (10/20 wt.%)is **t**he combination of 10 wt.% PLAF and 20 wt.% WLF balances the mechanical contribution of both fibers, ensuring proper dispersion and optimized interfacial bonding. This fraction maintains a workable resin matrix fraction of 70 wt.%. Resin fractions were adjusted to complement fiber content and ensure adequate wetting, curing, and consolidation of the composite. For high fiber content composites (30 wt.% fibers), the epoxy matrix is 70 wt.%, providing sufficient matrix to encapsulate fibers, prevent voids, and maintain structural integrity.

Table **IV.2** presents the weight percentage (wt.%) compositions of the composite specimens, offering a detailed overview of their material compositions.

*Table **IV.2**: Weight Percentage Compositions of Wool and Plant Fiber-Reinforced Composites [8].*

Type of fiber	Type of treatment	Fiber Weight fraction (Wt. %)	Epoxy Resin weight fraction (Wt. %)
WLF	Untreated	30	70
NWLF	NaOH treated	30	70
PLAF	untreated	15	85
PLAF-WLF	Untreated (PLAF)-cold plasma treated (WLF)	10/20	70

II.3. Mechanical tests of the Composite materials

Following the fabrication of the four composite materials, each specimen underwent three distinct mechanical tests tensile, compression, and flexural to assess their behavior under various loading conditions. Tensile and compression tests were performed using the Zwick/Roell Z10 testing machine, operated with TestXpert software version 12.0 and fitted with a 10 kN precision force sensor. In contrast, flexural tests were conducted using the Zwick Z 2.5 machine, equipped with a 2 kN load cell. Figure **IV.13** displays both the universal Zwick/Roell Z10 machine for tensile and compression tests, and the Zwick Z 2.5 for flexural testing.

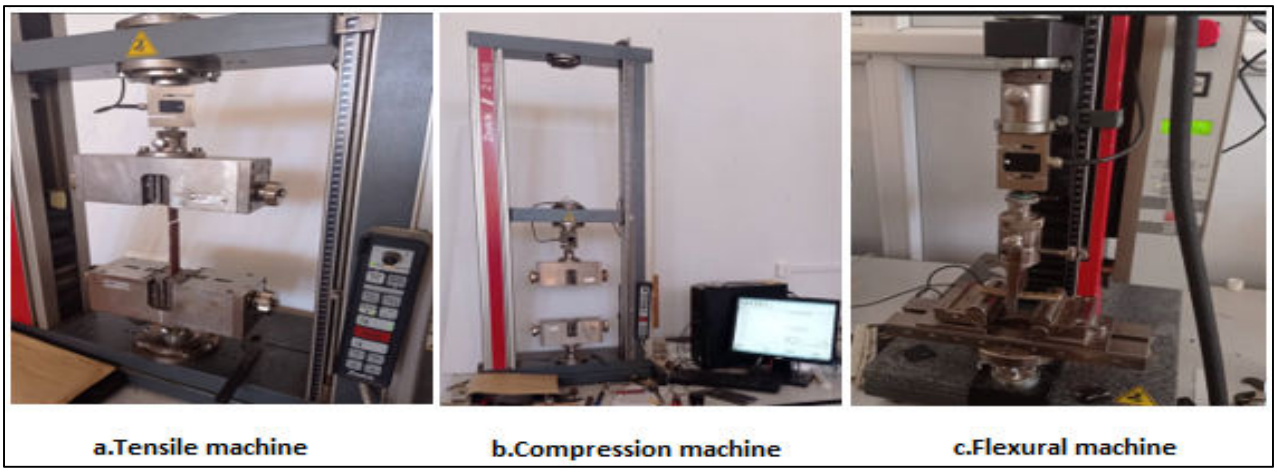

*Figure **IV.13**: Mechanical Test machines: (a) Universal Zwick/Roell Z10 for tensile test (b) Universal Zwick/Roell Z10 for compression teste, (c)Zwick Z 2.5 Flexural tester [8].*

To ensure reliable comparisons and optimal evaluation, five samples of each composite type were tested under consistent laboratory conditions, including ambient temperature and a fixed testing speed of 5 mm/min. These mechanical tests yielded critical information regarding the composites' performance, capturing data such as elongation, nominal strain, Young's modulus, and tensile strength. The dimensions of the test specimens are shown in Figure **IV.14**, while the shapes used for each test. The tests adhered to ASTM standards: ASTM D3039 for tensile, ASTM D790 for flexural, and ASTM D3410 for compression testing.

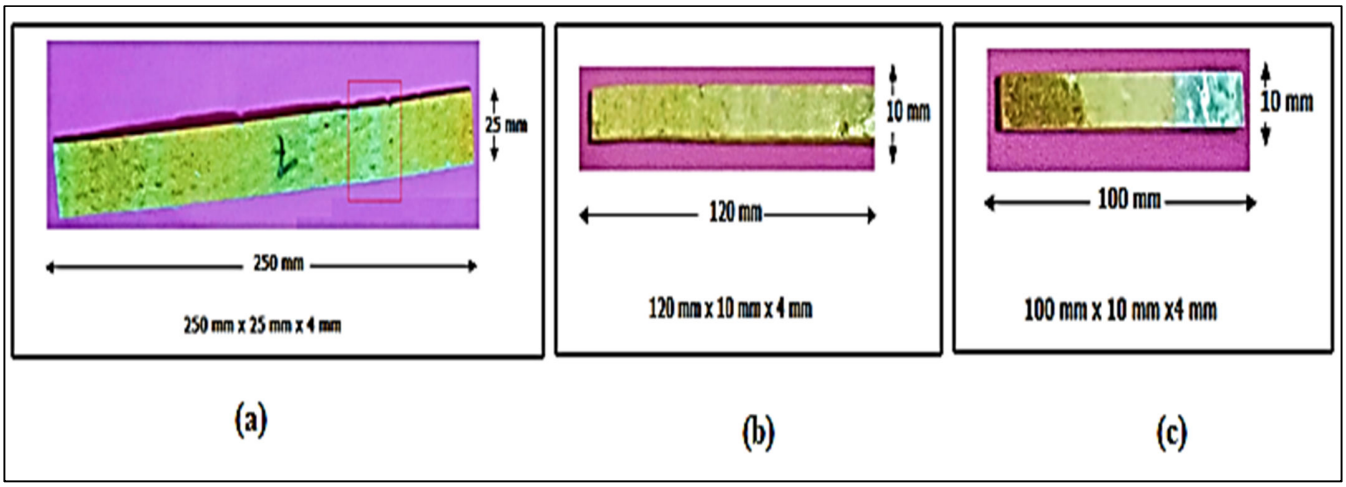

*Figure **IV.14**: The dimensions of the test specimens adhered to ASTM standards [8].*

III. Experimental II: Fabrication of Single Fiber-Reinforced Composites Using Horse Tail Hair Fiber (HHTF)

III.1. Materials

III.1.1. Natural Fibers Selection

III.1.1.1. Horse hair tail fiber (HHTF)

In this study, horse tail hair fibers were collected from the El Oued region of Algeria. Prior to any treatment, the fibers were carefully cleaned using distilled water to eliminate impurities such as dust, oils, and other debris that could negatively impact their performance as reinforcement in composite materials. This initial cleaning step was essential to ensure a clean surface for effective bonding with the matrix in subsequent processes.

III.1.2. Fiber treatment

II.1.2.1. Chemical treatment method

Following the cleaning process, the fibers were treated with a 1% sodium hydroxide (NaOH) solution to further enhance their surface characteristics. This alkaline treatment was performed at room temperature (25°C) for 1 hour. The purpose of the NaOH treatment was to remove remaining organic residues, increase surface roughness, and improve the wettability of the fibers. These modifications enhance the fiber's compatibility with the resin matrix, promoting stronger interfacial adhesion and improved mechanical performance of the final composite. A low concentration of NaOH (1%) was specifically selected to avoid fiber degradation, which can occur at higher concentrations.

III.1.3. Structural Characterization of Horse Hair Tail Fibers (HHTF)

The structural characterization procedures applied to Horse Hair Tail Fibers (HHTF) were the same as those used for Periploca laevigata fibers (PLAF) and Wool fibers (WLF), including Fourier Transform Infrared Spectroscopy (FTIR) for identifying chemical functional groups, X-ray Diffraction (XRD) for analyzing crystalline structure, and Scanning Electron Microscopy (SEM) for examining surface morphology, as detailed in Section **II.1.3**.

III.2. Fabrication of Composite Materials

The composite fabrication process using epoxy and horse tail hair fibers was carried out via the vacuum infusion molding technique. To begin, the mold was prepared and coated with a release agent to facilitate easy demolding. The horse tail hair fibers were then uniformly arranged inside the mold. The Duraclear Epoxy resin and hardener were blended in a 100:43 weight ratio, as recommended. A metallic mold measuring 250 × 300 × 4 mm^3 was used for the process. Careful fiber placement ensured consistent distribution for effective reinforcement. A vacuum pump was employed to apply negative pressure, compacting the fiber layers and eliminating entrapped air [76]. The resin was introduced into the mold through designated inlet points, guided by the vacuum pressure. After ensuring complete resin infusion,

the setup remained under vacuum while the composite cured at room temperature over 72 hours. To promote further cross-linking of the epoxy matrix and improve mechanical performance, a post-curing step at 25 °C was implemented [137]. Upon completion of the curing process, the mold was opened, the composite panel was demolded, and specimens were prepared for subsequent mechanical testing. The overall fabrication steps are depicted in Figure **IV.15**.

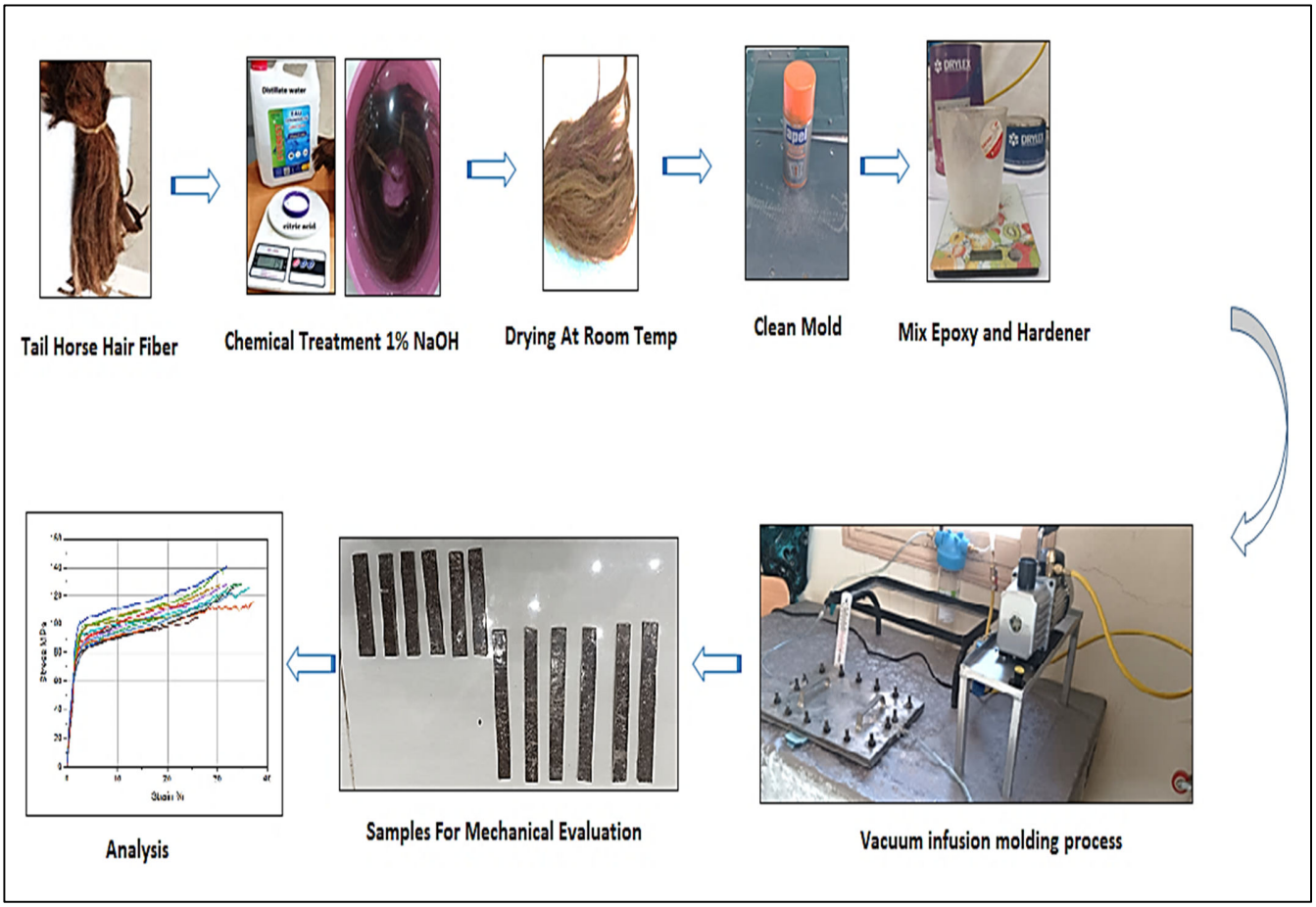

*Figure **IV.15**: Schematic representation of the composite fabrication process.*

III.3. Mechanical tests of the Composite materials

III.3.1. Tensile test

After fabricating the composite materials, all samples were subjected to three mechanical evaluations tensile, compressive, and flexural tests to analyze their responses under different loading scenarios. Tensile testing was conducted using the Zwick/Roell Z10 machine, equipped with a 10 kN precision load cell and operated via TestXpert software version 12.0. To ensure consistent and accurate comparisons between the various composite structures, five (05) specimens were tested for each configuration under

uniform testing conditions. These tests yielded valuable information on properties such as elongation, nominal strain, Young's modulus, and tensile strength. As illustrated in Figure IV.16, the tensile testing procedure followed the ASTM D 638 standard.

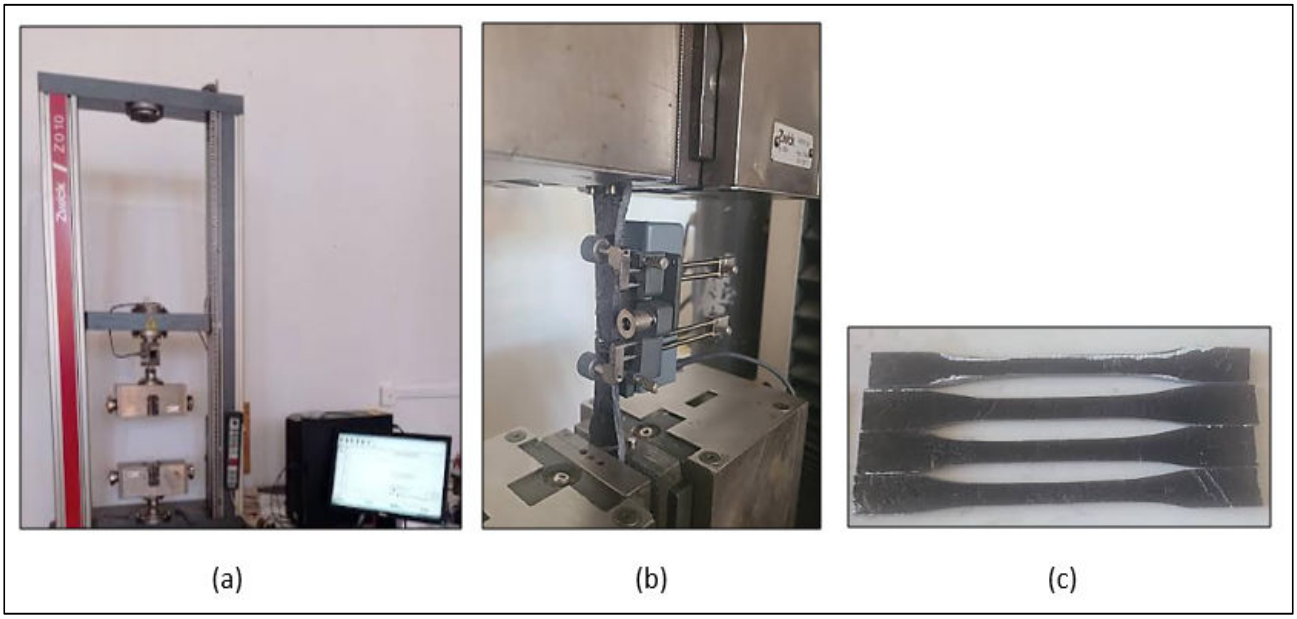

*Figure **IV.16**: Tensile test, (a) Tensile test machine, (b) Sample under tensile force, (c) THHF samples.*

III.3.2. Flexural test

The flexural tests were conducted on the Zwick Z 2.5 machine, which utilized a 2 kN force sensor. Figure **IV.17**, the Zwick/Roell Z10 and Zwick Z 2.5 machines used for these evaluations. The specimens are presented in Figure **IV.17c**. The procedures for the three tests adhered to ASTM D790 standard.

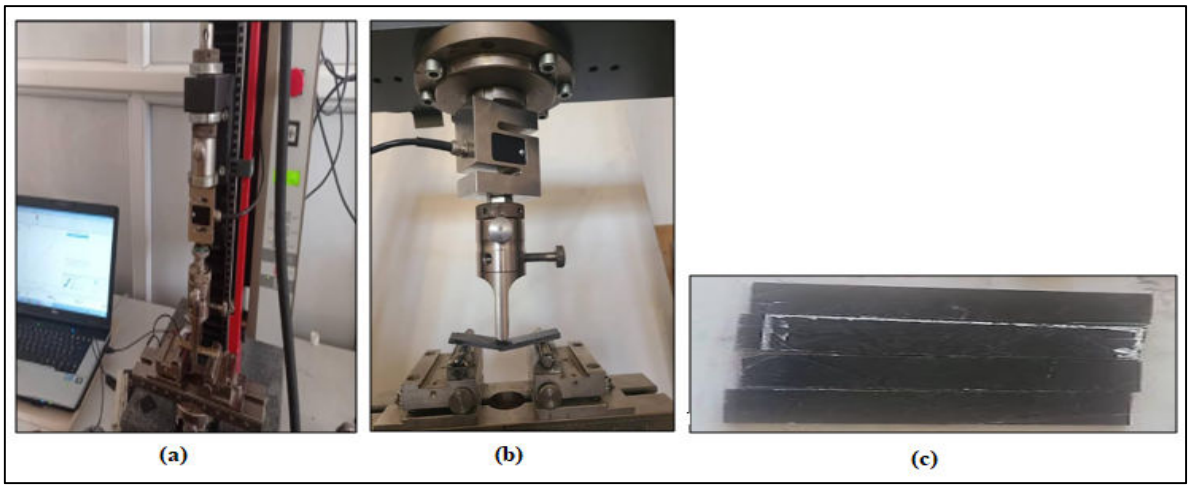

Figure 59

*Figure **IV.17**: Flexural test. (a) Flexural machine, (b) Sample under bending force, (c) Samples.*

III.3.3. Compression test

The compression tests were performed using the Zwick/Roell Z10 machine, operated with TestXpert software version 12.0 and equipped with a high-precision 10 kN force sensor. To ensure reliable comparisons of the mechanical performance across different composite structures, five specimens per configuration were tested under standardized conditions. The dimensions of the compressive specimens are presented in Figure **IV.18.** The procedures for the three tests adhered to ASTM D3410 standards.

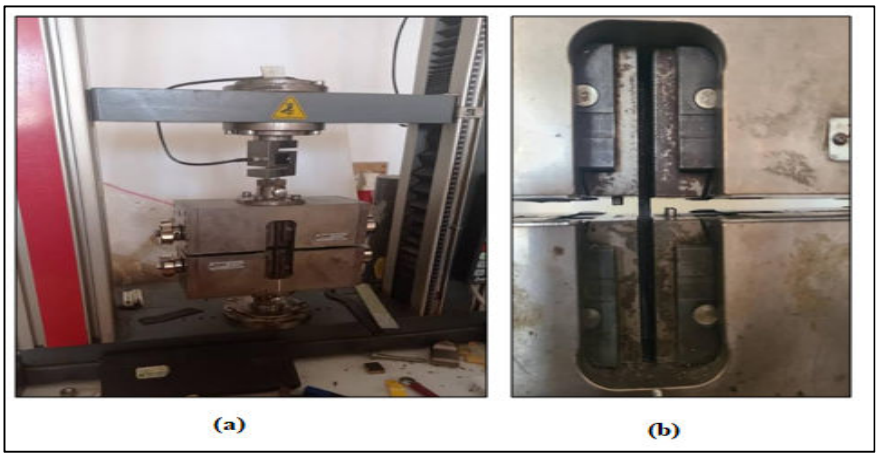

Figure 60

*Figure **IV.18**: Compression test, (a) Compression machine, (b) Sample under compression force.*

III.3.4. Mechanical characteristic of single horse hair tail fibers

As illustrated in Figure **IV.19,** the tensile characteristics of horse tail hair fibers are typically evaluated through single-fiber testing. The fiber's modulus and tensile strength are calculated based on its cross-sectional area, which is estimated by measuring the fiber's width and assuming a circular cross-section [138] To assess fiber length, 11 fibers were randomly chosen from the extracted horse tail samples. Each fiber's length was carefully measured using a ruler with a 0.2 mm precision, ensuring accurate and detailed length determination.

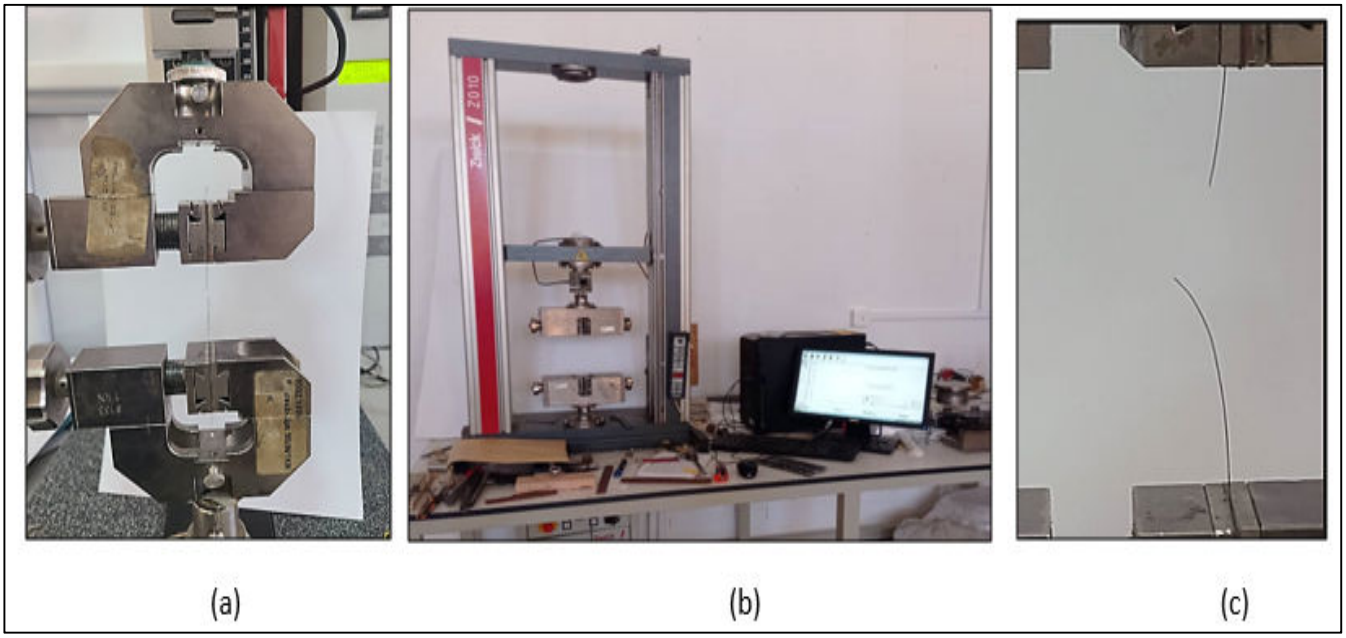

*Figure **IV.19**: Tensile test machine: (a) and (c) THHF under tensile force, (b) Zwick/Roell Z10 machine.*

IV. Experimental III: Failure Analysis of Periploca Laevigata Aiton-Wool Hybrid Composites Under Low-Velocity Impact

IV.1. Introduction

The increasing demand for sustainable and lightweight materials in fields like transportation, construction, and protective applications has driven the development of natural fiber-reinforced composites (NFRCs) that demonstrate enhanced mechanical properties. Among the essential assessment techniques for these materials, low-velocity impact (LVI) testing provides important information regarding their damage tolerance, energy dissipation characteristics, and structural dependability under dynamic loading. This research investigates the LVI response of four different composite systems reinforced with natural fibers: Periploca laevigata Aiton fiber (PLAF), untreated wool fiber (WLF), NaOH-treated wool fiber (NWLF), and a hybrid composite (PLAWLF) that combines plasma-treated wool with PLAF. Each composite was produced using vacuum infusion molding to guarantee consistent resin distribution and fiber wetting. The goal of this study is to assess their impact resistance at varying energy levels of 5 J, 10 J, 30 J, and 50 J by evaluating peak load, displacement at peak load, and energy absorbed. Particular emphasis is placed on the influence of fiber treatment (chemical or plasma) in altering interfacial properties, thus affecting the modes of failure. Figure **I.V.1** illustrates the step-by-step process involving fiber surface modification and impact testing, highlighting the experimental workflow that supports the study's conclusions.

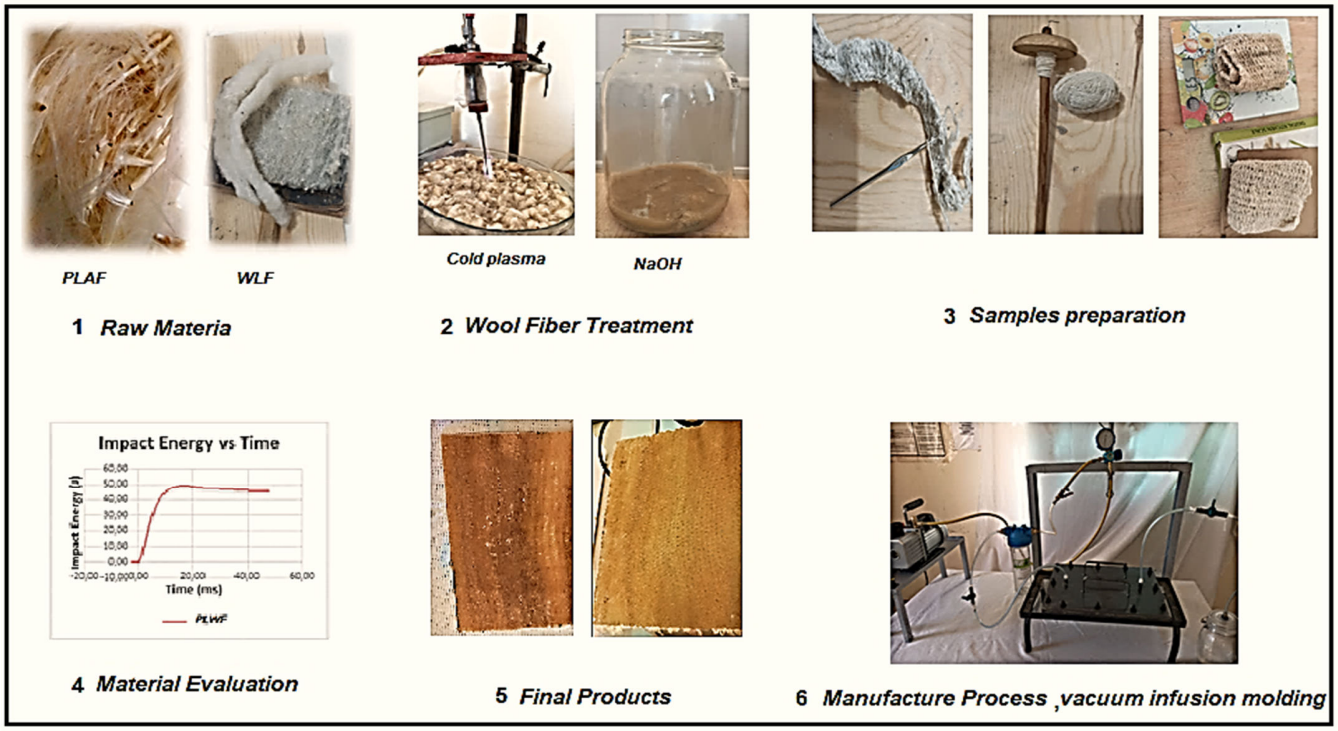

*Figure **IV.1**: The implemented approach.*

IV.2. Material

As discussed in the previous chapter, the composite materials examined in this study PLAF (Periploca laevigata Aiton fiber), WLF (untreated wool fiber), NWLF (wool fiber treated with a 0.1% NaOH solution), and PLAWLF (a hybrid composite reinforced with cold plasma-treated wool fiber and Periploca fiber) were fabricated using vacuum infusion molding techniques. The fibers underwent specific surface modification treatments to enhance interfacial bonding with the epoxy matrix. This chapter investigates the low-velocity impact performance of these composites to evaluate their energy absorption, peak load, and failure mechanisms.

CHAPTER V

Results and discussions

I. Experimental I: Fabrication of Single and Hybrid Composites Based on Wool Fiber and Periploca laevigata Aiton (PLA) Fibers

I.1. Water absorption

I.1.1. Periploca laevigata Aiton Fibers

Water absorption behavior was evaluated following the ASTM D570 standard. Sample weights were accurately recorded using a digital precision balance to calculate the percentage of water absorbed. As presented in Table **V.1**, Periploca laevigata Aiton fibers demonstrated water absorption values ranging from 7.22% to 11.09%. This low absorption rate underscores a key advantage of these fibers, alongside their lightweight characteristics. In comparison with other natural fibers such as cotton (32.5% to 50.5%), banana fibers (448.5% to 495%), and untreated areca fibers (698% to 851%) Periploca laevigata Aiton fibers exhibit remarkably reduced water uptake.

*Table **V.1**: Water absorption measurement for Periploca laevigata Aiton fiber.*

Samples	W1 (g)	W2 (g)	Water Absorption (%)
Sample 1	0,5707	0,6419	11,09
Sample 2	0,5641	0,6293	10,36
Sample 3	0,5744	0,621	7,50
Sample 4	0,5785	0,6247	7,40
Sample 5	0,5785	0,6235	7,22

I.1.2. Wool fiber

Wool is a protein-based polymer that contains multiple functional groups and a largely amorphous structure, which makes it highly receptive to moisture absorption. Under conditions of 65% relative humidity, wool is capable of absorbing between 13% and 18% of its dry weight in water. This absorption capacity can rise significantly, reaching up to 40% at full (100%) relative humidity.

I.2. Void content

The void content of the composite specimens was determined following the ASTM D2734-94 standard. Table **V.2** presents the void fraction of the composites, calculated based on the comparison between measured and theoretical density values.

*Table **V.2**: Measured Density and Calculated Void Fraction of Composite Specimens.*

Sample	ρ_t (g/cm3)	ρ_c (g/cm3)	V (%)
WLF	1,130	1,092	3,361
NWLF	1,130	1,095	3,095
PLAF-WLF	1,041	1,029	1,182
PLAF	0,887	0,877	1,098

The reduction in void fraction observed with the incorporation of Periploca laevigata Aiton fibers in the hybrid composite can be linked to several contributing factors. Primarily, the presence of these fibers helps to minimize empty spaces within the composite by promoting better fiber-matrix adhesion. This improved interaction also limits shrinkage and fiber buckling during the curing stage, resulting in fewer voids. Consequently, the material becomes more densely packed, and the available space for void formation decreases. This enhanced compaction and matrix infiltration lead to a noticeable decline in the overall void content.

I.3. Characterization Results of WLF, NWF, PLAF-WLF, and PLAF Natural Fibers

I.3.1. Fourier Transform Infrared Spectroscopy (FTIR)

The structural properties of all processed natural fibers were evaluated using Fourier Transform Infrared Spectroscopy (FTIR), X-ray Diffraction (XRD), and Scanning Electron Microscopy (SEM). The FTIR analysis, illustrated in Figure V.1 and detailed in Table **V.3**, highlights the chemical similarities and bonding characteristics between Periploca laevigata Aiton and wool fibers. A notable peak around 1519 cm^{-1}, corresponding to the bending deformation of the (-C-N-H) bond, indicates an interaction between C-N stretching and N-H bending. Additionally, peaks observed at 1585 cm^{-1}, 1566 cm^{-1}, 1681 cm^{-1}, and 1573 cm^{-1} in Figure**V.1a**, and Figure**V.1d** are attributed to the -CO stretching vibration of the amide group.

The broad peaks detected in Figure**V.1a,** Figure**V.1c**, and Figure**V.1d** within the 3699–3788 cm^{-1} range and around 3703 cm^{-1} in Figure V.1b correspond to the presence of hydroxyl (-OH) groups, suggesting minimal differences in moisture content among the samples. Notably, the Amide II band becomes more pronounced in treated fibers, with its position varying depending on treatment conditions. Furthermore, the peaks at 1288 cm^{-1}, 1276 cm^{-1}, and 1284 cm^{-1} in Figures 12b–d reflect the presence of both α-helical structures and disordered conformations. These spectral features offer valuable insights into the fibers' molecular configurations and structural characteristics.

*Table **V.3**: FTIR Spectroscopy Results of Treated and Untreated Natural Fibers.*

Samples	Amide III	Amide I	C–N -H	-OH

Untreated Wool fiber	1232 cm^{-1}	1573 cm^{-1}	1519 cm^{-1}	3699 –3788 cm^{-1}
Wool treated by NaOH	1288 cm^{-1}	1585 cm^{-1}	1519 cm^{-1}	3699 –3788 cm^{-1}
Plasma treated Wool	1276 cm^{-1}	1566 cm^{-1}	1519 cm^{-1}	3703 cm^{-1}
Untreated P-Laevigata	1284 cm^{-1}	1681 cm^{-1}	1519 cm^{-1}	3699 –3788 cm^{-1}

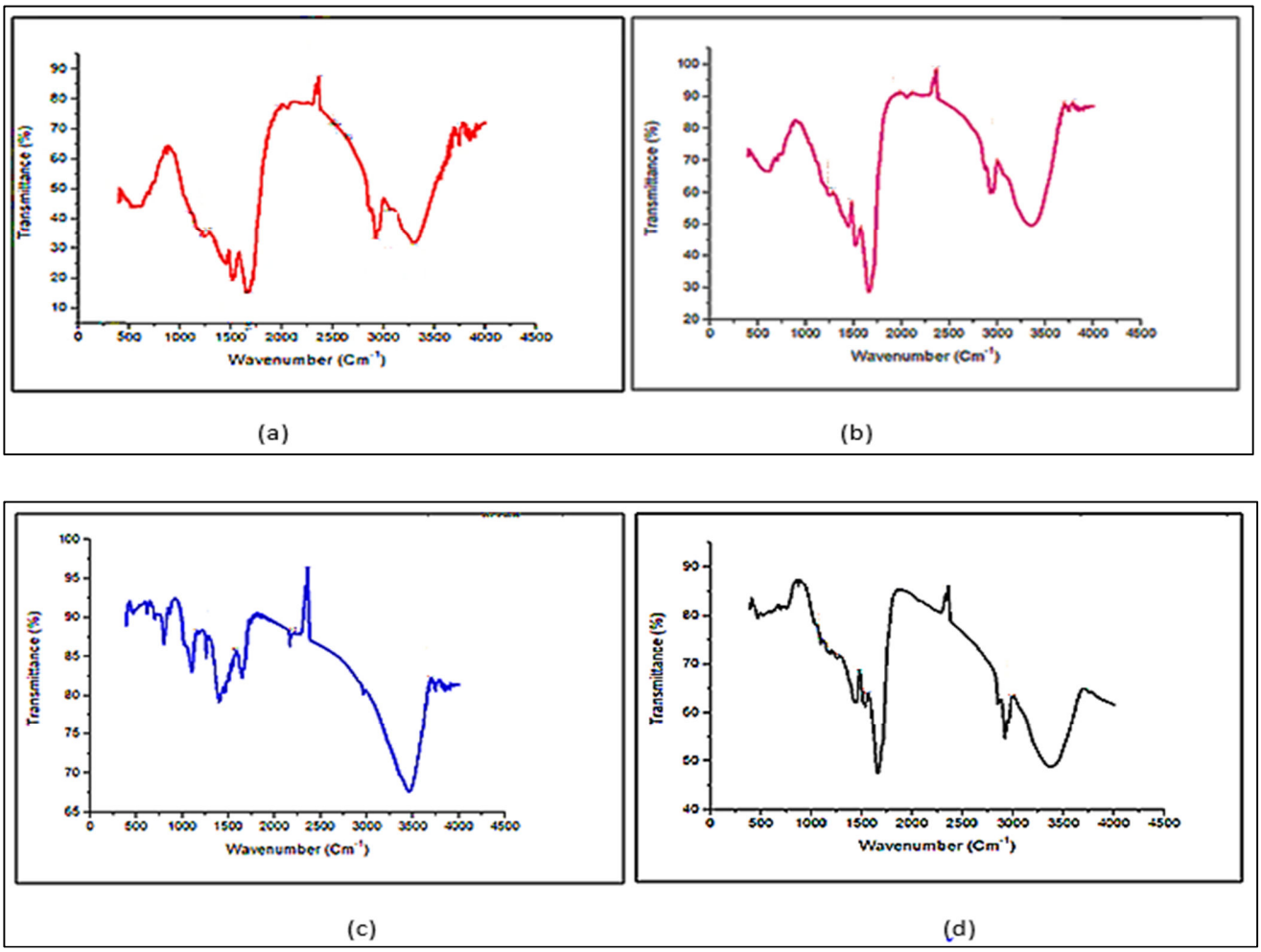

*Figure **V.1**: FTIR Spectroscopy Spectra of Natural Fibers, (a) PLAF-WLF hybrid fiber, (b) NWLF (NaOH-treated wool fiber), (c) PLAF (Periploca laevigata Aiton fiber), and (d) WLF (untreated wool fiber).*

I.3.2. XRD

The XRD results are presented in Figure**V.2a**, Figure **V.2b**, Figure**V.2c,** and Figure **V.2d**. In Figure **V.2c** and d, the untreated Periploca laevigata fiber and untreated wool fiber, respectively, reveal peaks

corresponding to the crystal structures of the studied samples. Specifically, the peak at an angle of 2θ = 25.62° in Figure **V.13c** aligns closely with the peak at 2θ = 26.67° in Figure **V.13b**. A similar observation is made in Figures **V.13a** and **V.13b**, which show the treated wool fiber with 0.1% NaOH and treated wool fiber with cold plasma, mixed with untreated Periploca laevigata fiber. In these cases, the peak at 2θ = 20.98° in Figure **V.2c** aligns closely with the peak at 2θ = 21.39° in Figure **V.13b**. These results suggest a relationship between wool fiber crystallinity and its chemical, physical, and mechanical properties. Specifically, the crystallinity of wool fiber was found to decrease following alkali treatment. This reduction is likely due to the degradation of the polypeptide chain during the alkali treatment, leading to partial decomposition of the crystal structure.

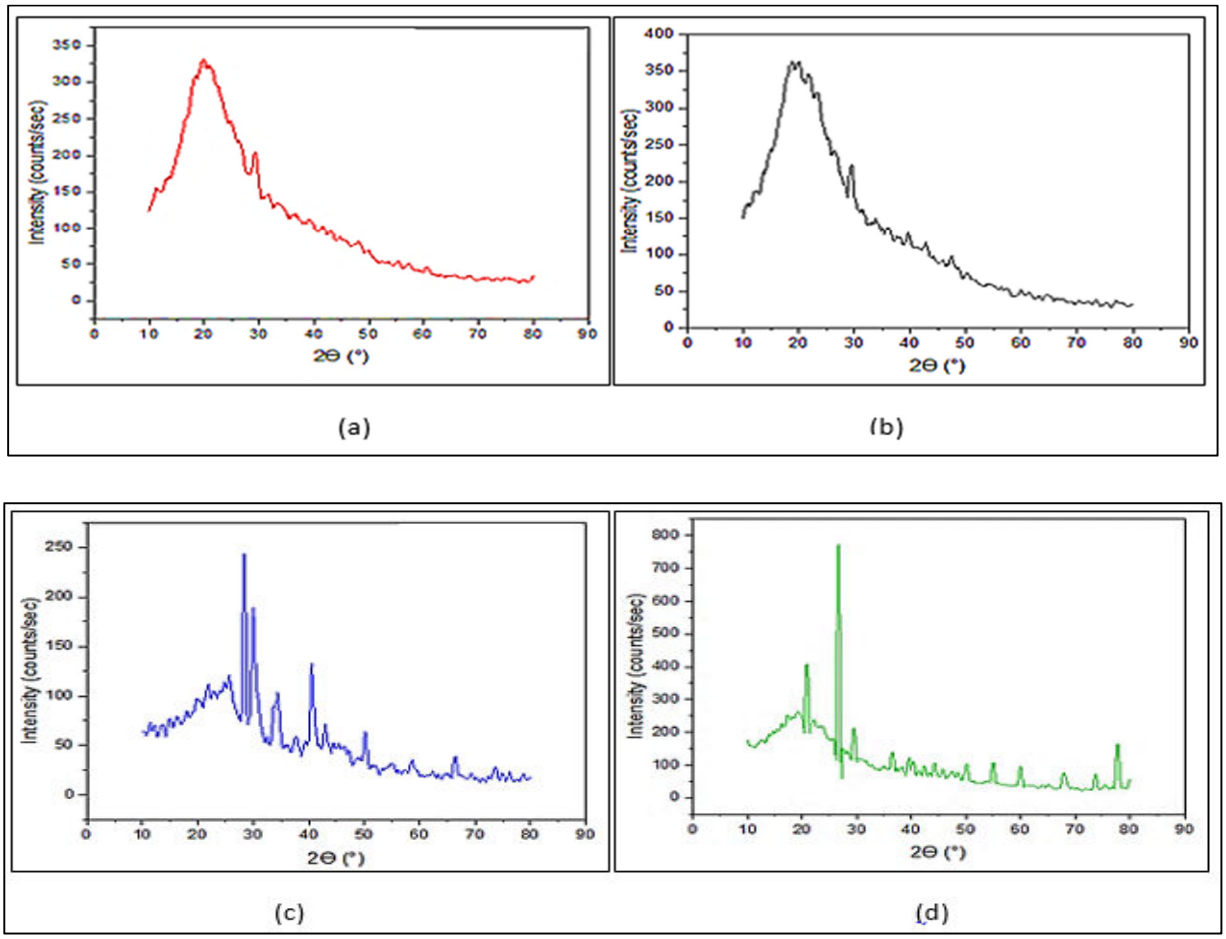

*Figure **V.2**: X-ray diffraction patterns: (a) NWLF, (b) PLAF-WLF, (c) PLAF, and (d) WLF.*

I.4. Evaluations of mechanical properties for the four composite materials

I.4.1. Tensile test results

The tensile test specimens were evaluated using a universal tensile testing machine to determine key mechanical properties such as ultimate tensile strength (MPa), Young's modulus (GPa), and ductility (%). The resulting data were presented as stress-strain curves. Figure **V.4** shows that the tensile stress-strain behavior follows a notably linear trend, which aligns with established theory, particularly in the fiber direction, where mechanical properties are largely dictated by the fibers and maintain a linear stress-strain relationship until fracture. The hybrid composite of PLAF-WLF exhibited the highest tensile strength of 26.02 MPa, which can be attributed to the strong bonding between wool fiber and Periploca laevigata Aiton fiber within the matrix. This strong bond was facilitated through the vacuum infusion process, emphasizing the significant influence of the reinforcement stacking sequence on the composite's properties. During the test, the composite's head withstood the maximum stress, delaying the initial fracture beyond expectations. This delay is due to the fiber's ability to absorb a substantial amount of the load, thereby enhancing the yield point. However, after some time, the material approached the necking stage, a point of increased vulnerability to fracture, which eventually led to crack propagation due to damage in the epoxy matrix.

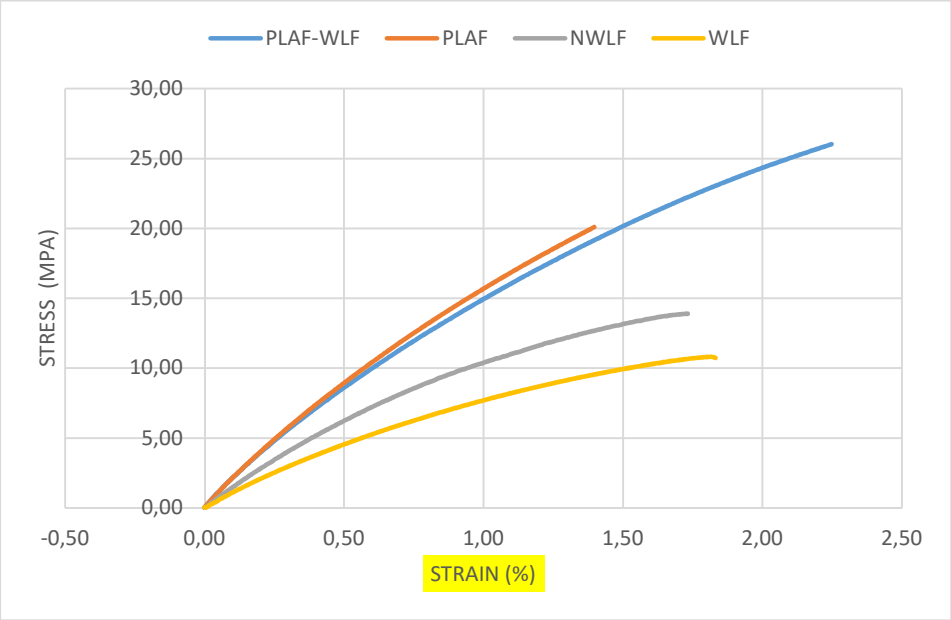

*Figure **V.4**: Stress vs Strain curves for tensile test.*

Figure **V.5** and Figure **V.6** display the force values and Young's Modulus for the composites. The composite with untreated wool fiber showed a tensile strength of 10.82 MPa and a Young's modulus of 1420.34 MPa (1.42 GPa). When treated with 0.1% NaOH, the composite demonstrated even better mechanical properties, with a tensile strength of 13.89 MPa and a Young's modulus of 1688.55 MPa (1.688 GPa). In contrast, the PLAF composite exhibited superior mechanical performance, with a tensile strength of 20.1 MPa and a Young's modulus of 2345.73 MPa (2.3457 GPa). The hybrid composite PLAF-WLF outperformed all others, achieving an impressive tensile strength of 26.02 MPa and a Young's modulus of 2350.50 MPa (2.350 GPa). These outstanding results highlight the synergistic effect of cold plasma treatment and the inclusion of Periploca laevigata Aiton fiber, leading to a composite with exceptional mechanical properties, ideal for applications requiring both strength and stiffness.

Untreated wool fiber composite (WLF) exhibited visible surface contaminants, which are known to impair bonding between the fiber and matrix, reducing the contact area between them. As reported by other researchers, these contaminants create weak interfacial bonding, resulting in isolated micro spaces that hinder stress transfer between the fiber and matrix, as shown in Figure **V.8**. As fiber loading increases, these obstructions also increase, resulting in greater stiffness. After treating the wool fiber with 0.1% NaOH, both tensile strength and Young's modulus improved. This enhancement is explained by the effective transmission of the load to the fiber during tensile testing, in accordance with fiber-reinforced polymer matrix theory, which boosts the overall composite modulus. The PLAF composite displayed remarkable mechanical performance, achieved due to the inherent properties and purity of the fiber, demonstrating excellent results without any modification, thanks to its natural light weight and thin structure.

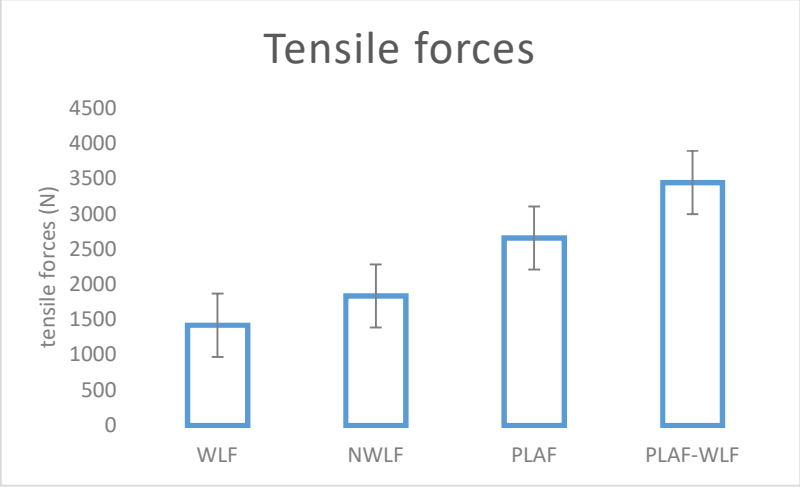

*Figure **V.5**:Tensile test forces.*

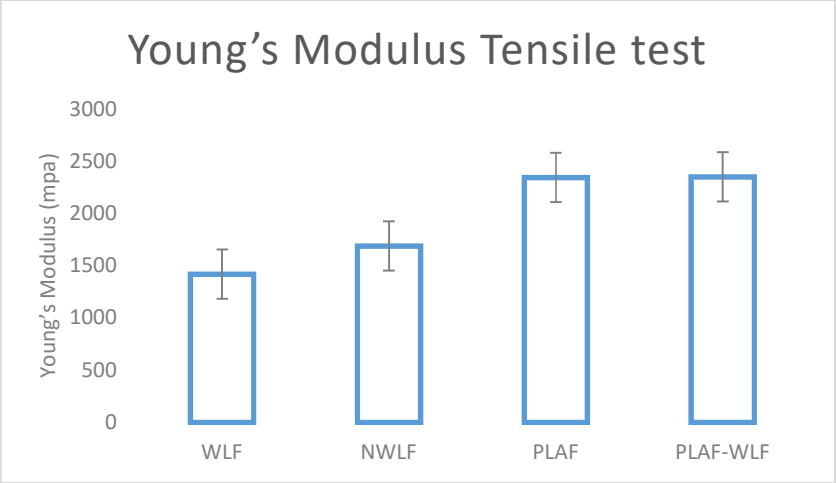

Figure V.7: Young's Modulus Tensile test.

The integration of Periploca laevigata Aiton fiber with cold plasma-treated wool fibers led to a marked enhancement in both Young's modulus and tensile strength. This notable improvement is largely due to the intrinsic organic and structural compatibility between Periploca laevigata Aiton and wool fibers, despite their differing natural origins. Evidence of their compatibility is supported by XRD and FTIR analyses. Cold plasma treatment modifies the wool fiber surface by introducing functional groups and altering surface energy, which improves interfacial compatibility with other materials. Depending on the specific treatment conditions, this method can strengthen the wool fiber through cross-linking or structural modification, thereby increasing its tensile strength and overall durability[49]. The altered surface also promotes improved adhesion between the fiber and the composite matrix, contributing to enhanced mechanical performance [139]

The addition of Periploca laevigata Aiton fiber to cold plasma-treated wool composites yielded substantial gains in tensile strength: a 58.57% increase for the untreated wool fiber composite (WLF), a 46.62% improvement for the NaOH-treated wool fiber composite (NWLF), and a 22.75% rise for the PLAF composite. These figures clearly demonstrate the reinforcing effect of Periploca laevigata Aiton fiber, especially for the untreated and chemically treated wool composites. The enhancements in Young's modulus are also significant, with a 39.57% increase for WLF and a 28.16% boost for NWLF, while the PLAF composite saw only a marginal improvement. This suggests that Periploca laevigata Aiton fiber played a crucial role in carrying a substantial share of the applied load, significantly improving the tensile behavior of the composite, particularly in WLF and NWLF variants.

The final composite exhibited outstanding mechanical characteristics, with a Young's modulus of 2.35 GPa indicating high stiffness and resistance to deformation and a tensile strength of 26.02 MPa. These values reflect the material's ability to endure substantial tensile stress without failure, highlighting its robustness and structural integrity. To better understand the tensile behavior and failure mechanisms, both macro and micro photographs were analyzed to examine fracture patterns in the tested specimens. Figure

V.8a, Figure V.8b, Figure V.8c, and d present macro-level images of the fracture surfaces from the tensile test samples.

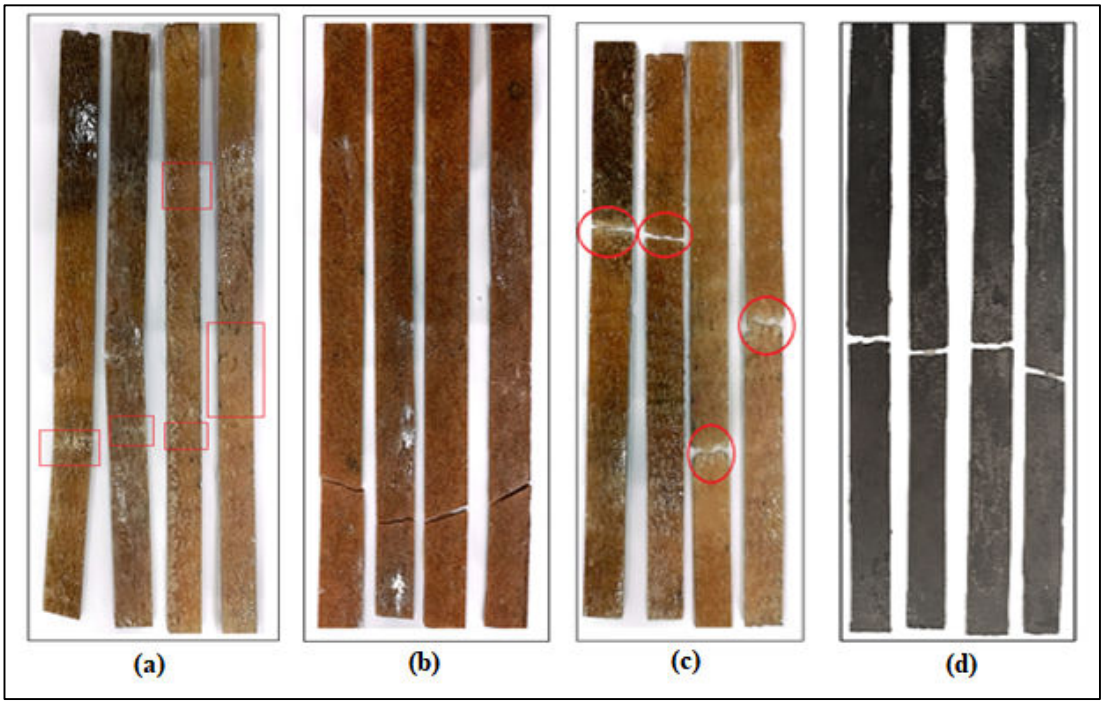

*Figure **V.8**: Tested Specimens Displaying Tensile Fracture.*

I.4.2. Flexural test

The flexural test assesses how a beam-shaped specimen responds to bending loads, providing measurements for both flexural strength and flexural modulus. This test was conducted following the ASTM D790 standard. The results were graphically represented through stress-strain and force-displacement plots.

As illustrated in Figure **V.9**, the PLAF-WLF hybrid composite demonstrates superior flexural strength in comparison to the other tested composites. Regarding deflection behavior, the WLF composite exhibited the highest deflection, followed by the NWLF composite, among the hybrid materials under investigation. The flexural test results clearly highlight the outstanding performance of the PLAF-WLF composite, which achieved a 72.70% increase in flexural strength over the WLF composite. This aligns with expectations due to the naturally high flexural strength of Periploca laevigata Aiton fiber, especially when reinforced with plasma-treated wool fiber.

Moreover, PLAF-WLF outperformed the NWLF composite by 67.84% and even exceeded the strength of the PLAF composite by 56.03%. These results emphasize the synergistic interaction between cold

plasma-treated wool and Periploca laevigata Aiton fibers, leading to a composite material with enhanced resistance to bending forces.

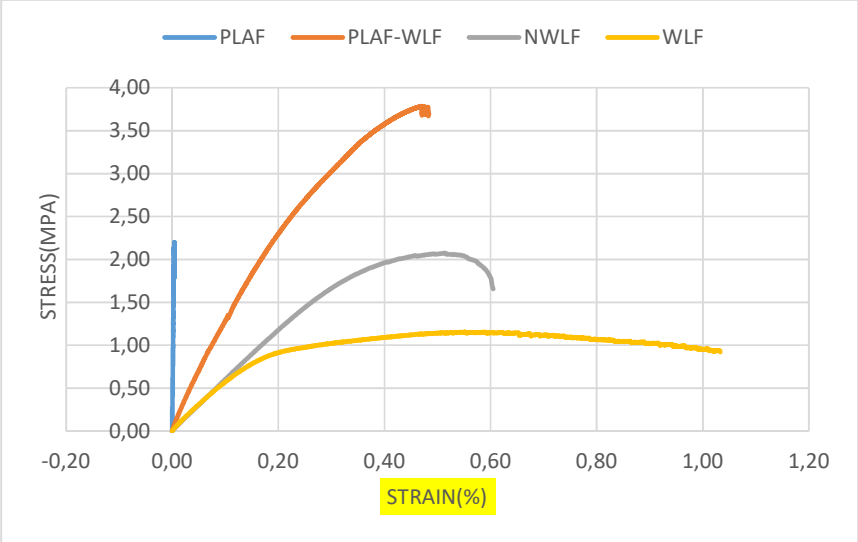

*Figure **V.9**: Stress–strain curves obtained from the flexural test for the four composite.*

Figure**V.10**, Figure **V.11**, and Figure **V.12** display the mechanical behavior of the composite specimens under applied loading conditions. Among them, the PLAF-WLF hybrid composite stands out, sustaining the highest peak load of 253.15 N and exhibiting a Young's modulus of 1210.93 MPa (1.21 GPa). This performance surpasses all other tested composites. The PLAF composite, composed solely of Periploca laevigata Aiton fiber, also showed notable strength, with a peak force of 111.29 N and Young's modulus of 623.2 MPa (0.6223 GPa). The NWLF composite, consisting of NaOH-treated wool, recorded a force of 81.39 N and a modulus of 588.5 MPa (0.588 GPa), indicating the positive effect of chemical treatment.

The WLF composite reinforced with untreated wool fibers displayed the lowest mechanical performance, bearing a force of just 69.09 N and having a Young's modulus of 524.83 MPa (0.524 GPa). These results clearly demonstrate the critical role of fiber treatment techniques in enhancing the structural and mechanical performance of composite materials. The integration of Periploca laevigata Aiton fiber with cold plasma-treated wool fibers in the hybrid PLAF-WLF composite presents a promising advancement in composite material design, delivering impressive mechanical benefits suitable for demanding applications.

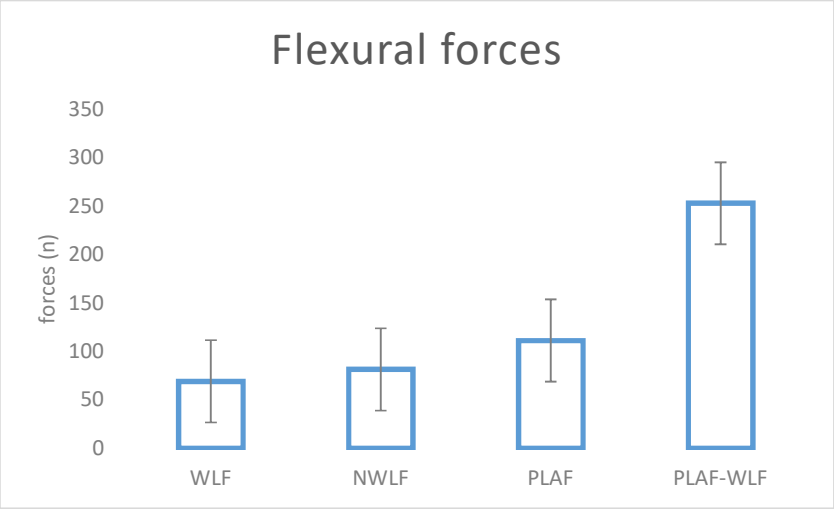

*Figure **V.10**: Flexural force values recorded during testing for the four composite materials.*

Figure **V.11** highlights that the hybrid composite PLAF-WLF demonstrates superior flexibility compared to the other composites. Unlike NWLF and PLAF, the WLF composite exhibits a more brittle behavior, making it less capable of enduring substantial flexural loads. During bending, the outer fibers in the composite structure are subjected to the greatest stress. The degree of resin infiltration into these fibers a critical factor for flexural strength is largely influenced by the interfacial adhesion between the fiber and the matrix. Additionally, previous studies have indicated that combining different natural fibers within a hybrid configuration often results in enhanced flexural properties compared to composites reinforced with a single type of fiber [140].

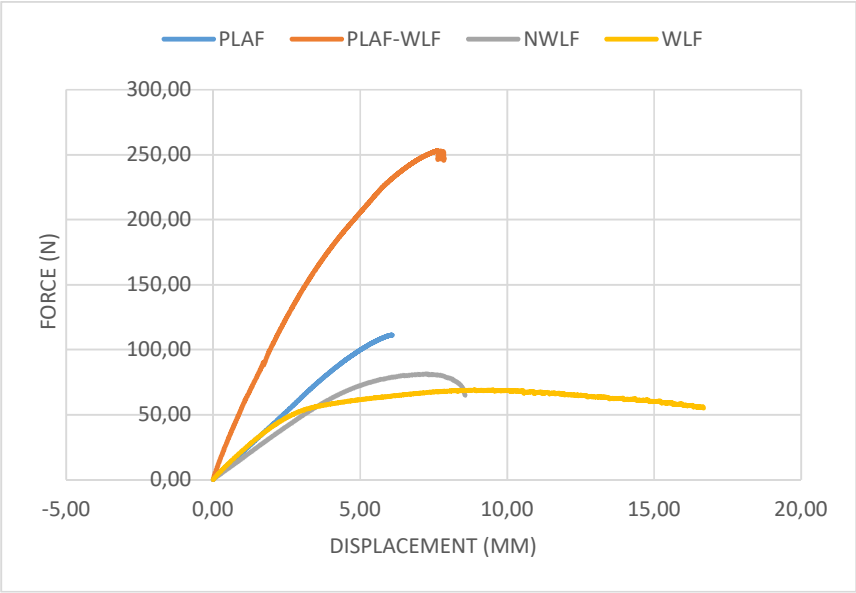

*Figure **V.11**: Load-Displacement Response Curves.*

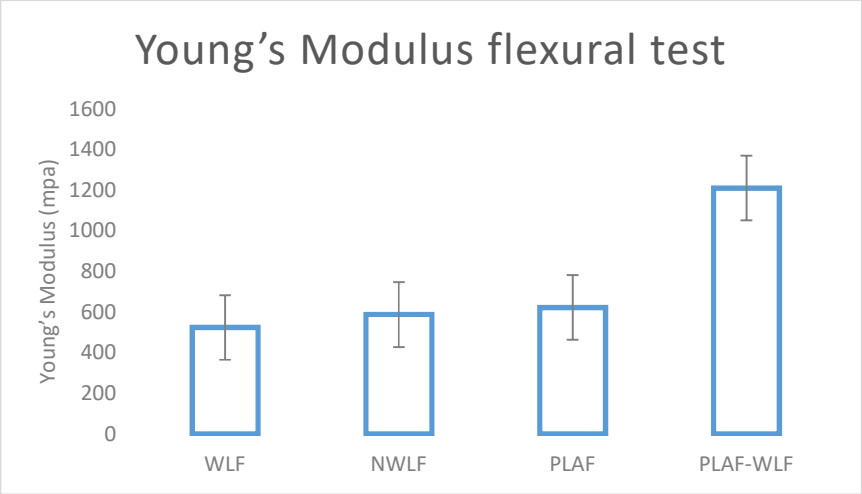

*Figure **V.12**: Young's Modulus via Flexural Testing.*

The effective penetration of resin into the fibers enhances the flexural strength and influences the adhesion between the fibers and the matrix. Hybridizing natural fibers improves the flexural strength compared to using individual fibers. The bending test results shown in Figure**V.13a**, Figure **V.13b**, Figure **V.13c** and Figure **V.13d**, and d for PLAF-WLF, NWLF, PLAF, and WLF, respectively, reveal that integrating Periploca fibers into wool fibers increases their bending capacity without fracture. This demonstrates an improvement in ductility. After analyzing the failure mode of the specimens during bending tests, it was determined that the addition of Periploca fibers effectively transformed the brittle failure behavior of untreated wool fibers under concentrated loads into a more ductile mode. Consequently, incorporating Periploca fibers into wool fibers aids in the transfer of tensile stress along the sample axis, thereby enhancing the ductility of the hybrid composite.

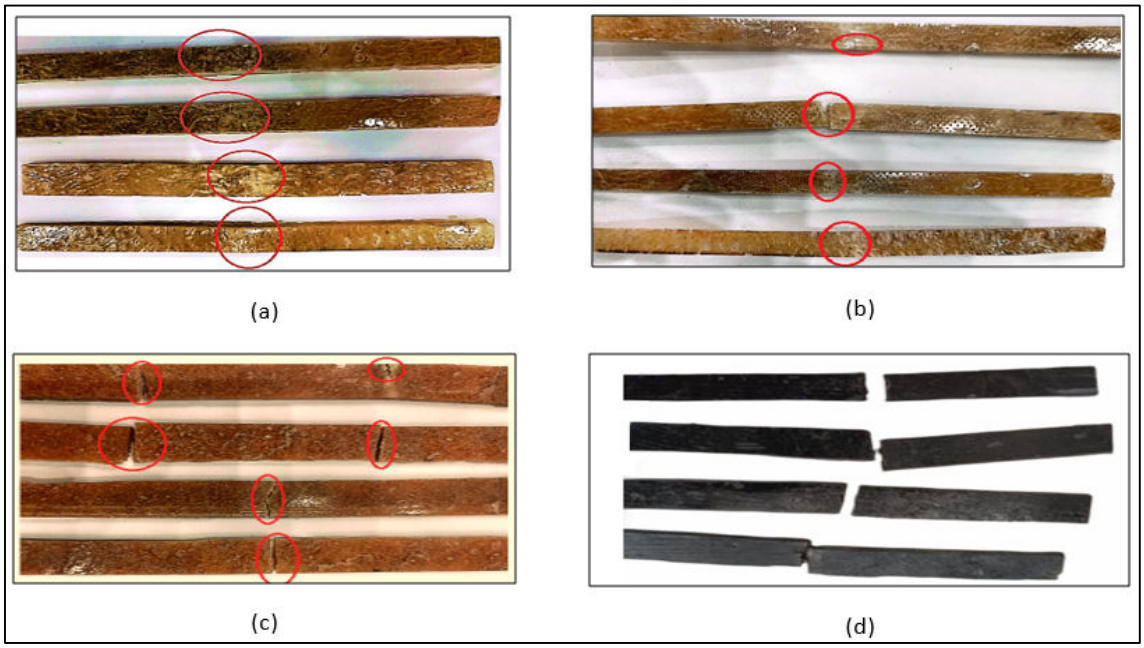

*Figure **V.13**: Post-Flexural Test Examination of Composite Specimens: PLAF-WLF, NWLF, PALF, and WLF.*

I.4.3. Compression test

The mechanical performance of the four composites was further assessed through a compression test, where all specimens were subjected to compressive stress to evaluate their response to this type of loading. Figure **V.14** and Figure **V.15** illustrate the compressive strength and Young's Modulus of each composite. The PLAF composite demonstrated a notable Young's Modulus of 500 MPa (0.5 GPa) and a compressive strength of 44.75 MPa. Although it did not possess the highest load-bearing capacity at 2755.19 N, PLAF still exhibited substantial strength and stiffness. The hybrid PLAF-WLF composite showed exceptional mechanical properties, with a load-bearing capacity of 4369.19 N and the highest compressive strength of 59.56 MPa among all tested specimens. Additionally, its Young's Modulus reached 500 MPa (0.5 GPa), further emphasizing its remarkable rigidity. The NWLF composite demonstrated a load-bearing capacity of 1829.25 N, with a Young's Modulus of 450 MPa (0.45 GPa) and a compressive strength of 36.87 MPa, showing significant improvements in strength compared to the untreated WLF composite. The untreated WLF composite displayed the lowest load-bearing capacity at 1134.18 N, with a Young's Modulus of 0.4 GPa and a compressive strength of 36.12 MPa. These results underscore the importance of fiber treatment or modification to enhance load-bearing capacity, as evidenced by the improvements in the NaOH-treated wool fiber composite NWLF and the hybrid composite PLAF-WLF compared to the untreated WLF composite. The compressive strength data clearly highlight the variations in performance among the different composites.

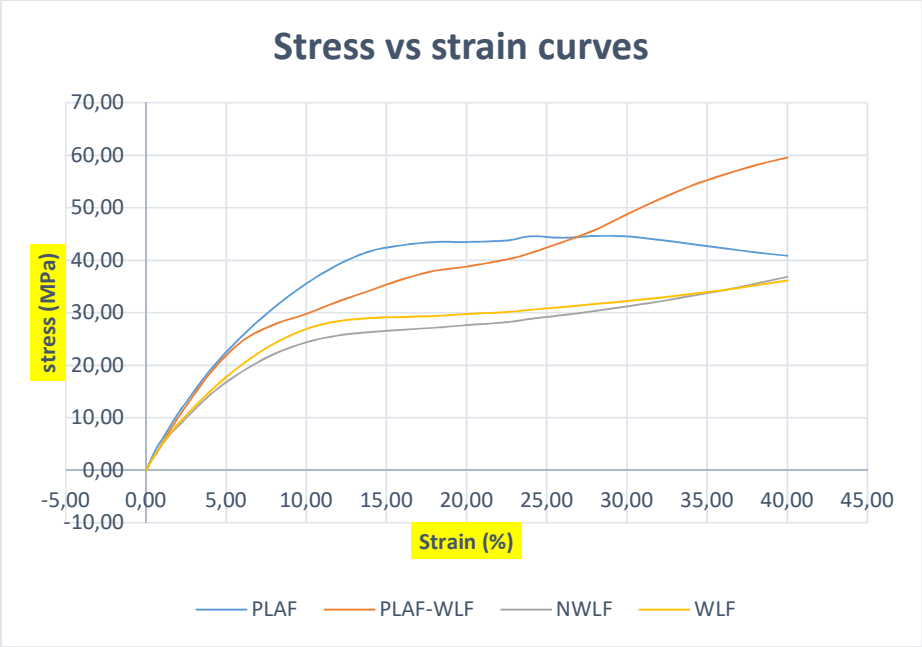

*Figure **V.14**: Compressive test stress vs Strain curves.*

The hybrid composite demonstrated the highest compressive strength at 59.56 MPa, while the WLF composite showed the lowest at 36.12 MPa. The PLAF composite, with a fiber/epoxy ratio of 17.65%, achieved a compressive strength of 44.76 MPa. In comparison, the PLAF-WLF composite, which had a fiber/epoxy ratio of 14.29% Periploca laevigata Aiton fiber and 28.57% treated wool fiber via cold plasma, matched the hybrid composite's compressive strength of 59.56 MPa. The NWLF and WLF composites, both with a high wool fiber/epoxy ratio of 42.86%, recorded compressive strengths of 36.87 MPa and 36.12 MPa, respectively. These results clearly highlight that the inclusion of Periploca laevigata Aiton fiber significantly enhances the strength and stiffness of the wool fiber. Notably, the compressive strength of the wool fiber composite increased by approximately 39.35% due to the synergistic effect of incorporating Periploca laevigata Aiton fiber. In a comparative analysis, the PLAF composite outperforms the WLF composite, offering a 19.30% higher load-bearing capacity and an impressive 20% greater Young's Modulus, showcasing superior strength and stiffness. Furthermore, the hybrid PLAF-WLF composite achieves a 38.09% improvement in load-bearing capacity over the pure NWLF composite, demonstrating exceptional strength, although with a slight trade-off in stiffness.

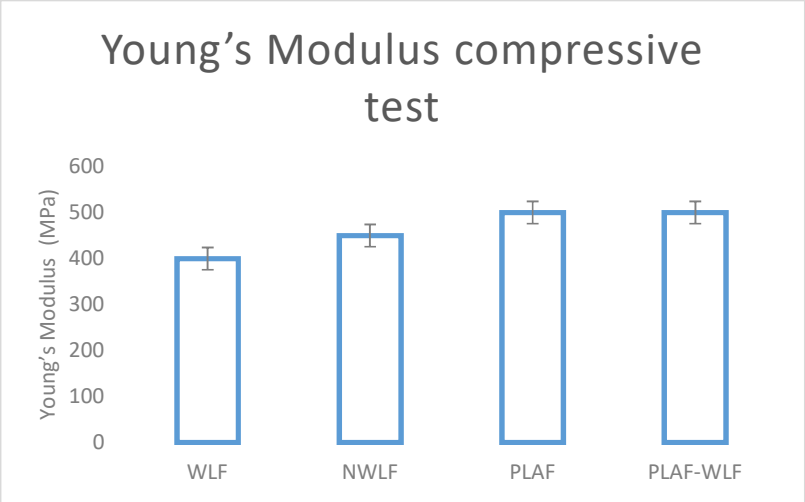

*Figure **V.15**: Young's Modulus compressive test.*

This study demonstrates the successful integration of Periploca laevigata Aiton fiber into composite materials, improving interfacial bonding and overall performance. Four composite materials were created: a composite with untreated Periploca laevigata Aiton fiber (PLAF), a hybrid composite of cold plasma-treated wool fiber and untreated Periploca laevigata Aiton fiber (PLAF-WLF), and composites with untreated wool fiber (WLF) and wool fiber treated with 0.1% NaOH (NWLF). The study revealed that treated fibers had lower adhesion rates compared to untreated ones. Mechanical testing showed that the hybrid composite (PLAF-WLF) outperformed the single fiber composites (PLAF, WLF, and NWLF) in terms of tensile, compressive, and flexural strength. The addition of Periploca laevigata Aiton fiber enhanced the tensile properties of the composites. The vacuum infusion molding process used ensured consistent quality and reduced defects, such as voids, in the composite. The results highlight the compatibility of Periploca laevigata Aiton fiber for hybridization, particularly with wool fiber, leading to significant improvements in mechanical properties. This makes it a versatile and lightweight material for industries aiming to enhance performance. In conclusion, the integration of Periploca laevigata Aiton fiber offers a promising alternative in materials engineering, with potential applications across various industries.

I.5. Scanning electron microscopy (SEM)

Scanning electron microscopy (SEM) was employed to examine the morphology of the four composite materials. Figure **V.3a**, Figure **V.3b,** Figure **V.3c**, and Figure **V.3d** show the SEM micrographs, which clearly depict the surface characteristics of the samples. When observing the surface of untreated wool fiber after conventional cleaning, as seen in Figure **V.3b**, the fibers exhibit distinct scales at the edges, sharp scale structures, and a smooth cuticle layer, attributed to the presence of amino acids. In contrast, Figure**V.3a** and Figure **V.3d** display changes in the surface morphology of the wool-reinforced composites that underwent chemical and cold plasma treatments. The SEM images show that the chemical treatment resulted in a reduction of scale edges, suggesting some smoothing or removal of the scales. On the other

hand, cold plasma treatment introduced a roughness to the cuticle surface. For Periploca laevigata Aiton fiber, shown in Figure **V.3c** and Figure **V.3d**, the surface appears smooth, indicating that the cuticle layer remains in its natural, untreated form. Interestingly, the SEM images in Figure **V.3b** and Figure **V.3c** reveal similar cell structures on the outer layer of both untreated wool fiber and untreated Periploca laevigata Aiton fiber. This shared feature could potentially improve adhesion between the fibers and the resin.

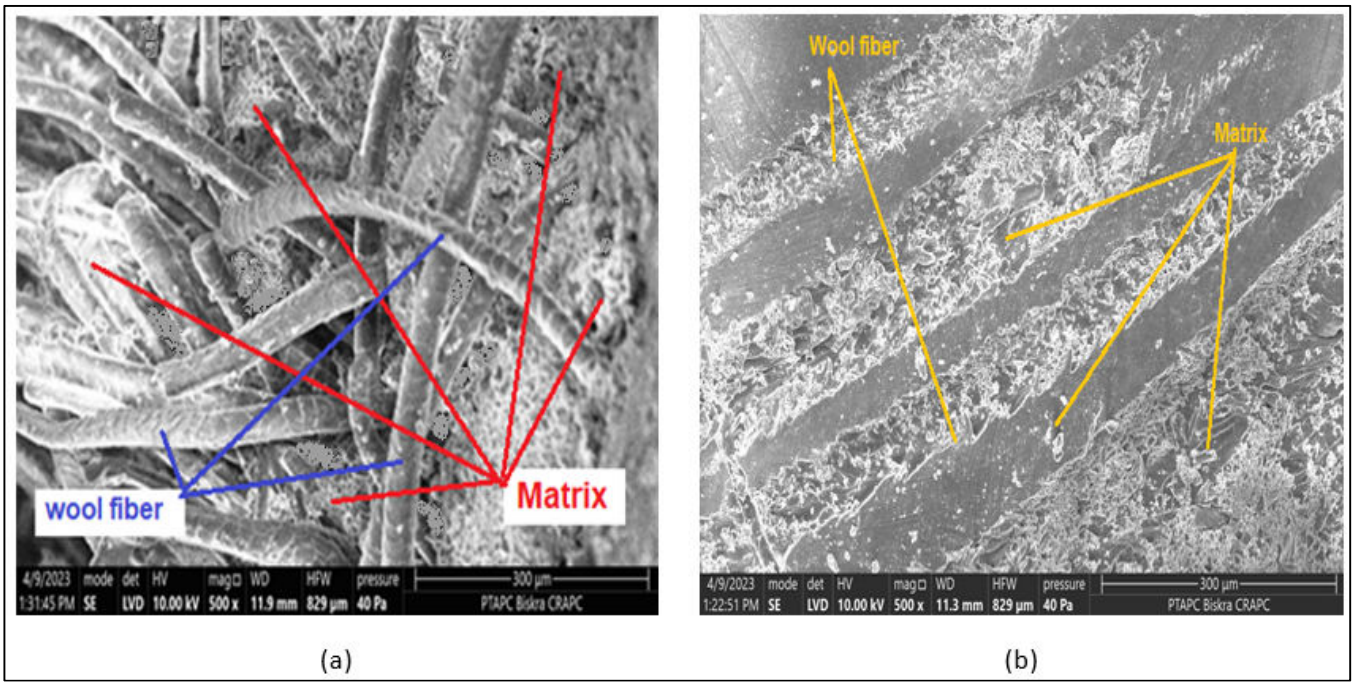

(a) (b)

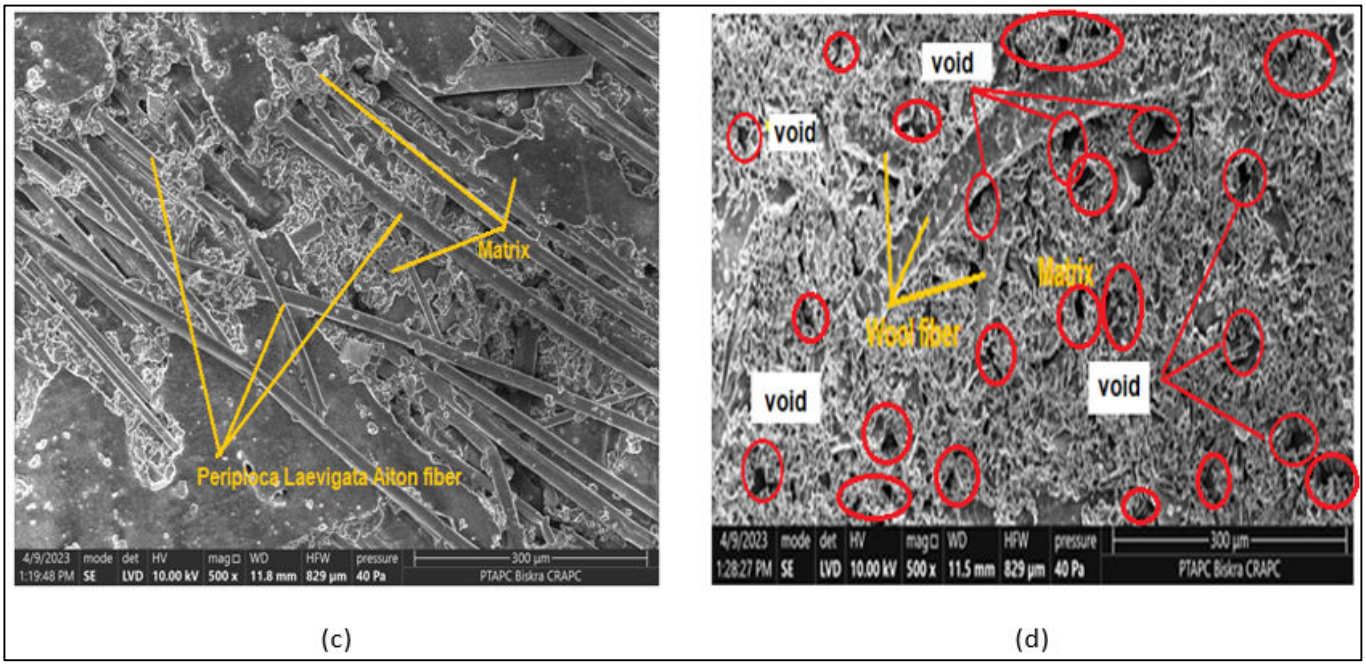

*Figure **V.3**: Scanning Electron Microscopy: (a) PLAF-WLF, (b) NWLF, (c) PLAF, (d) WLF.*

I.6. Conclusion

This study examined the impact of hybridization on composite materials, focusing on the performance of blends of wool and Periploca laevigata Aiton fibers. The hybrid composites demonstrated impressive mechanical properties, including tensile, flexural, and compressive strengths of 26.02 MPa, 2.53 GPa, and 109.22 MPa, respectively, along with Young's modulus values of 2.35 GPa, 1.21 GPa, and 0.50 GPa. These results highlight the potential of these composites as strong alternatives for engineering applications. The combination of cold plasma-treated wool fibers and Periploca laevigata Aiton fibers offers a pioneering solution, providing excellent structural strength, low density (0.45 g/cm³), and remarkable stiffness and durability. Additionally, the Periploca laevigata Aiton fibers possess antibacterial and antioxidant properties, making them appealing for industries focused on long-term durability and opening opportunities in various engineering fields.

II. Experimental III: Fabrication of Single Fiber-Reinforced Composites Using Horse Tail Hair Fiber (HHTF)

II.1. Water absorption

The water absorption of horse hair tail fibers was measured following ASTM D570 standards. The fibers were first dried in an oven at 60°C for 3-4 hours to remove moisture. Their initial weight was recorded, and then they were immersed in water for 24 hours to absorb moisture. After immersion, excess surface water was blotted away to ensure accurate weight measurements. Table **V.4** shows a significant

difference in water absorption between treated and untreated horse tail hair fibers. The treated fibers absorb between 7% and 9% of water, while the untreated fibers absorb much more, ranging from 20% to 23%. This highlights the advantage of treated fibers, particularly their lower hydrophilicity compared to untreated ones.

*Table **V.4**: Water Absorption of Treated and Untreated Horse Tail Hair Fiber.*

Fiber Type	W1 (g)	W2 (g)	Water Abs (%)
Treated horse tail hair	10.0	10.7 - 10.9	7% - 9%
Untreated horse tail hair	10.0	12.0 - 12.3	20% - 23%

II.2. Void content

The presence and morphology of voids significantly influence the performance of composite materials, especially in structural applications, where voids can serve as stress concentrators and compromise mechanical integrity. Understanding how voids form is essential for reducing their occurrence and controlling their distribution. In this study, the density of each composite specimen was evaluated following ASTM D792–08 standards. The theoretical density was calculated using the rule of mixtures, while the experimental density was obtained using the Archimedes principle, which involves measuring the specimen's mass in both air and water. The void content (V%) was then determined by comparing the theoretical and experimental densities. Table **V.5** presents the necessary data for calculating the theoretical density of the composite materials. This calculation is based on the rule of mixtures, which takes into account the densities and weight fractions of both the fiber and the matrix components in each composite. The values provided in the table include the individual densities of the fiber and matrix, along with their respective weight percentages, enabling accurate estimation of the theoretical density for each composite configuration.

*Table **V.5**: The values used for the calculation of the theoretical density of the composite.*

Parameter	Value	Unit
Density of horse hair fiber ρ_f	1.30	g/cm³
Density of epoxy resin ρ_m	1.07	g/cm³
Volume fraction of fiber V_f	0.40	
Volume fraction of matrix V_m	0.60	
Theoretical density of composite ρ_{th}	1.162	g/cm³

The experimental density of a composite is measured using ASTM D792, which calculates density by weighing the specimen in air and in water, helping identify material quality and internal voids. The experimental densities of the composites, shown in Table V.6, were calculated using a constant air weight (Wair = 10 g) and their corresponding fluid weights (Wfluid), following ASTM D792 guidelines.

*Table **V.6**: The experimental densities.*

Samples	Wair (g)	Wfluid (g)	ρ_{exp} (g/cm3)
THTHF-1	10	1,297	1,149
THTHF-2	10	1,282	1,147
THTHF-3	10	1.304	1,150

Table **V.7** presents the final void content results of the composite materials, calculated using both theoretical and experimental density values.

*Table **V.7**: Void content analysis for treated horse tail hair fiber composites.*

Sample	ρ_{th} (g/cm3)	ρ_{exp} (g/cm3)	V (%)
THTHF-1	1,162	1,149	1,131
THTHF-2	1,162	1,147	1,308
THTHF-3	1,162	1,150	1,043

II.3. FTIR analysis

To identify the functional groups, present in horse tail hair fibers, both untreated (UHTHF) and sodium hydroxide-treated (THHF) samples were examined using a Shimadzu IR Affinity-1 FTIR spectrophotometer equipped with an attenuated total reflectance (ATR) accessory. The analysis was performed in transmittance mode across a spectral range of 400–4000 cm^{-1}, with 20 scans recorded for each sample. As illustrated in Figure V.16b and Table **V.8**, notable changes in the chemical structure and functional groups were observed following 1% NaOH treatment. The peak at 3950 cm^{-1} indicates O–H stretching vibrations, which became more pronounced after treatment, suggesting increased hydroxyl group exposure due to the disruption of hydrogen bonds. The peak at 3475 cm^{-1} also corresponds to O–H stretching, representing both free and hydrogen-bonded hydroxyl groups. The 2830 cm^{-1} peak signifies aliphatic C–H stretching from methylene and methyl groups, while the 2345 cm^{-1} peak may reflect carbon dioxide or interactions introduced during treatment. The presence of a carbonyl group is confirmed by the

peak at 1819 cm^{-1} (C=O stretching), and the 1502 cm^{-1} peak indicates N–H bending vibrations, associated with amide groups and the protein structure of the fibers.

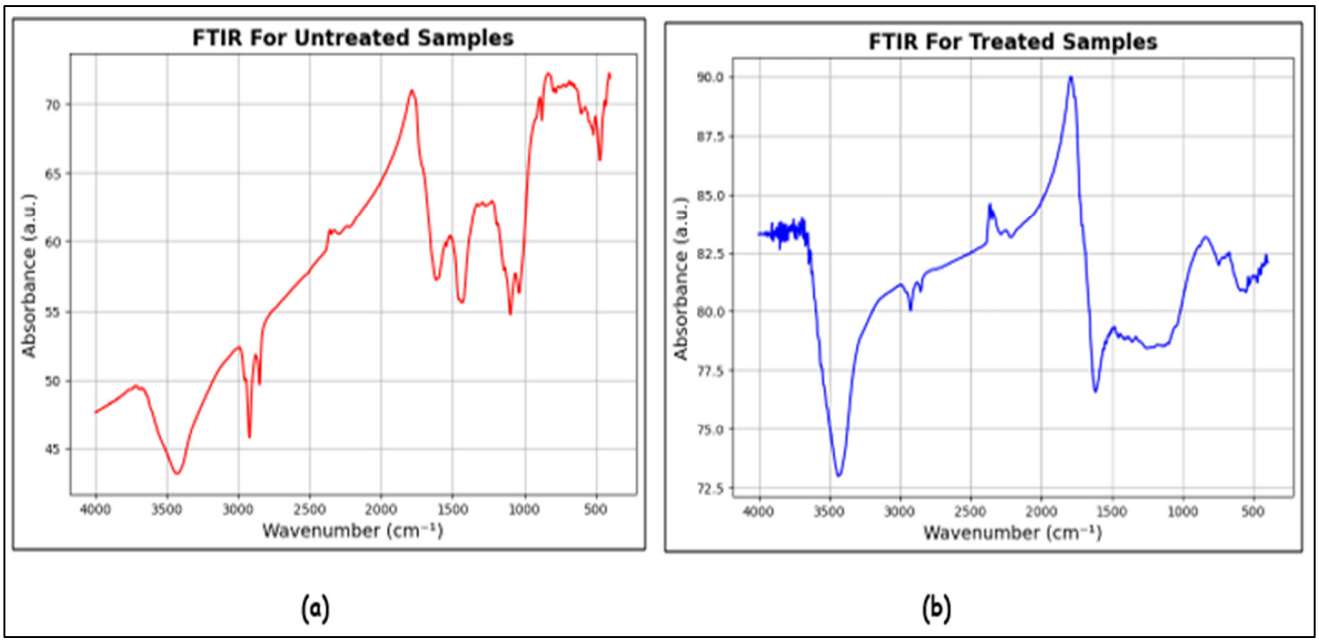

*Figure **V.16**: FTIR, (a) Untreated horse hair fiber, (b) NaOH Treated Horse Hair Fiber (THHF).*

*Table **V.8**: FTIR Peaks of horse tail hair fibers treated with 1% NaOH.*

Wavenumber (cm^{-1})	Functional Group
3950	O–H Stretching
3475	O–H Stretching
2830	C–H Stretching
2345	Weak Peak
1819	C=O Stretching
1502	N–H Bending

As illustrated in Figure **V.16a** and Table **V.9**, the FTIR spectrum of untreated horsetail fiber reveals distinct peaks indicative of its chemical composition. The broad peak at 3500 cm^{-1} signifies the presence of hydroxyl (-OH) groups, suggesting alcohols or phenolic compounds that contribute to the fiber's hydrophilic nature. Peaks around 3000 cm^{-1} and 2750 cm^{-1} correspond to C-H stretching vibrations,

indicating the presence of aliphatic hydrocarbons such as methylene (-CH_2-) and methyl (-CH_3) groups. A peak at 2345 cm^{-1} is attributed to the -CO stretching of amide groups. The 1750 cm^{-1} peak represents carbonyl (C=O) stretching, pointing to the presence of esters or ketones. The peak near 1500 cm^{-1} is associated with C=C stretching or aromatic compounds, suggesting unsaturated or aromatic structures. Additionally, the 1200 cm^{-1} peak reflects C–O stretching vibrations typical in alcohols, ethers, and esters, while the 925 cm^{-1} peak is linked to specific C–O stretches in polysaccharides, highlighting key structural components of the fiber.

*Table **V.9**: FTIR Peaks of untreated horse tail hair fibers.*

Wavenumber (cm^{-1})	Functional Group
3500	Hydroxyl groups (-OH)
300	C-H stretching
2750	C-H stretching
2345	Carbon dioxide
1750	Carbonyl (C=O)
1500	C=C stretching
1200	C-O stretching
925	C-H bending

II.4. Scanning electron microscopic analysis

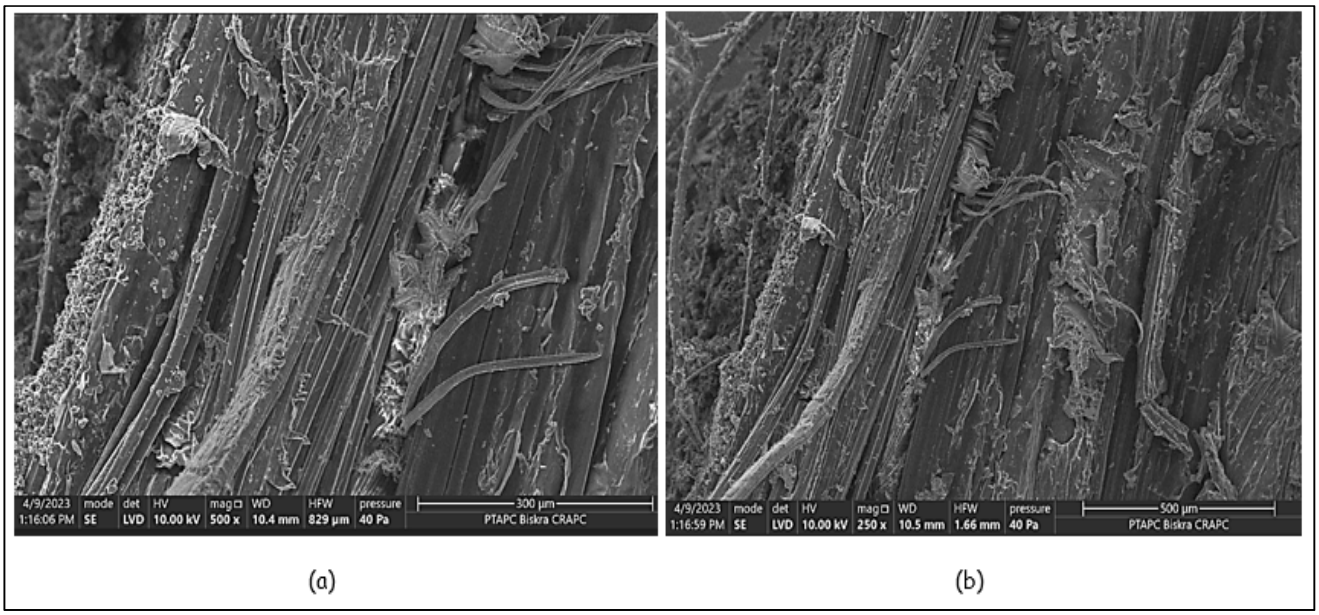

*Figure **V.17**. Scanning Electron Microscopy (SEM) images of NaOH-treated Horse Tail Hair Fiber (THTHF): (a) at 300× magnification, showing surface roughness and exposed fibrils; (b) at 500× magnification, highlighting increased porosity and microstructural*

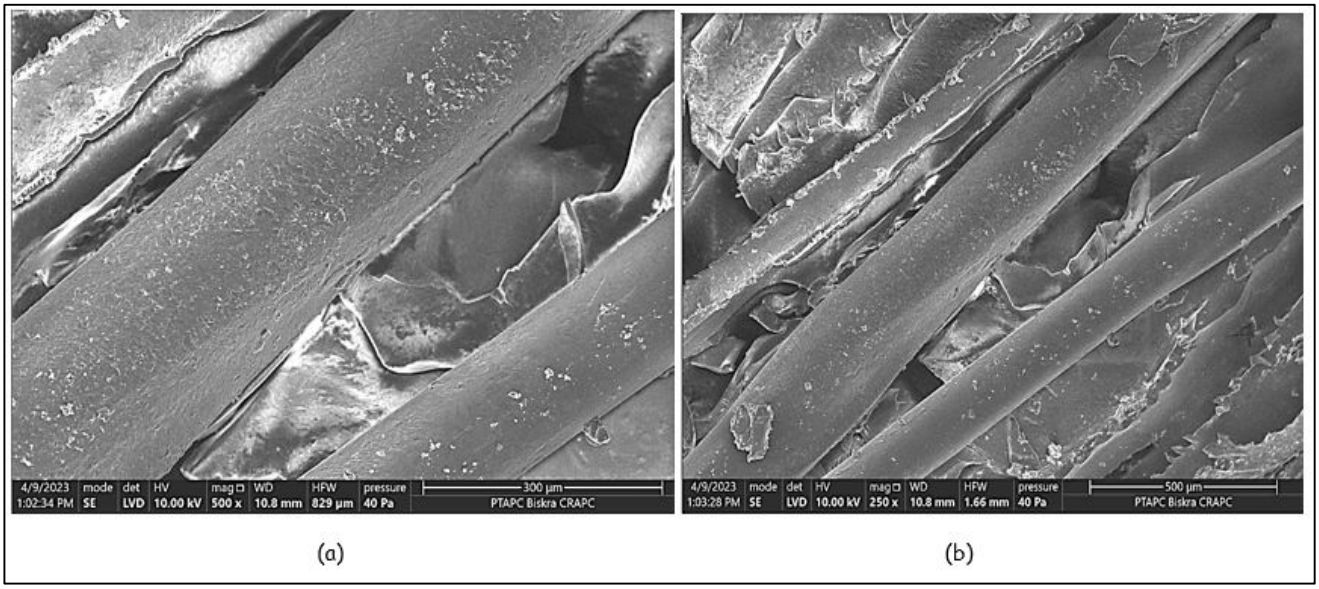

*Figure **V.18**: Scanning Electron Microscopy (SEM) images of Untreated Horse Tail Hair Fiber (UHTHF): (a) at 300× magnification, displaying a relatively smooth surface with minimal surface features; (b) at 500× magnification, illustrating limited porosity.*

II.5. Evaluations of mechanical properties for the four composite materials

II.5.1. Tensile test results

The tensile test specimens of the THHF composite to determine the mechanical properties, including tensile strength (MPa), Young's modulus (GPa), and elongation (%). The results were presented through stress-strain curves, offering a comprehensive understanding of the composite's behavior under tensile loading. The stress-strain relationship exhibits a pronounced linear region, indicative of fiber-dominated mechanical behavior. This linearity is consistent with the established mechanics of composite materials, where properties along the fiber direction are primarily governed by the reinforcing fibers' stiffness and strength. Notably, the composite maintained linearity until fracture, suggesting no plastic deformation occurred in the matrix typical of brittle composites [141]. The high tensile strength observed is attributed to the 1% NaOH treatment of horse tail hair fibers, which enhanced fiber-matrix interfacial adhesion by removing surface impurities and roughening the fiber surface [142, 143]. The vacuum infusion molding technique was also critical in eliminating voids and ensuring uniform resin distribution, thereby further enhancing the composite's mechanical properties [144]. As show in Figure **V.19**, young's modulus of 3.66 GPa underscoring the composite's stiffness, this modulus reflects the treated fibers' ability to support a substantial portion of the applied load before matrix cracking occurs [145]. The treated fibers demonstrated good energy absorption, delaying fracture [146, 147]. The 1% NaOH treatment notably improved the mechanical performance by increasing the fiber's wettability with the epoxy matrix [143]. The fiber to matrix ratio of 30/60 was optimized, ensuring efficient load transfer lead to avoid void formation or poor bonding typically seen with higher fiber contents [148].

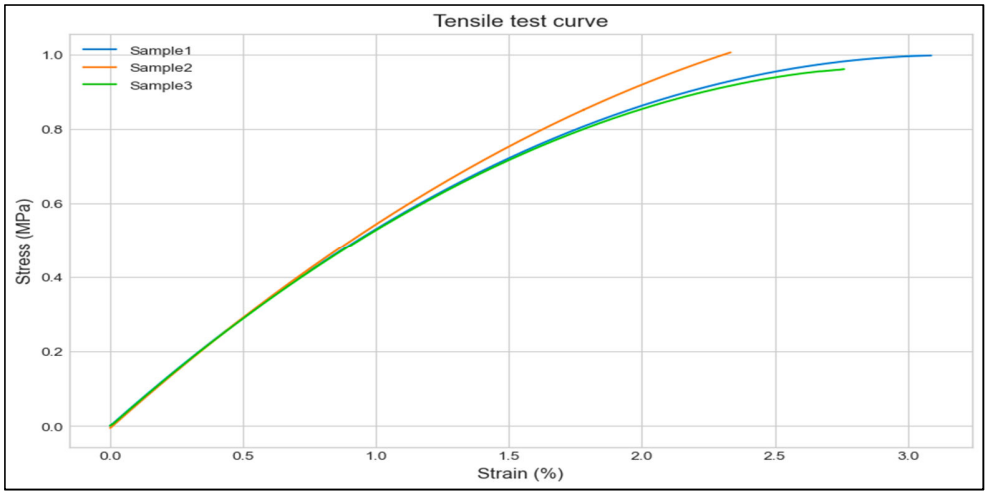

*Figure **V.19**: Stress vs Strain curves for tensile test.*

As shown in the Figure V.19 and Figure V.20 are presents tensile strength and tensile modulus of animal fiber-reinforced composites. The tensile strength and tensile modulus of the treated horse hair fiber (THHF) composite significantly outperform most animal fiber-reinforced composites, indicating its

remarkable mechanical performance. For the THHF composite, the tensile strength values range from 59.797 MPa to 60.295 MPa across three samples. This is considerably higher than that of the animal fiber composites, where the tensile strengths range from 23.2 MPa (treated leather fiber) to 34.95 MPa (treated mixed cow hair and chicken feather with ZnO filler). Even with treatments like 1% NaOH and ZnO fillers, the animal fiber composites show a tensile strength increase of 3% to 94% compared to their untreated counterparts, but these values are still far lower than the THHF composite, which demonstrates nearly 2 to 2.5 times greater tensile strength. The tensile strength of THHF can be attributed to the enhanced fiber-matrix bonding achieved by the NaOH treatment, which improves wettability and fiber surface roughness, resulting in better stress transfer between the fiber and matrix.

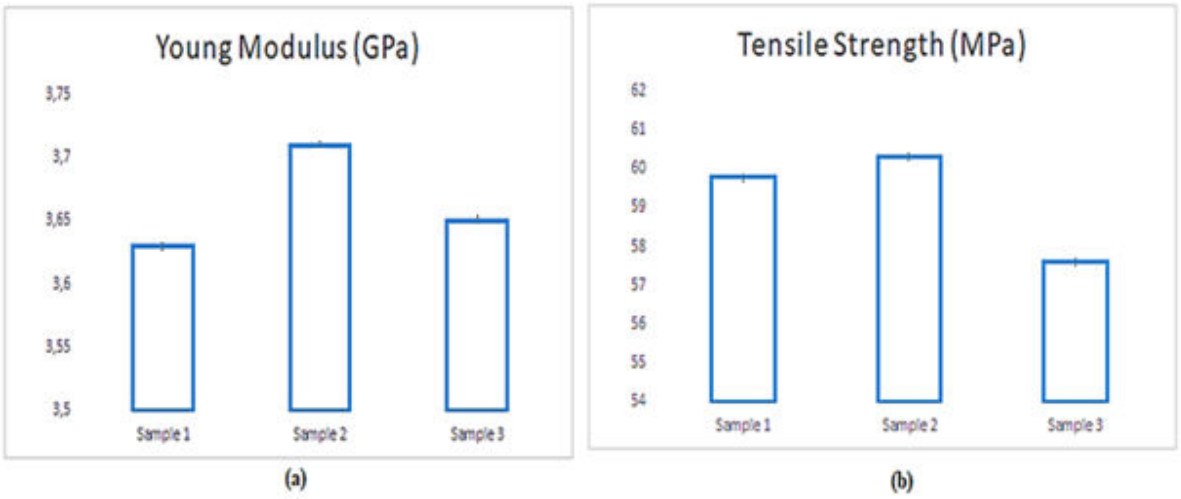

*Figure **V.20**: Tensile test, (a) Young modulus, (b) Tensile Strength.*

II.4.2. Flexural test

The THHF (Treated Horse Hair Fiber) composite demonstrated good performance with flexural strength values between 46.16 MPa and 63.27 MPa. These results, illustrated in Figure **V.21** and Figure **V.22.**

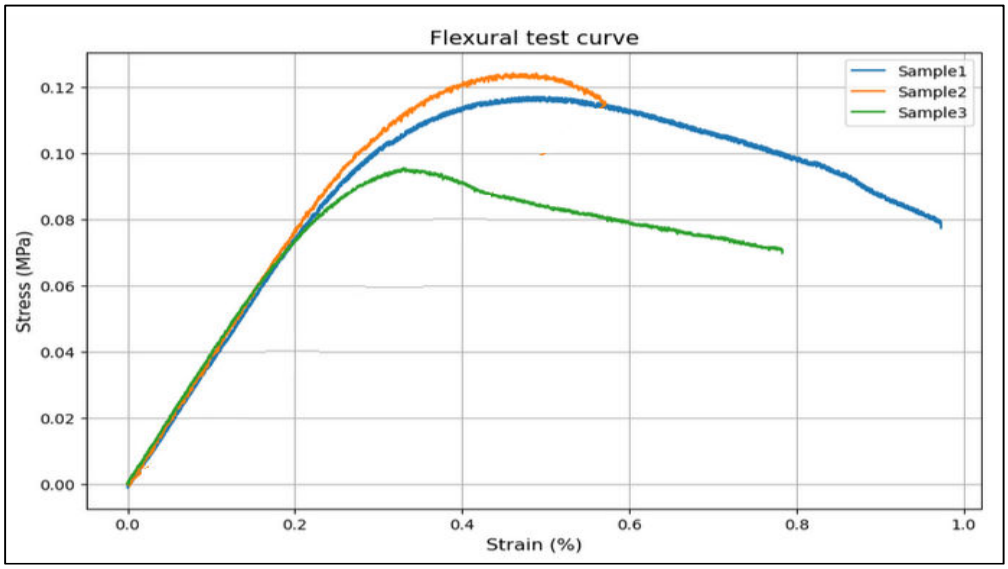

*Figure **V.21**: Stress vs Strain curves for flexural test.*

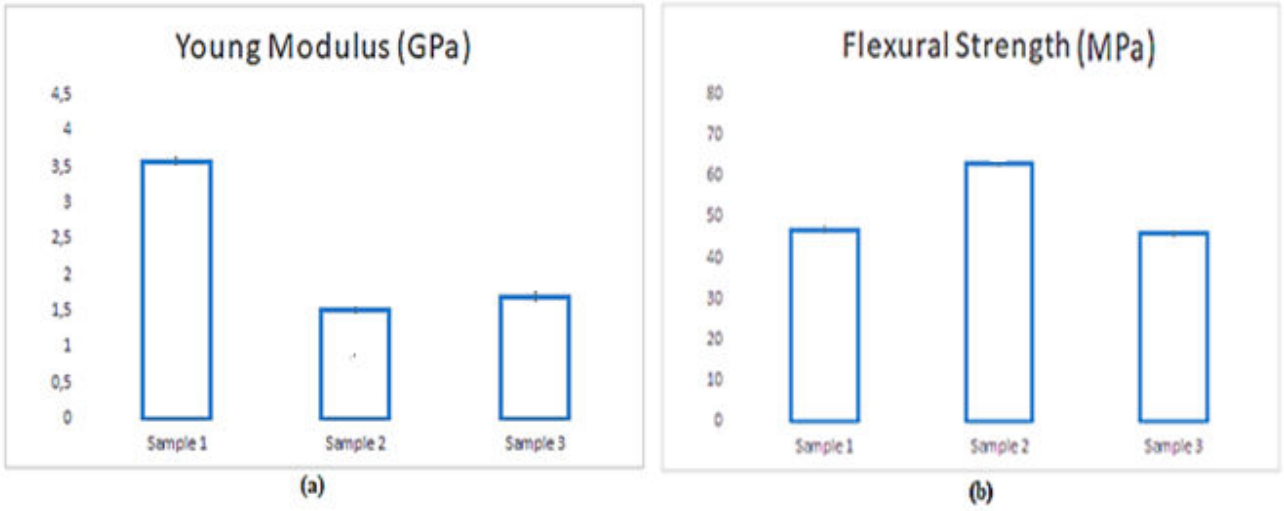

*Figure **V.22**: Flexural test, (a) Young modulus, (b) Flexural Strength.*

II.4.3. Compression test

To ensure reliable comparisons of the mechanical performance across different composite structures, five specimens per configuration were tested under standardized conditions. The procedures for the three tests adhered to ASTM D3410 standards.

Figure **V.23** and Figure **V.24** illustrate the compressive strength range (66.14–78.82 MPa) for the composite material, emphasizing its uniform mechanical performance across samples with only minor

variations. This narrow range strongly suggests a controlled fabrication process, including effective fiber alignment, consistent resin matrix distribution, and good curing quality [149]. Such uniformity is critical for ensuring reliable and predictable mechanical behavior, particularly in structural applications. The average compressive strength of 71.97 MPa positions this composite material within the medium-high strength category for composites. The composite's compressive strength indicates reliable bonding at the fiber-matrix interface, reducing the likelihood of localized stress concentrations that could lead to premature failure. An average Young's modulus of 1.96 GPa highlights the composite's relatively high stiffness under compression, meaning it can resist deformation effectively before reaching its failure point. This stiffness is crucial for maintaining structural integrity under compressive loads, as it reduces the likelihood of buckling or significant dimensional changes during use [150]. The high rigidity also suggests that the composite can retain its shape and performance under sustained loading conditions, further enhancing its suitability for structural applications. When compared to other fiber-reinforced composites, the compressive strength and stiffness of this material make it an good candidate for medium-load applications, such as in construction, automotive components, or lightweight structural frameworks [151]. Its performance reflects a well-optimized design that balances strength, stiffness, and ductility, making it a versatile material for applications requiring a combination of moderate strength and high reliability. The compressive strength and stiffness of the composite material underscore its mechanical robustness and reliability. The uniform range of compressive strength, coupled with a high Young's modulus, reflects a well-engineered fiber-matrix interaction that minimizes failure risks and enhances structural performance [152]. These properties, combined with the gradual failure behavior, position the composite as a safe and efficient material for applications demanding consistent mechanical properties and resistance to compressive deformation.

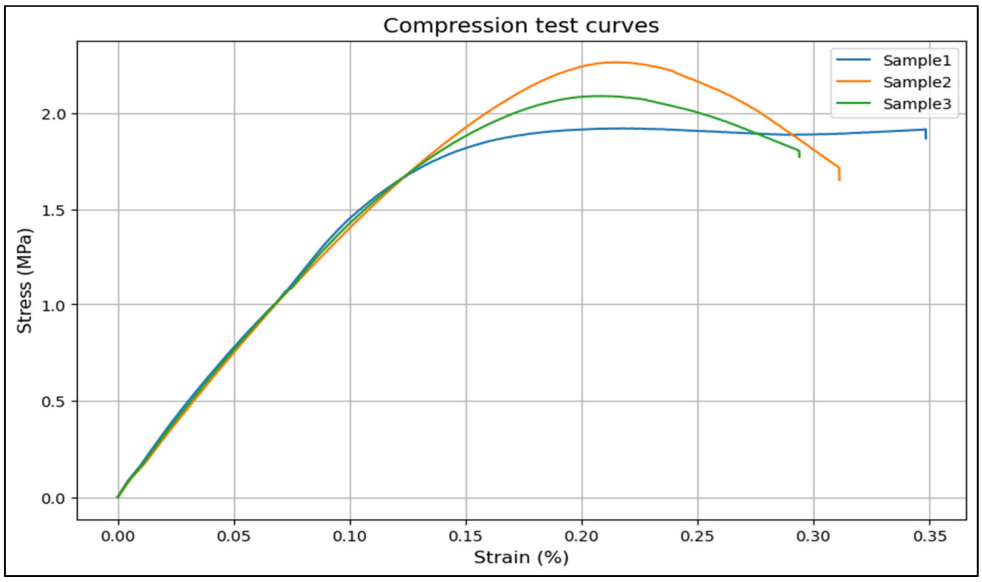

*Figure **V.23**: Stress vs Strain curves for compression test.*

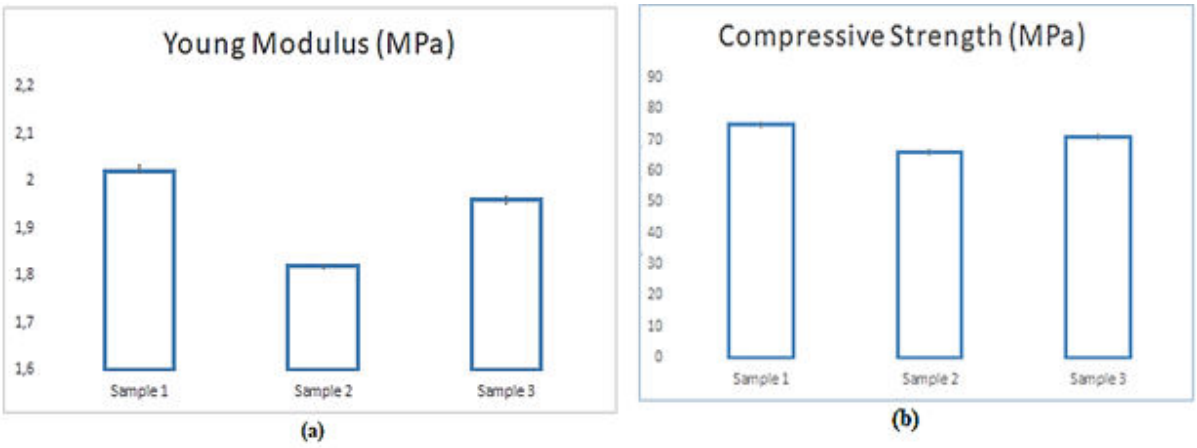

*Figure **V.24**: Compression test, (a) Young modulus, (b) Compressive Strength.*

II.5. Conclusion

The treated horse tail hair fiber (THHF) composites exhibit exceptional mechanical performance, surpassing most animal fiber-reinforced composites and highlighting their potential as a sustainable and high-performing reinforcement material. The tensile strength of THHF composites ranges from 59.797 MPa to 60.295 MPa, reflecting their capability to withstand substantial tensile loads, which is critical for structural applications. Similarly, their flexural strength, peaking at 63.27 N/mm² in Sample 2, demonstrates competitive bending performance, while the compressive strength, ranging from 66.14 MPa to 78.82 MPa, underscores the material's uniformity and reliability. This consistency is attributed to precise fiber alignment, optimized resin matrix distribution, and high curing quality during fabrication. The superior performance of THHF composites stems from the intrinsic properties of the single treated horse tail hair fibers, which possess an average tensile strength of 129.34 MPa and a Young's modulus of 5.72 GPa, indicating high stiffness and load-bearing capacity. These properties form a strong foundation for the composite's reinforcement capabilities, enabling efficient load transfer and excellent mechanical integrity. The application of alkaline surface treatment plays a pivotal role in enhancing the mechanical performance of THHF composites. This treatment removes residual organic impurities, increases surface roughness, and significantly improves fiber-matrix adhesion, thereby boosting load transfer efficiency. It also mitigates potential fiber pull-out, ensuring robust interfacial bonding and increased durability under mechanical stress. Additionally, the treatment reduces the fibers' water absorption by approximately 60% to 65%, ensuring long-term stability in humid environments. The composites exhibit remarkable stiffness and strength, with bending strength values reaching 63.27 MPa and a Young's modulus up to 1.68 GPa, ensuring excellent resistance to deformation and flexural loads. This balance of high strength and stiffness positions THHF composites as a versatile material for advanced structural applications, capable of withstanding demanding performance requirements while maintaining durability and reliability. These findings firmly establish THHF composites as a promising, eco-friendly alternative to conventional reinforcing materials. Their superior mechanical performance, combined with their environmental sustainability, makes them an ideal candidate for next-generation composite solutions. By leveraging the

outstanding properties of treated horse tail hair fibers, these composites address the increasing demand for high-performance, sustainable materials in diverse industrial applications, from construction to automotive and aerospace engineering. The synergy of mechanical excellence and sustainability ensures that THHF composites will play a pivotal role in advancing material engineering and promoting eco-conscious innovation.

III. Experimental III: Failure Analysis of Periploca Laevigata Aiton-Wool Hybrid Composites Under Low-Velocity Impact

III.1. Impact Test

The composite was created using the vacuum infusion molding method, chosen for its ability to produce high-quality, void-free structures with superior fiber wetting. A metal mold measuring 250 × 300 × 4 mm³ was used throughout the procedure. For single-fiber composites, a solitary layer of randomly oriented fibers was uniformly spread over the mold surface. Conversely, the hybrid composites featured woven reinforcement designs, integrating wool and Periploca laevigata Aiton fibers in a well-organized arrangement to enhance mechanical synergy. During the fabrication process, epoxy resin was introduced into the mold under a vacuum pressure of about 0.32 MPa, ensuring uniform resin infiltration and complete impregnation of the fiber network. This method markedly decreased the presence of voids and enhanced the interfacial bonding between the fibers and the matrix. The epoxy resin system was blended at a 2:1 volume ratio (resin to hardener), resulting in a viscosity of 280 mPa·s and a mixed density of 1.07 g/cm³ at 25°C. The pot life of the mixture was roughly 90 minutes, offering sufficient time for the infusion process.

To ensure complete cross-linking, the composites were left to cure for seven days at room temperature following the infusion procedure. If deemed necessary, a post-curing procedure was carried out in accordance with the resin manufacturer's instructions to enhance the composites' mechanical and thermal properties even more.

In assessing the best fiber-to-resin ratio, earlier research has explored volume fractions that range from 30/70 to 50/50 (fiber/matrix). A 30/70 ratio is typically regarded as the minimum threshold for sustaining adequate mechanical performance, as a further decrease in fiber content can lead to a notable drop in structural integrity. While a 50/50 mixture improves reinforcement, it usually results in increased moisture absorption, which could jeopardize the composite's durability. Likewise, although a 60/40 ratio provides better chemical resistance, it may hinder fiber dispersion and restrict matrix availability for optimal wetting and bonding. When fiber content surpasses 50%, mechanical performance may deteriorate due to a lack of matrix material, causing poor load transfer and weak interfacial adhesion.

After the curing process, composite laminates were sliced into test samples with dimensions of 60 mm × 60 mm utilizing a water jet cutting method. This size was chosen to guarantee compatibility with the IMATEK IM10T drop-weight impact testing apparatus and to allow sufficient surface area for monitoring damage progression while preserving specimen integrity during dynamic loading.

To investigate the damage mechanisms and assess various impact parameters, the composite was impacted with energies of 5 J, 10 J, 30 J, and 50 J, leading to complete sample perforation. For every energy level, at least three (03) impact tests were conducted on each composite material system to guarantee consistent and dependable results. These tests were carried out using a drop-weight testing machine following ASTM D7136, the recognized testing standard for measuring the damage resistance of fiber-reinforced polymer composites under drop-weight impact conditions.

The drop-weight impact tests were performed utilizing the IMATEK IM10T instrumented falling-weight impact test apparatus, as illustrated in Figure III.1a and Figure III.1b This device was coupled with the IMATEK Impact Analysis software to gather comprehensive impact data. The impact force was captured using a piezoelectric load cell, which has the capability of gathering 32,000 data points, and was mounted in the impactor. The system possesses a peak force accuracy of 1%. The software calculates essential parameters, including force-time data, velocity, displacement, and energy absorption by the specimen.

During the experiments, a striker attached to a weight was lowered onto the specimen at a predetermined impact speed. The impactor utilized was hemispherical, measuring 20 mm in diameter and weighing 1.223 kg (total drop mass: 14.56 kg). The specimens, sized at 60 mm x 60 mm x 4 mm, were secured at the ends. The drop height was modified to attain the target impact energy levels of 5 J, 10 J, 30 J, and 50 J. The respective velocities were 0.885 m/s, 1.147 m/s, 2.125 m/s, and 2.582 m/s for each energy level, respectively.

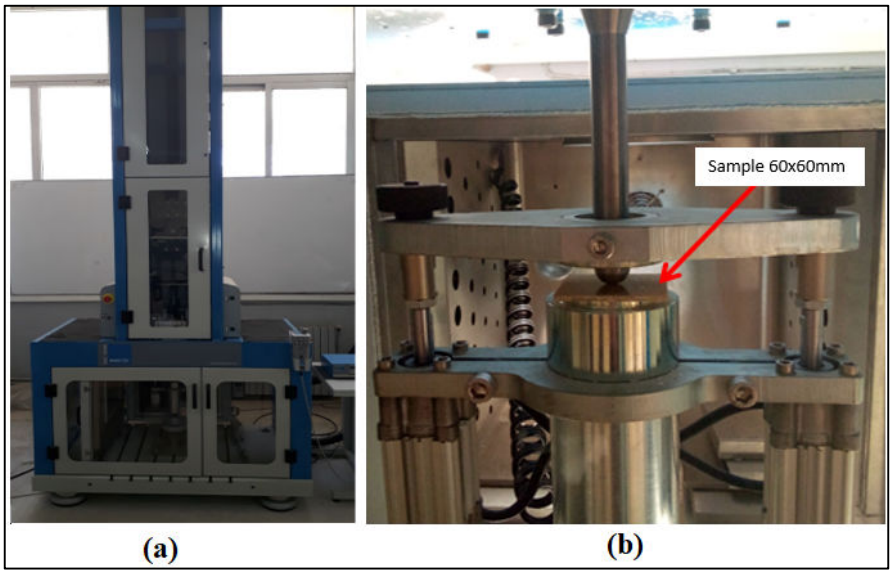

*Figure **V.25**: (a): Drop weight test machine, (b): Fixture and weight location.*

III.2. Results and Discussions

III.2.1. Energy vs. Time Curves

As shown in Figure **V.25** the energy–time (E–t) curves of the impacted composites reveal distinct behaviors characteristic of composite materials under low-velocity impact. Initially, the energy as a function of time increases rapidly, corresponding to the transfer of kinetic energy from the impactor to the composite, this phase ends at the maximum energy point, representing the total kinetic energy of the impactor. After this peak, the energy decreases, reflecting dissipation mechanisms within the composite, such as deformation, matrix cracking, and fiber breakage. The final energy value on the curve represents

the total energy absorbed by the composite material. Comparing different composites, materials with higher toughness or better fiber-matrix bonding demonstrate a broader curve with a slower decline after the peak, indicating better energy dissipation and impact resistance. Hybrid composites PLAWLF exhibit superior energy absorption due to the combination of stiffness and flexibility in their structure[153]. These composites effectively dissipate energy over time, reducing the risk of catastrophic failure. In contrast, untreated fiber composites show a steeper energy decline, indicating lower absorbed energy and reduced toughness. The energy–time curves provide valuable insights into the impact performance of composites, highlighting the critical role of material design in enhancing energy absorption and resistance to damage. PLAWLF absorbed the most energy across all impact levels, particularly at 50 J, where its fiber synergy effectively dissipated impact forces, preventing high damage. NWLF absorbed more energy compared to WLF and PLAF, attributed to its improved fiber-matrix interface [154]. PLAWLF consistently demonstrated the highest peak forces and stiffness, indicating superior resistance to penetration and deformation [155]. NWLF performed better than untreated WLF, showing that chemical treatments like NaOH significantly enhance performance. At lower energies, all composites showed significant energy rebound, but PLAWLF exhibited delayed rebound, reflecting its ability to absorb and dissipate energy elastically. At 5 J, energy absorption is limited across all composites, with PLAWLF and NWLF showing slightly higher values compared to untreated WLF, highlighting their improved ability to withstand low-energy impacts. PLAWLF absorbs energy more effectively due to its hybrid structure, which combines the toughness and flexibility of plasma-treated wool fibers with the stiffness of Periploca laevigata Aiton fibers, enabling better dissipation of impact energy[156, 157]. At 10 J, energy absorption increases significantly for PLAWLF outperforms others, absorbing more energy than WLF and PLAF individually, reflecting its superior resistance to crack propagation and its ability to dissipate higher impact forces efficiently [158]. The NaOH-treated NWLF also demonstrates enhanced energy absorption compared to untreated WLF, attributed to the improved fiber-matrix adhesion, which reduces fiber pull-out and promotes effective load transfer [159]. At 30 J, PLAWLF maintains its good properties in energy absorption, showcasing its ability to resist failure under higher impact energies. The hybrid structure ensures better load distribution and minimizes internal damage, NWLF also performs well at this energy level but falls behind PLAWLF, indicating that hybridization offers a more robust solution, and for impact energy of 50 J, PLAWLF demonstrates exceptional energy absorption, maintaining structural integrity despite increased impact energy. The hybrid composite's ability to delay crack propagation and manage energy dissipation[156, 157, 159]. PLAWLF absorbs significantly more energy across all tested impact energies, making it the most effective composite for resisting and dissipating impact forces. Its hybrid structure provides a balanced combination of stiffness and toughness, ensuring superior energy absorption and impact resistance compared to single-fiber or chemically treated composites [153].

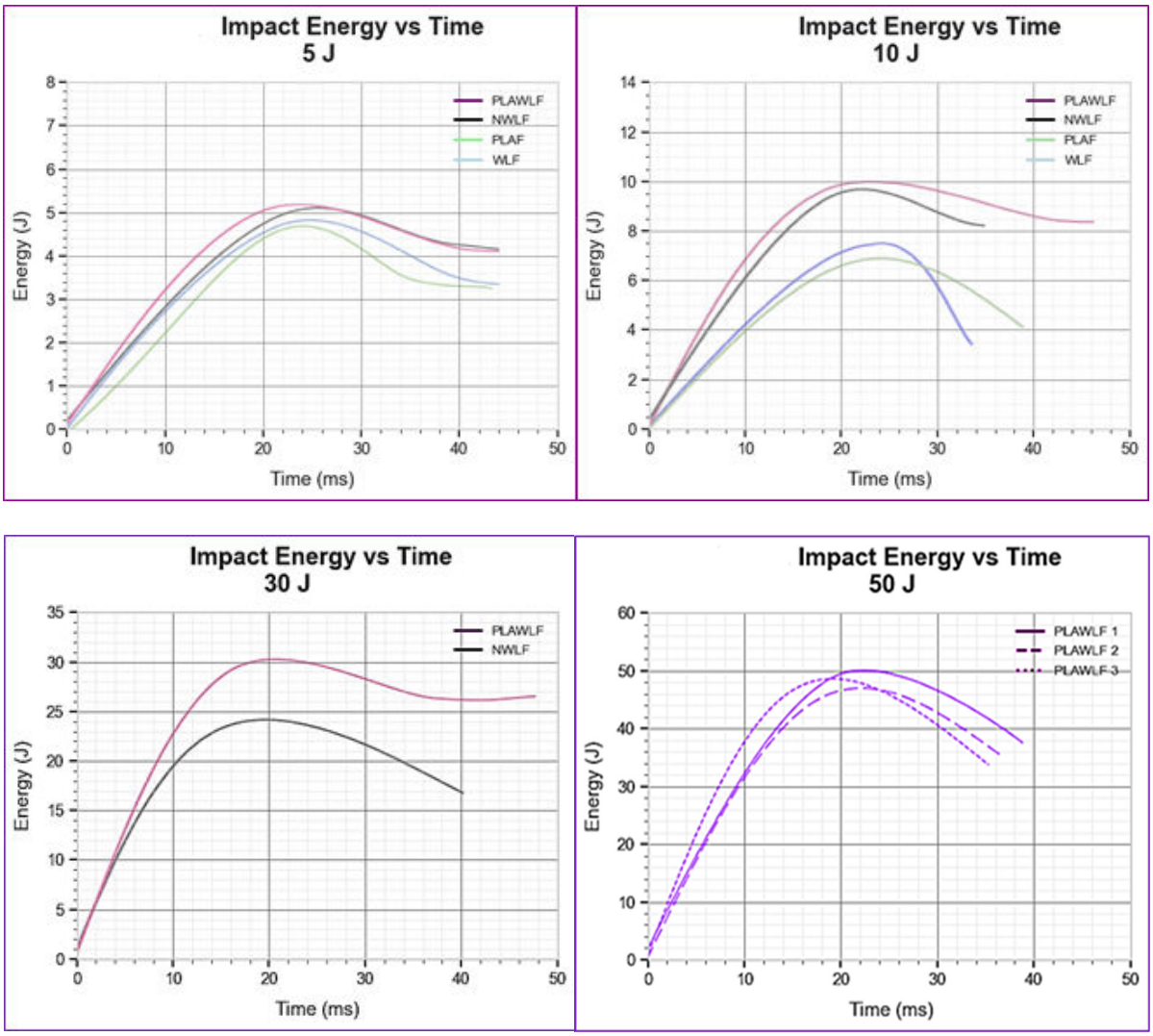

*Figure **V.26**: Diagrams Impact energy vs. time.*

As shown in Figure V**.26** and Figure **V.27**, At an impact energy of 5 J, PLAWLF exhibited the highest absorbed energy, demonstrating its superior impact resistance. Compared to PLAF, PLAWLF showed a significant improvement of 30.23%, while NWLF showed a 29.79% increase. Similarly, PLAWLF absorbed 17.65% more energy than WLF, whereas NWLF showed a comparable improvement of 17.29% over WLF. On the other hand, PLAF absorbed the least energy, 23.26% lower than PLAWLF and 22.98% lower than NWLF, indicating its lower toughness and energy dissipation capacity. WLF, while better than PLAF by 10.69%, still lagged significantly behind both NWLF and PLAWLF. The close performance of NWLF and PLAWLF highlights the effectiveness of chemical treatments and hybridization in enhancing the energy absorption of composites. At an impact energy of 10 J WLF absorbed the least energy, 33.75% less than PLAF, and 64.37% less than PLAWLF. PLAF absorbed 50.71% less energy than NWLF and 52.33% less than PLAWLF, indicating its poor performance in terms of energy dissipation and impact

resistance. The superior performance of PLAWLF and NWLF highlights the benefits of hybridization and chemical treatment in enhancing energy absorption, making them more resilient to impact damage compared to untreated or single-fiber composites like PLAF and WLF [153, 160].At an impact energy of 30 J, the absorbed energies for the composites NWLF absorbed 26.823 J, while PLAWLF absorbed 16.232 J. NWLF absorbed 65.39% more energy than PLAWLF, but despite this high energy absorption, the composite experienced full penetration, indicating its failure under the higher impact energy. PLAWLF absorbed 39.61% less energy than NWLF, yet it withstood the impact without full penetration, demonstrating superior impact resistance and structural integrity compared to NWLF. The full penetration of NWLF suggests that while it has a high energy absorption capacity, its ability to dissipate energy is limited under high-impact conditions, leading to failure. On the other hand, PLAWLF, although absorbing less energy, managed to maintain its form, making it a more reliable material for impact-resistant applications at higher energy levels. At an impact energy of 50 J, the absorbed energies for the three PLAWLF samples were 35.102 J, 36.541 J, and 37.254 J. While these composites absorbed a significant portion of the impact energy, two samples experienced full penetration, and one sample showed damage but did not fully penetrate. The absorbed energy values showed slight variations: the second composite absorbed 6.15% more energy than the first, and the third absorbed 1.95% more energy than the second. These results indicate that PLAWLF can absorb a substantial amount of energy (up to 74.51% of the total impact energy), but its performance is inconsistent at high energy levels, leading to failure in some samples. The full penetration in two of the composites suggests that while PLAWLF is effective at dissipating energy, it has limitations under extreme impact conditions, with some samples unable to resist the 50 J energy fully

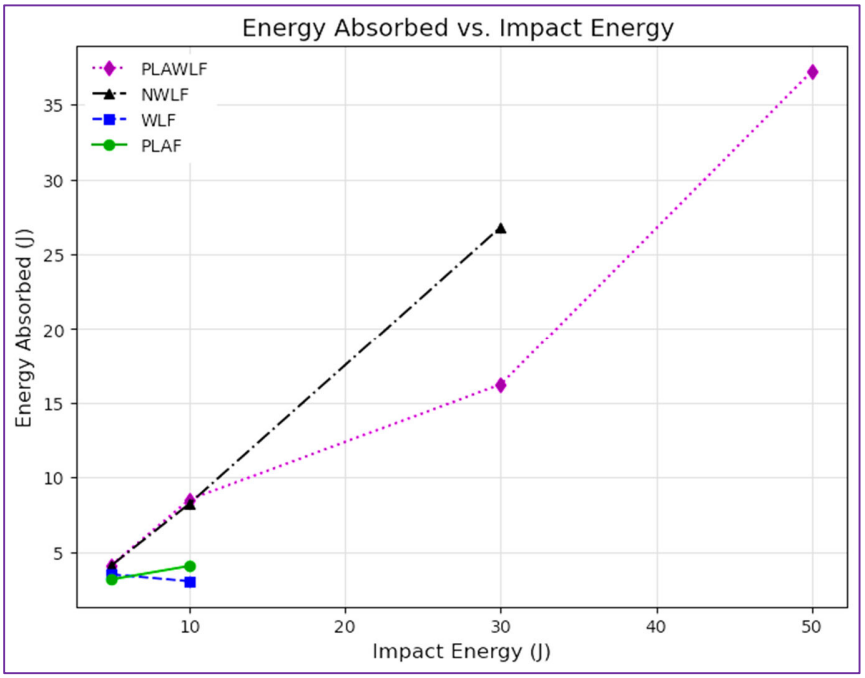

*Figure **V.27**: Impact energy vs. Absorbed energy.*

As shown in Table **V.10**, at 5 J untreated wool fiber (WLF) has the lowest peak load of 0.912 KN, indicating lower resistance to impact. PLAWLF and NWLF have nearly identical peak loads of 1.0115 KN and 1.0123 KN, showing similar resistance under low energy. For impact energy of 10 J PLAWLF achieves the highest peak load of 1.495 KN, significantly higher than NWLF of 1.402 KN and other composites. WLF remains the lowest peak load of 1.121 KN. NWLF shows improvement over untreated WLF due to chemical treatment, which enhances fiber-matrix bonding[7].The increased peak load with energy indicates that composites require greater force to deform under higher energy. Table **III.2**shows the result for Impact energy of 10 J, the hybrid composite PLAWLF demonstrates the highest peak load of 1.495 N and a displacement of 5.00 mm, outperforming PLAF and WLF, which exhibit lower peak loads of 1.203 KN and 1.121 KN, respectively, and higher displacements.

*Table **V.10**. Peak load and displacement at peak load for Energy Level of 5 J*

Composite	Peak Load(KN)	Displacement at Peak Load(mm)
PLAF	0.992	4.125
WLF	0.912	4.281
NWLF	1.0123	4.253
PLAWLF	1.0115	4.254

This good performance of PLAWLF is due to the hybridization of Periploca laevigata Aiton fibers and wool fibers treated by plasma, which combines the stiffness and load-bearing capacity of Periploca with the flexibility and toughness of the wool, resulting in enhanced energy dissipation and crack resistance[161]**.**Chemical-treated of wool fiber (NWLF) shows a significant improvement in peak load of 1.402 KN at 10 J compared to untreated wool fiber (WLF) 1.121 KN, along with reduced displacement, reflecting the effect of NaOH treatment in enhancing fiber-matrix bonding, reducing fiber pull-out, and improving load transfer efficiency [162].

Table **V.11**. Peak load and displacement at peak load for Energy Level of 10 J.

Composite	Peak Load(KN)	Displacement at Peak Load(mm)
PLAF	1.203	6.252, ± 0.0130
WLF	1.121	6.253, ± 0.0140
NWLF	1.402	5.000, ± 0.0075
PLAWLF	1.495	5.000, ± 0.0060

Table **V.12** presents results at higher impact energy levels, such as 30 J and 50 J, the hybrid composite PLAWLF maintains superior toughness and energy absorption, indicating its ability to delay crack propagation and resist failure [163]. At an impact energy of 30 J, PLAWLF shows the highest peak load of 2.921 KN, indicating good resistance to impact forces. NWLF follows with a peak load of 2.253 KN, showing a significant improvement compared to its performance at 10 J of 1.402 KN. PLAWLF's hybrid structure allows it to withstand higher loads due to its synergistic combination of stiffness from Periploca and flexibility from wool fiber treated by plasma, enabling better load distribution and crack

resistance[72].NWLF, with improved fiber-matrix bonding due to NaOH treatment, exhibits enhanced performance but still lags behind PLAWLF, reflecting its limited structural integration compared to hybrid composites. The increasing peak load with energy for both composites highlights their ability to resist higher forces before deformation or damage[164].

*Table **V.12**. Peak load and displacement at peak load for Energy Level of 30 J.*

Composite	Peak Load(KN)	Displacement at Peak Load (mm)
NWLF	2.253	7.532
PLAWLF	2.921	6.321

AS shown in Table **V.13**, Peak Load at impact energy of 50 J for PLAWLF 1, PLAWLF 2, and PLAWLF 3 are 4.120 KN, 3.981 KN, and 3.721 KN respectively. Despite the variations in composition, PLAWLF maintains effective energy absorption and deformation at 50 J. This indicates that PLAWLF's hybrid nature contributes significantly to energy dissipation and impact resistance[165]. However, the slight reduction in peak load from PLAWLF 1 to PLAWLF 3 suggests that uniform distribution and consistency in composite composition play a role in maintaining peak load resistance.

.

*Table **V.13**. Peak load and displacement at peak load for Energy Level of 50 J.*

Composite	Peak Load(KN)	Displacement at Peak Load (mm)
PLAWLF 1	4.120	7.022
PLAWLF 2	3.981	7.500
PLAWLF 3	3.721	7.981

III.2.2. Load vs. Time Curves

The impact response of the four composite samples, PLAF, WLF, NWLF, and PLAWLF, under impact energies ranging from 5 J to 50 J, is illustrated in the Load–time (L–t) histories. At low energy levels**,** the force peaked quickly and dropped off sharply, indicating elastic deformation and rebound for all composites[166]. PLAWLF exhibited the highest peak load, showcasing better resistance to initial penetration. At higher energy levels**,** the curves became broader, with prolonged impact durations, reflecting greater energy absorption and material deformation. PLAWLF again demonstrated the highest peak force and prolonged resistance, indicating its ability to withstand and dissipate higher energy without failure[156]. As shown in and above tables, at 5 J, the untreated wool fiber composite (WLF) shows the lowest peak load of 0.912 KN, indicating poor impact resistance[167]. In contrast, PLAWLF and NWLF exhibit higher peak loads of 1.0115 KN and 1.0123 KN, respectively, due to improved fiber-matrix bonding and hybridization. At 10 J, PLAWLF achieves the highest peak load of 1.495 KN, surpassing NWLF (1.402 KN), PLAF (1.203 KN), and WLF (1.121 KN). The superior performance of PLAWLF is attributed to the combined stiffness of Periploca fibers and the flexibility of plasma-treated wool fibers, enhancing energy dissipation and crack resistance[167, 168]. NWLF shows significant improvement over WLF due to NaOH treatment, which strengthens fiber-matrix adhesion. At 30 J, PLAWLF continues to lead with the highest peak load of 2.921 KN, demonstrating its ability to resist deformation and delay

crack propagation. NWLF, with 2.253 KN, shows notable improvement but remains behind PLAWLF. At 50 J, PLAWLF samples achieve peak loads of 4.120 KN, 3.981 KN, and 3.721 KN, reflecting consistent energy absorption and deformation resistance[156]. These results highlight the role of uniform fiber distribution in maintaining performance. In conclusion, PLAWLF consistently achieves the highest peak loads across all energy levels, making it the most impact-resistant composite due to its optimized hybrid structure that combines stiffness, flexibility, and toughness[153].

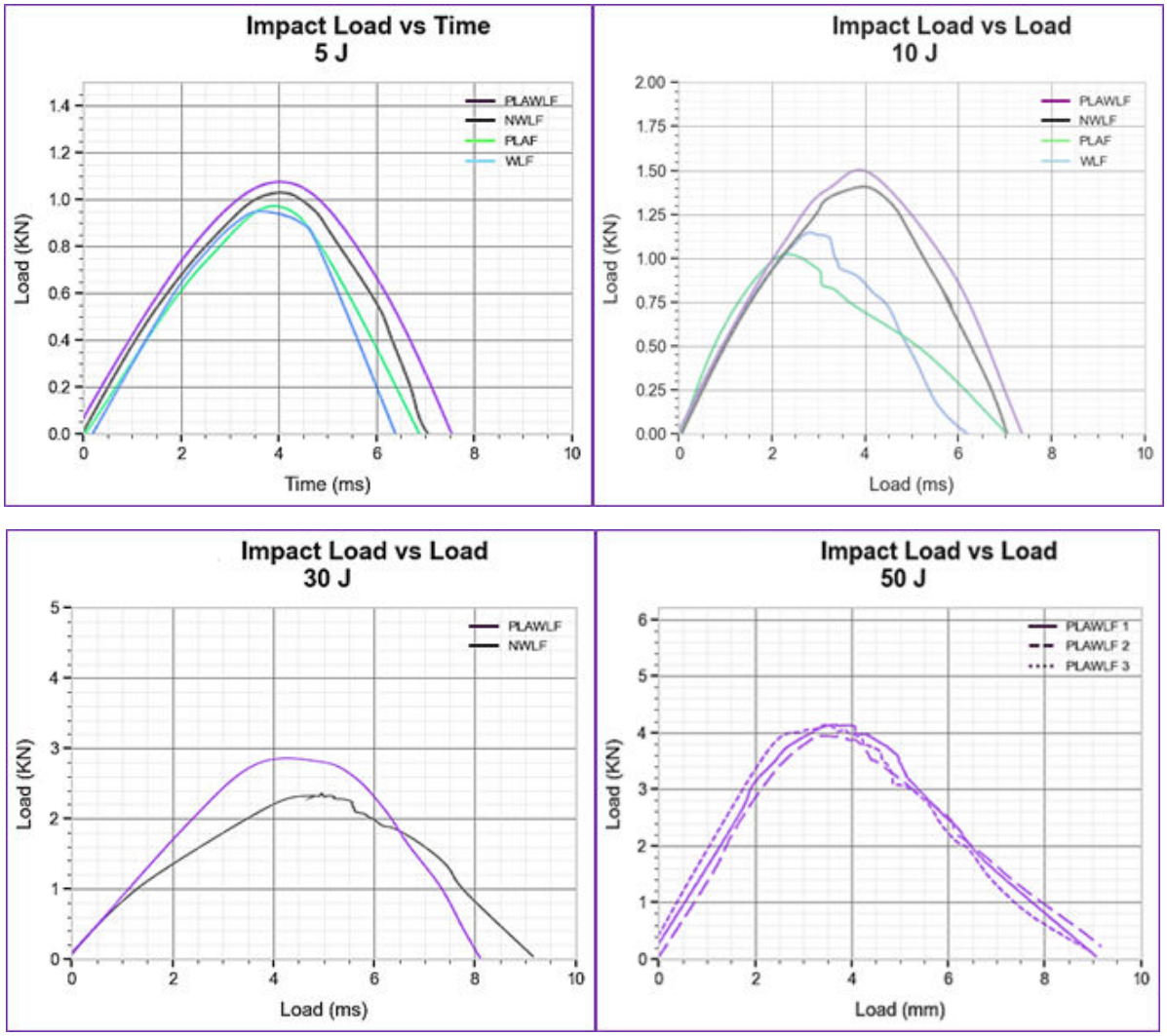

*Figure **V.28**: Diagrams Impact Load vs. Time.*

The maximum force at the maximum displacement corresponds to the maximum energy absorbed by the composite. This point represents the peak of the material's ability to dissipate energy through deformation and damage mechanisms such as matrix cracking[169]. Beyond this point, the composite begins to rebound, transferring the stored elastic energy back to the impactor[170]. At impact, with energy of 30 J for NWLF and 50 J for PLAWLF, the load–time curves reveal distinct behaviors indicative of the materials' failure mechanisms. For NWLF at 30 J, a sudden drop in force after reaching the maximum

force suggests the onset of perforation[171].This behavior points to the failure mechanisms dominated by fiber breakage, and matrix cracking leading to a rapid loss of resistance[156, 171].For PLAWLF at 30 J, the curve displays a symmetric shape without fluctuations, highlighting the composite's ability to absorb and dissipate energy effectively up to the point of perforation. The absence of significant fluctuations in the force response reflects a more controlled failure mechanism, where energy is absorbed through progressive matrix cracking and fiber-matrix interaction rather than sudden catastrophic failure[156].

III.2.3. Load vs. Displacement Curves

As shown in Figure**V.29**,Figure **V.30**, and the above tables, the Load-displacement curves reveal the materials' stiffness, ductility, and permanent deformation under impact[172].At 5 J and 10 J, all composites displayed smaller displacements at peak load, signifying elastic behavior and minimal damage. PLAWLF showed the steepest slope (highest stiffness) and the lowest permanent deformation, confirming its superior structural integrity[157, 173].At 30 J and 50 J, the composites displayed more pronounced permanent displacements, indicating damage initiation. PLAWLF maintained a steeper curve initially, reflecting higher stiffness, and exhibited the least permanent deformation due to its hybrid.

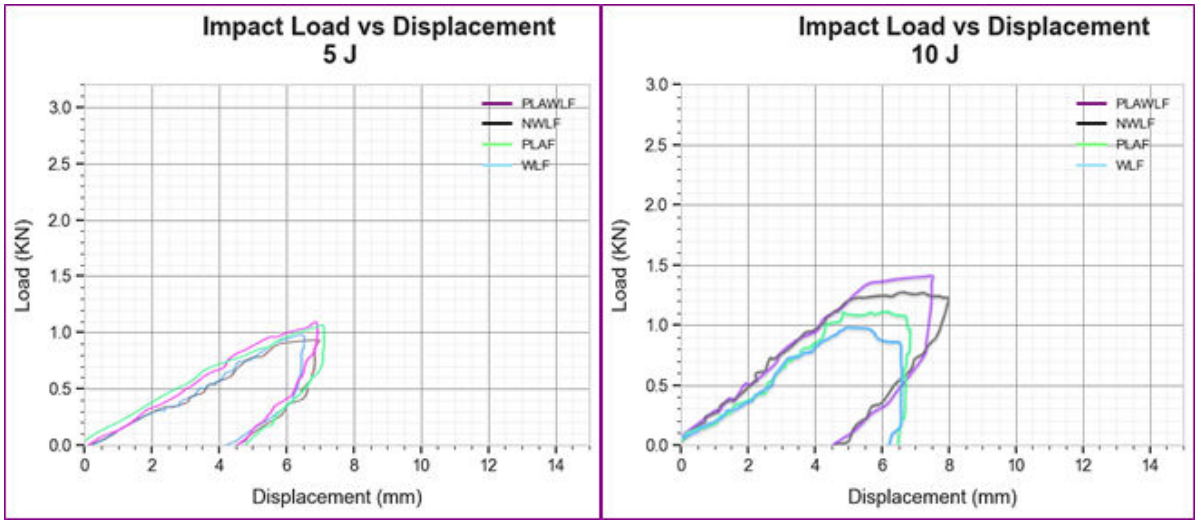

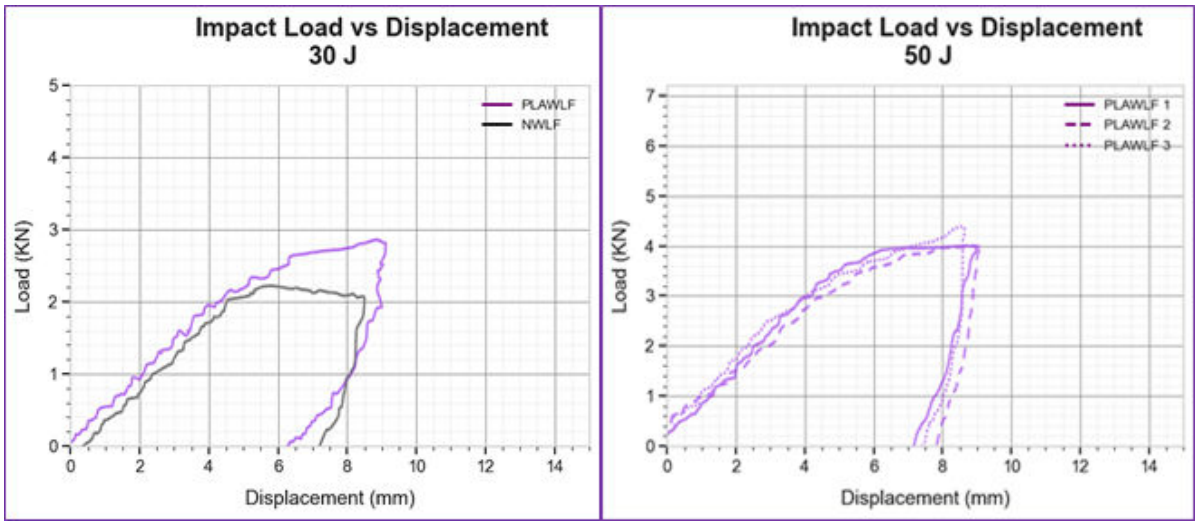

*Figure **V.29**. Diagrams Impact Load vs. Displacement.*

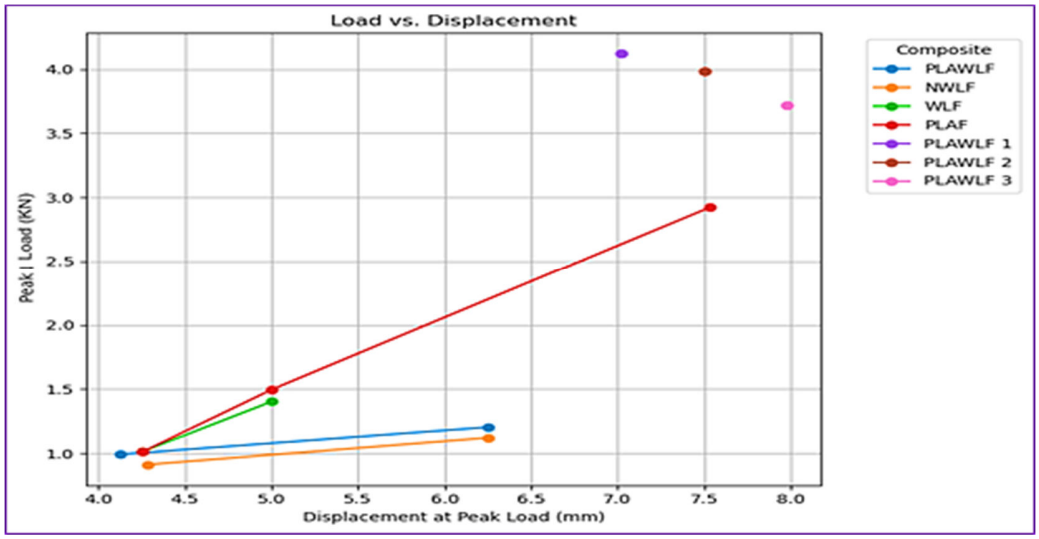

*Figure **V.30:** Impact Load vs. Displacement t peak load.*

Figure **V.29** shows at 5 J WLF represents the highest displacement of 4.281 mm, indicating lower stiffness[156]. PLAF shows the lowest displacement of 4.125 mm, reflecting its remarkable stiffness. NWLF and PLAWLF exhibit displacements of 4.253 mm and 4.254 mm, respectively. At 10 J PLAF and WLF show significant increases in displacement of 6.252 mm and 6.253 mm due to their limited resistance under higher impact energy. NWLF and PLAWLF maintain a consistent displacement of 5.00 mm, indicating enhanced toughness and better energy absorption without excessive deformation[174].Lower

displacement at higher energy for NWLF and PLAWLF demonstrates their improved ability to resist deformation, reflecting effective energy absorption.

At 30 J NWLF exhibits a displacement of 7.532 mm, higher than PLAWLF (6.321 mm). The displacement of NWLF increases significantly from 5.00 mm at 10 J, reflecting greater material deformation under higher energy. PLAWLF shows displacement even at 30 J, increasing from 5.00 mm at 10 J to 6.321 mm. The lower displacement of PLAWLF under higher energy indicates good toughness and effective energy dissipation without excessive deformation, which is critical for impact resistance [173, 174]. NWLF, although improved by chemical treatment, shows greater deformation, which may lead to earlier failure compared to PLAWLF. The balance between displacement and load in PLAWLF demonstrates its ability to absorb and dissipate energy efficiently, reducing the risk of damage[154].The displacement at 50 J for the three samples PLAWLF 1, PLAWLF 2, and PLAWLF 3 are 7.022 mm, 7.500 mm, and 7.981 mm respectively. The results show that PLAWLF 1 and PLAWLF 2 provide superior peak load resistance and controlled displacement at 50 J, compared to PLAWLF 3 and other composites tested at this energy level. PLAWLF's hybrid structure, combining stiffness and flexibility, optimizes energy dissipation and impact resistance, with variations in composition (PLAWLF 1, PLAWLF 2, and PLAWLF 3) affecting peak load and displacement performance [175].Figure **V.31**, PLAWLF composites show behavior under impact energy, particularly at 50 J, where they display a balance of high peak load resistance and displacement, which is essential for effective energy dissipation and toughness.

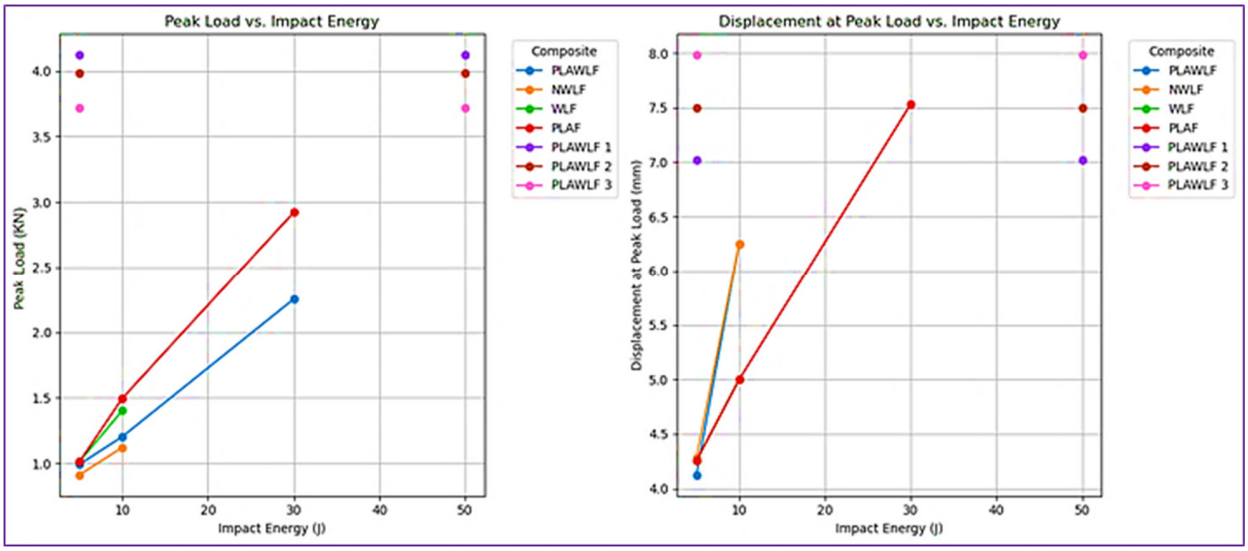

*Figure **V.31**: Diagrams Peak Load vs. Energy and Displacement at Peak Load vs. Energy.*

As shown at the above Figures and Tables, the energy-time, force-time, and force-displacement curves collectively demonstrate that the PLAWLF composite outperforms the other three composites across all impact energy levels. Its hybrid structure, combining stiffness and toughness, makes it highly effective in resisting and dissipating impact forces, reducing internal damage and permanent deformation[172, 175]. NWLF, benefiting from NaOH treatment, also shows improved performance compared to untreated WLF and PLAF but remains less effective than PLAWLF

III.2.4. Crack and Failure Mechanisms for Low-Velocity Impact

The crack and failure mechanisms of these composites under varying impact energies are strongly influenced by the fiber-matrix bonding, flexibility, and deformation ability of the material. PLAWLF stands out with its ability to absorb and dissipate energy effectively, especially at higher energies, due to its hybrid structure. NWLF shows improvements over untreated WLF but still fails at higher energies due to insufficient toughness. PLAF and WLF fail more rapidly, with matrix cracking, fiber breakage at higher energy levels[153].

Several researchers have examined the influence of the matrix on low-velocity impact behavior. Studies on composites with flexible matrices revealed that the resulting damage morphology is strongly influenced by the geometry of the impactor. These investigations also identified common failure modes, including fiber breakage, interfacial debonding, and matrix cracking[176]

III.2.4.1. PLAWLF (Hybrid composite)

PLAWLF's performance under varying impact energies reveals that its hybrid structure combining the stiffness of PLAF and the elasticity of WLF enables effective energy dissipation and enhances its resistance to failure. At low energy levels (5 J and 10 J), the failure is primarily driven by matrix cracking at the fiber-matrix interface[177]. The cracks typically remain localized, and fiber pull-out is the dominant mechanism of energy absorption[178]. Due to the flexibility of WLF, the cracks do not propagate extensively, preventing catastrophic failure. The fiber-matrix bond plays a crucial role in preventing large-scale failure, allowing the composite to deform without significant structural damage. As the energy increases to 30 J, matrix cracking becomes more widespread, and cracks propagate through the matrix. The material starts to experience fiber breakage as the fibers are subjected to higher stresses. Despite this, PLAWLF still shows considerable energy dissipation through plastic deformation and the interaction between the fibers and the matrix, this allows the composite to absorb more energy before catastrophic failure occurs[179]. The material's ability to deform significantly and distribute the stresses throughout the matrix and fibers reduces the risk of sudden failure, demonstrating its resilience at moderate impact levels[180]. At 50 J, crack propagation becomes more extensive, but the composite still manages to absorb a substantial amount of energy, despite the increased severity of the failure mechanisms, such as fiber breakage, the material's capacity to dissipate energy through significant deformation prevents catastrophic failure. This allows PLAWLF to maintain structural integrity even at high-energy impacts, proving its superior toughness and impact resistance[181]. Advantageous features were attributed to the Periploca laevigata Aiton fiber inherent toughness, such as the formation of matrix-rich regions at crimped fiber bundles supporting plastic flow, and crack propagation aligned with the curvature of fiber [176].

As shown in Figure **V.32**, the hybrid composite PLAWLF demonstrated superior resistance to these damage modes due to its optimized structural integration. The presence of Periploca laevigata Aiton fibers improved the stiffness and load-bearing capacity of the matrix, delaying the initiation and propagation of micro-cracks. Plasma treatment of wool fibers enhanced fiber-matrix adhesion and ensured efficient stress transfer. The hybridization combined the stiffness of Periploca fibers with the flexibility of wool fibers, providing an effective balance of energy dissipation and resistance to fracture. PLAWLF showed better resistance due to its hybrid structure, which delayed crack initiation. At high energy levels (50 J), fiber

fracture dominated the failure process. PLAWLF exhibited superior toughness, as its hybrid structure effectively distributed stresses, delaying catastrophic failure. The behavior exhibited by the specimens analyzed in this study is both fascinating and promising for potential applications in protective measures and possibly in structural contexts due to the significant fracture toughness of the matrix [176].

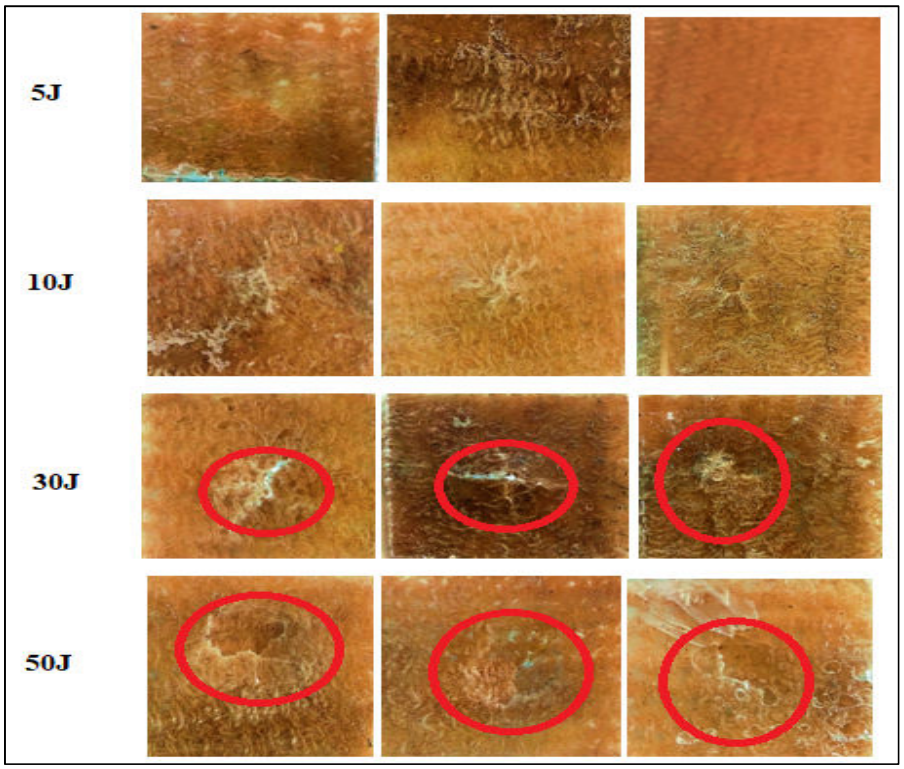

*Figure **V.32**: Images of the PLAWLF specimens from the drop-weight impact tests. (a) 5J, (b) 10J, (c) 30J, (d) 50J.*

III.2.4.2. NWLF (NaOH-Treated Wool Fiber)

The NaOH treatment significantly enhances the fiber-matrix bonding, improving energy absorption and reducing fiber pull-out, but at higher impact energy levels, the composite exhibits faster failure compared to PLAWLF due to a lack of sufficient toughness. At low energy levels (5 J and 10 J), the primary failure mechanism is matrix cracking around the fiber-matrix interface[182]. The NaOH treatment improves the fiber-matrix bond, which enhances the load distribution, reducing fiber pull-out and allowing the composite to absorb energy more effectively. Small delamination may occur at the interface, but these cracks generally do not propagate significantly, and the material absorbs energy primarily through fiber pull-out and localized cracking without catastrophic failure. This indicates that the NaOH-treated composite can withstand lower energy impacts through efficient energy dissipation and load transfer. At intermediate energy levels (30 J), the matrix cracking becomes more pronounced as the impact energy exceeds the composite's ability to absorb and dissipate it. Fiber breakage begins to occur as the fibers fracture under the stress. The NaOH treatment helps maintain the fiber-matrix bonding to some extent, but delamination at the fiber-matrix interface becomes more apparent, reducing the composite's ability to

absorb additional energy. As delamination propagates, the composite's overall energy absorption capacity declines and the material transitions more quickly to failure.

Figure **V.33**shows the NaOH-treated wool fiber composite (NWLF) demonstrates enhanced impact resistance compared to untreated wool fiber composites (WLF) due to improved fiber-matrix bonding. However, it is still outperformed by the hybrid composite (PLAWLF), which benefits from its synergistic combination of fibers. The damage mechanisms in NWLF during impact testing include micro-cracking in the matrix, fiber bending, and partial fiber fracture. These mechanisms, although mitigated by NaOH treatment, significantly influence NWLF's performance at various impact energy levels.

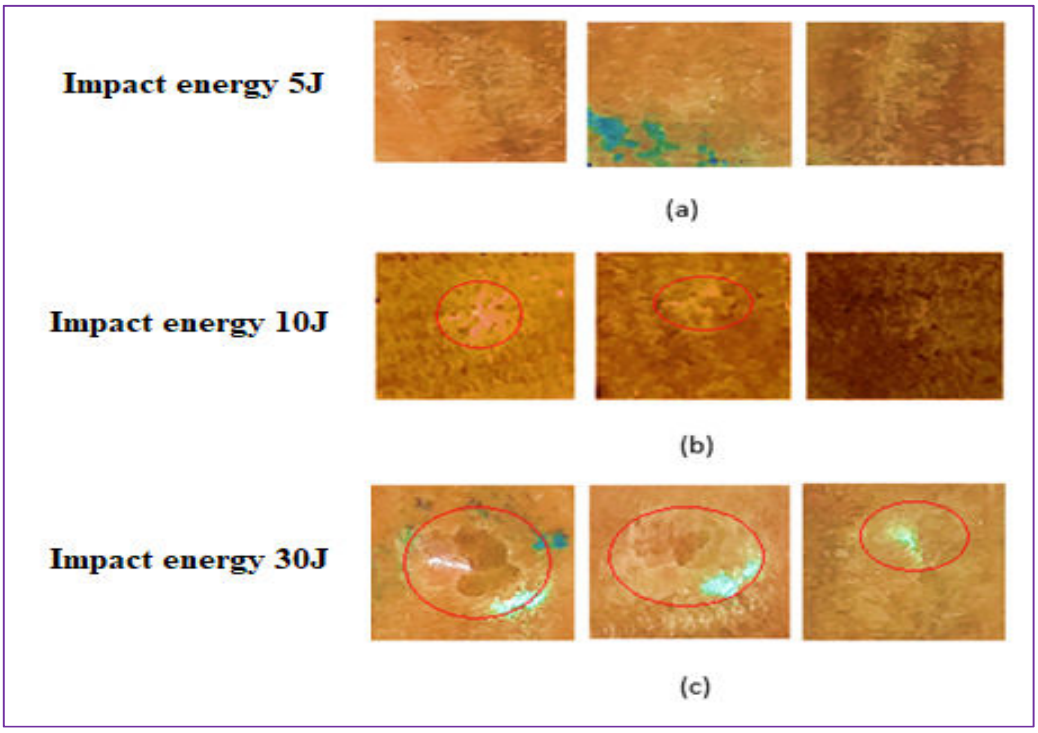

*Figure **V.33**: Images of the NWLF specimens from the drop-weight impact tests. (a) 5J, (b) 30J, (c) 50J.*

NWLF demonstrates significant improvement over untreated WLF due to the NaOH treatment, which enhances fiber-matrix adhesion and delays damage progression. It performs well at low and medium impact energies, absorbing energy more effectively and resisting micro-cracking. However, at higher energy levels, NWLF experiences extensive fiber fracture and, limits its performance. While NWLF is a viable improvement over untreated composites, it remains less effective than hybrid composites like PLAWLF, which benefit from the synergistic combination of stiffness, flexibility, and toughness. Bottom of Form in NWLF, micro-cracking in the polymer matrix is the first stage of damage under impact. The NaOH treatment significantly enhances fiber-matrix bonding, reducing the size and extent of these cracks compared to untreated WLF. This good interface bond prevents cracks from propagating rapidly, allowing the composite to absorb and dissipate impact energy more effectively before penetration occurs. However, at 30 J, the matrix's capacity to contain these cracks is exceeded, contributing to eventual failure. Wool

fibers in NWLF play a key role in absorbing impact energy by bending under load. The NaOH treatment increases fiber surface roughness, improving adhesion with the matrix. This enhanced adhesion ensures that fibers bend uniformly and share the impact load more efficiently. The bending of fibers temporarily stores energy, delaying their ultimate fracture.

Modifying fibers through chemical treatments can further enhance the interfacial bonding between the matrix and fibers, consequently affecting the composite's response to impact. Additionally, the choice of matrix material and fiber reinforcement plays a crucial role in determining the dominant damage mechanisms under impact loading, such as matrix cracking, fiber breakage [183].

This mechanism contributes to energy absorption but is insufficient to prevent penetration entirely at 30 J. The strong interfacial bond ensures that more energy is dissipated within the composite system, delaying the progression of damage. At 30 J, the interface bond is overwhelmed, leading to fibers to direct stress. This stress accelerates fiber fracture, ultimately leading to penetration. Under 30 J impact energy, fiber fracture becomes a dominant failure mechanism in NWLF. While NaOH treatment delays this stage by enhancing adhesion and load transfer, the fibers eventually reach their tensile and bending limits. Fiber fracture reduces the composite's ability to resist further damage, allowing the impactor to penetrate. The composite's energy dissipation capacity is surpassed by the energy delivered, leading to structural failure.

Matrix failure and fiber separation are identified as the primary mechanisms of impact damage in composite materials. Matrix failure typically involves cracking, deformation, or fragmentation of the resin, which compromises load transfer between fibers. Fiber separation, on the other hand, occurs when the bond between the fibers and matrix weakens or breaks, leading to phenomena such as fiber pull-out or interfacial debonding. These mechanisms not only reduce the structural integrity of the composite but also influence the extent and propagation of damage under impact loading [183].

III.2.4.3. PLAF (Periploca Laevigata Aiton Fiber)

PLAF exhibits relatively low energy absorption due to its stiffness, which limits its ability to deform significantly under impact. This stiffness results in rapid failure compared to PLAWLF, particularly at higher energy levels. At low energy of 5 J, the failure mode is primarily matrix cracking [184]. The rigidity of PLAF restricts significant deformation, leading to cracks forming around the fiber-matrix interface. Fiber pull-out is observed, but the lack of flexibility prevents the cracks from propagating extensively.

Figure **V.34** shows the Images of the PLAF specimens from the drop-weight impact tests (5 and 10 J). At 10J PLAF, the impact load initially induces micro-cracking within the epoxy matrix. The inherent stiffness of the Periploca laevigata Aiton fibers helps constrain crack propagation, limiting damage in the early stages. The fibers in PLAF, being naturally stiff, resist bending under impact[185]. This stiffness enables PLAF to withstand greater loads, reaching a peak load of 1.203 KN, higher than WLF. The energy is dissipated primarily through matrix cracking at the fiber-matrix interface[184, 186]. As the impact progresses, cracks propagate along the fiber-matrix interface. PLAF's fibers exhibit limited flexibility, and their inability to bend significantly causes localized stress concentrations, eventually leading to fiber fracture and penetration at lower displacement levels compared to WLF[154, 156].

Due to their inferior mechanical properties, these composites exhibit accelerated fracture propagation and more rapid fiber failure compared to PLAF composite, resulting in reduced damage resistance and lower perforation thresholds[183]. PLAF demonstrates better load-bearing capacity than WLF, its lack of flexibility reduces its ability to absorb energy through deformation. The composite fails primarily due to brittle fracture of the fibers [175].

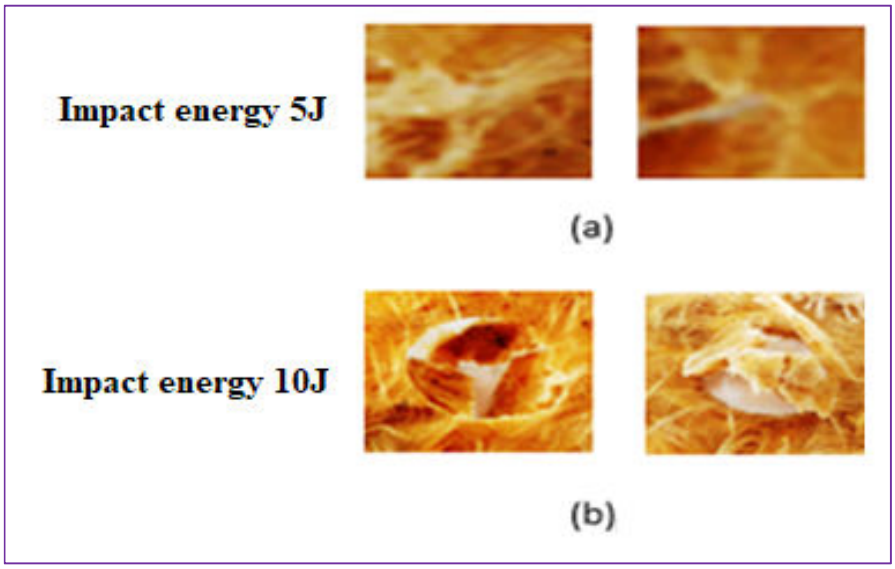

*Figure **V.34**: Images of the PLAF specimens from the drop-weight impact tests. (a) 5J, (b) 10J.*

III.2.4.4. WLF (Untreated Wool Fiber)

WLF demonstrates the weakest performance among the composites due to its poor fiber-matrix bonding and lack of effective energy dissipation mechanisms, as the impact energy increases, failure occurs more rapidly, and the material shows limited capacity to absorb and distribute energy. At low energy levels (5 J and 10 J), the failure mechanism is primarily matrix cracking, with cracks forming around the fiber-matrix interface. As the impact energy increases from 5 J to 10 J, the composite's structural integrity deteriorates more rapidly, resulting in early failure and reduced capacity to absorb and redistribute impact forces effectively.

Figure **V.35**shows the Images of the WLF specimens from the drop-weight impact tests (5 and 10 J). At 10 J WLF, being inherently flexible, absorbs energy through extensive fiber bending. However, the weak interface between untreated wool fibers and the epoxy matrix allows micro-cracks to propagate more freely, leading to widespread matrix damage at the early stages of impact due to the absence of strong fiber-matrix bonding resulting in reducing energy absorption efficiency. At the same impact energy level, PLAF shows superior peak load and crack resistance due to the natural stiffness of Periploca fibers, but its lack of flexibility limits its energy absorption capacity. These results emphasize the trade-offs between

stiffness and flexibility in natural fiber composites, highlighting the potential of hybrid approaches to optimize performance under impact.

These findings highlight the crucial balance between flexibility and stiffness in natural fiber composites, while flexibility can help dissipate energy through deformation, adequate fiber–matrix bonding is essential to prevent premature matrix cracking[186]. Conversely, stiff fibers enhance load-bearing capacity and crack resistance but may compromise overall toughness. Therefore, this study reinforces the importance of hybrid composite strategies (such as PLAWLF) to harness both stiffness and energy dissipation capabilities, optimizing performance for structural applications subjected to impact loading.

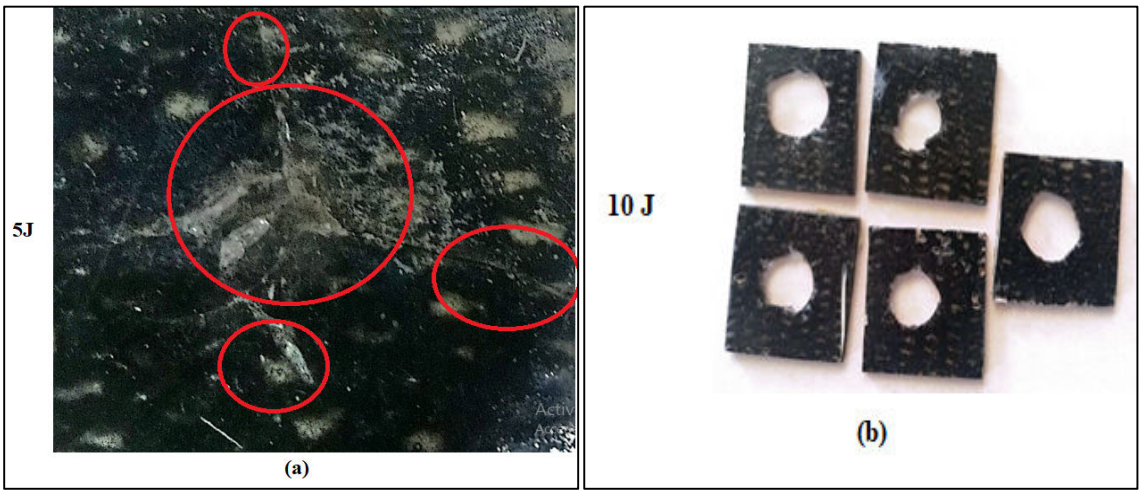

*Figure **V.35**: Images of the WLF after the drop-weight impact tests. (a) 5 J, (b) 10 J.*

III.3. Conclusions

This research examines the mechanical properties of four composite materials reinforced with natural fibers: Periploca laevigata Aiton (PLAF), untreated wool fiber (WLF), NaOH-treated wool fiber (NWLF), and a hybrid composite (PLAWLF), which merges cold plasma-treated wool fiber with PLAF. The composites underwent low-velocity impact testing at various energy levels of 5 J, 10 J, 30 J, and 50 J. The evaluation centered on essential performance indicators such as peak load, displacement at peak load, and energy absorption, providing insights into the potential of these composites for high-impact applications.

The study specifically sought to assess the impact of different fiber treatments chemical (NaOH treatment) and physical (cold plasma treatment) on the impact response of the composites. Epoxy-based composites reinforced with natural fibers have been attracting interest for their sustainable and lightweight features, yet their capacity to endure high-impact scenarios continues to be a significant challenge. By utilizing controlled vacuum infusion molding, this research guaranteed uniform fiber allocation and steady resin flow, resulting in consistent composite structures[139, 187] . This technique allowed for dependable and repeatable mechanical performance evaluations across the various energy levels tested (5 J, 10 J, 30 J, and 50 J). The low-velocity impact tests disclosed considerable differences in the mechanical behavior of the four composite materials. WLF, as a natural fiber, demonstrated relatively inferior performance regarding peak load resistance and energy absorption, mainly because of the intrinsic hydrophilic

character and weaker fiber–matrix bonding[188]. Conversely, NaOH-treated NWLF composites exhibited significant enhancements in peak load and energy absorption, which were due to the improved fiber–matrix adhesion resulting from the alkali treatment. The hybrid composite PLAWLF, which combined the benefits of both NaOH-treated wool and PLAF, demonstrated good performance at all tested energy levels, attaining the highest peak load and minimal displacement, thereby positioning it as a promising option for applications that demand heightened impact resistance and energy dissipation. This thorough analysis not only emphasizes the mechanical behavior of these natural fiber-based composites under low-velocity impact conditions but also show the advantages of fiber treatment and hybridization in enhancing their toughness and energy absorption capabilities. These results are vital for promoting the utilization of natural fiber composites in high-impact structural applications, where both strength and durability are critical[159].

PLAWLF consistently demonstrated superior performance across all energy levels, particularly at higher energy levels of 30 J and 50 J. This composite benefits from the synergy between the stiffness of periploca laevigata Aiton fiber and the flexibility of the wool fiber, resulting in enhanced energy dissipation and crack resistance. The high displacement and peak load observed at these energy levels indicate that PLAWLF can absorb significant energy before failure, making it a good candidate for applications requiring high-impact resistance[189]. The NaOH treatment applied to WLF to create NWLF proved beneficial, especially at the higher impact energy levels of 30 J. The treatment enhanced the fiber-matrix bonding, and improved load transfer, leading to better energy absorption and higher displacement values than untreated WLF[190].

The experimental findings revealed that surface modification significantly influences impact resistance. The NWLF composite demonstrated improved peak load and energy absorption relative to WLF, highlighting the effectiveness of alkali treatment in enhancing fiber–matrix adhesion and reducing interfacial voids. More notably, the hybrid PLAWLF composite exhibited the highest peak load values and the lowest displacements across all energy levels tested. At 10 J, it outperformed PLAF by 24% in load resistance and reduced displacement by 20%, indicating an optimal balance between stiffness and ductility. At 30 J and 50 J, PLAWLF maintained structural integrity, with up to 30% higher load-bearing capacity than NWLF, confirming the superior energy dissipation and crack-arresting synergy between plasma-treated wool and stiff PLAF fibers.

PLAF and WLF, when tested alone, exhibited lower energy absorption and less effective performance under energy level 10 J. These materials show limited deformation and energy dissipation capabilities, leading to rapid failure when subjected to higher impacts. PLAF, being a stiffer material, and WLF, composed of natural fibers, both lack the toughness needed to withstand and absorb significant impact energy, making them less suitable for applications where high impact resistance is essential[159, 191]. The failure mechanism of PLAWLF was characterized by its toughness and flexibility, allowing it to deform significantly and absorb more energy without catastrophic failure[192]. The increased displacement at peak load and the higher peak loads observed at the 30 J and 50 J energy levels highlight the composite's ability to handle higher energies without rapid failure[180]. PLAF and WLF failed more quickly with less deformation and energy absorption, which limited their effectiveness under high-impact conditions. The NaOH treatment of WLF to form NWLF also shows significant potential for improving energy absorption properties, especially in hybrid composite applications. However, PLAF and WLF, due

to their inherent limitations in toughness and energy dissipation capacity, may be more suitable for lower-impact applications or where rigidity is a key design requirement. This study provides valuable insights into the failure mechanisms, material behaviors, and performance characteristics of these composite materials under low-velocity impact conditions, contributing to the development of advanced composites for high-performance applications.

The critical innovation of this study lies in demonstrating the efficacy of combining physical (plasma) and chemical (NaOH) treatments with natural fiber hybridization to significantly improve the toughness, energy absorption, and damage tolerance of bio-composites under impact loading. The PLAWLF hybrid emerges as a promising sustainable material solution for applications demanding high impact resistance, such as protective gear, automotive panels, and aerospace components. These insights contribute to the growing body of knowledge on natural fiber-reinforced composites and encourage further research on fiber treatment optimization and hybrid design strategies to tailor composite performance for specific engineering applications.

GENERAL CONCLUSION

I. General conclusion

This research underscores the significant potential of natural fiber-reinforced composites, particularly those utilizing hybrid and chemically treated fibers, as high-performance and sustainable alternatives for engineering applications. The hybrid composite composed of cold plasma-treated wool and Periploca laevigata Aiton fibers exhibited outstanding mechanical properties tensile, flexural, and compressive strengths of 26.02 MPa, 2.53 GPa, and 109.22 MPa, respectively paired with low density (0.45 g/cm³) and enhanced structural integrity. The antibacterial and antioxidant properties of Periploca laevigata further position these composites as valuable materials for long-term and multifunctional applications.

The significant influence of fiber surface treatment and hybridization on enhancing the impact performance of epoxy-based natural fiber composites has been evaluated. The comparison of Periploca laevigata Aiton fiber (PLAF), untreated wool fiber (WLF), NaOH-treated wool fiber (NWLF), and a hybrid composite comprising plasma-treated wool with PLAF (PLAWLF) under low-velocity impact revealed notable differences in mechanical behavior. While WLF and PLAF demonstrated limited energy absorption and early failure due to inadequate fiber-matrix interaction and low toughness, the NWLF composite showed improved impact resistance attributed to enhanced interfacial bonding from alkali treatment. Notably, the PLAWLF hybrid composite exhibited superior performance across all tested energy levels (5 J, 10 J, 30 J, and 50 J), effectively combining stiffness and flexibility to achieve excellent energy dissipation and structural integrity. The integration of plasma-modified wool with rigid PLAF resulted in reduced displacement and increased peak load resistance, validating the effectiveness of hybrid and surface modification techniques. These findings underscore the potential of tailored natural fiber composites for high-performance applications in sectors such as automotive, aerospace, and protective structures, where sustainability, toughness, and impact resistance are critical. Future studies should focus on exploring long-term durability and optimizing treatment conditions to further improve the functionality and applicability of bio-based composite systems.

Complementing this, the treated horse tail hair fiber (THHF) composites demonstrated exceptional mechanical performance, with tensile strengths exceeding 60 MPa and compressive strengths approaching 79 MPa. These properties stem from the synergistic effects of fiber alignment, optimal matrix distribution, and alkaline surface treatment, which significantly improved fiber-matrix adhesion and reduced water absorption. The intrinsic strength and stiffness of THHF, combined with its environmentally friendly profile, highlight its value as a reinforcement material capable of withstanding rigorous mechanical demands.

This thorough study emphasizes the transformative capabilities of natural fiber-reinforced composites, especially those utilizing surface treatment and fiber hybridization techniques, as high-performance, sustainable substitutes for synthetic materials. The composite that merges cold plasma-treated wool and Periploca laevigata Aiton fibers shows an impressive balance of strength, stiffness, and low weight, achieving tensile, flexural, and compressive strengths of 26. 02 MPa, 2. 53 GPa, and 109. 22 MPa, respectively, with a density of only 0. 45 g/cm³. The additional antibacterial and antioxidant attributes of Periploca laevigata boost its potential for multifunctional and prolonged use. The low-velocity impact assessment further validated the benefits of fiber surface treatment and hybridization, with the PLAWLF

composite surpassing other configurations at every energy level due to enhanced interfacial bonding and synergistic mechanical properties. Likewise, the THHF composites demonstrated remarkable mechanical performance tensile strength over 60 MPa and compressive strength approaching 79 MPa resulting from efficient alkali treatment, better fiber-matrix interaction, and lower water sensitivity. Collectively, these results confirm that both single-fiber and hybrid-treated composites are promising options for structural applications that require durability, lightweight construction, and environmental stewardship. This research significantly contributes to the advancement of bio-based composite technologies and establishes a robust foundation for future innovations in automotive, aerospace, and infrastructure sectors in line with global sustainability objectives.

These findings establish both hybrid and single-fiber-treated composites as promising candidates for next-generation structural materials. Their excellent mechanical performance, coupled with sustainability, makes them well-suited for diverse industrial applications such as automotive, aerospace, and civil infrastructure. By integrating renewable resources and surface modification techniques, this work contributes to advancing eco-conscious material engineering and encourages the broader adoption of green composite technologies.

Recommendations and Future Research research

Recommendations and Future Research Directions

The advancement of composite materials requires an integrated strategy that simultaneously addresses scientific innovation, industrial scalability, long-term durability, digital transformation, and environmental sustainability. Based on the findings of this research, the following recommendations and future research directions are proposed.

1. Integrated Policy and Industrial Strategy

Governments and industrial stakeholders should establish national strategic frameworks to accelerate the development of advanced composite materials. Collaboration between academia, research institutions, and industrial leaders such as Boeing and Airbus demonstrates how coordinated investment significantly enhances composite innovation. Key recommendations include:

- Development of standardized testing and certification protocols for advanced composites.
- Financial incentives for sustainable and recyclable composite systems.
- Investment in automated manufacturing technologies (AFP, RTM, additive manufacturing).
- Establishment of pilot-scale composite production facilities to bridge laboratory research and industrial deployment.
- Economic modeling of composite manufacturing scale-up in emerging markets.
- Optimization of automated production systems using digital twin technologies.
- Integration of Industry 4.0 tools for defect reduction and process monitoring.

2. Machine Learning for Composite Design and Property Prediction

The integration of machine learning (ML) into composite materials research should transition from exploratory studies to standardized engineering tools. A centralized composite materials database incorporating microstructural parameters, processing variables, and mechanical performance metrics is essential. Research institutions should:

- Combine physics-based models with ML algorithms.
- Develop interpretable AI models for material property prediction.
- Implement real-time ML monitoring systems during manufacturing.
- Physics-informed neural networks for fatigue and damage prediction.
- Generative AI for inverse composite design.
- ML-based prediction of interfacial strength and delamination resistance.
- Hybrid FEM–ML frameworks for multiscale structural analysis.

3. Fatigue and Long-Term Mechanical Performance

Long-term reliability remains one of the primary limitations of fiber-reinforced composites. Standardized accelerated aging methodologies should be developed to simulate real service environments, including moisture, temperature variation, and cyclic loading. It is recommended to:

- Implement multi-axial fatigue testing protocols.
- Develop embedded structural health monitoring systems.

- Study creep–fatigue interaction under realistic service conditions.
- Multiscale modeling linking nano-interfacial damage to macro-structural failure.
- Crack propagation modeling under mixed-mode loading.
- Development of self-healing composite systems.
- Long-term durability assessment under combined environmental stressors.

4. Environmental Sustainability and Circular Economy

Sustainability must become a primary design criterion in composite development. Industries such as Vest as increasingly require recyclable blade materials, highlighting the urgency of circular composite systems. Key recommendations include:

- Adoption of Life Cycle Assessment (LCA) as a mandatory evaluation tool.
- Promotion of bio-based resins and natural fiber reinforcements.
- Design for disassembly and recyclability.
- Implementation of carbon fiber recycling technologies.
- Fully recyclable thermoplastic composite systems.
- Low-energy curing technologies.
- Biodegradable nanocomposites.
- Comparative carbon footprint analysis of thermoset versus thermoplastic systems.
- Upcycling strategies for composite waste streams.

5. Cross-Cutting Strategic Research Directions

Future composite research should converge toward multifunctional and intelligent systems. Emerging research directions include:

- Smart composites with embedded sensing capabilities.
- Energy-storing structural composites.
- Fire-resistant and extreme-environment composite systems.
- Hybrid natural–synthetic fiber composites.
- AI-driven autonomous materials discovery platforms.

References

References

1. Manivannan, J., et al., *Tensile and Hardness Properties of Sheep Wool Fiber Reinforced Polyester Composite.* Materials Science Forum, 2019. **969**: p. 266-270.
2. Shah, I., et al., *A Review on Chemical Modification by using Sodium Hydroxide (NaOH) to Investigate the Mechanical Properties of Sisal, Coir and Hemp Fiber Reinforced Concrete Composites.* Journal of Natural Fibers, 2021. **19**: p. 1-19.
3. Murillo, M., et al., *Use of animal fiber-reinforcement in construction materials: A review.* Case Studies in Construction Materials, 2024. **20**: p. e02812.
4. Thu Huyen, B., et al., *Determination and Review of Physical and Mechanical Properties of Raw and Treated Coconut Fibers for Their Recycling in Construction Materials.* Fibers, 2020. **8**: p. 37.
5. Ezeh, E. and P. Agu, *Application of Selected Chemical Modification Agents on Banana Fibre for Enhanced Composite Production.* Cleaner Materials, 2022. **5**: p. 100131.
6. Pokhriyal, M., et al., *Effect of alkali treatment on novel natural fiber extracted from Himalayacalamus falconeri culms for polymer composite applications.* Biomass Conversion and Biorefinery, 2023. **14**: p. 1-17.
7. Khan, M., et al., *Characterisation Studies and Impact of Chemical Treatment on Mechanical Properties of Sisal Fiber.* Composite Interfaces, 2011. **18**.
8. Rahmani, L., et al., *Evaluation of the Mechanical Performance and Structural Characterization of Hybrid Green Composites Based on Periploca laevigata Aiton and Wool Natural Fibers.* 2024.
9. Islam, M.R., H. Beg, and A. Gupta, *Characterization of Alkali Treated Kenaf Fibre Reinforced Recycled Polypropylene Composites.* Journal of Thermoplastic Composite Materials, 2012. **27**.
10. Jaiswal, D., et al., *Review on extraction, characterization, surface treatment and thermal degradation analysis of new cellulosic fibers as sustainable reinforcement in polymer composites.* Current Research in Green and Sustainable Chemistry, 2022. **5**: p. 100271.
11. R, V., et al., *Characterization of Chemical Treated and Untreated natural fibers from Pennisetum orientale grass- A potential reinforcement for lightweight polymeric applications.* International Journal of Lightweight Materials and Manufacture, 2020. **4**.
12. John, M. and R. Anandjiwala, *Recent developments in chemical modification and characterization of natural fiber-reinforced composites.* Polymer Composites, 2008. **29**: p. 187-207.
13. Kumer, A., et al., *Surface Modification of Silk Fiber with Chitosan and studies of dyeing enhance ability with antimicrobial properties.* International Journal of Innovative Research in Science Engineering and Technology, 2017. **4**: p. 4776-4784.
14. Naveen, P.N.E. and D. Raju, *Evaluation of Mechanical Properties of Coconut Coir Fiber Reinforced Polymer Matrix Composites.* Journal of Nano Research, 2013. **24**: p. 34-45.
15. Mann, G., et al., *Green Composites Based on Animal Fiber and Their Applications for a Sustainable Future.* Polymers, 2023. **15**: p. 601.
16. Ngo, T., *Introduction to Composite Materials*. 2020.
17. Sun, W., et al., *Compressive failure analysis of unidirectional carbon/epoxy composite based on micro-mechanical models.* Chinese Journal of Aeronautics, 2017. **30**.
18. Molla, A., et al., *Plant fiber-reinforced green composite: A review on surface modification, properties, fabrications and applications.* Materials Open Research, 2024.
19. B a, P., et al., *Experimental Investigation on Density and Volume Fraction of Void, and Mechanical Characteristics of Areca Nut Leaf Sheath Fiber-Reinforced Polymer Composites.* International Journal of Polymer Science, 2022. **2022**: p. 1-13.

20. Dias, J., et al., *Biopolymers Derived from Forest Biomass for the Sustainable Textile Industry.* Forests, 2025. **16**: p. 163.
21. Balakrishnan, T.S., et al., *Selection of Natural Fibre for Pultruded Hybrid Synthetic/Natural Fibre Reinforced Polymer Composites Using Analytical Hierarchy Process for Structural Applications.* Polymers, 2022. **14**: p. 3178.
22. Tabassum, F., et al., *Mechanical and Frictional Behavior of Jute-Textile-Reinforced Polymer Composites With Matrix Modification.* Advances in Materials Science and Engineering, 2025. **2025**: p. 1-18.
23. Ru, S., et al., *Effect of Coir Fiber Surface Treatment on Interfacial Properties of Reinforced Epoxy Resin Composites.* Polymers, 2022. **14**: p. 3488.
24. Murugan, A., et al., *A Review on the Effect of Various Chemical Treatments on the Mechanical Properties of Renewable Fiber-Reinforced Composites.* Advances in Materials Science and Engineering, 2022. **2022**.
25. Singh, M.K., et al., *A comprehensive review of various factors for application feasibility of natural fiber-reinforced polymer composites.* Results in Materials, 2023. **17**: p. 100355.
26. Bahrami, M., et al., *Characterization of hybrid biocomposite Poly-Butyl-Succinate/Carbon fibers/Flax fibers.* Composites Part B: Engineering, 2021. **221**: p. 109033.
27. Fang, C., et al., *Cold nitrogen plasma treated glass fiber warp knitted structural composites: mechanical properties and response surface analysis.* Journal of Industrial Textiles, 2022. **52**: p. 152808372211219.
28. Khayal, O., *ADVANCEMENTS IN POLYMER COMPOSITE STRUCTURES*. 2019.
29. Abdul, H., A. Alkazraji, and H. Jasim, *Advances in Composite Materials for Structural Mechanics Applications.* 2025.
30. Hannula, S.-P., et al., *Processing and Properties of Metal Matrix Composites Synthesized by SHS.* Materials Science Forum, 2003. **426-432**: p. 1971-1978.
31. Altenbach, H., J. Altenbach, and W. Kissing, *Mechanics of Composite Structural Elements*. 2018: Springer Nature Singapore.
32. Sharma, A.K., et al., *Matrix materials used in composites: A comprehensive study.* Materials Today: Proceedings, 2020. **21**: p. 1559-1562.
33. Jose, J. and K. Joseph, *Advances in Polymer Composites: Macro- and Microcomposites - State of the Art, New Challenges, and Opportunities*. 2012. p. 1-16.
34. Kumar, S., et al., *Physical and Mechanical Properties of Natural Leaf Fiber-Reinforced Epoxy Polyester Composites.* Polymers, 2021.
35. Sapiai, N., A. Jumahat, and R.N. Hakim, *Tensile and compressive properties of hybrid carbon fiber/ kenaf polymer composite.* Advances in Environmental Biology, 2014. **8**: p. 2655-2661.
36. Saxena, M., et al., *Composite Materials from Natural Resources: Recent Trends and Future Potentials*. 2011.
37. Englund, K., *Tribology of natural fiber polymer composites.* Materials Today - MATER TODAY, 2009. **12**: p. 45-45.
38. Bai, J., *Advanced Fibre-Reinforced Polymer (FRP) Composites for Structural Applications*. 2013. 1-906.
39. Kiruthika, A., *A review of leaf fiber reinforced polymer composites.* Journal of Engineering and Applied Science, 2024. **71**.
40. Kashtalyan, M., *Introduction to Composite Materials Design– Third edition E. J. Barbero CRC Press, Taylor & Francis Group, 6000 Broken Sound Parkway NW, Suite 300, Boca Raton, FL, 33487-2742, USA. 2018. Distributed by Taylor & Francis Group, 2 Park Square, Milton Park,*

Abingdon, OX14 4RN. xxxv; 535pp. Illustrated. £92. (20% discount available to RAeS members via www.crcpress.com using AKQ07 promotion code). ISBN 978-1-1381-9680-3. The Aeronautical Journal, 2018. **122**: p. 2048-2049.
41. Patsiaoura, D., et al., *Lignocellulosic-Based/High Density Polyethylene Composites: A Comprehensive Study on Fiber Characteristics and Performance Evaluation.* Applied Sciences, 2024. **14**: p. 3582.
42. Kalia, S., B.S. Kaith, and I. Kaur, *Cellulose Fibers, Bio-, and Nano- Polymer Composites*. 2011.
43. Shaker, K. and Y. Nawab, *Lignocellulosic Fibers: Sustainable Biomaterials for Green Composites*. 2022.
44. Mohanty, A., et al., *Natural Fibers, Biopolymers, And Biocomposites*. 2005. p. 1-36.
45. Di Bella, G., V. Fiore, and A. Valenza, *Natural Fibre Reinforced Composites*. 2012. p. 57-90.
46. Welker, C., et al., *Engineering Plant Biomass Lignin Content and Composition for Biofuels and Bioproducts.* Energies, 2015. **2015**: p. 7654-7676.
47. Ovalı, S. and O. Eryılmaz, *Physical and Chemical Properties of a New Cellulose Fiber Extracted from the Mentha pulegium L. (Pennyroyal) Plant's Stem.* Çukurova Üniversitesi Mühendislik Fakültesi Dergisi, 2024. **39**: p. 211-220.
48. Chopra, L. and Manikanika, *Extraction of cellulosic fibers from the natural resources: A short review.* Materials Today: Proceedings, 2021. **48**.
49. Mohankumar, D., et al., *Extraction of plant based natural fibers – A mini review.* IOP Conference Series: Materials Science and Engineering, 2021. **1145**: p. 012023.
50. Yue, L., et al., *MECHANICAL RESEARCH AND OPTIMIZATION OF BANANA STALK FIBER EXTRACTION.* Engenharia Agrícola, 2024. **44**.
51. Gebru, K., et al., *Extraction and Characterization of Fiber and Cellulose from Ethiopian Linseed Straw: Determination of Retting Period and Optimization of Multi-Step Alkaline Peroxide Process.* Polymers, 2023. **15**: p. 469.
52. Zhang, X., et al., *Green Degumming Technology of Hemp and a Comparison between Chemical and Biological Degumming.* ACS Omega, 2021. **6**(50): p. 35067-35075.
53. Subash, M. and P. Muthiah, *Eco-friendly degumming of natural fibers for textile applications: A comprehensive review.* Cleaner Engineering and Technology, 2021. **5**: p. 100304.
54. Cheng, L., et al., *Ramie-degumming methodologies: A short review.* Journal of Engineered Fibers and Fabrics, 2020. **15**: p. 155892502094010.
55. Yadav, A., et al., *Coupling chemical degumming with enzymatic degumming of ultrasound pre-treated ramie fiber using Bacillus subtilis ABDR01.* Environmental Technology & Innovation, 2022. **28**: p. 102666.
56. Roblin, N., et al., *Development of a More Environmentally Friendly Silk Fibroin Scaffold for Soft Tissue Applications.* Journal of Functional Biomaterials, 2023. **14**: p. 230.
57. Wu, Y., et al., *A Novel endo-β-1,4-xylanase xyl-1 from Aspergillusterreus HG-52 for High-Efficiency Ramie Degumming.* Journal of Natural Fibers, 2022. **19**.
58. Patil, H., K. Surve, and A. Athalye, *Green Process for Degumming of Tussar Silk by Sapindus Extract.* Journal of the Textile Association, 2023. **84**: p. 190-195.
59. Sahai, R., et al., *Effect of alkali and silane treatment on water absorption and mechanical properties of sisal fiber reinforced polyester composites.* Metallurgical and Materials Engineering, 2022. **28**: p. 641-656.
60. Rohit, K. and s. Dixit, *A Review - Future Aspect of Natural Fiber Reinforced Composite.* Polymers from Renewable Resources, 2016. **7**: p. 43-60.

61. Prome, F., et al., *Different Chemical Treatments of Natural Fiber Composites and Their Impact on Water Absorption Behavior and Mechanical Strength.* Hybrid Advances, 2025. **8**.
62. Ouerghi, H., et al., *Effect of Chemical Treatment on the Mechanical and Hygroscopic Properties of an Innovative Clay–Sand Composite Reinforced with Juncus acutus Fibers.* Materials, 2025. **18**: p. 177.
63. Rothenhäusler, F., et al., *Influence of sodium hydroxide, silane, and siloxane treatments on the moisture sensitivity and mechanical properties of flax fiber composites.* Polymer Composites, 2024. **45**: p. 1-12.
64. Suarsana, I., et al., *Flexural strength of hybrid composite resin epoxy reinforced stinging nettle fiber with silane chemical treatment.* AIMS Materials Science, 2021. **8**: p. 185-199.
65. Wu, S., et al., *Interface Enhancement and Tribological Properties of Cattle Manure-Derived Corn Stalk Fibers for Friction Materials: The Role of Silane Treatment Concentration.* Polymers, 2024. **17**: p. 22.
66. Sood, M. and G. Dwivedi, *Effect of fiber treatment on flexural properties of natural fiber reinforced composites: A review.* Egyptian Journal of Petroleum, 2017. **27**.
67. T G, Y., et al., *Natural Fibers as Sustainable and Renewable Resource for Development of Eco-Friendly Composites: A Comprehensive Review.* Frontiers in Materials, 2019. **6**.
68. Duppala, A. and A. Lakshumu Naidu, *A STUDY ON DIFFERENT CHEMICAL TREATMENTS FOR NATURAL FIBER REINFORCED COMPOSITES.* 2018. **8**: p. 143-152.
69. Luz, S.M., et al., *Cellulose and cellulignin from sugarcane bagasse reinforced polypropylene composites: Effect of acetylation on mechanical and thermal properties.* Composites Part A: Applied Science and Manufacturing, 2008. **39**(9): p. 1362-1369.
70. Fridman, A., *Plasma Chemistry I*. 2008.
71. Lu, X., et al., *Cold atmospheric-pressure air plasma jet: Physics and opportunities.* Physics of Plasmas, 2021. **28**: p. 100501.
72. Macedo, M., et al., *Surface modification of kapok fibers by cold plasma surface treatment.* Journal of Materials Research and Technology, 2020. **9**.
73. Thibodeaux, N., et al., *Effect of Cold Plasma Treatment of Polymer Fibers on the Mechanical Behavior of Fiber-Reinforced Cementitious Composites.* Fibers, 2021. **9**: p. 62.
74. Shadhin, M. and B. Engineering, *Comparative Evaluation of Flax, Cattail, and Hemp Fiber Composites*. 2021.
75. Venugopal, J., et al., *Effect on Compression Molding Parameters in Mechanical Properties of MWCNT/Glass Fiber/Epoxy Composites.* Advances in Polymer Technology, 2022.
76. Agwa, M., et al., *Integrated vacuum assisted resin infusion and resin transfer molding technique for manufacturing of nano-filled glass fiber reinforced epoxy composite.* Journal of Industrial Textiles, 2022. **51**: p. 152808372093233.
77. Koay, S.C., et al., *Properties of corn husk fibre reinforced epoxy composites fabricated using vacuum-assisted resin infusion.* Journal of Physical Science, 2020. **31**: p. 17-31.
78. Doppelbauer, L., et al., *A macroscopic model of the compaction process during compression molding of carbon fiber sheet molding compounds.* Composites Part A Applied Science and Manufacturing, 2023. **169**.
79. Xie, J., et al., *Process Optimization for Compression Molding of Carbon Fiber–Reinforced Thermosetting Polymer.* Materials, 2019. **12**: p. 2430.
80. Masta, M., *Design analysis of mold cavity and core on compression molding of composite material.* Jurnal Polimesin, 2023. **21**.

81. Oladele, I., et al., *Fabrication of animal shell and sugarcane bagasse particulate hybrid reinforced epoxy composites for structural applications.* Polymers and Polymer Composites, 2024. **32**.
82. Prabhu, P., et al., *Study on Machining Parameters and Mechanical Properties of Hybrid Agave Sisalana and Glass Fiber-reinforced Polyester Composites (A/GFRP).* Journal of Natural Fibers, 2022. **19**: p. 1-14.
83. Abdurohman, K., et al., *A comparison process between hand lay-up, vacuum infusion and vacuum bagging method toward e-glass EW 185/lycal composites.* Journal of Physics: Conference Series, 2018. **1130**: p. 012018.
84. Orman, S., M. Dogu, and B. Ozbek, *Optimization of the Filament Winding Process for Glass Fiber-Reinforced PPS and PP Composites Using Box–Behnken Design.* Polymers, 2024. **16**: p. 3488.
85. Kivirenko, O., et al., *Fiberglass Pipeline Continuous Filament Winding Automation.* International Journal of Mechatronics and Applied Mechanics, 2023. **2023**: p. 241-247.
86. Shrigandhi, G. and B. Kothavale, *Biodegradable composites for filament winding process.* Materials Today: Proceedings, 2021. **42**.
87. Kikuchi, T., et al., *Mechanical Properties of Jute Composite by Spray up Fabrication Method.* Energy Procedia, 2014. **56**: p. 289–297.
88. Jeon, J., et al., *Effect of Fiber Entanglement in Chopped Glass Fiber Reinforced Composite Manufactured Via Long Fiber Spray-Up Molding*. 2023.
89. Serban, D., *SURFACE TEXTURING METHODS FOR THERMOPLASTIC COMPOSITES INJECTION MOLDING by Daniiel Serban*. 2023.
90. Yewale, P. and S. Kulkarni, *Optimization of Injection Molding Process for Kenaf and Polypropylene Composite to Improve Its Tensile Strength.* International Journal for Research in Applied Science and Engineering Technology, 2022. **10**: p. 1952-1958.
91. Jetty, B., F. Wittemann, and L. Kärger, *Modeling Approach for Reactive Injection Molding of Polydisperse Suspensions with Recycled Thermoset Composites.* Polymers, 2024. **16**: p. 2245.
92. Tan, M., et al., *Multi-Objective Optimization of Injection Molding Parameters for Manufacturing Thin-Walled Composite Connector Terminals.* Materials, 2024. **17**: p. 3949.
93. Buragohain, M.K., *Composite Structures: Design, Mechanics, Analysis, Manufacturing, and Testing*. 2017: CRC Press.
94. Jones, R.M., *Mechanics Of Composite Materials*. 1998: Taylor & Francis.
95. Hancox, N., *Book Review: Engineering with Fibre-Polymer Laminates.* Engineering Plastics, 1994. **2**: p. 147823919400200.
96. Hertzberg, R.W., R.P. Vinci, and J.L. Hertzberg, *Deformation and Fracture Mechanics of Engineering Materials*. 2012: Wiley.
97. Rand, O. and V. Rovenski, *Analytical Methods in Anisotropic Elasticity: with Symbolic Computational Tools*. 2007: Birkhäuser Boston.
98. Hult, J.A.H., J. Hult, and F.G. Rammerstorfer, *Engineering Mechanics of Fibre Reinforced Polymers and Composite Structures*. 1994: Springer Vienna.
99. Zhao, D., et al., *Vibration study of dielectric elastomer conical structure based on fractional viscoelasticity.* Scientific Reports, 2025. **15**.
100. Gibson, R.F., *Principles of Composite Material Mechanics, Third Edition*. 2011: Taylor & Francis.
101. Callister, W.D. and D.G. Rethwisch, *Fundamentals of Materials Science and Engineering: An Integrated Approach*. 2020: Wiley.
102. Gdoutos, E.E., *Fracture Mechanics: An Introduction*. 2005: Springer Netherlands.

103. Salit, M.S., et al., *Manufacturing of Natural Fibre Reinforced Polymer Composites*. 2015: Springer International Publishing.
104. Guedes, R.M., *Creep and Fatigue in Polymer Matrix Composites*. 2019: Woodhead Publishing.
105. LeMaitre, J., *Handbook of Materials Behavior Models, Three-Volume Set: Nonlinear Models and Properties*. 2001: Elsevier Science.
106. Carcione, J. and G. Casula, *Generalized mechanical model analogies of linear viscoelastic behaviour,l., 235-256.* Bollettino di Geofisica Teorica ed Applicata, 1992. **34**: p. 235-256.
107. Zoghi, M., *The International Handbook of FRP Composites in Civil Engineering*. 2013: Taylor & Francis.
108. Campbell, F.C., *Fatigue and Fracture: Understanding the Basics*. 2012: ASM International.
109. Hwu, C., *Anisotropic Elastic Plates*. 2010: Springer US.
110. Gay, D. and S.V. Hoa, *Composite Materials: Design and Applications, Second Edition*. 2007: CRC Press.
111. Soboyejo, W., *Mechanical Properties of Engineered Materials*. 2002: CRC Press.
112. Rösler, J., M. Baeker, and H. Harders, *Mechanical Behaviour of Engineering Materials: Metals, Ceramics, Polymers, and Composites: with 320 Figures and 32 Tables*. 2010.
113. Aboudi, J., S.M. Arnold, and B.A. Bednarcyk, *Micromechanics of Composite Materials: A Generalized Multiscale Analysis Approach*. 2013: Elsevier Science.
114. Landel, R.F. and L.E. Nielsen, *Mechanical Properties of Polymers and Composites*. 1993: CRC Press.
115. Kumar, S., et al., *Mechanism of Quiescent Nanoplastic Formation from Semicrystalline Polymers*. 2024.
116. Zhang, W., et al., *Stöber method to amorphous metal-organic frameworks and coordination polymers.* Nature Communications, 2024. **15**.
117. Nozawa, J., et al., *Polymorphic transitions during nonclassical nucleation and growth in the colloidal heteroepitaxy.* Communications Physics, 2025. **8**.
118. Godey, F., A. Fleury, and A. Soldera, *Local dynamics within the glass transition domain.* Scientific Reports, 2019. **9**.
119. Hyer, M.W. and S.R. White, *Stress Analysis of Fiber-reinforced Composite Materials*. 2009: DEStech Publications, Incorporated.
120. Reddy, J.N., *Mechanics of Composite Materials: Selected Works of Nicholas J. Pagano*. 2013: Springer Netherlands.
121. Testing, A.S.f. and Materials, *Annual Book of ASTM Standards*. 2007: ASTM.
122. Davis, J.R., *Tensile Testing, 2nd Edition*. 2004: ASM International.
123. Properties, A.S.D.o.M. and A.S.f.T. Materials, *Standard Test Methods for Flexural Properties of Unreinforced and Reinforced Plastics and Electrical Insulating Materials*. 1997: American Society for Testing Materials.
124. Aeronautics, U.S.N., et al., *NASA Reference Publication*. 1977: National Aeronautics and Space Administration, Scientific and Technical Information Branch.
125. 17, C.M.H., *Polymer Matrix Composites: Guidelines for Characterization of Structural Materials: CMH-17 Volume 1 - Revision H*. 2022: SAE International.
126. Agbabiaka, O., I. Oladele, and O. Daramola, *Mechanical and Water Absorption Properties of Alkaline Treated Coconut (cocosnucifera) and Sponge (acanthus montanus) Fibers Reinforced Polypropylene Composites.* American Journal of Materials Science and Technology, 2015.
127. Hüner, Ü., *Effect of water absorption on the mechanical properties of flax fiber reinforced epoxy composites.* Advances in Science and Technology Research Journal, 2015. **9**: p. 1-6.

128. Testing, A.S.f. and Materials, *Standard Test Method for Compressive Properties of Polymer Matrix Composite Materials with Unsupported Gage Section by Shear Loading*. 2016: ASTM International.
129. Hosford, W.F., *Mechanical Behavior of Materials*. 2005: Cambridge University Press.
130. Zito, P., et al., *Essential oils composition of Periploca laevigata Aiton subsp. angustifolia (Labill.) Markgraf (Apocynaceae – Periplocoideae).* Natural product research, 2012.
131. Mezhoud, S., et al., *Flavonoid glycosides from Periploca laevigata (Asclepiadaceae) from Algeria.* 2016. **8**: p. 129-131.
132. Hariharan, H. and G. Rajeshkumar, *Investigation of Mechanical Properties of Sisal Fiber and Sugar Palm Fiber Reinforced Hybrid Composites*. 2024.
133. Lee, C.H., A. Khalina, and S.H. Lee, *Importance of Interfacial Adhesion Condition on Characterization of Plant-Fiber-Reinforced Polymer Composites: A Review.* 2021. **13**(3): p. 438.
134. Chikkol Venkateshappa, S., *Abaca Fiber Reinforced Epoxy Composites: Evaluation of Impact Strength.* International Journal of Sciences: Basic and Applied Research (IJSBAR), 2014. **18**: p. 305-317.
135. Sun, C., et al., *Effect of Atmospheric Pressure Plasma Treatment on Adhesive Bonding of Carbon Fiber Reinforced Polymer.* Polymers, 2019. **11**: p. 139.
136. Cui, H. and X. Gao, *Surface Modification on Polyimide Yarn by Plasma Treatment to Enhance Adhesion with Polypropylene Resin.* 2022. **14**(19): p. 4232.
137. Wang, F., et al., *Preparation and curing process optimization of an asymmetric impregnated vacuum bag-only prepreg.* Frontiers in Materials, 2022. **9**.
138. Soatthiyanon, N., A. Crosky, and M. Heitzmann, *Comparison of experimental and calculated tensile properties of flax fibres*. 2015. 116-120.
139. Vaidya, U.K., et al., *Low Velocity Impact Response of Resin Infusion Molded Foam Filled Honeycomb Sandwich Composites.* 1998. **17**(9): p. 819-849.
140. Subramanyam, S.P., et al., *Plain-Woven Areca Sheath Fiber-Reinforced Epoxy Composites: The Influence of the Fiber Fraction on Physical and Mechanical Features and Responses of the Tribo System and Machine Learning Modeling.* ACS Omega, 2024. **9**(7): p. 8019-8036.
141. Deng, Y., et al., *The temperature-dependent fracture models for fiber-reinforced ceramic matrix composites.* Composite Structures, 2016. **140**.
142. Workiye, A. and E. Woldesenbet, *Flexural Strength and Porosity of NaOH-Treated Maize Stalk Cellulose-Fibers-Reinforced Geopolymer Composites.* Proceedings of Engineering and Technology Innovation, 2023. **25**: p. 44-53.
143. Santhiarsa, I.G.N. and I.G.B. Kusuma, *Mechanical Characterization of NaOH-Treated Agel Fiber-Cotton Composites.* Journal of Mechanical Engineering Science and Technology (JMEST), 2023. **7**: p. 214.
144. Shevtsov, S., et al., *Numerical Study of Thin-Walled Polymer Composite Part Quality When Manufactured Using Vacuum Infusion with Various External Pressure Controls.* Polymers, 2024. **16**: p. 654.
145. Nayan, A., M. Yusuf, and D. Siska, *Tensile Strength Comparison of Polymer Composite Materials Reinforced by Three Types of Bamboo Fiber Treated With 5% aq. NaOH Solution.* International Journal of Engineering, Science and Information Technology, 2023. **3**: p. 37-46.
146. Xia, Z. and W.A. Curtin, *Multiscale Modeling of Tensile Failure in Fiber-Reinforced Composites*. 2007. p. 37-82.
147. Ghaffari, S., G. Seon, and A. Makeev, *Effect of Fiber–Matrix Interface Friction on Compressive Strength of High-Modulus Carbon Composites.* Molecules, 2023. **28**: p. 2049.

148. Ziaee, S., et al., *Effect of High Fiber Content on Properties and Performance of CFRTP Composites.* Journal of Composites Science, 2024. **8**: p. 364.
149. Gu, Y., et al., *Temperature Distribution and Curing Behaviour of Carbon Fibre/ Epoxy Composite during Vacuum Assisted Resin Infusion Moulding Using Rapid Heating Methods.* Polymers and Polymer Composites, 2015. **23**: p. 11-19.
150. Zhu, S., et al., *Effect of the stiffener stiffness on the buckling and post-buckling behavior of stiffened composite panels – Experimental investigation.* Composite Structures, 2014. **120**.
151. Blanco Gómez, D., et al., *Lightweight Structural Materials in Open Access: Latest Trends.* Materials, 2021.
152. Boey, J.Y., C.K. Lee, and G.S. Tay, *Factors Affecting Mechanical Properties of Reinforced Bioplastics: A Review.* 2022. **14**(18): p. 3737.
153. Ashraf, M., et al., *Effect of Fibre Hybridization and Stacking Sequence on the Low Velocity Impact Response of Flax/Basalt/Aluminum Composite-Metal Joints.* Composite Structures, 2024. **331**.
154. Xiong, X., et al., *Simulation and Experiment on the Low-Velocity Impact Response of Flax Fabric Reinforced Composites.* Materials, 2023. **16**: p. 3489.
155. Khoob, A., M. Ramezani, and S. Mousavi Ojarestaghi, *Low-Velocity Impact Resistance of Glass Laminate Aluminium Reinforced Epoxy (GLARE) Composite.* Recent Progress in Materials, 2023. **5**.
156. Jakubczak, P., et al., *Experimental Investigation on the Low Velocity Impact Response of Fibre Foam Metal Laminates.* Materials (Basel), 2021. **14**(19).
157. Lee, G.-H., et al., *Low-Velocity Impact Analysis in Composite Plates Incorporating Experimental Interlaminar Fracture Toughness.* Materials, 2024. **17**: p. 5768.
158. Najeeb, M., et al., *Low-Velocity Impact Analysis of Pineapple Leaf Fiber (PALF) Hybrid Composites.* Polymers, 2021. **13**: p. 3194.
159. Bogahawaththa, M., et al., *Low-velocity impact response and energy absorption of Menger sponge-inspired fractal structures fabricated by selective laser melting.* Engineering Structures, 2024. **321**.
160. Bahrami, M., et al., *Impact properties of flax-carbon hybrid composites under low-velocity impact*. 2022.
161. Shishevan, F.A., H. Akbulut, and M.A. Mohtadi-Bonab, *Low Velocity Impact Behavior of Basalt Fiber-Reinforced Polymer Composites.* Journal of Materials Engineering and Performance, 2017. **26**(6): p. 2890-2900.
162. Nassef, M., et al., *Manufacturing and utilization of novel sustainable composites using pulled wool fibers waste from leather tanneries: Mechanical, physical, and dynamic characterization.* Journal of Industrial Textiles, 2022. **51**: p. 1-20.
163. Reis, P.N.B., et al., *Impact response of Kevlar composites with filled epoxy matrix.* Composite Structures, 2012. **94**(12): p. 3520-3528.
164. Vasudevan, A., et al., *Advanced 3D and 2D damage assessment of low velocity impact response of glass and Kevlar fiber reinforced epoxy hybrid composites.* 2018. **4**.
165. Zhang, D., et al., *Bridging the low-velocity impact energy versus impact damage and residual compression strength for composite laminates.* Journal of Reinforced Plastics and Composites, 2021. **40**: p. 378-390.
166. Albayrak, M., M. Kaman, and I. Bozkurt, *The effect of lamina configuration on low-velocity impact behaviour for glass fiber/rubber curved composites.* Journal of Composite Materials, 2023. **57**: p. 002199832311649.

167. Samlal, S. and R. Santhanakrishnan, *Low-Velocity Impact Behavior of Foam Core Sandwich Panels with Inter-Ply and Intra-Ply Carbon/Kevlar/Epoxy Hybrid Face Sheets.* Polymers, 2022. **14**: p. 1060.
168. Abdelgader Ali, A., A. Seeahmed, and R. Mohmmed, *LOW-VELOCITY IMPACT OF WOVEN GLASS FIBER/EPOXY COMPOSITE USING DIFFERENT FIBER ORIENTATION AND NUMBERS OF LAYERS: EXPERIMENT AND SIMULATION.* International Journal of Engineering Applied Sciences and Technology, 2022. **6**: p. 1-5.
169. Bencheikh, A., et al., *Mechanical properties and low-velocity impact analysis of camel hair and hybrid camel hair/flax fibre-reinforced epoxy.* Journal of the Brazilian Society of Mechanical Sciences and Engineering, 2024. **46**.
170. Ahmad, M., D. Feng, and W. Ali, *Low Velocity Impact of Composite Materials Glass Fiber Laminates.* European Journal of Applied Science, Engineering and Technology, 2024. **2**: p. 59-68.
171. Srivastava, V., *Dynamic Fracture Toughness Behaviour of CFRP-Foam-CFRP Sandwich Composite and Particles Filled Hybrid Glass Fiber Cloth, Graphene Nanoplates Coated Glass Fiber Strand Composite Materials under Low Impact Velocity.* Journal of Materials Science Research, 2022. **11**: p. 70.
172. Go, S.-H., et al., *The impact fracture behaviors of CFRP/EVA composites by drop-weight impact test.* Carbon letters, 2017. **21**: p. 23-32.
173. Huang, Y., et al., *Research on Low-Velocity Impact Response of Novel Short-Fiber-Reinforced Composite Laminates.* Polymers, 2023. **15**: p. 840.
174. Shah, S., et al., *Impact resistance and damage tolerance of fiber reinforced composites: A Review.* Composite Structures, 2019. **217**.
175. Yang, B., et al., *Study on the low-velocity impact response and CAI behavior of foam-filled sandwich panels with hybrid facesheet.* Composite Structures, 2015. **132**: p. 1129-1140.
176. Vescovini, A., et al., *Experimental investigation on low-velocity impact behavior of glass, Kevlar, and hybrid composites with an elastomeric polyurethane matrix.* Composites Part C: Open Access, 2023. **13**: p. 100426.
177. Sun, J., et al., *Low-Velocity Impact Behaviour of Titanium-Based Carbon-Fibre/Epoxy Laminate.* Materials, 2024. **17**: p. 5380.
178. Meireman, T., et al., *Low-Velocity Impact Resistance and Compression After Impact Strength of Thermoplastic Nanofiber Toughened Carbon/Epoxy Composites with Different Layups.* Polymers, 2024. **16**: p. 3060.
179. Erkek, B., E. Kosedağ, and H. Adin, *Hybridization effect on energy absorption capacity of composite crash boxes.* Polymer Composites, 2024. **45**.
180. Liu, Z., K. Zou, and Z. Zhang, *Energy Absorption Behavior of Carbon-Fiber-Reinforced Plastic Honeycombs under Low-Velocity Impact Considering Their Ply Characteristics.* Materials, 2024. **17**: p. 4257.
181. Xiao, Y., et al., *Experimental and Numerical Investigation of Dynamic Damage and Load Transfer of PBX Substitute Material under Low Velocity Impact.* Polymers, 2024. **16**: p. 1235.
182. Kharshiduzaman, M., et al., *Characterization of Mechanical Properties of Woven Jute, Kenaf & Woven E-Glass Hybrid Composite Laminates and their Response to Low Velocity Impact.* SSRN Electronic Journal, 2024.
183. Siddiqui, M.A.S., M. Rabbi, and S. Dewanjee, *Low-Velocity Impact Response of Natural Fibre Reinforced Composites: A Comprehensive Review on Influential Parameters.* Composites Part C: Open Access, 2023. **12**: p. 100422.

184. Charca, S., L.J. Wang, and C. Santiuste, *Influence of Reinforcement Architecture on Behavior of Flax/PLA Green Composites under Low-Velocity Impact.* Materials, 2024. **17**: p. 2958.
185. Xie, J., et al., *Effect of prestressed loading on low-speed impact performance for carbon fiber/epoxy resin composite laminates.* AIP Advances, 2024. **14**.
186. Amorim, L., et al., *Low velocity impact study of vacuum bag infused bouligand inspired composites.* Polymer Composites, 2024.
187. Almazán, J., et al., *Enhanced Low-Velocity Impact Properties for Resin Film Infusion-Manufactured Composites by Flow-Control Approach.* Polymers, 2021. **13**.
188. Militello, C., et al., *Low-velocity impact behaviour of green epoxy biocomposite laminates reinforced by sisal fibers.* Composite Structures, 2020. **253**: p. 112744.
189. Rahmani, H., S.H. Mahmoudi Najafi, and A. Ashori, *Mechanical performance of epoxy/carbon fiber laminated composites.* Journal of Reinforced Plastics and Composites, 2014. **33**: p. 733-740.
190. Brooks, R., et al., *The Relationship Between the Extent of Indentation and Impact Damage in Carbon-Fibre Reinforced-Plastic Composites after a Low-Velocity Impact.* Applied Composite Materials, 2024.
191. Dorival, O., et al., *Experimental comparison of impact energy absorption by several foam-composite reinforced structures*. 2015.
192. Ng, L.F., et al., *Drop-weight Impact Responses of Kenaf Fibre-Reinforced Composite-Metal Laminates: Effect of Chemical Treatment and Fibre Composition.* Applied Science and Engineering Progress, 2023.

ANNEXES

ANNEXE.1Published Article 1

Wiley
International Journal of Polymer Science
Volume 2024, Article ID 9405259, 27 pages
https://doi.org/10.1155/2024/9405259

WILEY

Research Article

Evaluation of the Mechanical Performance and Structural Characterization of Hybrid Green Composites Based on *Periploca laevigata* Aiton and Wool Natural Fibers

Lalmi Rahmani,[1] **Mohammed Taher Gherbi**,[1,2] **Atibi Chouaib**,[3] **H. S. S. Aljibori**,[4] **M. N. Mohammed**,[5] **Salah Al-Zubaidi**,[6] **Oday I. Abdullah**,[7,8,9] **and Mohammed Fouad Ferhat**[10]

[1]*UDERZA Laboratory, University of El Oued, El Oued 39000, Algeria*
[2]*Department of Mechanical Engineering, University of El Oued, El Oued 39000, Algeria*
[3]*Research Unit: Materials, Processes and Environment, Boumerdes University, Boumerdès, Algeria*
[4]*Al-Warith Center for Crowd Engineering and Management Research, University of Warith Al-Anbiyaa, Karbala, Iraq*
[5]*Mechanical Engineering Department, College of Engineering, Gulf University, Sanad 26489, Bahrain*
[6]*Department of Automated Manufacturing Engineering, Al-Khwarizmi College of Engineering, University of Baghdad, Baghdad 10071, Iraq*
[7]*Energy Engineering Department, College of Engineering, University of Baghdad, Baghdad, Iraq*
[8]*Department of Mechanics, Al-Farabi Kazakh National University, Almaty 050040, Kazakhstan*
[9]*College of Engineering, Gulf University, Sanad 26489, Bahrain*
[10]*Faculty of Technology, Department of Process Engineering, University of El Oued, Al Oued 39000, Algeria*

Correspondence should be addressed to Salah Al-Zubaidi; salah.salman@kecbu.uobaghdad.edu.iq

Received 16 January 2024; Revised 2 June 2024; Accepted 17 August 2024

Academic Editor: Ulrich Maschke

The current research is focused on developing and evaluating new composite materials that are reinforced with natural fibers to enhance sustainability and create environmentally friendly composites. The use of both wool and *Periploca laevigata* Aiton fibers was chosen in the construction of the hybrid composite due to their similar organic composition, while also taking into account their different properties such as weight, density, and water absorption capabilities. This combination created a composite material that is not only lightweight but also has little water absorption. To further improve the quality of the wool, a treatment involving cold plasma has been carried out to enhance the bonding between individual fibers. Vacuum infusion technology is used during the manufacturing process to ensure the quality of the composite materials by eliminating trapped air, allowing for consistent purity in each repetition. The fibers used in this study include untreated wool fibers, NaOH-treated wool fibers, and cold plasma-treated wool fibers. Wool fibers were treated with a 5% sodium hydroxide solution for 30 min, resulting in fiber degradation. The concentration of the solution was gradually reduced until it reached a practical level of 0.1%. The hybrid composite incorporates wool that has undergone plasma treatments, which are crucial for removing organic contaminants from surfaces, strengthening the surface layer, and altering the chemical structure. The electric field applied had a strength of 9 kV and a frequency of 60 Hz. Atmospheric air was employed as the gas, with a flow rate of 800 L/min, and the fiber treatment lasted for 60 min. An analysis of natural fibers using Fourier transform infrared (FTIR) and X-ray diffraction (XRD) unveiled similarities in the organic structures and chemical bonds shared between *Periploca laevigata* Aiton fiber and wool fibers, despite their unique origins. While wool fibers are animal-derived, *Periploca laevigata* Aiton fibers stem from plants. By identifying these parallels, a hybrid composite material was formulated by combining plasma-treated wool fibers with *Periploca laevigata* fibers. This resulted in a significant improvement in the tensile, flexural, and compressive properties of the composite, establishing it as a promising avenue for enhancing mechanical performance. The PLAF-WLF hybrid composite exhibited a remarkable tensile strength of 26.02 MPa and Young's modulus of 2.35 GPa, surpassing all other composites. In comparison,

the PLAF composite demonstrated an impressive tensile strength of 20.1 MPa and Young's modulus of 2.34 GPa. The PLAF-WLF hybrid composite exhibited the highest flexural load-bearing capacity of 253.15 N and Young's modulus of 1.21 GPa. PLAF-WLF demonstrates a hybrid compressive strength of 59.56 MPa, while its Young's modulus is 0.5 GPa. The mechanical analysis findings revealed that the hybrid composite incorporating cold plasma-treated wool fibers and *Periploca laevigata* Aiton fibers displayed superior mechanical characteristics. Additionally, the composite made of *Periploca laevigata* Aiton fibers, recognized for its lightweight nature, smooth surface, and high quality, showed notable mechanical properties as well.

Keywords: cold plasma; composites; epoxy; fiber; hybrid composite; mechanical characteristics; *Periploca laevigata* Aiton; polymer; vacuum infusion; wool

1. Introduction

The utilization of composite materials is increasing, progressively substituting conventional materials. To stay abreast of the swift technological advancements in various industries, it is crucial to concentrate on creating inventive alternative material designs. Polymer composites are deemed superior alternative materials because of their reduced weight, enhanced strength, and cost efficiency. Fiber reinforcement is commonly employed in polymer matrices like polyester and epoxy to produce fiber-reinforced polymer (FRP) composite materials. Nowadays, there are numerous synthetic fibers available, such as E-glass fiber and aramid fiber, that enhance mechanical properties across the board. However, these composites may face challenges in terms of environmental impact due to issues related to degradability, renewability, and recyclability [1]. With the progress in technology, it is now feasible to utilize the ecofriendly characteristics of plant-based materials, all while taking into account environmental issues and sustainability factors. Consequently, natural fiber composites are presently attracting more interest [2].

Therefore, green composites are now a mandatory substitute for nondegradable material due to the increasing demand for natural fiber–based products, which minimizes the environmental impact. Due to the promotion of sustainability, bioreinforced composites have gained attention from various industries, including agricultural crops, aerospace, construction, packaging, fire retardancy, and housings for laptop computers [3]. Academics are interested in integrating environmental fiber into modern engineering activities due to reducing the number of synthetic fibers in polymer composites obtained from petroleum resources [4].

A composite material comprising a polymer matrix and incorporated fibers has garnered widespread interest worldwide. In light of the prevailing global environmental challenges, there is a rising inclination among people to explore the optimal use of natural fibers in diverse applications [5]. Natural fibers offer numerous advantages for use in composite materials such as high elastic modulus, flexural strength, flexibility, low density, renewability, biodegradability, and recyclability. These characteristics have significantly increased the appeal of natural fiber–reinforced composites. However, natural fibers also come with inherent disadvantages, such as poor compatibility with polymer materials. The hydrophilic nature of natural fibers results in weak adhesion and moisture absorption, leading to compatibility issues in biocomposites. Therefore, pretreatment of natural fibers is necessary to enhance the biocompatibility between the fibers and matrix through the activation of the fiber's hydroxyl groups [6].

Polymers are typically hydrophobic, while natural fibers are hydrophilic. Material scientists are currently developing numerous polymer composites using natural fibers that are easily accessible. In order to enhance the mechanical properties and environmental performance of these composites, natural fibers need to undergo chemical modifications with suitable additives or be coated with appropriate resins. Recent applications of chemical treatments include acetylation, alkali, acylation, silane, and benzoylation [7]. Among these, alkali treatment stands out as the most cost-effective and commonly used method. This treatment works by breaking down the hydrogen bonds in fiber bundles into smaller fibers, thereby reducing hydrophilic clusters in the matrix/fiber interaction [8]. Various methods are used to improve the adhesion between fiber morphology and the polymeric matrix. Sodium hydroxide (NaOH) and cold plasma techniques are commonly employed for this purpose. Cold plasma treatment, a physical method, is utilized to enhance the compatibility of natural fibers with the matrix. The fiber-matrix interface plays a crucial role in determining the quality of a fiber-reinforced composite. Acting as a binder, this interface facilitates the transfer of stress between the fibers, and it is enhanced through the use of a chemical agent such as NaOH. During the treatment process, water is taken in a specific volume along with 0.1% NaOH. The fibers are then soaked in this solution for a duration of 1 h. Subsequently, the fibers are meticulously washed with distilled water to eliminate any remaining alkali residues [9].

Plant, animal, and mineral fibers are categorized into broad classifications. Plant fibers consist of cellulose, hemicellulose, and lignin, whereas animal fibers contain various types of functional amino acids. Notably, cotton, jute, wool, and silk fibers are significant natural fibers that find extensive use in apparel clothing [10]. Wool plays a significant role in textile manufacturing as one of the key animal fibers. Like other hairs, animal horns, and fingernails, wool consists of a special protein called keratin, which sets it apart with its high sulphur content. With a chemical formula of $NH_2.CHR.COOH$, wool is preferred over other fibers for its exceptional natural properties including feel, moisture absorption, strength, and its ability to hang. In contrast, wool stands out as the most contaminated natural fiber. A ton of raw wool typically comprises around 150 kg of lanolin, 40 kg of saint, 150 kg of dirt, 20 kg of vegetable matter, and merely 640 kg of wool fiber. Prior to its utilization in textile production, wool must undergo several treatment

procedures [11]. *Periploca laevigata* Aiton (PLA) subsp. angustifolia (Labill.) Markgraf, also known as *P. laevigata* Aiton or *P. angustifolia* Labill., is a plant species native to the Mediterranean and Saharan regions. It can be found growing naturally in the lower and middle basin areas, extending southwards into the northern and central Sahara. It is highly desired due to its conventional healing attributes and its significance in pastoral and erosion prevention, owing to its acclaimed medicinal properties. The *Periploca* species that have been extensively researched exhibit a range of biological activities, including antiproliferative, antitumor, and hypotensive effects [12].

Natural FRP composite is currently growing in industrial applications and scientific research due to their renewable nature, low cost, partially or completely recyclable, and biodegradability. Researchers have developed composite manufacturing techniques that use biodegradable natural fibers such as flax, cotton, hemp, jute, sisal, pineapple, banana, wood, date palm, and other fibers to manufacture products that have good mechanical properties and cost-effectiveness while minimizing environmental impact [13]. The reinforcement fibers are classified into two main groups: synthesized and natural fibers. Some plant fibers are good substitutes for synthesized fibers in different applications [14–16]. Animal fibers have low density and low cost. They are also readily available, with a constant supply, and they are safe to handle [17]. Animal fibers have diverse applications and are used in various sectors such as biomedical, construction, and automotive [18]. The producers of keratin fibers are largely dependent on the sheep wool fibers that play as raw materials for the textile industry. Some attempts were carried out to examine their thermal properties. For example, Zach et al. [19] examined the suitability of wool as thermal insulation in buildings and evaluated the wool at different temperatures. According to the findings, sheep wool insulation is comparable in performance with mineral or rock insulation. In some cases, it even performs better.

The materials are evaluated for their physical aspects as well as their mechanical properties to develop a better product and reach customer satisfaction [20]. Understanding natural fiber's physical and chemical properties, as well as mechanical characteristics, is required to increase composite material performance [21]. Depending on the nature and structural properties of the natural fiber, the use of natural fiber in the polymeric matrices allows us to adjust or improve some essential characteristic behaviors such as mechanical, thermal, acoustical, processing, and free volume [22]. The poor surface adhesion between the fiber and the polymer matrix is due to the hydrophobic nature of the fiber. Moisture penetration into composites can damage their mechanical characteristics in three different ways: the first mechanism involves the diffusion of water molecules into microgaps across polymer chains, the second mechanism involves the movement of filaments through gaps and defects in the fiber matrix contacts, and the third mechanism involves swelling effects, which cause microcracks to propagate in the matrix [23]. Several chemical treatments can be applied to the fiber surfaces to improve interfacial interaction and moisture absorption in natural fiber composites. Alkaline solution treatments improve the removal of partially amorphous elements such as hemicellulose, lignin, waxes, and oils soluble in alkaline solution and reduce the fiber diameter and degree of fiber clumping. The rough surface improves fiber/matrix adhesion [24]. There are some physical and chemical processes used in the treatment of fiber morphology to promote adhesion with the polymeric matrix. For instance, chemical treatment by NaOH and cold plasma methods. Cold plasma represents a form of physical treatment employed to enhance the compatibility of natural fiber with the matrix. Surface modification depends on the type and nature of the gas used [25]. Alkaline treatment represents the most commonly utilized method for treating plant fiber composites due to its low cost. This process effectively removes noncellulosic components from the fiber surface, resulting in a smooth and textured surface that enhances interfacial adhesion [17]. Alkaline treatment helps remove hydrogen bonds from the network structure of the fiber, which effectively reduces moisture absorption and reduces the diameter of the fiber, which raises the aspect ratio. Alkaline treatment enhances surface roughness, which increases mechanical cross-linking and exposes more cellulose on the surface of the fiber [18]. The NaOH procedure aims to enhance the contact area by reducing the presence of hydrophilic groups that result in an inadequate polymer matrix and weak fiber-matrix adhesion. The fibers undergo treatment with a NaOH chemical solution to enhance the interfacial adhesion between the fibers and matrix, thereby achieving tensile strength through a well-established interface along the fiber surface [4].

There are a number of studies that promote the use of sheep's wool as a toughening agent in an epoxy matrix. In order to assess the mechanical properties of composites, various forms of sheep wool were tested as toughening agents in an epoxy matrix [26, 27]. Therefore, wool fibers can be used as good strengtheners for polymeric matrix not only for the improvement of the thermal properties but also it is extended to mechanical properties as will be seen in the current study.

The exploration of a new hybrid composite, which combines cold plasma–treated wool fiber (WLF) and PLA, represents a cutting-edge project in materials science. A thorough investigation of the existing literature reveals no documented cases where this specific compound has been synthesized. By subjecting wool fibers to cold plasma treatment and incorporating *P. laevigata* Aiton fibers (PLAF), this innovative approach aims to capitalize on the unique properties of both fibers to improve composite performance. The production of such a hybrid composite highlights the pioneering nature of this research, opening up possibilities for new applications and developments in the field of composite materials. As the scientific community aims to push the frontiers of materials science forward, the synthesis of animal-based wool fibers treated in a cold plasma environment with plant-based PLA emerges as a promising and unprecedented method for developing advanced hybrid composites.

The main contribution of the current study is to manufacture and investigate the performance of a new hybrid

green composite processed from the reinforcement of epoxy resin with untreated PLAF and WLF. For comparison purposes, another three composites were fabricated with epoxy resin reinforced with untreated WLF, chemically treated NWLF by NaOH, and untreated PLA. The structure of four fibers was characterized by Fourier transform infrared (FTIR), X-ray diffraction (XRD), and scanning electron microscopy (SEM). Four composite materials were fabricated from different volume fractions of natural fibers and epoxy resins by the vacuum infusion method. All composites were subjected to three mechanical tests, namely, tensile, flexural, and compression tests, to show the effectiveness of hybridizing the PLAF-WLF composite with PLAF fiber.

2. Materials and Procedures

This section presents a description of the two natural fibers being used in this study, namely, PLA and wool fibers. Also, it illustrates how these two fibers are prepared and treated to examine their structures by using FTIR and XRD. It also describes how the composite materials were produced. Further, it shows how the produced composite materials are subjected to tensile, compression, and flexure tests.

Figure 1 depicts the adopted methodology in this study which shows the steps mentioned above. It reveals that the applied methodology consists of several steps to reach the proposed objectives of the current study. These steps are described in the following subsections.

2.1. Preparation of the Natural Fibers

2.1.1. PLAF. PLA is actually a heat-loving, perennial, deciduous shrub that is widespread in different regions. It is native to the Mediterranean region and can be found in countries such as Spain, Algeria, Libya, Tunisia, Karpathos, Egypt, Crete, Malta, and Sicily [28]. PLA has drooping leaves and an entire, narrowly lanceolate branch. The flowers are distributed in short auxiliary cymes with reddish-brown lobes bordered in greenish-yellow and alternated with incurved purplish filaments. The fruit is dry and made up of two smooth and fissured follicles that contain anemocorous seeds [29]. These fibers are short and very lightweight; they fly in the air after the lobes become dry, and they crack naturally, as shown in Figures 2(a), 2(b), and 2(c). It has not undergone any processing due to its delicate structure and natural characteristics. The PLA lobes were manually extracted by opening the lobes and separating the seeds from the fiber. The fibers were washed extensively with distilled water at 25°C. This temperature maintains the structural characteristics of the fiber. The fiber was filtered and then subjected to a 24-h drying process at room temperature.

Archimedes' principle was employed to determine the density of PLAF. The fibers of 4.5 g mass were impressed in a 100 mL water container to calculate the volume difference. The fiber's mass (4.5 g) is divided by its volume (0.01 L) to get the fiber density of 0.45 g/cm^3.

2.2. Preparation and Treatment of Wool Fiber. Sheep wool, alpaca hair, goat hair, horse hair, and other hairy mammal fiber are examples of animal fiber [30]. Wool has long been used in the clothing and textile industries, and it will continue to assume a significant role in a number of new and future uses [31]. Shearing, washing, drying, grading, sorting, carding, spinning, weaving, and finishing are all important processes in the process of turning wool from sheep into fabrics [30]. Wool samples are taken from sheep in the Ghardaia region (Algeria), and the wool was sheared from sheep in the spring, resulting in greasy raw wool that contained a lot of dirt, sand, oil, and dry sweat. A part of this wool was manually cleaned of dirt and dust; another part was treated with a NaOH solution with a concentration of 0.1%, and the last part was cleaned with cold plasma. The next two sections (2.2.1 and 2.2.1) describe how the WF has been treated by the second and third methods (i.e., chemical and cold plasma methods).

After cleaning the wool with the three previously mentioned methods, it is combed as it is passed through a series of thin metal teeth that work to loosen wrinkles and tangles in the fiber, and then it is arranged in the form of a flat strip called a weave, which later turns into thin threads. After the fibers are carded, the threads are stretched and twisted to make them thinner, just as the fibers are pulled to become very thin and ready for spinning. Figure 3 shows the manufacturing process depicted in the study.

2.2.1. Chemical Treatment Method. Natural fiber is hydrophilic in nature and has seen significant obstacles in polymeric composites due to the presence of its hydroxyl groups like lignin, cellulose, and waxes [32]. Because of their negative sensitivity to water, it is difficult to combine natural fiber with a hydrophobic matrix [33]. Therefore, the natural fibers must be treated before processing any green composite materials. The chemical treatment is generally applied to the natural fiber to remove impurities and other particles from the surface of the fiber, tightening the surface of the fiber and matrix to enhance the interfacial bonding between them [34, 35]. Alkaline treatment helps remove hydrogen bonds from the network structure of the fiber, which effectively reduces moisture absorption and reduces the diameter of the fiber, which raises the aspect ratio. Alkaline treatment enhances surface roughness, which increases mechanical cross-linking and exposes more cellulose on the surface of the fiber [36]. NaOH is one of the most important alkaline chemical treatments in this field [37]. Therefore, the NaOH treatment was nominated to process the fibers. We immersed the wool in a 5% solution of NaOH for 30 min, and the fiber started to degrade. Treatment of wool fiber with NaOH at different concentrations, specifically 5% and 3%, results in varying degrees of fiber structure breakdown. The concentration of the solution was gradually reduced until it reached a practical concentration of 0.1%, with every treatment taking 1 h. At this point, there is a rough surface with uniform roughness. The treated wool fibers were washed with distilled water and dried at ambient temperature (25°C) for 3 days. As a result, 0.1% NaOH was used during the fiber chemical treatment process in this experiment.

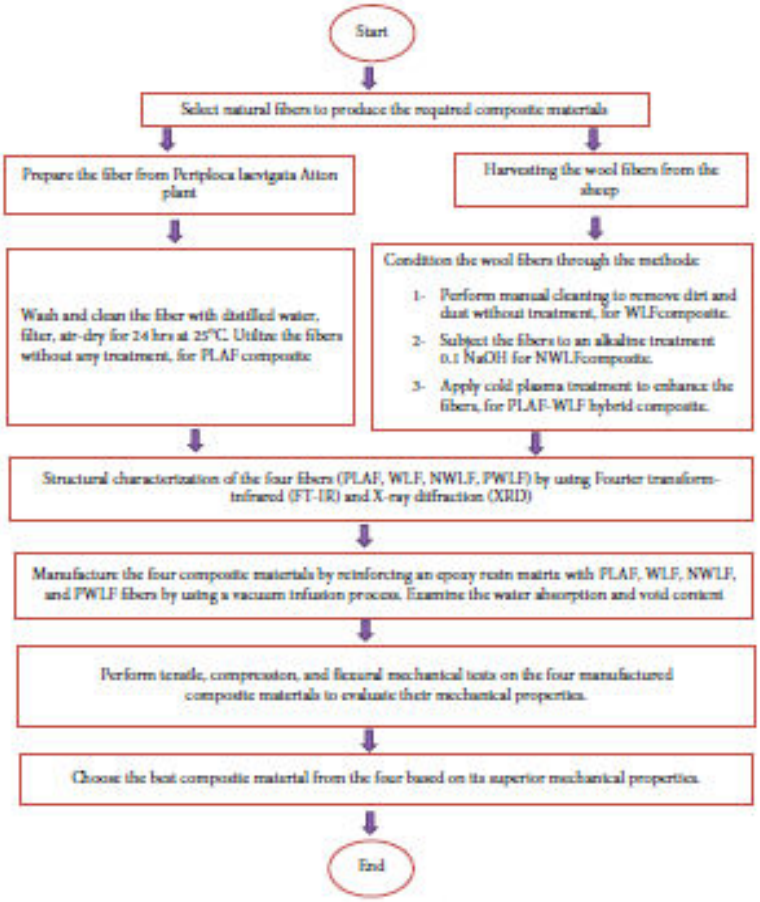

Figure 1: Applied methodology.

2.2.2 *Cold Plasma Treatment Method.* Plasma surface treatment is very important in the industrial field due to its efficiency and environmental friendliness [38]. The cold plasma treatment can be used to modify the surface of short glass, carbon, cellulose, polyimide, aramid, and other fibers. The surface of cellulose fiber was altered by air plasma treatment, which was employed to augment the adhesion between the thermoplastic starch matrix and the fiber. SEM analyses of the fractured surfaces demonstrate a considerable increase in adhesion between treated cellulose fiber and the thermoplastic starch matrix [39]. The applied electric field was generated using a gliding ARC discharge with a power source set at 9 kV at a frequency of 60 Hz. The atmospheric air was used as a gas, with a flow rate of 800 L/min. As shown in Figures 4 and 5, the plasma jet discharge extended approximately 5 cm, giving a direct measurement of the cold plasma's effect on natural fiber. The gliding arc discharge reactor consists of two diverging stainless steel electrodes with a thickness of 1 mm, located at the bottom of the feed gas nozzle. The fibers were put in a container 10 cm in diameter and 1 cm thick. The wool was treated with cold plasma inside a container containing distilled water. For a set period of time, the fiber was moved randomly inside the container under the effect of the plasma jet at ambient air temperature. During processing, the fiber was maintained 5 cm away from the flow of liquid plasma. Jet plasma treatment was applied to the fiber for a period of 60 min. Plasma-treated wool fiber was left in ionized water for 4 h. The wool fiber was washed with distilled water and left to dry at room temperature for 3 days before utilization, and the drying procedure was accomplished by subjecting it to an oven at a temperature of 60°C for a duration of 24 h.

(a) (b) (c)

Figure 2: *Periploca laevigata* plant and its fibers: (a) the *Periploca laevigata* Aiton plant, (b) lobes with fibers, and (c) extracted fibers.

2.3. *Epoxy and Hardener.* The resin matrix that is intended to be strengthened in this study by the natural fibers is Duraclear Epoxy. It is provided by AGEL Chemicals Company, and its properties and specifications are tabulated as Table 1 shows.

2.4. Structural Characterization of WF and PLA Natural Fibers

2.4.1. Analysis via FTIR. Researchers have experimented with a variety of chemical treatments to enhance the cellulose content, mechanical characteristics, surface roughness, and so on, and this method can be used to determine the chemical changes occurring in the functional groups. Analysis using the FTIR [41]. The samples were examined using FTIR (Shimadzu, IR Affinity-1, FTIR, Resolution 8). To study changes in chemical composition, 0.02 g of each sample was grinded and mixed with 0.198 g of KBr powder before being grinded on a KBr disk and compressed at a pressure of 70 kN for 2 min. FTIR uses a wavenumber range of 400–4000 cm^{-1}, and 20 scans were performed in each case..

2.4.2. Analysis Using XRD. X-ray crystallography is the most extensively utilized method for identifying the molecular and crystal structures of any crystalline substance, whether natural or synthetic [42]. The recording pattern is based on measuring diffraction line intensities by transmitting source and detector steps. We were able to record the diffraction pattern on the investigated material using the XRD instrument. XRD spectroscopy with wavelength $\lambda_{CuK\alpha} = 1.54°A$ at 2θ scan angles ranging from 10° to 90°, whereas this approach allows for the determination of diffraction lines based on Bragg's law.

2.4.3. SEM. The SEM test would provide a complete view of the structural characterization of all natural fibers being used in the current study. All those fibers were subjected to SEM

Figure 3: Preparation of the wool fiber: (a) cold plasma treatment, (b) treatment by 0.1% NaOH, and (c) manual cleaning.

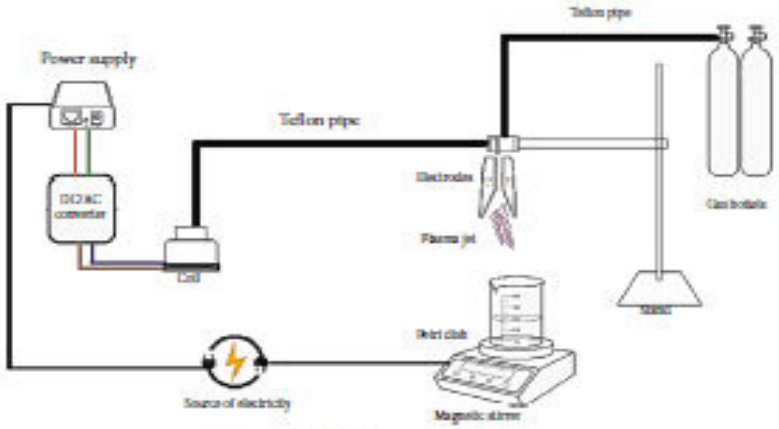

Figure 4: Cold plasma treatment process.

examination. It is a helpful tool in scanning and illustrating the surface features of all fibers.

The SEM (Leo Supra 55, Zeiss Inc., Oberkochen, Germany) was operated with specific settings for effective analysis. The voltage was set at 10 kV, the beam current at 5 μA, and the spot size at 10 nm. Additionally, the acceleration angle was adjusted to optimize the investigation of the morphology of the four composites. These meticulously chosen parameters aimed to ensure precise and detailed imaging during the SEM analysis.

2.5. *Fabrication of Composite Materials.* The vacuum infusion molding process was used in this study to manufacture composite material. This process can solve challenges with manual lay-up and spray-up methods. One of the modern composite manufacturing processes that could potentially replace the traditional method is the vacuum infusion molding process. The idea behind vacuum infusion is to create a vacuum and draw air into the mold through negative pressure while sucking the resin into the mold, thereby impregnating the reinforcement in the resin. The vacuum infusion molding process eliminates the risk of trapped air in the composite, and this process enables the composite to be manufactured in repetition with the same purity because it is dependent on the design of the equipment rather than the operator's competence [43].

Figure 5: Wool fiber under cold plasma jet.

Table 1: Properties and specifications of Duraclear Epoxy [40].

Item	Specifications
Density (specific density at 25°C)	1.12 epoxy, 0.97 hardener
Mix ratio (volume)	2:1
Mix ratio (weight)	100:43
Viscosity (A/B/mixed at 25°C)	1850/35/280
Mixed density-specific density at 25°C	1.07
Pot life at 25°C	90 min
Tack free time at 35°C	24 h
Color	White
pH	7–9
Recommended full cure	7 days at 25°C
Gel time @ 22°C in a 150-g mass	5.5 h
Maximum casting depth	1.27–2.54 cm

After the resin layer and matrix have been produced, excess resin will be extracted from the mold through suction. This method ensures homogeneous thickness distribution along the part. The material produced by the vacuum infusion technique has a greater fiber-to-resin ratio than the material produced by the hand lay-up method, resulting in a stronger and lighter composite material [44]. The mold has a dimension of 300 mm × 250 mm × 4 mm. Initially, fibers were weighed using a sensitive balance, and the amount of epoxy and hardener needed was calculated. The fibers, regardless of the type or treatment conditions, were dried in an oven at 60°C to prevent voids, moisture, and poor fiber–matrix adhesion. The mold surface was carefully cleaned, and a mold-releasing agent was coated all over the mold surface for easy removal and an excellent product surface finish. The fiber was placed in the mold once it had been prepared; after that, the mold was covered with another layer of mold. In Figure 6, we present the experimental setup, offering a clear depiction of the apparatus used for our study. The hose used for the inlet is attached to the resin tank, while the outlet hose is connected to the resin trap. After connecting and completing the circuit vacuum pump installation, it began to operate, and the resin flowed through the input section and entered the mold due to the pressure differences until it reached the output section. The vacuum pressure used to suction epoxy resin is 30 mHg. In Figures 7(a), 7(b), 7(c), 7(d), and 7(e), we outline the sequential steps involved in the manufacturing of the composites. The specimens depicted in Figures 8(a), 8(b), 8(c), and 8(d) were carefully positioned within a controlled environment. Previous findings in the literature suggest that the increase in wool fiber content has minimal influence on tensile stress or elastic modulus [45]. Various studies have employed volume fractions ranging from 30/70, 40/60, to 50/50. Notably, a volume fraction of 30/70 is considered the minimum, as any reduction below this ratio results in a decline in mechanical properties. Similarly, a volume fraction of 50/50 is considered the maximum, but the composition with a ratio of 50-50 exhibits higher moisture absorption compared to the composition with a ratio of 60-40, while the 60-40 composition demonstrates greater chemical absorption than the 50-50 composition [46]. When the fiber content surpasses 50%, the mechanical properties also deteriorate. To create a lightweight composite with favorable mechanical properties, our research highlights the significance of reducing the wool percentage and incorporating plant fibers. This combination enhances properties such as low water absorption, low density, and lightweight. Therefore, we selected a fiber percentage of 30% and maintained the same proportion when introducing plant fibers. As a result, we decreased the wool percentage in the composite. Table 2 presents the weight percentage compositions of the composite specimens, offering a comprehensive overview of their material compositions.

2.6. Mechanical Tests of the Composite Materials. After the fabrication of the four composite materials, all specimens were subjected to three mechanical tests, namely, tensile, compression, and flexural tests, to evaluate their response to different types of loading. The tensile and compression tests were conducted using the Zwick/Roell Z10 machine, which was controlled by test pert software Version 1.2.0 and equipped with a precision 10 kN force sensor. Conversely, for flexural examinations, it was utilized the Zwick Z 2.5 machine, which featured a 2 kN sensor. Figure 9 shows the universal Zwick/Roell Z10 tensile and compression and Zwick Z 2.5 Flexural tester. In order to compare the mechanical performance of each composite and achieve optimal results, we conducted assessments on five specimens for each structure. These assessments were carried out under consistent conditions, incorporating conditions such as ambient temperature and a testing speed of 5 mm/min. The tests provided valuable insights into the specimen's behavior, encompassing measurements such as elongation, nominal strain, Young's modulus, and tensile strength. Figure 10 outlines the dimensions of the tensile, compressive, and flexural specimens, as illustrated in Figure 11. The three tests were conducted according to ASTM D3039, ASTM D790, and D3410, respectively.

3. Water Absorption

3.1. PLAFs. The behavior of water absorption is commonly investigated in accordance with ASTM D 570. The

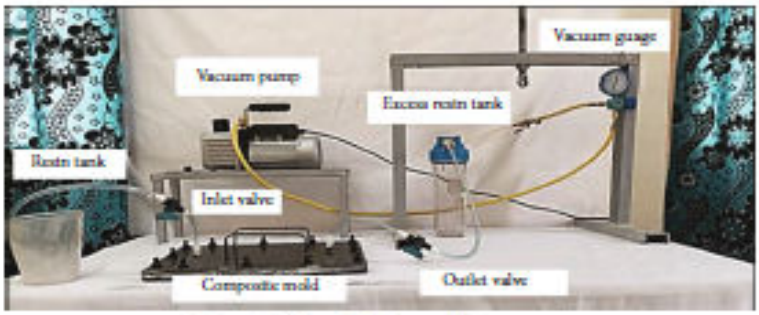

Figure 6: Vacuum infusion molding process.

Figure 7: Manufacturing of composites by vacuum infusion molding: (a) *Periploca laevigata* Aiton fiber, (b) WLF, (c) NWLF, (d) PLAF-WLF, (e) epoxy and hardener, (f) closed mold, and (g) composite after curing time.

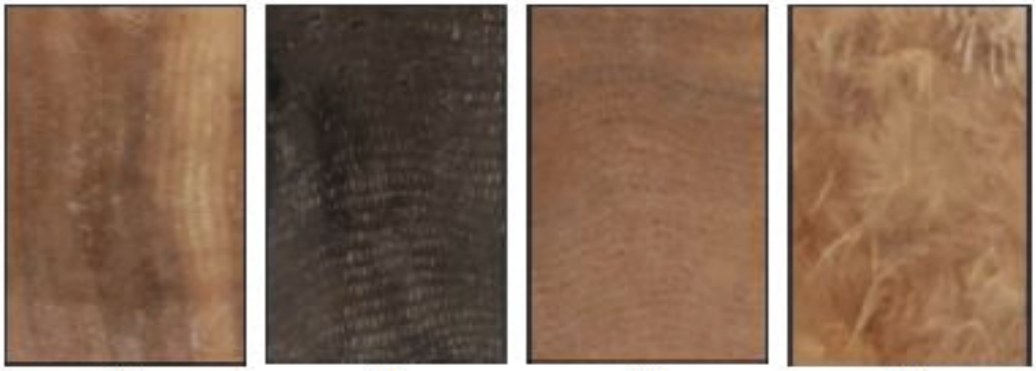

(a) (b) (c) (d)

Figure 8: Final composites specimens: (a) NWLF, (b) WLF, (c) PLAF-WLF, and (d) PLAF.

Table 2: Compositions of the composite specimens in weight percentage.

Type of fiber	Type of treatment	Fiber weight fraction (wt.%)	Epoxy resin weight fraction (wt.%)
WLF	Untreated	30	70
NWLF	NaOH-treated	30	70
PLAF	Untreated	15	85
PLAF-WLF	Untreated (PLAF), cold plasma–treated (WLF)	10/20	70

percentage increase in water absorption is calculated using a specific Equation (1) [47].

$$\text{Water absorption\%} = \frac{W2 - W1}{W2} \times 100 \quad (1)$$

where W_1 is the weight before soaking in water (gram) and W_2 is the weight after soaking in water (gram).

To begin the process, the samples were meticulously cleaned and then placed in individual containers filled with distilled water. They were left in the water for a duration of 10 min at room temperature. Each sample had a weight indicated in Table 3. Once the immersion period was complete, the samples were carefully removed from the containers. To facilitate the absorption of surface moisture, the fiber samples were positioned between a pair of filter papers and a pair of circular disks. The pressure exerted by the circular disk allowed the filter paper to absorb the moisture. Finally, the weights of the samples were measured using a precise digital balance machine in order to determine the percentage of water absorption [48].

As shown in Table 3, the water absorption of PLA ranges from 11.09% to 7.22%. This finding highlights another significant advantage of PLAFs, in addition to their lightweight nature.

Compared to various other natural fibers, such as cotton fibers (which can absorb water between 32.5% and 50.5%), banana fibers (which can absorb water between 495% and 448.5%), and raw areca fibers (which can absorb water between 698% and 851%), PLAFs exhibit a significantly lower rate of water absorption [28].

3.2. Wool Fibers. Wool, being a protein polymer, possesses various functional groups and an amorphous region, enabling it to readily absorb water molecules. It can retain water from 13% to 18% of its dry weight at 65% relative humidity, and this percentage can increase up to 40% at 100% relative humidity [49].

3.3. Void Content. Physical attributes play a crucial role alongside mechanical properties in assessing the suitability of a composite material for specific applications. Among these attributes, density stands out as a key factor. The theoretical density (Td) of composite samples measuring 25 mm × 25 mm × 4 mm, relative to their weight fraction, is calculated using Equation (2) as per ASTM D2734-94 [50].

$$Td = \frac{100}{R/D + r/d} \quad (2)$$

The actual density (Md) of the composite material is determined by dividing the weight by the volume. The composite void fraction (V) can be calculated using Equation (3) as per the ASTM D2734-94 standard. In this equation, Td represents the theoretical density in grams per cubic centimeter, R represents the weight fraction of resin, D represents the density of resin in grams per cubic centimeter, r

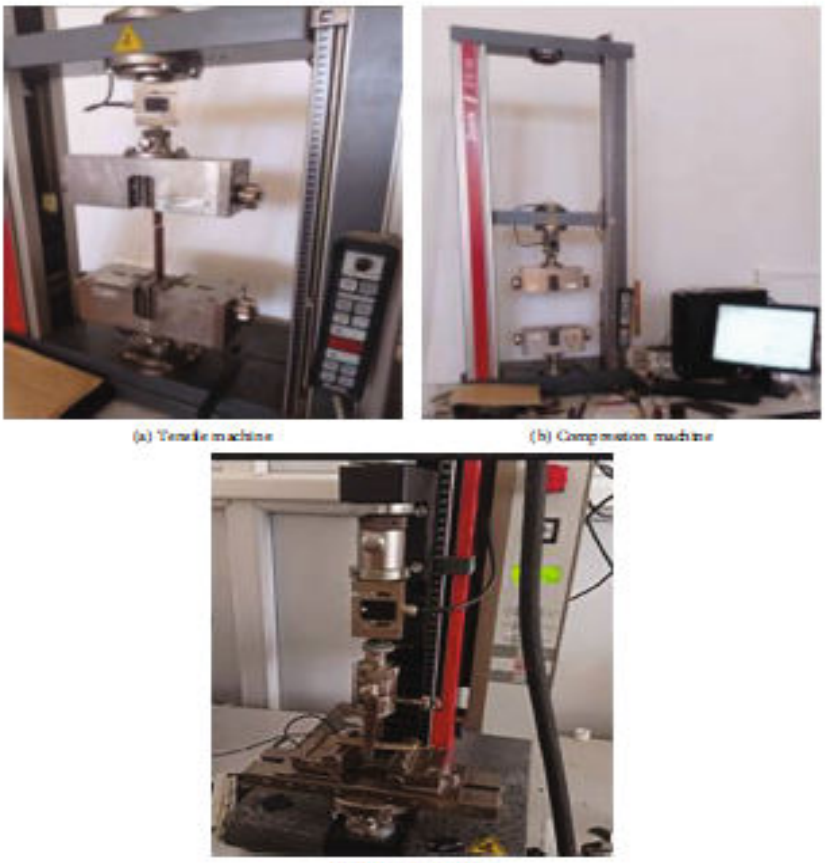

(a) Tensile machine (b) Compression machine

(c) Flexural machine

Figure 9: Test machines: (a, b) universal Zwick/Roell Z10 tensile and compression tester and (c) Zwick Z 2.5 Flexural tester.

represents the weight fraction of fiber, and d represents the density of fiber in grams per cubic centimeter [50].

$$V = \frac{100(Td - Md)}{Td} \quad (3)$$

The void fraction, denoted as V, is expressed in volume percentage. Td represents the theoretical density of composites in grams per cubic centimeter, while Md represents the actual (measured) density of composites, also in grams per cubic centimeter.

The table provided in Table 4 displays the void fraction in relation to the measured and theoretical densities of the composites.

The decrease in void fraction observed when blending PLAFs in the hybrid composite can be attributed to multiple factors. The addition of these fibers reduces the presence of voids or empty spaces between the fibers. This is due to enhanced interaction between the fibers and the matrix, as well as a decrease in shrinkage and buckling during the curing process. As a result, the total area available for voids is reduced, leading to a denser arrangement of materials in the composite and a lower void ratio. This improved filling efficiency ultimately contributes to the reduction in void fraction.

4. Results and Discussions

As aforementioned above, the structural characteristics of untreated PLA and treated and untreated WLF fibers were analyzed by using FTIR, XRD, and SEM. On the other hand, the composite materials, which were processed from those

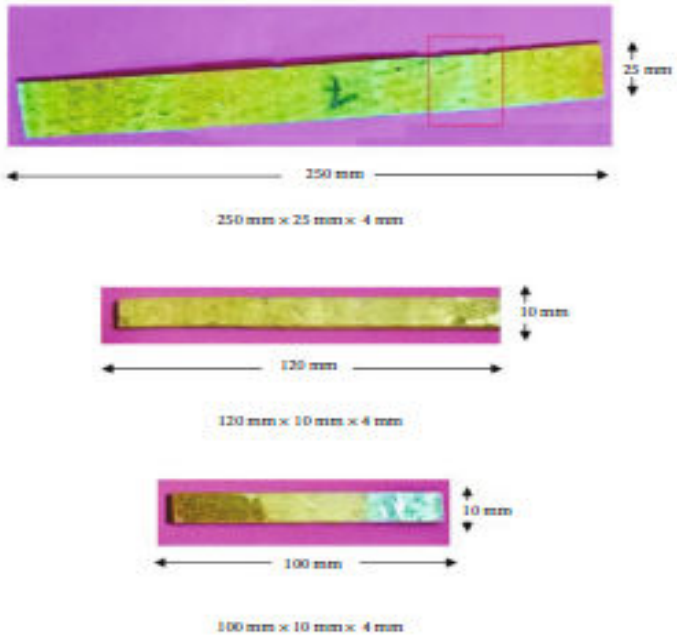

Figure 10: Specimen dimensions for tensile, flexural, and compression tests.

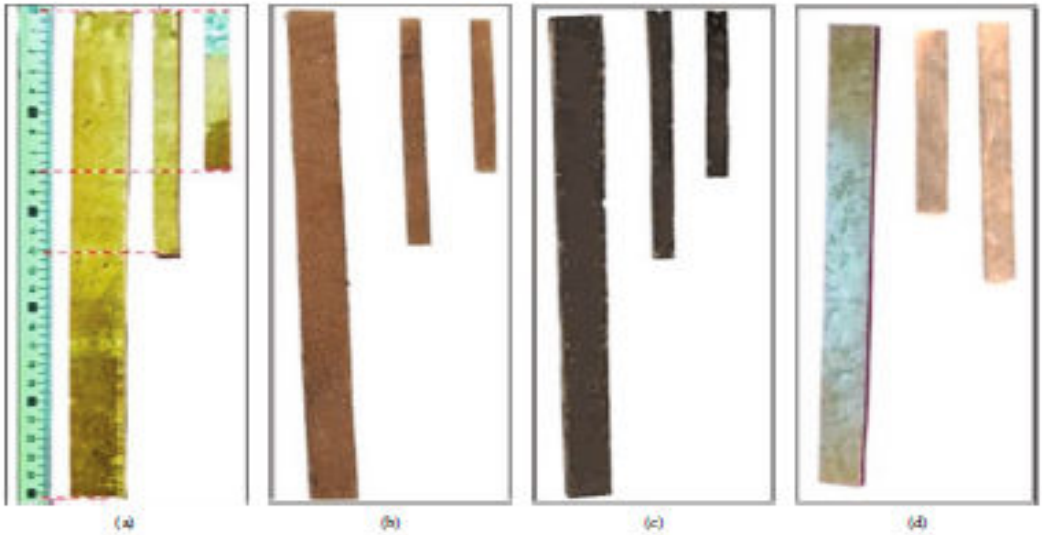

Figure 11: Tensile, compression, and flexural standard specimens of (a) PLAF-WLF, (b) WLF, (c) NWLF, and (d) PLAF composite materials.

Table 3: Water absorption of *Periploca laevigata* Aiton fiber.

Sample	W_1 (g)	W_2 (g)	Water ABS %
1	0.5707	0.6419	11.09
2	0.5641	0.6298	10.36
3	0.5744	0.621	7.50
4	0.5785	0.6247	7.40
5	0.5785	0.6235	7.22

Table 4: The density and void fraction of the specimen samples.

Sample	Td (g/cm^3)	Md (g/cm^3)	V (%)
WLF	1.130	1.092	3.361
NWLF	1.130	1.095	3.095
PLAF-WLF	1.041	1.029	1.182
PLAF	0.887	0.877	1.098

four fiber groups and epoxy resins, have been mechanically tested by tensile, compression, and flexural tests. Accordingly, the next two subsections present and analyze the collected findings of the fiber characterization and mechanical properties of the four composite materials.

4.1. Characterization Results of WLF, NWF, PLAF-WLF, and PLAF Natural Fibers. The structures of all the processed natural fibers were characterized by FTIR, XRD, and SEM tests. First, the FTIR spectroscopy results are presented in Figure 12 and Table 5 which indicate similarities in organic structures and chemical bonding between PLA and wool fibers. The peak around 1519 cm^{-1} in Figure 12 is known as the (-C-N-H) bond's bending deformation peak, and it demonstrates that C-N stretching is closely connected to N-H bending. The peaks at 1585, 1566, 1681, and 1573 cm^{-1} shown in Figures 12(a), 12(b), 12(c), and 12(d) are caused by the -CO stretching bond of the amide group. The peak in Figures 12(a), 12(c), and 12(d) is around 3699–3788 cm^{-1}, while the peak in Figure 12(b) is approximately 3703 cm^{-1}, proving that the water (-OH) in the samples indicates minimal variation in the peaks. The Amide II peak became more evident in the treated samples since its location changed based on the treatment conditions. In Figures 12(b), 12(c), and 12(d), the presence of peaks at 1288, 1276, and 1284 cm^{-1} is indicative of components associated with both α-helical conformation and disordered structure. These spectral features provide insights into the molecular composition and structural characteristics.

Second, the XRD results are shown in Figures 13(a), 13(b), 13(c), and 13(d). Through the two resulting curves shown in Figures 13(c) and 13(d) of untreated *P. laevigata* fiber and of untreated wool fiber, respectively, which record information about the crystal structures present in the studied samples, we notice that the peak corresponding to the angle $2\theta = 25.62°$ in Figure 13(c) is closely related to the peak of the angle $2\theta = 26.67°$ in Figure 13(b). The same observation was recorded through two curves shown in Figure 13(a) of treated wool fiber by 0.1% NaOH and Figure 13(b) of treated wool fiber by cold plasma mixed with untreated *P. laevigata* fiber, which noticed information on the crystal structures found in the samples during the study. We find that the peak corresponding to the angle $2\theta = 20.98°$ in Figure 13(c) is closely related to the peak of the angle $2\theta = 21.39°$ in Figure 13(b). As a result of the two curves shown in Figures 13(a) and 13(b), we conclude that the wool fiber crystallinity is linked to its chemical, physical, and mechanical characteristics. The crystallinity of wool fiber was observed to decrease as a result of alkali treatment. This reduction in crystallinity can likely be attributed to the damage inflicted upon the polypeptide chain during the alkali treatment process. Specifically, due to the decomposition of a portion of the crystal structure, a modest decrease in crystallinity was observed, as confirmed by [51].

Third, SEM was utilized to examine the morphology of the four composites. In Figures 14(a), 14(b), 14(c), and 14(d), SEM micrographs vividly depict the surface characteristics of these specimens. When studying the surface of untreated wool fiber following conventional cleaning, as seen in Figure 14(b), these fibers exhibit prominent scales elevated at the edges, sharp scale structures, and a smooth cuticle layer, owing to the presence of amino acids. Figures 14(a) and 14(d), however, reveal observable alterations in the surface morphology of the chemically treated and cold plasma-treated wood-reinforced composites. Notably, the micrographs illustrate that the chemical treatment has resulted in a reduction of scale edges, indicative of some degree of smoothing or scale removal on the wool-reinforced composites. Conversely, the micrographs indicate that the cold plasma treatment has introduced a degree of roughness on the cuticle surface. For PLAF displayed in Figures 14(c) and 14(d), the presence of a smooth surface suggests that the cuticle layer remains in its raw, untreated, and natural state, without any specific treatment or modification applied. Notably, the SEM images in Figures 14(b) and 14(c) reveal identical cells on the outer layer of untreated wool fiber and untreated PLAF for each species. This shared characteristic holds the potential for enhancing adhesion between the fiber and the resin.

To sum up the findings of the structural characterization of fibers, it can be said that the XRD revealed no variations in crystallinity, showing that plasma treatment caused degradation only on the surface of cellulosic materials [52]. FTIR analysis of the *P. laevigata* fiber revealed a close similarity in organic structures and chemical bonds to wool fiber. This similarity indicates that the two types of fiber share common functional groups and molecular arrangements. The FTIR analysis provides valuable information about the chemical composition and bonding characteristics of the fiber. XRD analysis confirmed the similarity between the fiber structures of *P. laevigata* fiber and wool fiber. The results of XRD analysis indicated that the *P. laevigata* fiber exhibits similar patterns to wool fiber, suggesting similarities in the arrangement of molecules and crystalline structure. The close overlap between wool fiber and *P. laevigata* fiber in terms of their organic structures and chemical bonds contributes to the formation of a hybrid composite (PLAF-WLF) with improved hardness and strength. SEM can

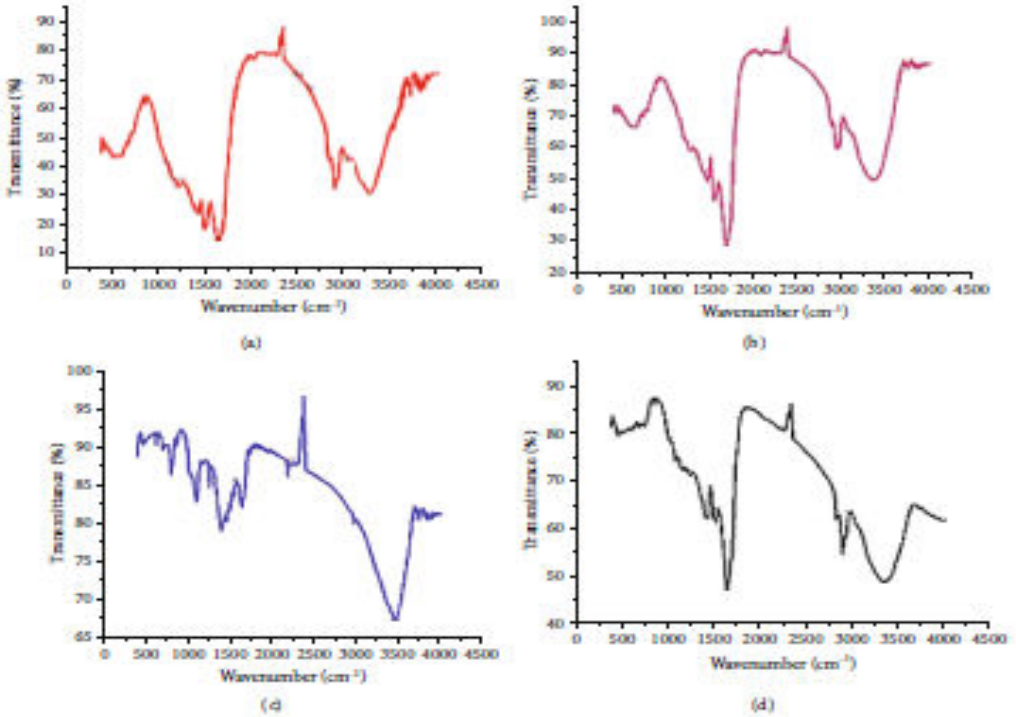

Figure 12: FTIR spectroscopy plots: (a) PLAF-WLF, (b) NWLF, (c) PLAF, and (d) WLF.

Table 5: FTIR spectroscopy results.

Sample	Amide III	Amide I (–C=O)	C–N-H	-OH
Untreated wool fiber	1232 cm^{-1}	1573 cm^{-1}	1519 cm^{-1}	3699–3788 cm^{-1}
Wool treated by NaOH	1288 cm^{-1}	1585 cm^{-1}	1519 cm^{-1}	3699–3788 cm^{-1}
Wool treated by plasma	1276 cm^{-1}	1566 cm^{-1}	1519 cm^{-1}	3703 cm^{-1}
Untreated *Periploca laevigata*	1284 cm^{-1}	1681 cm^{-1}	1519 cm^{-1}	3699–3788 cm^{-1}

indeed reveal the inherent compatibility between *P. laevigata* and wool fiber treated by cold plasma.

4.2. Evaluations of Mechanical Properties for the Four Composite Materials. After the characterization of the fibers, which were processed under different conditions, the fabricated four composites were subjected to three mechanical tests, namely, tensile, compression, and flexural tests, to show the composite's response to different types of loadings. The collected results are presented, analyzed, and discussed in detail, as shown in the below sections.

4.2.1. Tensile Test Results. The tensile test specimens were tested by using a universal tensile test machine to provide them with a set of mechanical properties such as ultimate tensile strength (megapascal), Young's modulus of elasticity (gigapascal), and ductility (percentage). The collected data were plotted in the form of the stress–strain curves.

Figure 15 demonstrates that the tensile stress–strain relations exhibit significantly linear behavior. This is consistent with established theory, particularly regarding mechanical properties in the fiber direction, which are predominantly influenced by fiber properties that maintain a linear stress–strain relationship up to the point of fracture [53]. The hybrid composite PLAF-WLF demonstrated the highest tensile strength of 26.02 MPa, which can be attributed to the effective bonding between the wool fiber and the PLAF within the matrix. This strong bonding was achieved through the vacuum infusion process, and this observation highlights the substantial impact of the stacking sequence

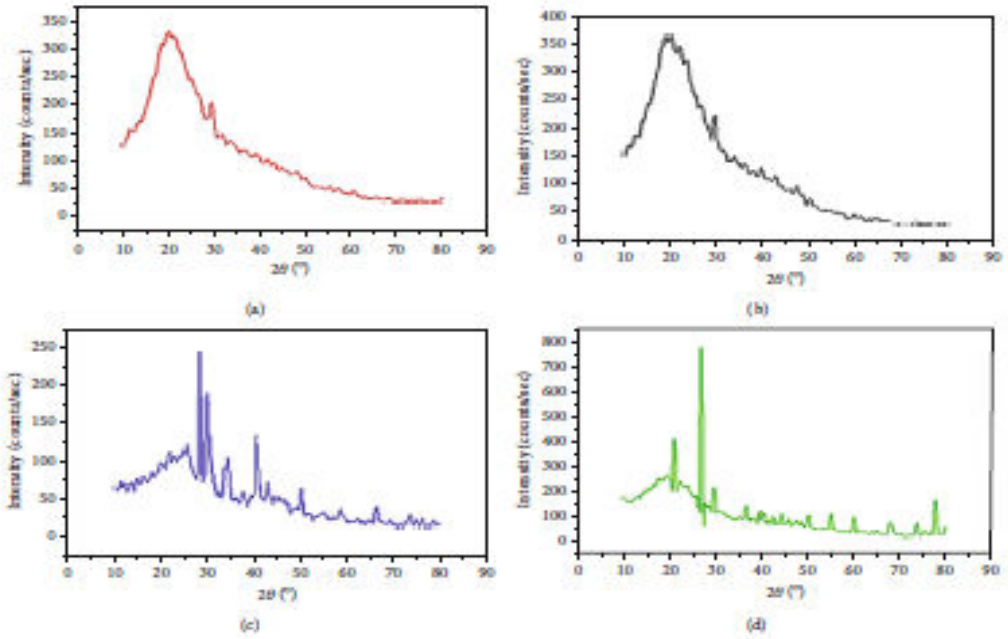

Figure 13: X-ray diffraction pattern: (a) NWLF, (b) PLAF-WLF, (c) PLAF, and (d) WLF.

of reinforcements on the overall properties of the composite [54]. During the test, the composite head endured the maximum amount of stress, which delayed the occurrence of the initial fracture beyond the expected time frame. This delay can be attributed to the fiber's ability to absorb a significant portion of the load, effectively boosting its yield point. However, after a short while, the fiber approaches the necking point, indicating the stage where the material is vulnerable to fracture, leading to crack propagation, which is caused by the damage of the epoxy matrix.

Figures 16 and 17 show the values of the forces and Young's modulus. The composite, consisting of untreated wool fiber, demonstrated a tensile strength of 10.82 MPa and Young's modulus of 1420.34 MPa (1.42 GPa), and the composite treated with 0.1% NaOH exhibited even more impressive mechanical properties, achieving a tensile strength of 13.89 MPa and Young's modulus of 1688.55 MPa (1.688 GPa). In comparison, the composite PLAF stands out with higher mechanical performance, showcasing a remarkable tensile strength of 20.1 MPa and Young's modulus of 2345.73 MPa (2.3457 GPa). However, the hybrid composite PLAF-WLF surpasses them all with an impressive tensile strength of 26.02 MPa and Young's modulus measuring 2350.50 MPa (2.350 GPa). These remarkable results highlight the synergistic effect of cold plasma treatment and the addition of PLAF, yielding a composite with remarkable mechanical properties, making it a compelling choice for applications demanding both strength and stiffness. Untreated wool fiber composite WLF, when not subjected to any treatment, exhibits noticeable accumulations of contaminants visible on their exterior. As previously noted by other researchers, these contaminants present on the surface of the fiber lead to suboptimal bonding between the fiber and the matrix material, primarily because of the restricted contact area between the two components [55]. Weak interfacial bonding leads to the creation of partially isolated microspaces that impede the transfer of stress between the fiber and the matrix, as seen in Figure 18. As the fiber loading increases, the level of obstruction also increases, resulting in heightened stiffness [56]. Following the treatment of wool fiber with 0.1% NaOH, there was an observed improvement in both tensile strength and Young's modulus. This outcome can be analyzed from various perspectives. To begin with, in accordance with the theory of fiber-reinforced polymeric matrices, the overall composite modulus experiences enhancement because the load exerted on the matrix gets effectively transmitted to the fiber during the tensile procedure [57]. The PLAF composite displayed exceptional mechanical performance, and these remarkable mechanical properties are a result of the fiber's inherent qualities and purity. It is worth noting that this plant fiber achieved such performance without any treatment or modification, emphasizing its natural lightweight and thin characteristics.

The incorporation of PLAF into cold plasma-treated wool resulted in a significant improvement in terms of both

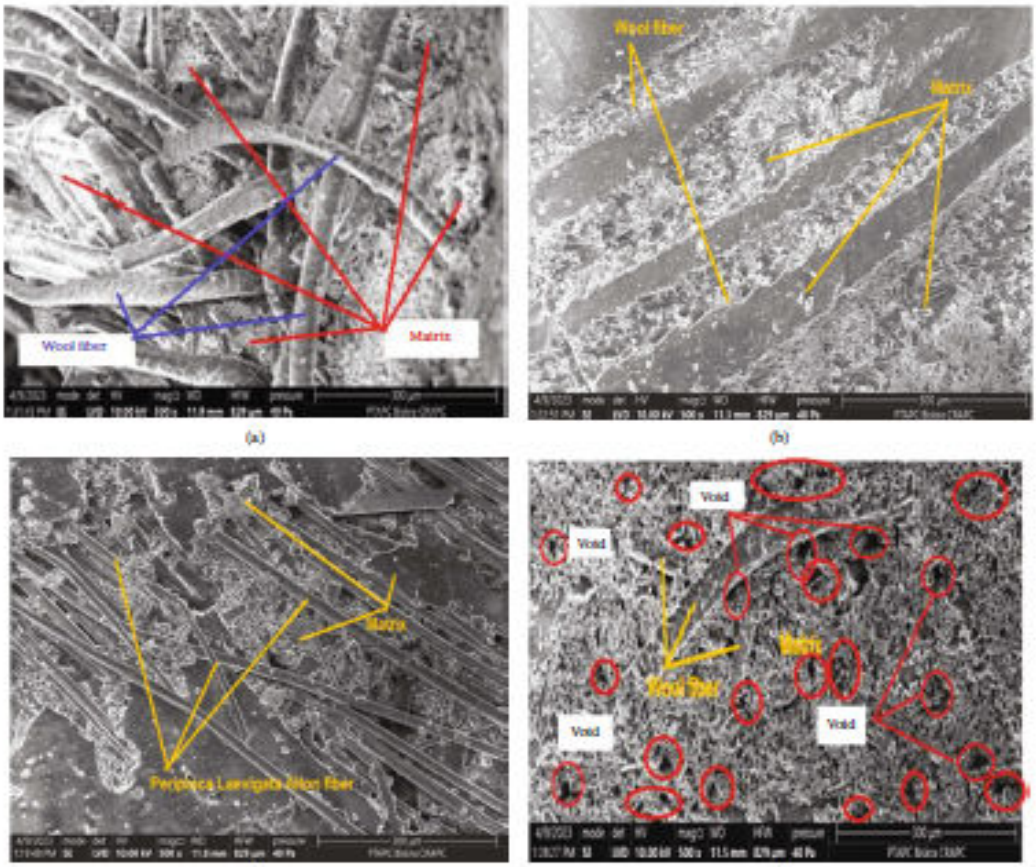

Figure 14: Scanning electron microscopy: (a) PLAF-WLF, (b) NWLF, (c) PLAF, and (d) WLF.

Young's modulus and tensile strength. This improvement can be attributed to the remarkable organic and structural similarities between PLA and wool fibers, despite their distinct natural origins. However, their organic compatibility has been proven by XRD and FTIR analysis. Cold plasma treatment alters the surface properties of wool fiber; it can introduce functional groups and change the surface energy, which can enhance its compatibility with other materials. Depending on the specific treatment parameters, cold plasma can strengthen wool fiber by cross-linking or modifying the fiber's structure, and this can result in improved tensile strength and durability [58]. The modified surface of plasma-treated wool fiber can promote better adhesion to other materials or matrices in composite materials, resulting in improved mechanical properties [59]. The addition of PLAF to WLF results in substantial improvements in tensile strength. Specifically, it leads to a remarkable increase of 58.57% in tensile strength for untreated wool fiber composite WLF, a significant enhancement of 46.62% for NaOH-treated wool fiber composite NWLF, and a notable rise of 22.75% for PLAF composite. This demonstrates the positive impact of incorporating PLAF into the composite, highlighting its potential to significantly enhance the tensile properties of these materials, especially for untreated and NaOH-treated wool fiber. It leads to significant improvements in Young's modulus; impressively, it leads to a substantial 39.57% increase in Young's modulus for WLF and a noteworthy 28.16% improvement for NWLF composite. However, the effect is negligible, increasing for PLAF composite. This indicates that PLAF played a significant role in bearing a considerable percentage of the applied stress force on the sample. It underscores the positive impact of incorporating PLAF into the composite, highlighting their potential to significantly enhance the tensile properties of

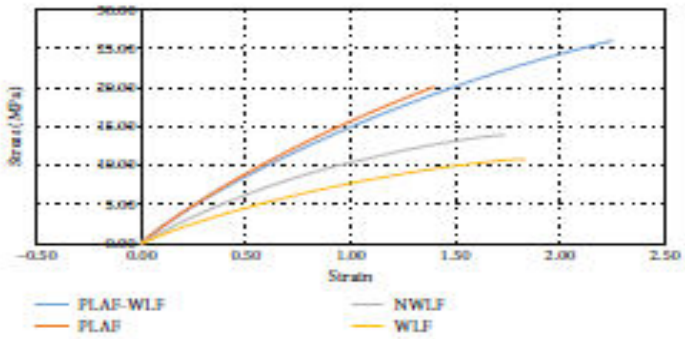

Figure 15: Stress versus strain curves for tensile test.

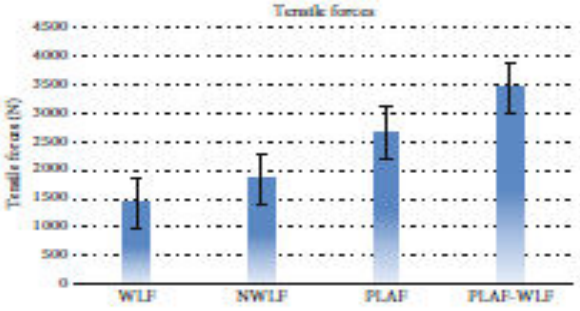

Figure 16: Tensile test forces.

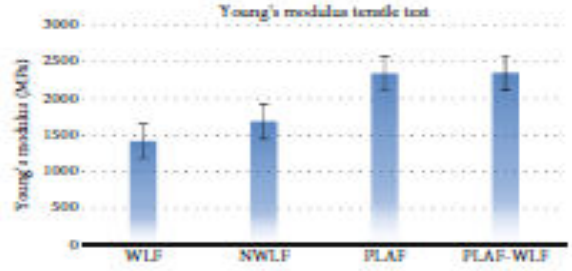

Figure 17: Young's modulus tensile test.

these materials, particularly in the case of WLF and NWLF composites. Young's modulus is remarkably high, with a value of 2.35 GPa. This indicates that the composite is rigid and shows great resistance to deformation under load. The tensile strength is also large, at 26.02 MPa. Indeed, the substantial increase in both Young's modulus and tensile strength in the composite material indicates its ability to withstand significant tensile stress without breaking. This correlation between these two material characteristics underscores its strength and durability.

Macro- and microphotographs were utilized to assess the fractures in the tensile test specimens and identify the

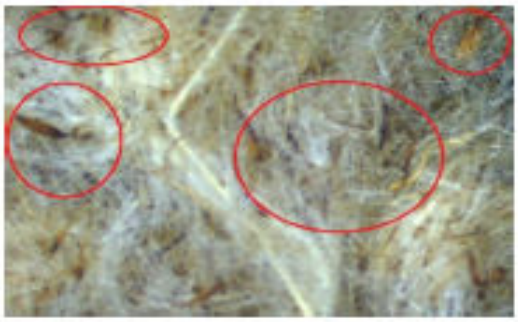

Figure 18: Optical microscope image of microscope image of untreated wool fiber indicates the presence of the impurities.

features of the tensile test results. Figures 19(a), 19(b), 19(c), and 19(d) exhibit macroimages of the fracture in a tensile test specimen.

Figures 20(a), 20(b), 20(c), and 20(d) display the various types of tensile fracture observed in WLF, NWLF, PLAF-WLF, and PLAF specimens, respectively, at microscopic scales. Fiber pullout is a common failure mechanism in NWLF and WLF specimens, indicating inadequate adhesion of the matrix to the fibers. The fracture structure of the PLAF-WLF composite, depicted in Figure 20(c), does not exhibit interlaminar cracks, confirming satisfactory adhesive strength. Additionally, the fractured structure shows minimal defects like microspores and fiber elongation, suggesting the potential for enhancing mechanical properties through process optimization [5]. Fracture-type analysis demonstrates that the hybridization of wool fibers and PLAFs contributes to improved interlaminar properties and increased mechanical strength.

Table 6 demonstrates a comparison between the results and those of alternative composite materials that utilize natural fibers for reinforcement.

4.3. Flexural Test. The flexural test examines the response of the beam specimen to the bending loading and determines its flexural strength and flexural modulus. The test was carried out according to the ASTM D790 standard. The achieved data was plotted in the stress–strain and force-displacement forms.

Figure 21 shows the flexural strength values for the four composites. Notably, the PLAF-WLF composite exhibits a higher flexural strength compared to the other composites. In terms of deflection, the WLF composite was found to have the maximum deflection, followed by the NWLF composite, among the hybrid composites investigated in the study. The results of the flexural test, as illustrated in Figure 21, demonstrate the remarkable performance of the hybrid composite PLAF-WLF. It exhibits a notable 72.70% increase in flexural strength compared to WLF composite, aligning with expectations due to the inherent higher flexural strength of PLAF when combined with plasma-treated wool fiber. Furthermore, the hybrid composite PLAF-WLF surpasses the NWLF composite by a substantial 67.84% and even outperforms the PLAF composite by 56.08%. These findings underscore the synergistic effect achieved by integrating WLF with PLAF, resulting in a composite material with exceptional resistance to flexural forces. Figures 22, 23, and 24 show the mechanical properties of composite materials under applied forces. Notably, the hybrid composite PLAF-WLF emerges as a standout candidate, displaying exceptional strength by withstanding a peak force of 253.15 N and boasting Young's modulus of 1210.93 MPa (1.21 GPa). This outstanding performance surpasses that of all other materials examined. Additionally, PLAF composite, derived from PLAF, demonstrates significant strength, recording a force of 111.29 N and Young's modulus of 623.2 MPa (0.6223 GPa). Furthermore, the NWLF composite exhibited a force value of 81.39 N, accompanied by Young's modulus of 588.5 MPa (0.588 GPa), highlighting the beneficial effects of chemical treatment on their mechanical properties. Conversely, the WLF composite exhibited the lowest force values at 69.09 N, coupled with Young's modulus of 524.83 MPa (0.524 GPa), underscoring the importance of treatment processes in enhancing material characteristics. These findings unequivocally underscore the remarkable and advantageous impact achieved through the amalgamation of PLA and wool fiber, particularly when the latter undergoes cold plasma treatment within the hybrid composite, promising innovations in material engineering and applications.

Figure 23 illustrates that the hybrid composite PLAF-WLF exhibits greater flexibility when compared to another composite. In contrast to both NWLF and PLAF composites, the WLF composites display a brittle nature and are incapable of withstanding significant flexural loads. When bending forces are exerted on a composite, the fiber located on the outer surface experiences higher levels of stress. The effective penetration of resin into the fiber, which contributes to flexural strength, depends significantly on the adhesive properties between the fiber and the matrix. It has also been noted that hybridizing natural fiber tends to enhance flexural strength compared to using single fiber alone [54].

Figures 25(a) and 25(b) show PLAFs and wool fibers under an optical electron microscope. The pure structural nature and low density of *Periploca laevigata* fibers, not subjecting them to any physical or chemical treatments, gave the composite remarkable stiffness and low elongation, which enhanced the bending strength and flexural Young's modulus of the PLAF.

Wool fiber has different functional groups like hydroxyl (-OH), amino (-NH2), amide (-CONH-), and carboxyl (-COOH) groups [49]. The O-H and C-OOH groups on the fiber surface are exposed when waxy substances dissolve, resulting in increased polarity and decreased acidity of the fiber's surface topography. Surface functional groups are linked by interactions between energized plasma species and the substrate surface, whereas surface bridges are typically created by reactions between excited surface species [63].

Effective penetration of the resin into the fibers contributes to the strength of the flexural test and affects the adhesion properties between the fibers and the matrix. Hybridization of natural fibers tends to enhance flexural

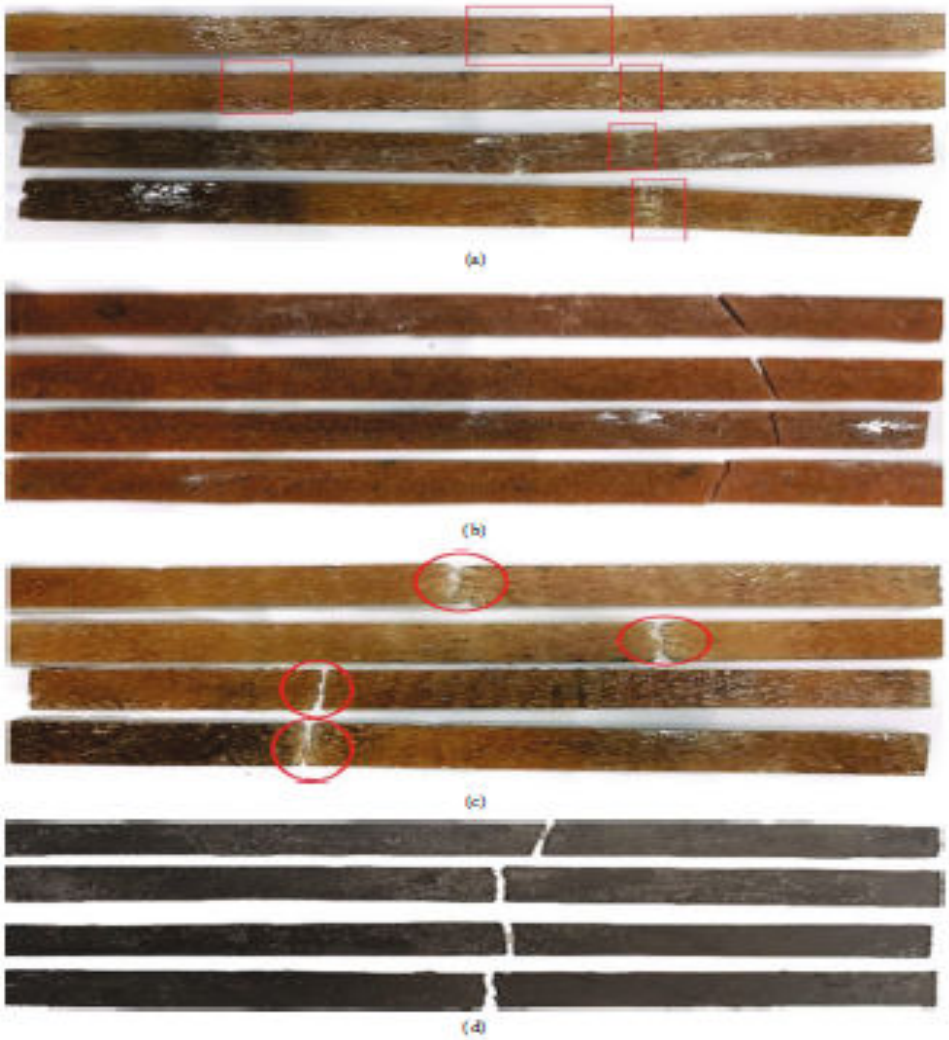

Figure 19: Specimens after the tensile test.

strength compared to using single fibers alone [54]. The results depicted in Figures 26(a), 26(b), 26(c), and 26(d) from bending tests of PLAF-WLF, NWLF, PALF, and WLF, respectively, demonstrate that incorporating *Periploca* into wool fibers enhances their capacity to bend without fracturing. This indicates that the inclusion of these fibers boosts ductility. Following an examination of the failure mode exhibited by the specimens in bending tests, it was conclusively determined that the addition of *Periploca* fibers to the composite hybrid effectively altered the brittle behavior of untreated wool fibers under concentrated loading to a more ductile failure mode. As a result, the incorporation of *Periploca* fibers into wool fibers facilitates the transmission of tensile stress along the sample axis, ultimately increasing the ductility of the hybrid composite.

4.4. Compression Test Results. The mechanical performance of the four composites was additionally evaluated when they were subjected to another type of mechanical test represented by the compression test. In this test, all specimens were subjected to compressive stress to show their response to this type of loading.

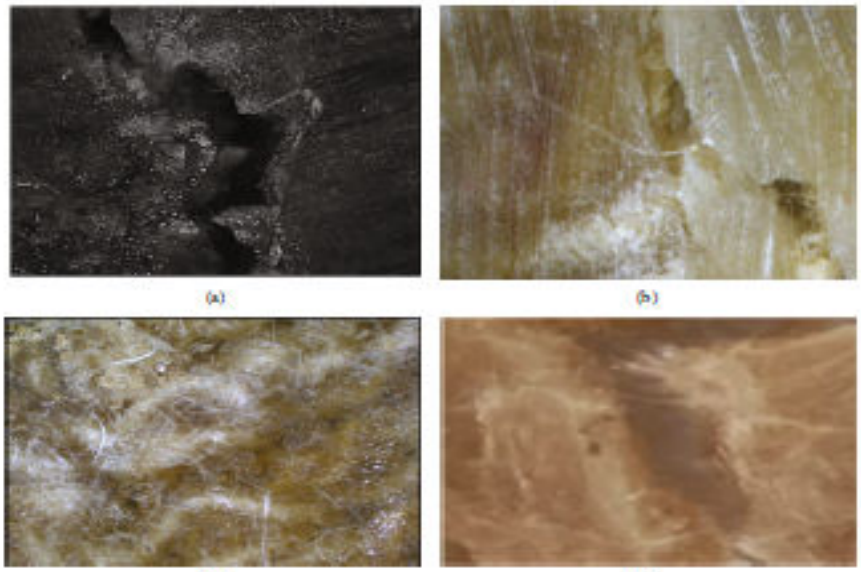

(a) (b) (c) (d)

Figure 20: Tensile fracture specimen of NWLF, WLF, PLAF, and PLAF.

Table 6: The tensile strength and modulus of the current study with some literatures of different composites.

Composites	Description	Young's modulus (GPa)	Tensile strength (MPa)	References
KRFP (90° D)	Kenaf with fiber orientation of 90°	0.33	3.52	[60]
KRFP (0° D)	Kenaf with fiber orientation of 0°	2.43	42.38	
HYBRID CKFRP (90° D)	Hybridization of carbon kenaf with fiber orientation of 90°	3.43	43.11	
H	Composite laminate RFFFR (ramie/3 layer of flax/ramie)	0.98	54	[54]
G	Composite laminate FRRRF (flax/3 layer of ramie/flax)	0.96	39.08	
HH/PLA	Horsehair fiber-based polylactic acid	4.52	30.33	[61]
Untreated luffa	Untreated luffa fiber	2.37	11.43	[62]
Treated luffa	Treated using benzoyl chloride and NaOH	3.54	14.54	
S10	Coconut fiber treated with KOH and polypropylene	1.03	23.17	[60]
S2	Coconut fiber treated with KOH and polypropylene compositions	0.62	21.76	
PLAF-WLF	*Periploca laevigata* Aiton fiber/wool fiber treated by cold plasma	2.35	26.02	
PLAF	*Periploca laevigata* Aiton fiber	2.34	20.1	
NWLF	Wool fiber treated with NaOH	1.688	13.89	
WLF	Untreated wool fiber	1.42	10.82	

Figures 27 and 28 demonstrate the compressive strength and Young's modulus of the PLAF composite, characterized by its noteworthy Young's modulus of 500 MPa (0.5 GPa) and compressive strength of 44.75 MPa. Despite not having the highest load-bearing capacity among the tested materials at 2755.19 N, PLAF composite still displays substantial

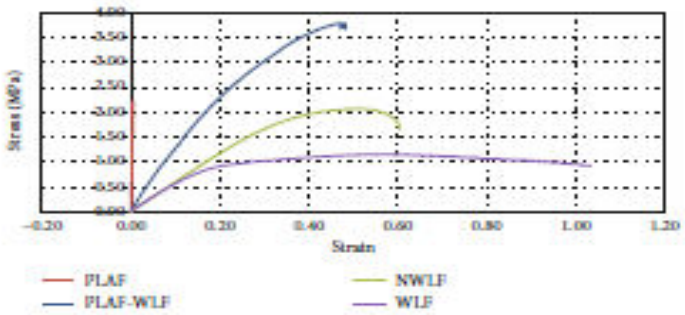

Figure 21: Stress versus strain curves for the flexural test.

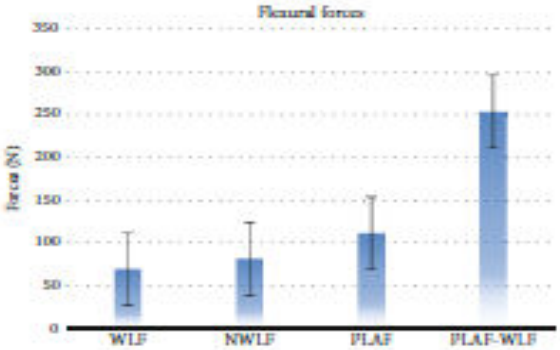

Figure 22: The flexural test forces.

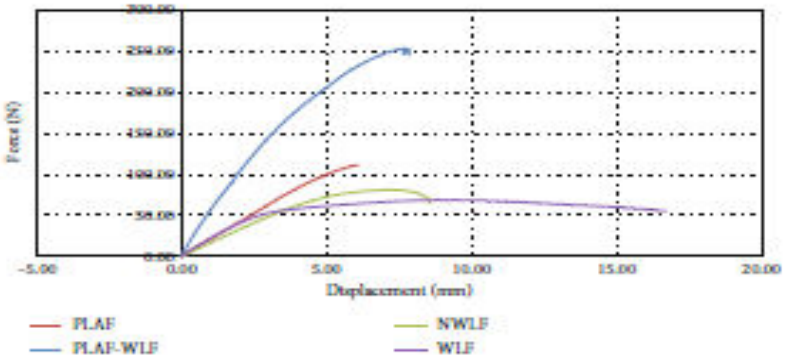

Figure 23: Force versus displacement curves.

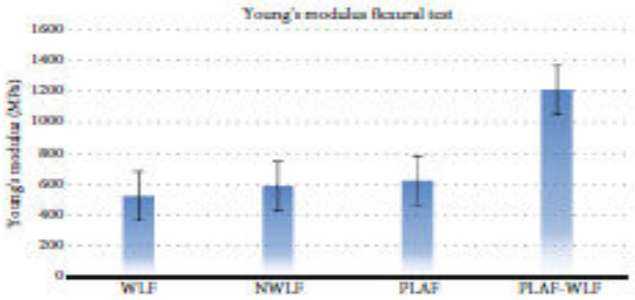

Figure 24: Young's modulus flexural test.

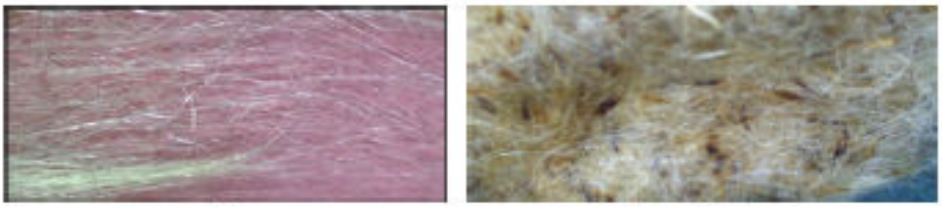

Figure 25: (a) *Periploca laevigata* Aiton fibers and (b) wool fibers under an optical electron microscope.

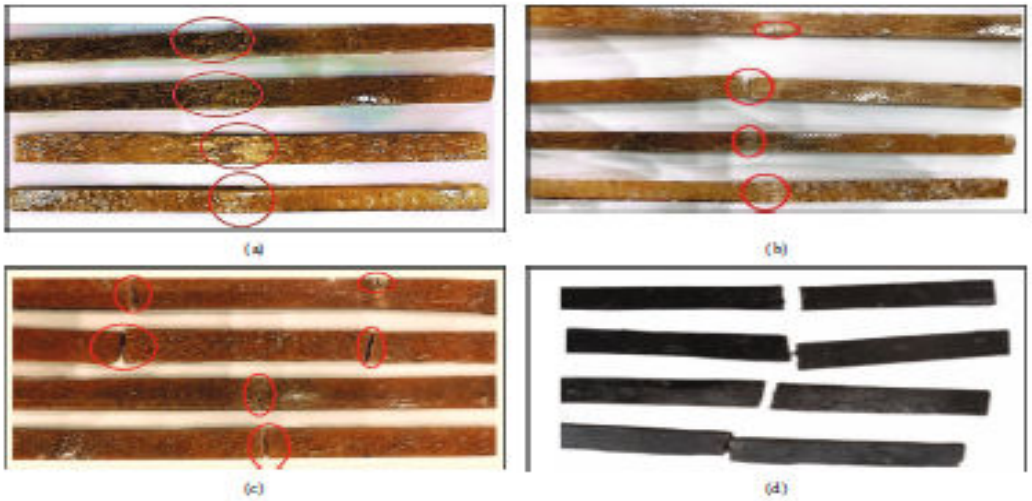

Figure 26: The specimens of composites: PLAF-WLF, NWLF, PALF, and WLF after the flexural test.

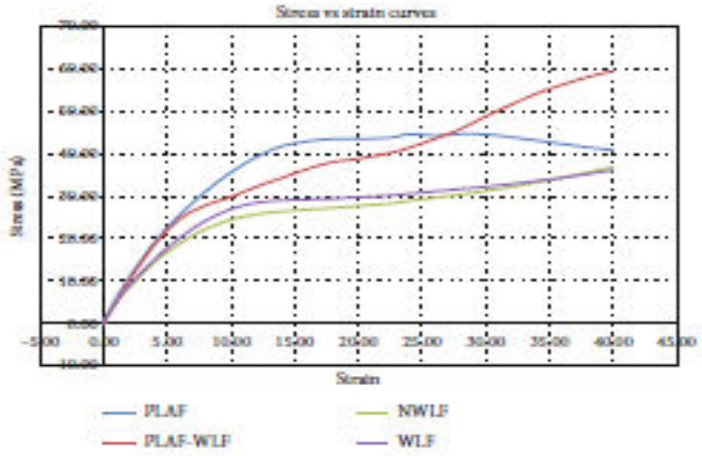

Figure 27: Stress versus strain curves for the compressive test.

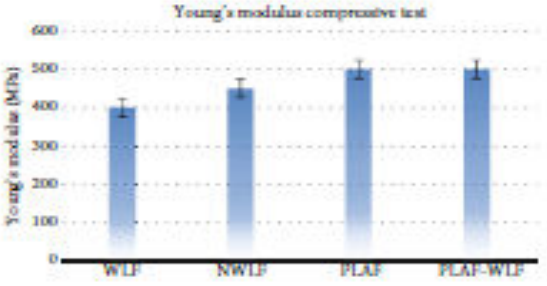

Figure 28: Young's modulus compressive test.

strength and rigidity. PLAF-WLF, a hybrid, demonstrates exceptional mechanical properties. With a load-bearing capacity of 4369.19 N, it achieved the highest compressive strength of 59.56 MPa among all tested specimens. Furthermore, its Young's modulus measures an impressive 500 MPa (0.5 GPa), highlighting its remarkable stiffness. NWL composite displays a load-bearing capacity, achieving a load measurement of 1829.25 N, and it possesses Young's modulus of 450 MPa (0.45 GPa) and compressive strength of 36.87 MPa. This marked improvement in strength compared to untreated wool composite WLF strongly indicates that the NaOH treatment has effectively reinforced the material. WLF composite, comprising untreated wool fiber, displays the lowest load value among the tested materials, with a load measurement of 1134.18 N. Furthermore, it has Young's modulus of 0.4 GPa and compressive strength of 36.12 MPa. These results emphasize the importance of fiber treatment or modification to enhance its load-bearing capacity, as demonstrated by the improvements seen in NaOH-treated wool fiber composite NWL and hybrid composite PLAF-WLF when compared to the untreated wool fiber composite WLF. The compressive strength results reveal significant variations in the performance of different composites.

The hybrid composite achieved the highest compressive strength at 59.56 MPa, while the WLF composite exhibited the lowest at 36.12 MPa. Interestingly, the PLAF composite, with a fiber/epoxy ratio of 17.65%, achieved a compressive strength of 44.76 MPa. In contrast, the PLAF-WLF composite, with a fiber/epoxy ratio of 14.29% PLAF and 28.57% treated wool fiber through cold plasma, reached the same impressive compressive strength as the hybrid composite at 59.56 MPa. Finally, the NWLF and WLF composites, both with a high wool fiber/epoxy ratio of 42.86%, achieved compressive strengths of 36.87 and 36.12 MPa, respectively. These results unequivocally demonstrate that the inclusion of PLAF provides substantial additional strength and stiffness to the wool fiber. Notably, the compressive strength of the wool fiber composite increased by approximately 39.35% due to the synergistic effect of incorporating PLAF. In a comparative analysis of mechanical properties, PLAF composite stands out as a superior material when compared to WLF composite, showcasing a remarkable 19.30% higher load-bearing capacity and an astonishing 20% greater Young's modulus, underscoring its exceptional strength and stiffness. Additionally, the hybrid composite PLAF-WLF displays an impressive 38.09% increase in load-bearing capacity over pure NWLF composite, highlighting its exceptional strength, although it does involve a slight compromise in stiffness.

It confirms the successful integration of the fiber and supports the enhanced interfacial bonding and overall performance of the composite material. Four composite materials were created in this study, including a composite with PLAF. This composite consists of a PLAF and is used as the reinforcing component. The PLAFs are likely in their

untreated form and provide their inherent properties to the composite. A hybrid composite with wool fiber treated by cold plasma mixed with untreated PLAF (PLAF-WLF). In this composite, wool fibers are treated with cold plasma to improve their properties. The treated wool fibers were then combined with untreated *P. laevigata* fiber to create a hybrid composite material. The reinforcing component is untreated wool fiber. The wool fibers are used in their natural state without any additional treatment or modification. A composite with wool fiber treated chemically with 0.1% NaOH (NWLF) involves treating wool fiber chemically with a 0.1% solution of NaOH. The analysis was conducted for both treated (NaOH and plasma) and untreated fiber, revealing a decrease in fiber adhesion rates compared to untreated fiber. In the single composites, PLAF comprised 30% of the total weight, WLF accounted for 30%, and the remaining 70% was epoxy. In the hybrid composite (PLAF-WLF), PLA contributed 10%, wool contributed 30%, and epoxy made up the remaining 70%. Notably, in the PLAF and WLF composites, epoxy constituted 80% and 70% of the total weight, respectively. The mechanical behavior, including tensile, compressive, and flexural strength, of both single and hybrid composites was investigated in accordance with ASTM standards. The hybrid composite, PLAF-WLF, demonstrated superior mechanical properties under loading conditions as compared to the single fiber-reinforced composites (PLAF, WLF, and NWLF). The introduction of PLAF had a substantial positive impact on the tensile properties of composites. Table 6 shows the percentages of voids during the manufacturing process that may introduce defects in the composite, such as microvoids in the matrix. These imperfections can lead to localized stress concentration, ultimately causing potential failure. During compression, the composite characteristics are influenced by the quality of the fiber-matrix interface and the stiffness of the resin. A stiffer matrix offers improved lateral support to the fiber, thereby delaying fiber microbuckling and enhancing the strain to failure [64].

The vacuum infusion molding process was used in this study to manufacture composite material. This process can solve challenges with manual lay-up and spray-up methods. The vacuum infusion molding process eliminates the risk of trapped air in the composite, and this process enables the composite to be manufactured in repetition with the same purity because it is dependent on the design of the equipment rather than the operator's competence [43].

Based on the obtained mechanical properties, it can be said that one of the most compelling aspects of PLAF composites is their compatibility with hybridization, particularly when combined with wool fiber. This synergy results in significant enhancements across various mechanical properties, including tensile strength, Young's modulus, compressive strength, and flexural strength. This adaptability makes it a versatile choice for industries aiming to boost performance while maintaining a lightweight profile.

To sum up, the introduction of PLAF into composite materials represents a promising leap in materials engineering. It offers a lightweight, robust, and versatile alternative that has the potential to revolutionize a wide range of industries.

5. Conclusions

The study focused on evaluating the effect of hybridization on the properties of the resulting materials, with the aim of understanding how different fiber blends affect the overall performance of composites. The experimental approach allowed a detailed analysis of the mechanical and structural properties of the hybrid composites. The following conclusions can be drawn:

- The hybrid composite exhibits tensile, flexural, and compressive strengths, measuring 26.02 MPa, 2.53 GPa, and 109.22 MPa, respectively. In addition, it has Young's modulus of 2.35, 1.21, and 0.50 GPa, respectively.
- These results indicate that hybrid composites reinforced with wool and PLAFs have the potential to serve as viable alternative materials, providing significant structural strength for various engineering purposes.
- The combination of PLAFs and WLF provides a pioneering solution for the development of hybrid composites. This innovative technology offers many advantages, making it a valuable choice for diverse applications.
- It is worth noting that PLAFs exhibit an exceptionally low density property, measuring 0.45 g/cm^3.
- In tensile tests, these fibers showed Young's modulus value of 2.345 GPa, indicating exceptional stiffness and resistance to deformation. Furthermore, the PLAF composite showed a flexural strength of 15.58 MPa, displaying its ability to withstand bending forces, and a compressive strength of 12.5 MPa, highlighting its durability under compression.
- These outstanding properties make PLAF composites very attractive to industries that prioritize long-term structural strength and durability. It is worth noting that *P. laevigata* also possesses antibacterial and antioxidant properties, which increases its biological appeal and the possibility of introducing this fiber into several engineering fields.

6. Limitations and Scope for Further Research

The limitations and scope for further research are illustrated in the following points:

- Discover the diverse range of potential uses for *P. laevigata* fiber epoxy composites that extend beyond structural applications.
- Explore the potential of hybridizing *P. laevigata* fiber epoxy composites with other reinforcing materials (carbon fiber, glass fiber, and aramid fiber) to enhance their impact resistance and toughness.

- Investigate the effect of fiber architecture (unidirectional, woven, and random) on the impact resistance of *P. laevigata* fiber epoxy composites.
- Evaluate the impact resistance of *P. laevigata* fiber epoxy composites.
- Conduct comprehensive corrosion resistance testing of *P. laevigata* fiber epoxy composites in different corrosive environments.
- Investigate the susceptibility of *P. laevigata* fiber epoxy composites to bacterial growth, biofilm formation, and biofouling in marine, industrial, and biomedical environments.

Data Availability Statement

The data that support the findings of the study are available from the corresponding author upon request.

Conflicts of Interest

The authors declare no conflicts of interest.

Author Contributions

Conceptualization: Lalmi Rahmani, Mohammed Taher Gherbi, and Aribi Chouaib. Methodology: Lalmi Rahmani, Mohammed Taher Gherbi, and Aribi Chouaib. Experimental: Lalmi Rahmani, Mohammed Taher Gherbi, and Aribi Chouaib. Validation: Lalmi Rahmani, Mohammed Taher Gherbi, and Aribi Chouaib. Formal analysis: Salah Al-Zubaidi. Investigation: H.S.S. Aljibori and M.N. Mohammed. Resources: Lalmi Rahmani, Mohammed Taher Gherbi, and Aribi Chouaib. Data curation: Oday I. Abdullah and Mohammed Fouad Ferhat. Writing–original draft preparation: Lalmi Rahmani, Mohammed Taher Gherbi, and Aribi Chouaib. Writing–review and editing: Salah Al-Zubaidi. Visualization: Salah Al-Zubaidi. Supervision: Oday I. Abdullah. Project administration: Salah Al-Zubaidi and Oday I. Abdullah. Funding acquisition: M.N. Mohammed. All authors have read and agreed to the published version of the manuscript.

Funding

The authors received no specific funding for this work.

References

[1] P. Prabhu, K. Balakrishnan, R. Vannan, and B. Alagappan, "Dynamic mechanical analysis of silk and glass (S/G/S)/pineapple and glass (P/G/P)/flax and glass (F/G/F) reinforced Lannea coromandelica blender hybrid nano composites," *Journal of Materials Research and Technology*, vol. 15, pp. 2484–2496, 2021.

[2] P. Prabhu, V. Chokkalingam, S. Arunkumar, and P. Perumal, "The investigation on mechanical, thermal conductivity and water absorption characteristics of coir fiber-reinforced vinyl ester biocomposites," *Biomass Conversion and Biorefinery*, pp. 1–11, 2024.

[3] R. Payal, "Chapter 9 - Green composites: versatile uses and applications in life," in *Green Sustainable Process for Chemical and Environmental Engineering and Science*, T. Altalhi and Inamuddin, Eds., pp. 165–193, Elsevier, 2022.

[4] W. Ghori, N. Saba, M. Jawaid, and M. Asim, "A review on date palm (phoenix dactylifera) fibers and its polymer composites," *IOP Conference Series: Materials Science and Engineering*, vol. 368, no. 1, article 012009, 2018.

[5] P. Prabhu, A. Balaji, D. Jayabalakrishnan et al., "Study on machining parameters and mechanical properties of hybrid Agave sisalana and glass fiber-reinforced polyester composites (A/GFRP)," *Journal of Natural Fibers*, vol. 19, no. 15, pp. 11644–11657, 2022.

[6] S. Hosseini, M. Gaff, and D. Hui, "Effect of fiber treatment on physical and mechanical properties of natural fiber-reinforced composites: a review," *Reviews on Advanced Materials Science*, vol. 62, no. 1, 2023.

[7] S. Mishra and V. Choudhary, "Chemical treatment of reinforced fibers used for bio composite: a review," in *Advances in Engineering Materials*, Lecture Notes in Mechanical Engineering, B. P. Sharma, G. S. Rao, S. Gupta, P. Gupta, and A. Prasad, Eds., Springer, Singapore, 2021.

[8] P. Prabhu, K. Balakrishnan, R. Malar Vannan, and B. Alagappan, "Mechanical, thermal and morphological analysis of hybrid natural and glass fiber-reinforced hybrid resin nanocomposites," *Biomass Conversion and Biorefinery*, vol. 14, pp. 4941–4955, 2022.

[9] K. K. Gudiseva, R. Panda, S. Banothu, and K. Vinoya, "Synthesis and analysis of natural fibers reinforcement of synthetic resins," *Journal of Material Science & Engineering*, vol. 5, no. 5, 2016.

[10] A. Lakshmanan, "Physical and chemical properties of wool fibers," in *Wool Fiber Reinforced Polymer Composites*, pp. 49–71, Woodhead Publishing, 2022.

[11] D. Stanovoytova, "Wool grease recovery from scouring effluent at textile mill," *Journal of Agriculture, Pure and Applied Science and Technology*, vol. 10, pp. 1–9, 2014.

[12] P. Zito, M. Sajeva, M. Bruno, S. Rosselli, A. Maggio, and F. Senatore, "Essential oils composition of *Periploca laevigata* Aiton subsp. *angustifolia* (Labill.) Markgraf (Apocynaceae–Periplocoideae)," *Natural Product Research*, vol. 27, no. 3, pp. 255–265, 2013.

[13] K. Rohit and S. Dixit, "A review-future aspect of natural fiber reinforced composite," *Polymers from Renewable Resources*, vol. 7, no. 2, pp. 43–59, 2016.

[14] S. H. Bahrain, N. R. Mandek, J. Mahmud et al., "Morphological, physical, and mechanical properties of sugar-palm (*Arenga pinnata* (Wurmb) merr.)-reinforced silicone rubber biocomposites," *Materials*, vol. 15, no. 12, p. 4062, 2022.

[15] S. H. K. Bahrain, N. N. C. A. Rahim, J. Mahmud et al., "Hyperelastic properties of bamboo cellulosic fibre–reinforced silicone rubber biocomposites via compression test," *International Journal of Molecular Sciences*, vol. 23, no. 11, p. 6338, 2022.

[16] M. Abdulmawjod Alsheikhly, S. Al-Zubaidi, and S. Kamarul Bahrain, "State-of-the-art review of green composites for automotive applications," in *Biocomposite and Synthetic Composites for Automotive Applications*, pp. 347–375, Woodhead Publishing, 2021.

[17] M. K. Rycerd, M. T. Maria, M. Malgorzata, and B. B. Jorge, "Future of natural fibers, their coexistence and competition

with man-made fibers in 21st century," *Molecular Crystals and Liquid Crystals*, vol. 556, no. 1, pp. 200–222, 2012.

[18] G. S. Mann, N. Azum, A. Khan et al., "Green composites based on animal fiber and their applications for a sustainable future," *Polymers*, vol. 15, no. 3, p. 601, 2023.

[19] J. Zach, A. Korjenic, V. Petránek, J. Hroudová, and T. Bednar, "Performance evaluation and research of alternative thermal insulations: based on sheep wool," *Energy and Buildings*, vol. 49, pp. 246–253, 2012.

[20] Y. G. Thyavihalli Girijappa, S. Mavinkere Rangappa, J. Parameswaranpillai, and S. Siengchin, "Natural fibers as sustainable and renewable resource for development of eco-friendly composites: a comprehensive review," *Frontiers in Materials*, vol. 6, p. 226, 2019.

[21] K. Al-Kaabi, A. Al-Khanbashi, and A. Hammami, "Natural fiber reinforced composites from date palm fibers," in *11th European Conference on Composite Materials*, Greece: Rhodes, 2004.

[22] U. Soykan, "Development of turkey feather fiber-filled thermoplastic polyurethane composites: thermal, mechanical, water-uptake, and morphological characterizations," *Journal of Composite Materials*, vol. 56, no. 2, pp. 339–355, 2022.

[23] K. S. Meenalochani and V. V. G. Reddy, "A review on water absorption behavior and its effect on mechanical properties of natural fibre reinforced composites," *International Journal of Innovative Research in Advanced Engineering (IJIRAE)*, vol. 4, no. 4, 2017.

[24] K. C. Benini, H. Voorwald, and M. O. Cioffi, "Manufacturing and characterization of high impact polystyrene (HIPS) reinforced with treated sugarcane bagasse," *Journal of Research Updates in Polymer Science*, vol. 6, no. 1, pp. 2–11, 2017.

[25] F. M. Al-Oqla and M. S. Salit, "Natural fiber composites," in *Materials Selection for Natural Fiber Composites*, F. M. Al-Oqla and M. S. Salit, Eds., pp. 23–48, Woodhead Publishing, 2017.

[26] J. Manivannan, S. Rajesh, K. Mayandi et al., "Animal fiber characterization and fiber loading effect on mechanical behaviors of sheep wool fiber reinforced polyester composites," *Journal of Natural Fibers*, vol. 19, no. 11, pp. 4007–4023, 2022.

[27] M. Kulkarni, V. Gawande, P. Mahanwar et al., "Review on biomass sheep wool-based polymer composites," *Biomass Conversion and Biorefinery*, pp. 1–22, 2023.

[28] P. Zito, M. Sajeva, M. Bruno et al., "Essential oil composition of the fruits of Periploca laevigata Aiton subsp angustifolia (Labill.) Maire and Weiller (Apocynaceae-Periplocoideae)," *Natural Product Research*, vol. 25, no. 14, pp. 1339–1346, 2011.

[29] S. Methoud, H. Aissaoui, S. Desbré et al., "Flavonoid glycosides from Periploca laevigata (Asclepiadaceae) from Algeria," *Der Pharma Chemica*, vol. 8, pp. 129–131, 2016.

[30] M. Saxena, A. Pappu, A. Sharma, R. Haque, and S. Wankhede, *Composite Materials from Natural Resources: Recent Trends and Future Potentials*, IntechOpen, 2011.

[31] F. Alladi, M. S. Hossain, J. Lalung et al., "Advancements in applications of natural wool fiber: review," *Journal of Natural Fibers*, vol. 19, no. 2, pp. 497–512, 2022.

[32] O. P. Balogun, A. A. Adediran, J. A. Omotoyinbo, K. K. Alaneme, and I. O. Oladele, "Evaluation of water diffusion mechanism on mechanical properties of polypropylene composites," *International Journal of Polymer Science*, vol. 2020, Article ID 8865748, 12 pages, 2020.

[33] M. Asrayal, "Sodium hydroxide and potassium permanganate treatment on mechanical properties of coconut fibers," *IOP Conference Series: Materials Science and Engineering*, vol. 619, no. 1, article 012011, 2019.

[34] M. Asrayal and R. Soenoko, "The effects of sodium hydroxide and potassium permanganate treatment on roughness of coconut fiber surface," *MATEC Web of Conferences*, vol. 204, article 05004, 2018.

[35] C. H. Lee, A. Khalina, and S. H. Lee, "Importance of interfacial adhesion condition on characterization of plant-fiber-reinforced polymer composites: a review," *Polymers*, vol. 13, no. 3, p. 438, 2021.

[36] R. Punyamurthy, D. Sampathkumar, B. Bennehalli, R. Patel, and S. C. Venkateshappa, "Abaca fiber reinforced epoxy composites: evaluation of impact strength," *International Journal of Sciences: Basic and Applied Research (IJSBAR)*, vol. 18, no. 2, pp. 305–317, 2014.

[37] H. Hariharan and G. Rajeshkumar, "Investigation of mechanical properties of sisal fiber and sugar palm fiber reinforced hybrid composites," *Qeios*, 2024.

[38] C. Sun, J. Min, J. Lin, and H. Wan, "Effect of atmospheric pressure plasma treatment on adhesive bonding of carbon fiber reinforced polymer," *Polymers*, vol. 11, no. 1, p. 139, 2019.

[39] H. Cui and X. Gao, "Surface modification on polyimide yarn by plasma treatment to enhance adhesion with polypropylene resin," *Polymers*, vol. 14, no. 19, p. 4232, 2022.

[40] A. Chemicals, "Epoxy SL-technical data sheet. Agel Chemicals: p 3," https://agelchemicals.de/uploads/Files/pdf/EPOXY%25205L.pdf.

[41] D. Jaiswal, G. L. Devnani, G. Rajeshkumar, M. R. Sanjay, and S. Siengchin, "Review on extraction, characterization, surface treatment and thermal degradation analysis of new cellulosic fibers as sustainable reinforcement in polymer composites," *Current Research in Green and Sustainable Chemistry*, vol. 5, p. 100271, 2022.

[42] B. Kojić-Prodić, "A century of X-ray crystallography and 2014 international year of X-ray crystallography," *Macedonian Journal of Chemistry and Chemical Engineering*, vol. 34, no. 1, pp. 19–32, 2015.

[43] M. K. Singh, R. Tewari, S. Zafar, S. M. Rangappa, and S. Siengchin, "A comprehensive review of various factors for application feasibility of natural fiber-reinforced polymer composites," *Results in Materials*, vol. 17, p. 100355, 2023.

[44] A. H. Saputra and G. Setyarso, "Vacuum infusion equipment design and the influence of reinforcement layers addition to the resin infusion time," *IOP Conference Series: Materials Science and Engineering*, vol. 162, no. 1, article 012015, 2016.

[45] M. Tolessa and B. Singh, "A review on composite materials from natural plant resources: recent trends and future potentials," *International Journal of Innovative Research in Science, Engineering and Technology*, vol. 9, no. 1, 2023.

[46] K. Bharath, M. Pasha, and B. Nizamuddin, "Characterization of natural fiber (sheep wool)-reinforced polymer-matrix composites at different operating conditions," *Journal of Industrial Textiles*, vol. 45, no. 5, pp. 730–751, 2016.

[47] P. Sahu and M. Gupta, "Water absorption behavior of cellulosic fibres: polymer composites: a review on its effects and remedies," *Journal of Industrial Textiles*, vol. 51, 5 Supplement, pp. 7480S–7512S, 2022.

[48] T. R. T. Hosne Ara Begum and M. A. Shahid, "Analysis of water absorption of different natural fibers," *Journal of Textile Science and Technology*, vol. 7, no. 4, pp. 152–160, 2021.

[49] A. Patruccco, M. Zoccola, and A. Anceschi, "Exploring the potential applications of wool fibers in composite materials: A review," *Polymers*, vol. 16, no. 16, p. 2360, 2024.

[50] S. P. Subramanyam, D. K. Kotikalu, B. Benneballi et al., "Plain-woven areca sheath fiber-reinforced epoxy composites: the influence of the fiber fraction on physical and mechanical features and responses of the tribo system and machine learning modeling," *ACS Omega*, vol. 9, no. 7, pp. 8019–8036, 2024.

[51] O. Abdelkhoui, T. Hariti, and S. Mnif, "Effect of the chemical unhairing process on pulled wool characteristics," *Fibres & Textiles in Eastern Europe*, vol. 30, no. 3, pp. 70–78, 2022.

[52] M. J. P. Macedo, G. S. Silva, M. C. Feitor, T. H. C. Costa, E. N. Ito, and J. D. D. Melo, "Surface modification of kapok fibers by cold plasma surface treatment," *Journal of Materials Research and Technology*, vol. 9, no. 2, pp. 2467–2476, 2020.

[53] S. Sutharsenan, H. Haniel, A. K. Taufik, M. Tiopan, R. A. Himarosa, and M. A. Mufiikhun, "Tensile, compressive, and flexural characterization of CFRP laminates related to water absorption," *Journal of Composite Science*, vol. 7, no. 5, p. 184, 2023.

[54] D. Rajesh, N. Lenin, R. Cep, P. Anand, and M. Elangovan, "Experimental investigation of bi-directional flax with sunnie fibre-reinforced phenol-formaldehyde hybrid composites," *Polymers*, vol. 14, no. 22, p. 4887, 2022.

[55] M. H. Zin, K. Abdan, N. Mazlan, E. S. Zainudin, and K. E. Liew, "The effects of alkali treatment on the mechanical and chemical properties of pineapple leaf fibers (PALF) and adhesion to epoxy resin," *IOP Conference Series: Materials Science and Engineering*, vol. 368, no. 1, article 012035, 2018.

[56] J. Tasnim, N. S. Jenifar, and M. Hasan, "Effect of chemical treatment of jute fiber on thermo-mechanical properties of jute and sheep wool fiber reinforced hybrid polypropylene composites," *Journal of Thermoplastic Composite Materials*, vol. 35, no. 11, pp. 1981–1993, 2022.

[57] M. Bahrami, B. Enciso, C. M. Gaitani, J. Abenojar, and M. A. Martínez, "Characterization of hybrid biocomposite polybutyl-succinate/carbon fibers/flax fibers," *Composites Part B: Engineering*, vol. 221, p. 109033, 2021.

[58] S. Shahidi, A. Rashidi, M. Ghoranneviss, A. Anvari, and J. Wiener, "Plasma effects on anti-felting properties of wool fabrics," *Surface and Coatings Technology*, vol. 205, pp. 5349–5354, 2010.

[59] N. Bhat and D. Upadhyay, "Plasma-induced surface modification and adhesion enhancement of polypropylene surface," *Journal of Applied Polymer Science*, vol. 86, no. 4, pp. 925–936, 2002.

[60] O. G. Agbabiaka, I. O. Oladele, and O. O. Daramola, "Mechanical and water absorption properties of alkaline treated coconut (Cocosnucifera) and sponge (Acanthus montanus) fibers reinforced polypropylene composites," *American Journal of Materials Science and Technology*, vol. 4, no. 2, pp. 84–92, 2015.

[61] N. Kumar, A. Singh, K. Debnath, and R. Ranjan, "Mechanical characterization of animal fibre-based composites," *Indian Journal of Fibre & Textile Research*, vol. 45, no. 3, pp. 293–297, 2020.

[62] D. Chakrabarti, M. S. Islam, K. Jubair, and M. R. H. Sarker, "Effect of chemical treatment on the mechanical properties of luffa fiber reinforced epoxy composite," *Journal of Engineering Advancements*, vol. 1, no. 2, pp. 37–42, 2020.

[63] F. R. Oliveira, L. Erhens, R. Fangueiro, and A. P. Souto, "Surface modification of banana fibers by DBD plasma treatment," *Plasma Chemistry and Plasma Processing*, vol. 32, no. 2, pp. 259–273, 2012.

[64] N. Sapiai, A. Jumahat, and R. N. Hakim, "Tensile and compressive properties of hybrid carbon fiber/kenaf polymer composite," *Advances in Environmental Biology*, vol. 8, no. 8, pp. 2655–2661, 2014.

ANNEXE. 2Certificates of ParticipationNational Conferences in Algeria

Université Echahid Hamma Lakhdar - El-Oued
Faculté de Technologie
Département Génie Mécanique

Attestation de participation

Le président du comité d'organisation de la **Journée d'étude sur l'intelligence artificielle en électromécanique et ses applications industrielles (JEIAM'23)** qui s'est déroulée le **03-04 Mai 2023** atteste que

Mr. (Mme. Melle.) **Rahmani LALMI**

a présenté une communication intitulée :

Machin learning for material sciences with python

Co-auteur(s): Gharbi Mohamed Taher

LE PRÉSIDENT DU COMITÉ D'ORGANISATION

LE CHEF DU DÉPARTEMENT

ANNEXE. 2Certificates of Participation in International Conferences in Algeria

People's Democratic Republic of Algeria

Ministry of Higher Education and Scientific Research

University of Echahid Hamma Lakhdar – El Oued

Faculty of Exact Sciences

Department of Physics

CERTIFICATE
OF PARTICIPATION

The Second International Conference on Materials, Energy & Environment (MEE'2023)

This is to certify that Lalmi RAHMANI

Presented an Poster in "The Second International Conference on Materials, Energy & Environment (MEE'2023)" which took place on October 23-24, 2023 in El Oued – Algeria.

Title: Utilization of Algerian Desert Plant Species for the Development of High-Quality Composite Materials

Co-authors: GHERBI mohamed tahar

Prof. Mohammed El Hadi Attaf
General Chair

El Oued – Algeria
October 23-24, 2023

People's Democratic Republic of Algeria
Ministry of Higher Education and Scientific Research
Echahid Hamma Lakhdar University - El-Oued

International Pluridisciplinary PhD Meeting (IPPM'23)

2nd Edition, December 11-13, 2023

Artificial Intelligence (AI) Revolution:
Challenges, Prospects and Ethical Aspects

Certificate of Participation

This Certifies that

(Mr.; Ms.) Mr. Laalmi Rhmani
University of El Oued, Algeria

Has successfully participated at the IPPM'23 as
Member of Organizing Committee

Algeria, 13/12/2023

IPPM'23 Chairman

We look forward to your continued and outstanding contribution for our community in the future ...

A31